Screening of algal cells using microdroplet technology

Tina Leontidou

Hughes Hall

Department of Chemistry

University of Cambridge

A dissertation submitted for the degree of Doctor of Philosophy

November 2020

DECLARATION

This is to declare that this thesis is the result of my own work and includes nothing which is the outcome of work done in collaboration except as specified in the text.

This thesis is not substantially the same as any work that has already been submitted before for any degree or other qualification except as specified in the text.

Any references made to other research are acknowledged in the text and in the bibliography, as per the University of Cambridge's guidelines on plagiarism.

This thesis does not exceed the word limit of 60,000 words as specified by the Degree Committee for the Faculty of Physics and Chemistry.

Tina Leontidou

November 2020

ABSTRACT

The increased interest in algae as feedstock for biofuel and high value chemicals, has accentuated the need for a more in-depth study of algal cells at the single cell level. Droplet microfluidics has been established as a multifunctional platform, with many advantages for the study of biological systems in the microscale. In this thesis, droplet microfluidic technology was used to optimise and expand the application of a platform designed for the study and screening of single algal cells.

Single *Phaeodactylum tricornutum* (*Pt*) cells were encapsulated in microdroplets and their growth was monitored over 11 days and was found to be heterogeneous. To limit cell sedimentation during encapsulation and to increase the time over which the encapsulation procedure could be run, 10% v/v OptiPrep density matching medium was added to the cell suspension prior to the encapsulation.

A fluorescence-activated droplet sorting platform was used to detect the fluorescence of encapsulated algal cells. Following modifications to the optics of a previously used platform, the fluorescence measurement uncertainty was reduced from 87% to 8%. This improved platform was used to detect the chlorophyll fluorescence of encapsulated *Pt* and *Ng* (*N. gaditana*) cells, confirming that the screening of cells of different sizes and shapes is possible. Chlorophyll fluorescence sorting was used to isolate droplets containing cells from empty droplets to overcome the issue of the random encapsulation of the cells in droplets. There were no false negatives during the sorting procedure, minimising the loss of cells.

GFP fluorescence detection was used to sort GFP-expressing *Pt* cells from a mixture with wild type cells. Furthermore, droplet sorting was combined with droplet dispensing to collect single GFP-expressing cells and obtain monoclonal cell cultures. Single droplet dispensing enables the screening of mutagenized libraries of cells and the selection of potentially rare cell clones, which is much harder to achieve using other selection methods.

To screen cells based on their lipid content, *Pt* cells encapsulated in microdroplets were stained with BODIPY 505/515. The diffusion of the dye to and from the droplets was studied by fluorescence imaging. Furthermore, the BODIPY 505/515 fluorescence of the droplets was

detected with the laser-induced fluorescence detection platform. Several experimental parameters were modified to reduce the high fluorescence background caused by the dye dissolved in the oil surrounding the droplets.

A new cell staining method was developed using micelle/hydrogel composite beads loaded with BODIPY 505/515 for dye delivery. The success of this method was assessed with fluorescence microscopy and flow cytometry. The flow cytometry results showed that *Pt* cells could be stained by these beads within 30 minutes and that the beads could also stain other types of cells, such as *Ng* cells. The cells could still grow after the staining. The beads were co-encapsulated with *Pt* cells in microdroplets to test whether this was a viable solution to the issue of leakage of BODIPY 505/515 from the droplets over time.

With the microfluidic platform established and optimised, it is now possible to transition from mainly proof-of-concept experiments on algal cell fluorescence detection, to targeted experiments aimed towards answering specific biological questions.

DEDICATION

This thesis is dedicated to the memory of my supervisor, Professor Chris Abell, who recently passed away. His untimely passing was shocking and heart-breaking. He was a wonderful person, an outstanding scientist and a great source of inspiration for me. He will be dearly missed.

ACKNOWLEDGEMENTS

TABLE OF CONTENTS

LIST OF ABREVIATIONS

a.u.   arbitrary unit

B. braunii   *Botryococcus braunii*

BHQ1   Black hole quencher 1

BODIPY   4,4-difluoro-1,3,5,7-tetramethyl-4-bora-3a,4a-diaza-s-indacene

C. reinhardtii   *Chlamydomonas reinhardtii*

C. vulgaris   *Chlorella vulgaris*

CMC   carboxymethyl cellulose

COC   cyclic olefin copolymer

DAQ   data acquisition

DHA   docosahexaenoic acid

DMAEMA   2-(Dimethylamino)ethyl methacrylate

DMSO   Dimethyl sulfoxide

DNA   deoxyribonucleic acid

E. coli   *Escherichia coli*

E. gracilis   *Euglena gracilis*

EPA   eicosapentaenoic acid

et al.   *et alia*

FACS   fluorescence-activated cell sorting

FADS   fluorescence-activated droplet sorting

FITC   fluorescein isothiocyanate

FRET   Fluorescence Resonance Energy Transfer

GFP	green fluorescent protein
hr	hour
kDa	kilodalton
kHz	kilohertz
LD	light-dark
LED	light-emitting diode
LIF	laser-induced fluorescence
LL	light-light
M	mol per litre
M_n	number average molecular weight
mg	milligram
mL	millilitre
mm	millimeter
MTES	methyltriethoxysilane
mW	milliwatt
MW	molecular weight
MWCO	molecular weight cut-off
Ng	*Nannochloropsis gaditana*
nL	nanolitre
nm	nanometer
NMR	Nuclear Magnetic Resonance
OD	optical density
o/w	oil-in-water

PBS	phosphate-buffered saline
PDI	polydispersity index
PDMS	polydimethoxysilane
PEG	poly(ethylene glycol)
PFO	perfluorooctanol
pg	picogram
pL	picolitre
PMMA	poly(methyl methacrylate)
PMT	photomultiplier tube
Pt	*Phaeodactylum tricornutum*
PUFA	polyunsaturated fatty acid
PVA	poly(vinyl alcohol)
rpm	revolutions per minute
s	second
S. elongatus	*Synechococcus elongatus*
SAW	Surface Acoustic Wave
SERS	Surface Enhanced Raman Scattering
TAG	triacylglycerol
TCEP	tris(2-carboxyethyl)phosphine
TEOS	tetraethoxysilane
THF	tetrahydrofuran
TTL	transistor–transistor logic
UV	ultraviolet

V	Volt
v/v	volume to volume
w/o	water-in-oil
w/v	weight to volume
µg	microgram
µL	microlitre
µm	micrometre
µM	micromolar

LIST OF FIGURES

Chapter 1

Chapter 2

Chapter 3

Chapter 4

Chapter 5

CHAPTER 1

Introduction

1.1.   Algal biotechnology

In recent years, there has been an increasing interest in microalgae as a source of a wide range of chemicals, such as biodiesel, bioethanol, polyunsaturated fatty acids (PUFAs), proteins, vitamins, pigments and other compounds of interest.[1-3] Considerable efforts are currently being devoted to cultivating microalgal cells at an industrial scale and using them as raw material for the production of useful compounds. This increased interest in microalgae and their products has accentuated the need for a more in-depth study of algal cells at the single cell level to further our understanding of the biology of the cells and to identify cell strains that are more suited for industrial exploitation.

1.1.1. Microalgae

Microalgae are unicellular organisms, found in freshwater or marine environments, that contain high levels of oils, carbohydrates, sugars and proteins. There are estimated to be 200,000 – 800,000 species of microalgae worldwide, although only a small fraction of these microalgae have been identified and studied so far, and they display a great diversity in terms of their physiology, chemical composition and behaviour.[4] Microalgae play a very important role globally as they supply more than half of the oxygen in the atmosphere through photosynthesis and are also the primary producers of organic compounds in most ecosystems.

As microalgae perform photosynthesis to satisfy their energy needs, they require light, CO_2, water and inorganic salts as nutrients to sustain their growth. However, they can be grown using water resources unsuitable for cultivating agricultural crops, such as seawater or wastewater. Therefore, not only do they not take up arable land but also, when grown in wastewater, they can help purify water that is not suitable for other purposes. The combination of CO_2 fixation (during photosynthesis), high biomolecule production and

storage and the potential for wastewater treatment, make algae a particularly attractive resource for industrial applications.[5]

1.1.2. Algal biofuel

The reduction in fossil fuel levels over time, as well as the negative environmental effects associated with their use, have led to a concentrated effort to develop new and more environmentally friendly fuels. The generation of biofuels is part of this effort, as numerous studies have deemed that they are a viable alternative to fossil fuels and they have the potential to be carbon neutral.[6,7] Liquid biofuels are of particular interest, since they can be more easily integrated into the infrastructure currently used for traditional fossil fuels, especially in the transport sector.

Biofuel derived from various agricultural crops such as corn, sugarcane, soybean and rapeseed have been in development for several decades and are now commercially available. However, there are considerable concerns over the use of land-based crops for fuel production. A major argument against the culture of plants for energy harvesting is that these plants take up valuable arable land which is needed to cover the nutritional needs of the rapidly increasing World population.[8] With this issue in mind, research began into establishing new biofuel sources that do not take up arable land. As part of this effort, the production of biofuel from algae was proposed.[9]

Besides not competing with crops for arable land, microalgae display several characteristics that make them a good biofuel source, such as much faster growth rates than land-based crops, lower water consumption, the ability to use the CO_2 generated by industry as carbon source and high lipid content.[10]

Biofuel generated by microalgae include ethanol, hydrogen, methane and syngas,[11] however one of the main fuels that can be derived from algae is biodiesel. Biodiesel is produced through the extraction of the intracellular lipids of the cells and the transesterification of the triglycerides with an alcohol, mainly methanol (**figure 1.1**). This reaction is an equilibrium, but by adding a large excess of methanol the methyl esters (biodiesel) can be produced at more than 98% yield.[12]

$$H_2C\!-\!OCOR_1 \qquad\qquad\qquad H_2C\!-\!OH \qquad R_1\!-\!COOMe$$
$$HC\!-\!OCOR_2 \;+\; 3MeOH \;\rightleftharpoons\; HC\!-\!OH \;+\; R_2\!-\!COOMe$$
$$H_2C\!-\!OCOR_3 \qquad\qquad\qquad H_2C\!-\!OH \qquad R_3\!-\!COOMe$$
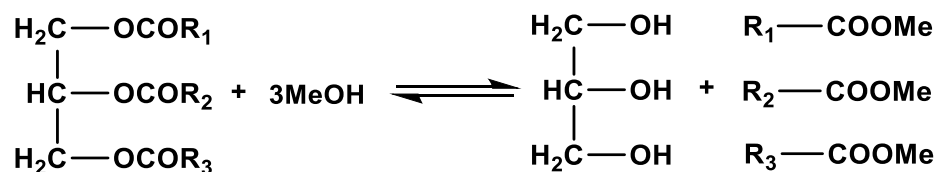
Figure 1.1: Transesterification of triglycerides to produce methyl esters (biodiesel), adapted from ref.12.

Biodiesel generated from vegetable oil or animal fat is currently one of the most common biofuels worldwide, second only to bioethanol in total energy production. In 2019, 47.4 billion litres of biodiesel were produced, accounting for approximately 35% of the global biofuel production.[13] It is distributed in the market either on its own or blended with petroleum diesel and is increasingly used as transportation fuel.[8] Currently, the generation of biodiesel from algal lipids is not economically viable, however, it is a more sustainable alternative to vegetable oil and animal fats.

1.1.3. Generation of high value products from microalgae

Despite extensive efforts into cultivating algae and generating algal biofuel on an industrial scale, the production of algal biofuel does not appear to be economically viable, due to the high costs of the extraction process and the lower than required lipid production from algal cells. This has led researchers to investigate other possible uses of algae and their products, to improve the economics of algal biorefineries. Algae can produce a range of high value products, including pigments, such as carotenoids and chlorophyll, poly-unsaturated fatty acids (PUFAs), various vitamins, such as vitamin A, B1, B2, B6, B12 and C, as well as proteins and antioxidants.[8,14] There is, therefore, considerable interest in the exploitation of algae by the nutritional, cosmetic and pharmaceutical industries. The production of such chemicals is more economically viable, so if it could be combined with biofuel production, an industry based on microalgae cultivation would be much more sustainable.[15]

1.1.4. Lipid biosynthesis in algae

Due to the large variations in morphology and in the habitats that microalgae occupy, the composition of microalgal lipids is also very diverse,[16] especially when compared to the lipid composition of higher plants.[17] This lipid composition changes over a cell's lifetime depending

on factors such as the cell growth phase, the culture age and the environmental conditions.[17] Algal lipids usually include, for the most part, neutral lipids, polar lipids, sterols, wax esters and hydrocarbons,[17] with the different lipids performing important functions in the cell. Under favourable growth conditions, microalgae will primarily synthesise fatty acids to form polar membrane lipids. These lipids take up 5 – 20 % of the dry cell weight and they are in the form of glycolipids and phospholipids.[17,18] However, if the cells are exposed to unfavourable conditions, the growth of the cells will halt and they will change their metabolic pathways to start producing neutral lipids, mainly triacylglycerols (TAGs), which accumulate in the cytoplasm of the cells in the form of lipid bodies. The TAGs act as a carbon and energy storage for the cells.[17] TAG accumulation will also take place in most cell strains when the stationary phase of growth is reached.[17,19]

1.1.4.1.   Polyunsaturated fatty acids (PUFAs)

Many algae, mainly marine microalgae, are an important source of ω-3 and ω-6 polyunsaturated fatty acids (PUFAs), mainly EPA and DHA (**figure 1.2**). Both EPA and DHA are ω-3 fats that are essential components of higher eukaryotes. Both fatty acids are a crucial part of the human diet due to the health benefits that they offer. DHA is important for the proper development of the eyes and the brain, while both EPA and DHA support good cardiovascular health, as well as supporting the brain and the nervous system.[20]
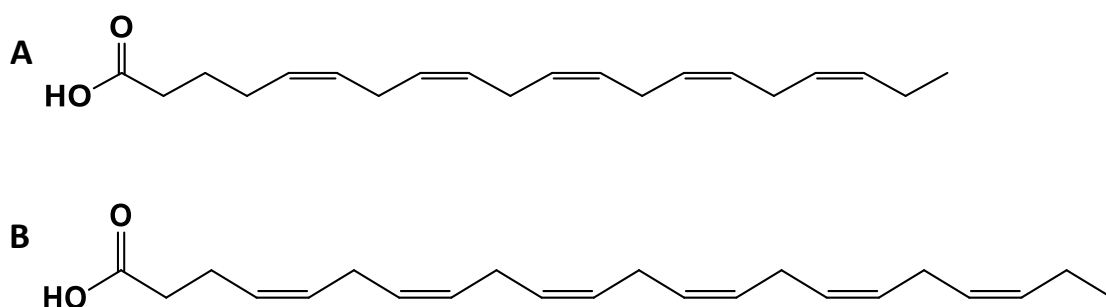
Figure 1.2: The chemical structures of A) EPA and B) DHA.

EPA and DHA are high value lipids which are traditionally obtained from fish and fish oil for use in dietary supplements, however, there is significant interest into exploring alternative sources of EPA and DHA, due to the gradual depletion of marine fish supply and the increasing risk of fish oils containing high levels of pollutants.[21]

1.1.5. Strategies to improve lipid accumulation

Several approaches are considered by researchers to enhance the production of lipids by microalgae. One such approach is the careful control over the cell culture conditions, as these affect the quantity and composition of the algal lipids.[19] Conditions, such as nutrient limitation, increased CO_2 supply, variation in light intensity, temperature and salinity can result in enhanced lipid production.[22] As some of these conditions can be harmful to cell growth, a two-stage cultivation strategy has been proposed,[23] whereby the microalgae are initially cultured under conditions optimal for cell growth to obtain maximum biomass and in the next stage they are exposed to culture conditions that trigger lipid accumulation. Other novel alterations that have been proposed to culture conditions include the use of phytohormones to promote cell growth, such as indole-3-acetic acid, kinetin and abscisic acid,[24] the addition of various chemicals to the cell cultures, such as azide[25] or surfactants,[26] the use of LEDs, dyes or paints to improve the light conditions[27,28] and the co-cultivation of microalgae with bacteria or yeast, as a possible symbiotic relationship between the two species could enhance microalgal cell growth.[29]

Another major strategy is the use of genetic engineering to generate new cell strains that display superior characteristics, such as enhanced growth rate or enhanced lipid production.[30] Furthermore, by modifying the biosynthetic pathways of the cells the composition of the algal lipids can be controlled and fatty acids of specific chain length or saturation levels can be obtained.[30]

The ratio of saturated to unsaturated fatty acids contained in microalgae is an important factor that determines if they are suitable as feedstock for biodiesel. Biodiesel generated from microalgae with lower saturated fatty acid content displays better cold temperature properties. On the other hand, biodiesel from microalgae with a high amount of unsaturated fatty acids oxidises more easily than conventional diesel affecting engine performance.[19]

1.1.6. Microalgae used in this project

1.1.6.1. *Phaeodactylum tricornutum*

The alga mainly used throughout this project was the marine diatom *Phaeodactylum tricornutum* (*Pt*) (**figure 1.3**). It is a model diatom and is therefore extensively studied by researchers. The genome of *Pt* has been fully sequenced, and several methods have been

applied to achieve the genetic transformation of *Pt* cells.[31,32] *Pt* can exist in different morphotypes – fusiform, triradiate or oval.[33] The cells used in this project were fusiform and approximately 20 µm in length. *Pt* cells have a doubling time of just one day and can accumulate large amounts TAGs, particularly in response to nutrient stress, which has led researchers to consider *Pt* as a major candidate for use in biofuel production. The cells can store lipids corresponding to 20-30% of the dry cell weight under standard culture conditions.[12] Besides TAGs, *Pt* is a major producer of PUFAs, mainly eicosapentaenoic acid (EPA), which constitutes up to 30% of its lipid content,[34] but also small amounts of docosahexaenoic acid (DHA).

Both characteristics make *Pt* a good candidate for use in high-value lipid production.[35] An additional advantage is that *Pt* is a marine alga and seawater is the most readily available and economic medium for algal cultivation. The growth of *Pt* cells in bulk has been extensively studied to determine the growth conditions that are optimum for lipid production[36,37] as well as the response of the cells to stress conditions, such as nitrogen[38-40] or light limitation.[41] Several methods to extract the lipids have also been considered, such as solvent extraction,[42] ultrasound-assisted extraction and microwave-assisted extraction.[43]

Figure 1.3: Image of fusiform *P. tricornutum* cells at 64x magnification.

1.1.6.2.   *Nannochloropsis gaditana*

N. gaditana (**figure 1.4**) is a marine microalga which is a well-known source of EPA[44] and whose relatively high growth rates[44] and high TAG productivity (38% of its dry weight)[45] also make it a strong candidate for use in biodiesel production.[46] While it has not been studied as extensively as *Pt*, its genome has been sequenced[47] and genetic transformation of *Ng* cells

has been demonstrated.[47,48] The response of *Ng* cells to stress conditions such as nitrogen limitation[45,49] and different light conditions[50] has been studied. *Ng* cells are spherical, with a diameter of approximately 2 μm.
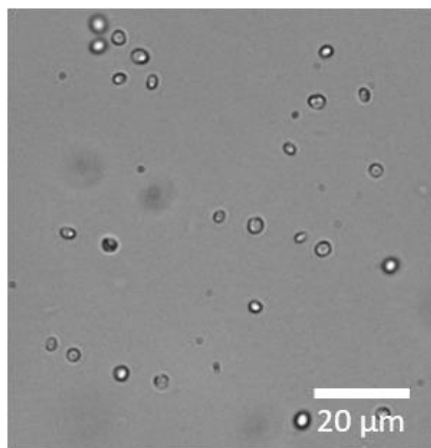
Figure 1.4: Image of *N. gaditana* cells at 64x magnification.

1.1.7. Single cell studies

The microalgae that are sought for algal lipid production at an industrial scale should ideally display a combination of the following attributes: high growth rates, high lipid content, ease of harvest and extraction,[7] tolerance of unfavourable environmental conditions such as high salinity, high temperatures and high light intensities and the production of by-products of commercial value.[18] To identify cell strains that display these favourable characteristics the screening of a large number of algal strains, either naturally occurring or genetically engineered, is required.

The conventional method used to screen algal cells based on their lipid content requires the extraction of the lipids using a solvent, followed by separation, concentration and gravimetric determination.[51] Despite its high accuracy, this method cannot be used for large scale screening of cell strains as it is time and labour-intensive and requires a substantial cell sample (more than 10-15 mg cells).[18] As it is also a bulk method, potentially critical information on the behaviour of the cell strains at the single cell level is lost.

Increasingly, single cell methods are used to study microalgae since they can reveal information about the heterogeneities in cell behaviour and the large variation that can occur within cell cultures. With the development of appropriate fluorescent tags and dyes,

fluorescence microscopy is now frequently used to study single algal cells in vivo.[52] Epifluorescence and confocal microscopy are high-resolution methods which can be used to study intracellular processes with high accuracy. When combined with automation and fast image analysis, the fluorescence of thousands of single cells can be assessed.[53]

Flow cytometry is also widely used to assess the light scattering and fluorescence of large populations of microalgae. In flow cytometry, a cell suspension is hydrodynamically focused to flow past a laser beam one cell at a time. Light scattering and fluorescence data of individual cells are then collected at a high throughput as they pass through the beam (**figure 1.5**). In algal research, flow cytometry has been used to monitor the cell cycle, enzymatic activity, and the viability of microalgae. It has also been used to identify cells with high pigment (chlorophyll, carotenoid) or high lipid content.[54] Flow cytometry can be further combined with fluorescence-activated cell sorting to isolate cells of interest.[54,55]
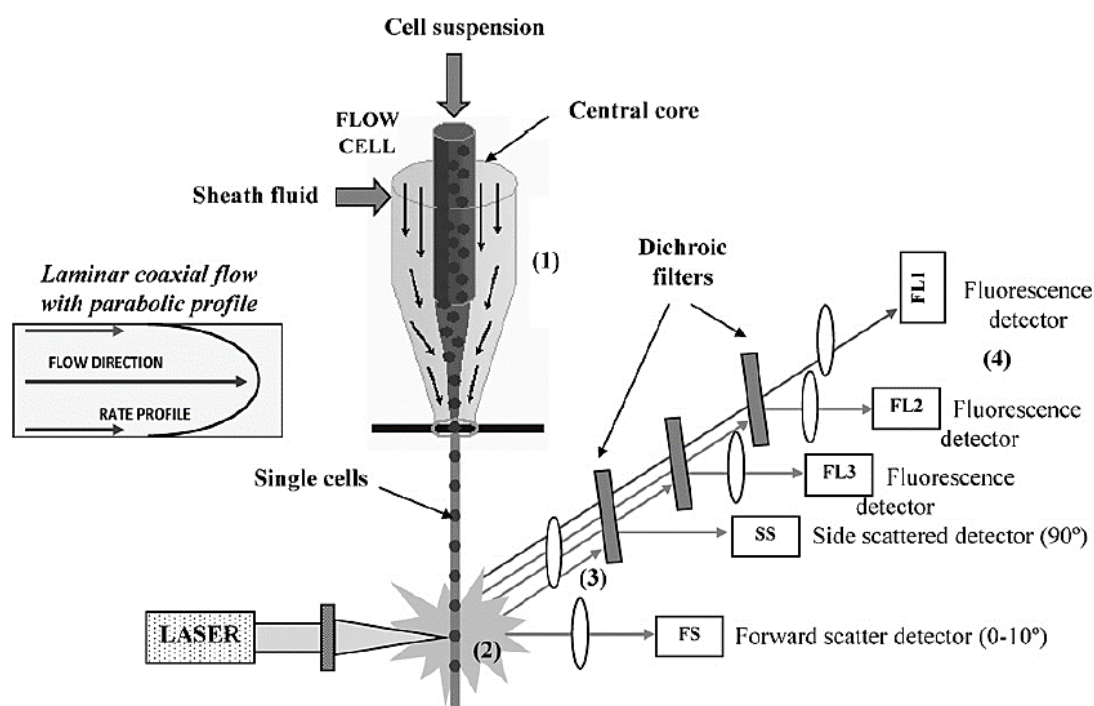
Figure 1.5: Flow cytometer operating principle, adapted from Diaz *et al*.[56] Through hydrodynamic focusing a single stream of cells is formed which passes through a laser beam. The scattered light and the fluorescence emitted by each cell are collected and split by a group of filters and mirrors according to wavelength. The light signals are then sent to separate detectors.

More recently, microfluidic systems and techniques have been applied to the algal biotechnology field to scale down cell cultures and enable high throughput single cell analysis and manipulation.[57,58]

1.2.   Droplet microfluidics

In the past three decades, advances in the instrumentation available have made possible the miniaturisation of analytical systems. The availability of such miniaturized systems has led to the development of microfluidics, a multidisciplinary research field which enables the study of chemical and biological systems in very small volumes.[59-61]

Scaling down reactions and processes and working with much smaller reagent volumes on a microfluidic chip offers multiple advantages. Firstly, as smaller volumes of chemicals are used, it can lead to significant reductions in research cost, as well as in the amount of waste generated.[60] At the same time, it drastically reduces the time needed to process and analyse large chemical or biological assays. Furthermore, the small size and the customisability of microfluidic devices allows for their easy integration into larger systems.

Single phase microfluidics involves the laminar flow of reagents through microfluidic channels. While useful for a variety of applications, there are several disadvantages which arise from the laminar flow regime which are detrimental in some applications, such as Taylor dispersion, the interaction of the solute with the surface of the microfluidic channels and cross-contamination which might arise due to interaction of the samples with the channel walls.[62]

Droplet microfluidics is a subset of microfluidics which has been developed to overcome the shortcomings of single-phase microfluidics. It involves the generation and manipulation of large numbers of droplets in microfluidic channels. The droplets are isolated from each other by an immiscible carrier phase (also known as the continuous phase) which acts as a barrier, stopping diffusion between the droplets from taking place, so each of the droplets can be regarded as a discrete miniature reaction vessel.[63] The droplets can be either oil-in-water (o/w) or water-in-oil (w/o) droplets depending on the required application. More complex emulsions, such as double emulsions or multiple emulsions, can also be generated due to the tunability and reproducibility offered by microfluidic methods.

1.2.1. Droplet microfluidics for single cell analysis

One particularly powerful application of droplet microfluidics is their use in the study of single cells. The individual w/o droplets formed in the microfluidic channels serve as an ideal method to separate and isolate cells.[59,64] The droplet generation methods used in droplet microfluidics enable the high throughput encapsulation of cells in droplets of tuneable size. The microdroplets act as microscale bioreactors, within which single cells can be monitored and analysed. The microdroplets, and the cells contained within, can be further manipulated by taking advantage of various droplet operations, such as droplet fusion and fission, droplet mixing and droplet sorting[65] (**figure 1.6**). The droplets can be analysed and screened at a high throughput and without the risk of contamination of the cells at any point during the experiment. At the same time, the environment of the cells can be more closely controlled, and a variety of experiments can be conducted, which would not be feasible through single phase microfluidics. As a result, complex biological assays can be performed on-chip.

By using only biocompatible reagents and materials, the viability of the encapsulated cells can be preserved. A fluorinert oil, such as Novec 7500 or FC-40, is usually used during droplet generation as the continuous phase. Fluorinert are stable fluocarbon-based oils that are noted for their high gas solubility.[72] The encapsulated cells can stay alive in the droplets for several days, as the oil prevents the contents of the microdroplets from diffusing, but still permits the diffusion of gases to and from the cells.[73]

Single cell experiments that have been performed using droplet microfluidics include, and are not limited to, the study of cell growth[74] and cell-to-cell interactions,[75] cell lysis,[76,77] the detection of molecules secreted by the cell,[78-81] as well as molecules within the cell,[82,83] cytotoxicity studies,[78,84] cell transfection,[85,86] single cell PCR[87,88] and single cell sequencing.[89]
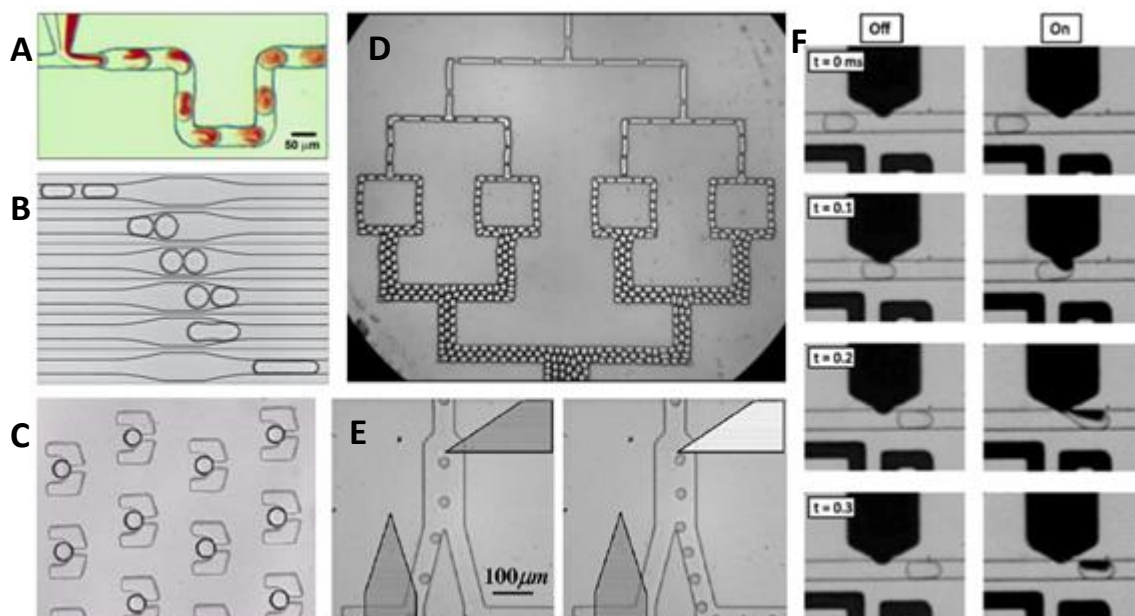
Figure 1.6: A) Mixing of the contents of microdroplets by chaotic advection as the droplets move through a winding microfluidic channel, adapted from ref.66, B) passive droplet fusion in an expanded channel, where two droplets collide, relax and separate again, leading to destabilisation of the droplet interface, adapted from ref.67, C) droplet trapping on-chip in an array of individual droplet traps, adapted from ref.68, D) passive droplet splitting occurring as droplets flow into a series of T-junctions where they are split into two side channels, adapted from ref.69, E) droplet sorting in a Y-shaped junction triggered by the application of an electric field – when the field is applied the droplets are deflected into the positive channel, while in the absence of an electric field, the droplets flow into the negative channel due to lower hydraulic resistance, adapted from ref.70, F) pico-injection of a new reagent into droplets triggered by the application of an electric field, adapted from ref.71.

1.2.2. Droplet generation

To generate monodisperse water-in-oil microdroplets, three different types of microfluidic device have been used. The first type of device is a T – junction, an example of which is shown in **figure 1.7A**. In this device, the aqueous phase is injected into the oil stream perpendicularly, resulting in the formation of aqueous droplets at regular intervals.[59]

The second type of device relies on flow-focusing for droplet generation (**figure 1.7B**). The flow-focusing geometry requires there to be two oil streams intersecting the aqueous stream.

The three converging streams subsequently flow through an orifice and the forces applied on the aqueous phase by the oil result in droplet formation downstream of the orifice.[59]

The third type of device used to generate microdroplets is a co-flowing device (**figure 1.7C**). In this approach, the aqueous phase is introduced into the co-flowing continuous phase using a microcapillary.[90] Other approaches to droplet formation have also been demonstrated which rely on the application of an external force to generate droplets on demand, for example using SAW[91] or an electric field[92] to trigger droplet formation and release.
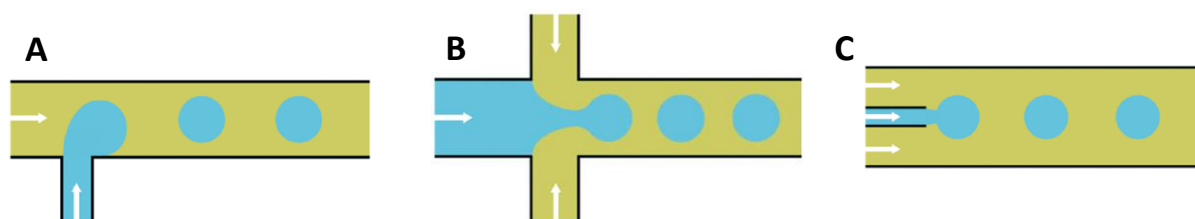
Figure 1.7: Microdroplet generation by A) a T-junction, B) a flow-focusing device, C) a co-flow device. The continuous phase is depicted in yellow, while the dispersed phase is shown in blue. The arrows indicate the direction of flow. Adapted from ref.93.

All three of the above usually-used methods result in the formation of microdroplets with less than 1–3% size dispersity.[59,91,94] Depending on the flow rates of the converging streams, droplet generation frequencies higher than 10 kHz can be achieved.[95] A surfactant that is added to the oil stream, helps control the interfacial tension and prevents droplet coalescence from taking place.[59] The size and properties of the generated microdroplets can be controlled by careful selection of the surfactant, the relative dimensions of the intersecting microfluidic channels and the relative flow rate of the two phases.[93]

1.2.3. Cell encapsulation in microdroplets

By suspending a cell sample in the aqueous phase during the droplet generation procedure, the cells can be easily encapsulated into microdroplets. However, as the flow of the cells in the microfluidic channel during the droplet generation is random, the number of cells within each of the generated droplets is defined by Poisson statistics[96] (**figure 1.8**). The probability of a droplet containing a certain number of cells is therefore defined as:

$$P(X = k) = \frac{e^{-\lambda}\lambda^k}{k!} \qquad \text{(Equation 1.1)}$$

where λ is the mean number of cells per droplet and k is the number of cells. This, unfortunately, means that to obtain droplets that contain only one cell a lot of empty droplets are generated, along with a few droplets that contain multiple cells. This is particularly undesirable in single cell studies since it results is a drastic increase in the time needed to screen a cell sample.
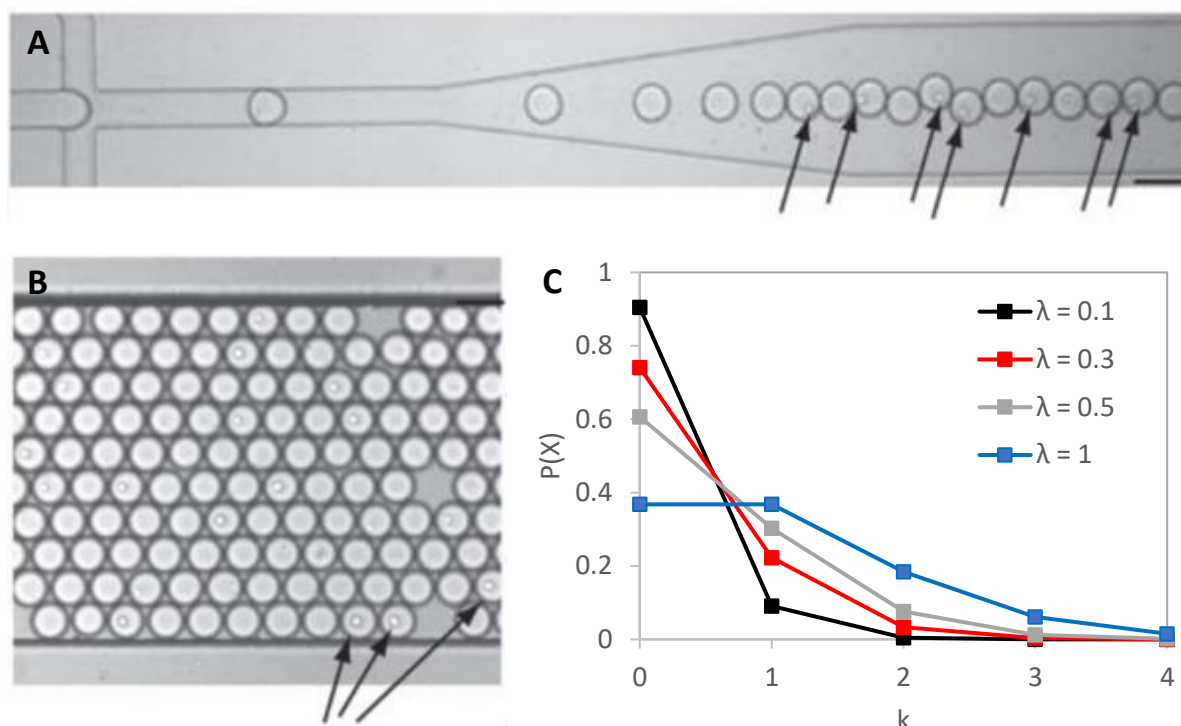
Figure 1.8: A) Random encapsulation of hybridoma cells in 33 pL droplets using a flow-focusing device, B) image of the generated droplets containing hybridoma cells (cells indicated by the arrows), adapted from ref.97, C) plot of the probability P(X = k) of finding k cells in each droplet for different λ values.

Alternative encapsulation methods have been proposed to eliminate Poisson statistics and improve the cell encapsulation efficiency. Edd *et al.*[98] proposed taking advantage of the self-organisation of cells when they flow rapidly through a high aspect-ratio microfluidic channel. Due to the even spacing between the cells under these conditions, a more ordered encapsulation can be achieved, resulting in ~80% of droplets containing single cells when a high-density cell suspension is used. A spiral channel has also been used to improve

encapsulation efficiency by using an inertial effect to order cells before encapsulation.[99] This method resulted in ~77% of droplets containing single cells. As considerable time and effort would be required to optimise these methods of encapsulation for new applications, they were not adopted in this thesis.

1.2.4. Analysis of microdroplet content

A great advantage of droplet microfluidics is that it can be combined with a range of analytical methods to analyse the contents of microdroplets in real time. The ability to probe the content of microdroplets qualitatively and quantitatively is vital for the conduction of chemical or biological assays in the droplets.[63] However, the very small volumes and low concentrations of the analytes in the microdroplets often make detection and analysis very challenging.[100]

Fluorescence-based methods are the most commonly used analytical methods in droplet microfluidics[61,71] due to their high sensitivity and selectivity.[61,63] Furthermore, fluorescence detection is ideally suited to probe the content of large numbers of droplets in a short timeframe as fluorescence measurements can be performed on a sub-millisecond timescale.[61] However, since fluorescence-based methods can only be used when fluorophores are available, other analytical methods have also been considered. Droplet microfluidics has been coupled with mass spectrometry[101,102] to analyse complex samples of small molecules and biomolecules. SERS (Surface Enhanced Raman Scattering) is also a promising technique that could be combined with droplet microfluidics to further increase the detection sensitivity.[103,104]

1.2.5. Droplet sorting

Once the contents of each droplet have been determined, it is often necessary to isolate droplets that have a specific constitution or specific desirable properties from the rest of the droplets to be studied separately. To satisfy this need, droplet sorting technology was developed.

A variety of methods has been applied to achieve the separation of microdroplets into subpopulations. Sorting platforms have been designed which rely on magnetic fields,[105] acoustic waves[106] or valves[107,108] for droplet actuation. However, the majority of microdroplet

sorting platforms rely on dielectrophoresis to induce droplet separation.[109,110] The principle behind this approach is that an electric field is applied on the droplets which have a different dielectric constant to the continuous phase. As a result, a net force acts on the droplets and redirects them. Using this method, higher sorting speeds have been achieved than through the other methods tested,[110] with sorting frequencies of up to 30 kHz having been reported.[111]

The first instance of microfluidic droplet sorting using dielectrophoretic force to redirect droplets was reported in literature is by Ahn *et al.* in 2006.[109] They designed a microfluidic device which had electrodes at a different layer than the microchannels through which the droplets would flow. These electrodes could be activated on demand and, by applying a dielectrophoretic force on the droplets flowing past, they would redirect droplets towards a different microfluidic channel. Through subsequent modifications to the electrode and the sorting device design, sorting efficiency has been significantly improved.[110]

By combining analytical methods with droplet sorting technology, high throughput screening of microdroplets based on their content can be achieved. FADS (Fluorescence-Activated Droplet Sorting) is an example of one such platform, which combines droplet microfluidics with the traditional fluorescence-activated cell sorting (FACS) (**figure 1.9**). It was first developed in 2009 by Baret *et al.*[70] who used it to sort *E. coli* based on their enzymatic activity. It is a very versatile technique that is capable of separating droplets with higher fluorescence without damaging the droplets or their contents.

To screen and sort the droplets based on their fluorescence, they are reinjected into a specifically designed sorting device. Spacing oil is used to adjust the distance between the droplets, which flow through a microfluidic channel and are subsequently intercepted by a laser beam. If the droplets contain fluorophores, then excitation will take place and the total fluorescence emitted by the droplet will be measured by a photomultiplier tube (PMT). The droplets will then flow towards the sorting junction and down the slightly wider 'negative' channel which has a lower hydraulic resistance. However, if the fluorescence signal detected by the PMT is above a certain threshold value, an electric pulse will be generated by the electrodes in the sorting device and an electric field will be applied in the microfluidic channel. As a result, a dielectrophoretic force will be exerted on the microdroplets which is enough to

redirect them towards a separate 'positive' channel. In this way, droplets that show higher fluorescence can be isolated from the rest.
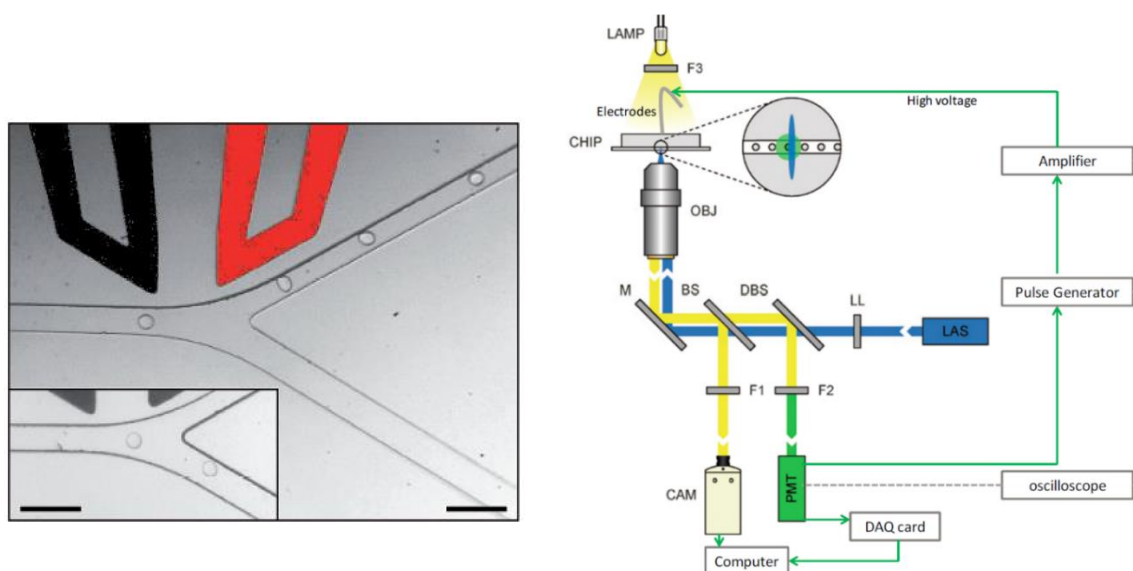
Figure 1.9: A) Trajectories of droplets passing past the sorting junction in the presence and absence (inset) of an electric field was applied across the electrodes (the scale-bar corresponds to 100 mm), B) Diagram of the optical and electronic setup for a FADS system. The beam emitted by the laser (LAS) is shaped into a laser line (LL) and transmitted through a microscope to the microfluidic sorting device (CHIP), where it excites the droplets as they flow past. The fluorescence emitted by the droplets is reflected by the dichroic beam splitter (DBS) to the PMT via a bandpass filter (F2). The signal recorded by the PMT is sent to a computer via a data acquisition (DAQ) card, to an oscilloscope for further monitoring and to a pulse generator, which triggers a square pulse when the fluorescence signal is above a certain threshold. The sorting procedure is monitored by a high-speed camera (CAM). Adapted from ref.70.

Droplet subpopulations that are selected through droplet sorting can be collected off-chip for subsequent analysis. The collected cells can be analysed in-droplet or they can be extracted from the droplets by the addition of perfluorooctanol (PFO) which disrupts the surfactant layer surrounding the droplets breaking them apart. The cells can then be transferred to plates to obtain cell cultures.

Droplet sorting has been used as an alternative method to isolate droplets containing cells from empty droplets after droplet generation. It can be applied to enrich the droplet pool with droplets that contain cells after the random cell encapsulation process. Best *et al.*[82] used fluorescence detection and sorting to successfully separate droplets containing *C. reinhardtii* cells from empty droplets based on the inherent chlorophyll fluorescence of the encapsulated cells. Some other sorting approaches used were the sorting of droplets based on their size in cases where droplets containing cells were larger than empty droplets[112,113] or image-based cell sorting, in which microscopy images of the droplets were captured and processed prior to sorting.[114]

In the case of single cell studies, individual droplets of interest can be isolated for further study off-chip by combining droplet sorting technology with droplet dispensing. During this process, the droplets, which are selected through droplet sorting, are directed towards an outlet nozzle and from there they are dispensed into the wells of a well plate,[115] or they are be printed and immobilised on a substrate where they can be studied individually[116] (**figure 1.10**). The well plate or substrate is controlled by a mechanised stage for high-throughput automated dispensing. Accurate droplet selection and dispensing are hard to achieve, and they require a suitable software and hardware control system.[81] Droplet dispensing is invaluable in applications such as cell line development, where it can be used to obtain monoclonal cell cultures from single cells of interest.[81]
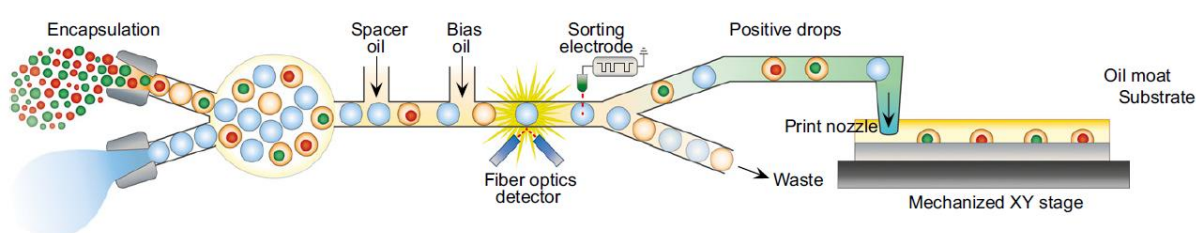
Figure 1.10: Single droplet printing on an oil moat substrate, adapted from ref.116. The printer consists of a droplet sorting platform connected to a print nozzle that automatically dispenses selected microfluidic droplets to a substrate under a cover of oil.

1.3.   Thesis overview

The increased interest in algae as feedstock for biofuel and high value chemicals, has accentuated the need for a more in-depth study of algal cells at the single cell level, to obtain

more information about the physiology and the behaviour of the cells and to identify cell strains that are more suited for industrial exploitation. The aim of this project was to develop a platform based on droplet microfluidics which can be used for the high throughput analysis and screening of algal cells, mainly focusing on the identification of algal cells which display superior lipid production.

While such a platform would have significant industrial potential, it would primarily be beneficial to researchers interested in algal biology and biotechnology. It would serve as a novel toolbox, which could be applied in the study of single algal cells to reveal potentially unknown information about algal cells. To be useful in this fashion, however, the platform must meet several requirements. Primarily, it must generate quantitative and reproducible experimental results. Furthermore, it must be robust and relatively straight-forward to use, even for researchers who are not familiar with microfluidic technology. Finally, it must be suitable for a range of different experiments, which cannot be easily performed through currently available methods and instruments. With these requirements in mind, the following objectives were set for this thesis:

(i)   To improve the performance of an established droplet-microfluidic platform which can be used to study single algal cells.[74,82]

(ii)   To improve the accuracy and the screening capabilities of a fluorescence-based platform which can be used to sort encapsulated algal cells based on useful fluorescence properties, such as chlorophyll fluorescence and GFP fluorescence and to expand the application of this platform to screen encapsulated cells based on their lipid content.

(iii) To test whether droplet sorting can be combined with droplet dispensing to collect single algal cells of interest and obtain monoclonal cell cultures.

(iv)   To develop a new staining method to improve the delivery of BODIPY 505/515, a lipophilic dye, to algal cells, whether they are in a bulk solution or encapsulated in droplets.

CHAPTER 2

Single microalga encapsulation in microdroplets

2.1. Introduction

The application of microfluidics to study algal cells has gained a lot of momentum in recent years, as it has become apparent that microfluidics facilitates the study of single cells and could potentially reveal previously unknown information about their behaviour.[58] Microfluidic systems serve as a useful platform to isolate algal cells and to study them in a controlled environment. They offer multiple advantages over the traditional methods used to study algal cells, which require the use of bioreactors, flasks, Petri dishes or well plates. In bulk studies, the data obtained correspond to the average of all the cells in the culture and it is assumed that all cells behave in a similar manner. By using microfluidics to isolate single cells, the cells are studied individually and their independent behaviours together with the heterogeneities in their behaviour are revealed.[74,117] Furthermore, the environment of individual cells can be carefully controlled allowing the study of the impact of various culture conditions on the cell growth, the cell morphology and the accumulation of metabolites in the cells.[58]

A number of microfluidic methods and devices have been used to isolate and study microalgal cells and they can be classified into three different categories: single-phase microfluidics, droplet microfluidics[118] and hydrogel droplet microfluidics (for the generation of microcapsules and hydrogel beads). These are analysed in some detail below.

2.1.1. Single-phase microfluidics

Single-phase microfluidic devices, that have been used to study microalgae, usually consist of arrays of microscale compartments or trapping modules, which are used to isolate the cells. In these devices, the cells can be cultured and analysed under different conditions over several hours or days. Some initial attempts to study single algal cells on chip were made using single phase microfluidics, as far back as 2003. Matsumura et al.[119-121] (**figure 2.1A**) trapped *C. reinhardtii* cells in microchambers etched on a glass slide in order to monitor the cell division process and perform measurements of the cell size and division time. Optical

tweezers were used to handle the cells, increasing the complexity of the system and making it difficult to scale-up.

Several other groups have, since then, developed their own microfluidic devices to immobilise and study microalgae on-chip. Ai *et al.*[122] (**figure 2.1C**) designed a PDMS – glass hybrid microwell device to track the flagellar length of *C. reinhartii* in real time. The impact of various environmental factors, such as the pH, on the flagella of the cells was investigated.

Multiple microfluidic devices have been developed to study *C. reinhardtii*, due to its role as a model organism for research in cell biology. Different designs used included C-shaped growth chambers (**figure 2.1B**),[123] microfluidic perfusion chambers[124] and agarose-based microchambers.[125] These devices enabled the study of the immobilised cells under different culture conditions, such as different sodium acetate (carbon source)[123] and ammonium (nitrogen source) concentrations.[125] These compounds act as the organic carbon source and the nitrogen source, respectively. The effect of the different conditions on the growth rate, the chlorophyll content and the lipid content of the *C. reinhardtii* cells was examined.

Besides nutrient limitation, the effect of the illumination conditions on cell growth was also examined. A microfluidic device composed of microchamber arrays was combined with a pixel-based irradiance platform to test the effect of a variety of illumination conditions of the growth of *S. elongatus* cells. This irradiance platform could accurately control the illumination intensity, the wavelength, as well as the variation of light intensity over time.[126] Kim *et al.* designed a multilayer microfluidic device which contained traps for cell capture.[127] This device was used to study the effect of different light conditions on the growth and the lipid content of *B. braunii*. They also designed a more sophisticated microfluidic device consisting of 1024 trapping modules that could be individually controlled (**figure 2.1D**). Within each of the modules they were able to capture a single *C. reinhardtii* cell and study the growth rate and the lipid content of each cell. They were then able to selectively release specific cells of interest from the traps to collect them off-chip.[128]

Overall, a variety of single-phase microfluidics devices have been used to culture and study algal cells. While these devices enable the study of individual cells, some issues might arise from cross-contamination.[58] A significant limitation of these devices can be the difficulty of extraction of the cells from the devices for further study both on and off-chip.
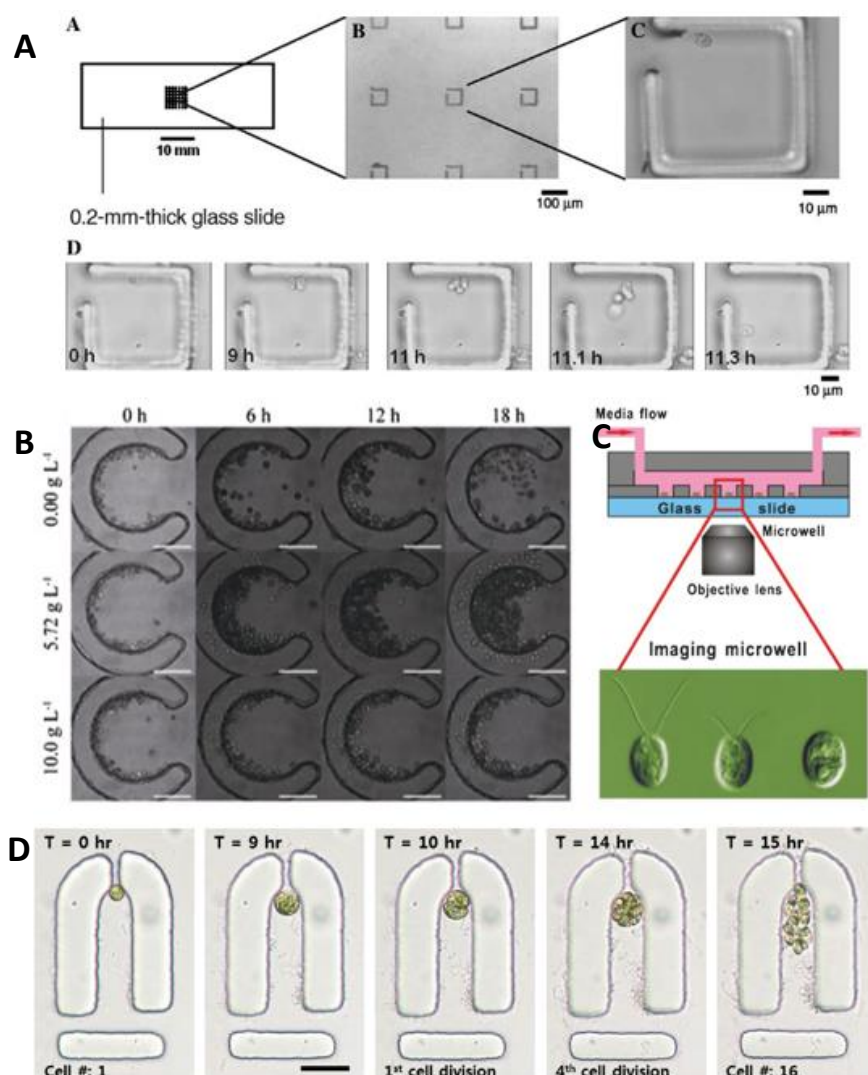
Figure 2.1: A) Studying the division process of *C. reinhardtii* single cells in microchambers on-chip, adapted from ref. 119, B) monitoring the growth of *C. reinhardtii* cells in C-shaped growth chambers, adapted from ref. 123, C) tracking the flagellar length of *C. reinhartii* in real time in a microwell device, adapted from ref. 122, D) monitoring the growth of *C. reinhardtii* cells capsured in trapping modules, adapted from ref. 128.

2.1.2. Droplet-based microfluidics

An alternate way of isolating algal cells is their encapsulation in microdroplets. The use of microdroplet technology to study algal cells offers unique advantages over the single-phase methods previously mentioned. The cells can be isolated with high throughput and studied in an environment which mimics the culture conditions used in bulk cultures, while at the same time avoiding contamination and providing full control over the cellular environment. In

addition, the microdroplets can be further manipulated on chip, enabling operations such as cell sorting.[65]

A droplet microfluidic platform for the encapsulation and study of single algal cells was developed by Pan *et al.*[74] They encapsulated single algal cells in microdroplets to track their growth within the droplets over 10 days. Three species of green algae were studied: *Chlamydomonas reinhardtii*, *Chlorella vulgaris* and *Dunaliella tertiolecta*. The droplets were collected within PDMS reservoir devices and they were imaged over time (**figure 2.2A**) to monitor the change in the number of encapsulated cells and to generate cell growth curves (**figure 2.2B**). Different growth conditions, such as nutrient limitation (**figure 2.2C**), pH and salinity, and different encapsulation parameters, such as droplet size and initial number of encapsulated cells, were tested and their impact on the encapsulated cells was studied.
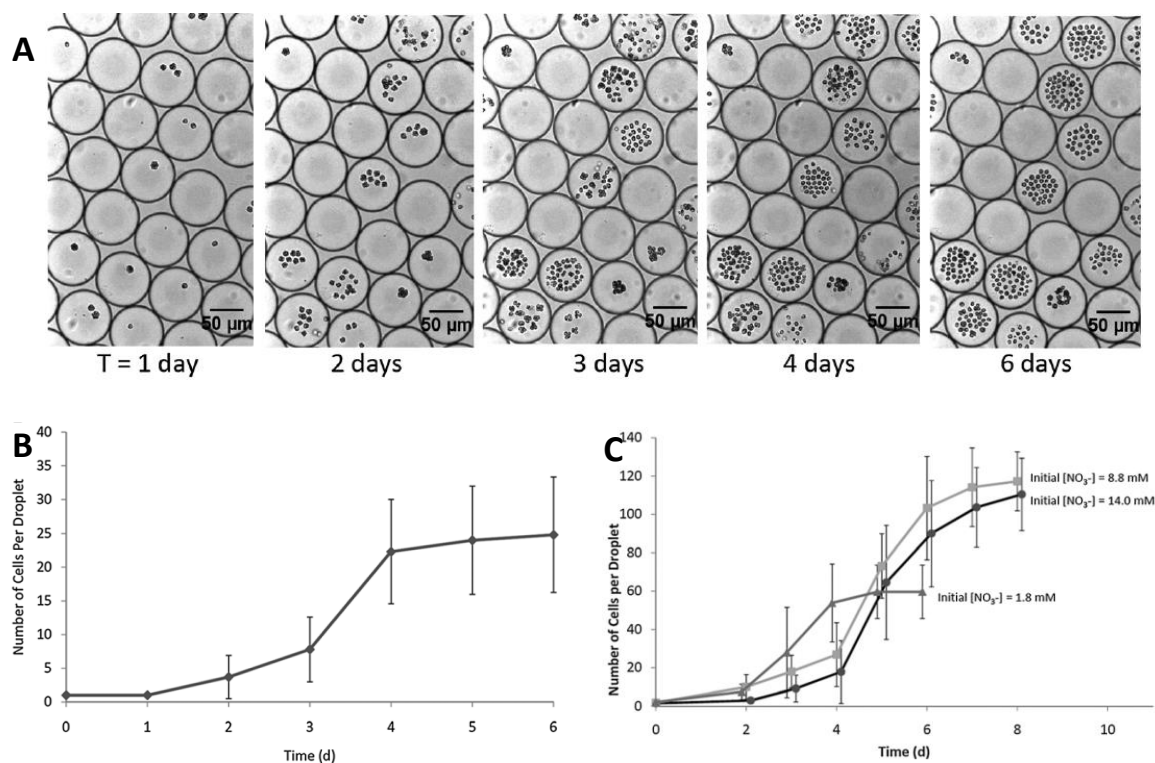
Figure 2.2: Studying the growth of *C. reinhardtii* cells encapsulated in microdroplets over one week: A) imaging of droplets incubating in a reservoir device, B) number of cells per droplet over time, C) effect of different nitrate concentrations on the growth of *C. vulgaris,* adapted from ref.74.

A variety of studies has been conducted on microalgae using droplet microfluidics. The growth kinetics and cell size distribution of *C. vulgaris* cells were investigated in nanolitre-size droplets. The droplets were formed by flowing the cell sample into specially designed microfluidic traps and generating static droplet arrays which could be stored on-chip for more than a month (**figure 2.3B**).[129] Sung *et al.* used a microfluidic device containing micropillars to immobilise and monitor microdroplets over 120 hours (**figure 2.3A**).[130] This platform was used to study the growth of *C. vulgaris* within the droplets under different CO_2 concentrations and under different light intensities. The effect of light intensity, temperature variation and nitrate limitation on the growth and the metabolic profile of *C. vulgaris* has also been studied using droplet microfluidics.[131,132]
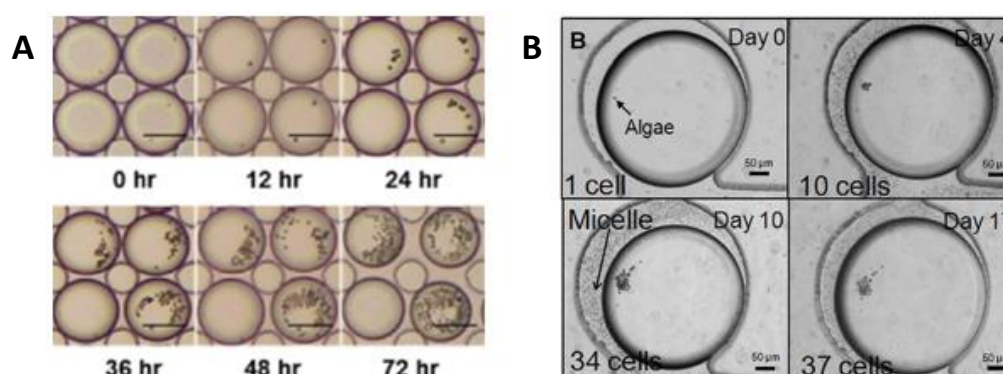
Figure 2.3: A) Monitoring of *C. vulgaris* growth in microdroplets immobilised by a reservoir device containing micropillars, adapted from ref.130, B) growth of *C. vulgaris* cells in microdroplets immobilised by microfluidic traps, adapted from ref.129.

A unique advantage that droplet microfluidic platforms have over single-phase microfluidics is the ability to manipulate the cells and their environment more accurately when they are encapsulated in the droplets. This enables researchers to perform a range of experiments that would otherwise be much more difficult to perform, such as co-encapsulation experiments or cell sorting after incubation. For example, Lagus *et al.*[133] used droplet microfluidics to co-encapsulate two different strains of *C. reinhardtii* in microdroplets, one cell of mating-type plus and one cell of mating-type minus *C. reinhardtii*. They then monitored the mating of the two cells within the droplets under nitrogen starvation conditions. The encapsulated cells could survive within the droplets for 17 days. *C. reinhardtii* cells were encapsulated in 150 nL droplets to study the cell growth kinetics of the *Chlamydomonas* cells over 140 hours. The

droplets were subsequently screened based on the chlorophyll fluorescence of the encapsulated cells and subpopulations of the cells were collected for further testing.[134]

2.1.3. Hydrogel droplet microfluidics

A further advantage of droplet microfluidics is that the microdroplet generation techniques can be combined with polymer chemistry, giving rise to new methods of isolating and studying algal cells. By encapsulating the cells in micromaterials, such as microcapsules or hydrogel beads, the encapsulated cells can be protected from outside contamination while still getting the nutrients that they need.[135] The cells that are encapsulated in this fashion can also be studied with techniques such as FACS (Fluorescence Activated Cell Sorting), which are not usually compatible with the encapsulation oil used to generate the droplets.[136]

Morimoto *et al.* developed a method of encapsulating *C. reinhardtii* cells within semi-permeable alginate-poly-L-lysine (PLL) microcapsules (**figure 2.4B**).[135] Since the membrane of the microcapsules was semi-permeable the cells could still get all the necessary nutrients from their environment, but they were kept isolated and safe from other microorganisms and contaminants. The cells could still grow and move around within the microcapsules. *Chlorella vulgaris*, *Chlamydomonas sp.*, and *Botryococcus braunii* cells have also been encapsulated in alginate microcapsules (**figure 2.4A**), so that their lipid content could be studied.[137]

E. gracilis and *C. reinhardtii* single cells were encapsulated in gelatin microdroplets and their growth within the droplets was monitored (**figure 2.4C**).[136] The gelatin droplets were kept liquid during this time by keeping the culturing temperature constant between 25 and 30 °C. However, when the droplets were incubated at 4 °C they would undergo a sol–gel transition. The solid hydrogel beads could then be transferred to an aqueous solution to be screened based on their fluorescence using FACS.

Co-encapsulation experiments have also been performed in gel microdroplets. *Chlorella sorokiniana* cells were co-encapsulated with various species of freshwater bacteria in agarose gel droplets by Ohan *et al.*[138] The gel microdroplets were incubated for at least one week and they were then transferred to aqueous media to be analysed and sorted through FACS.

Despite the multiple advantages offered by hydrogel technology, a disadvantage of encapsulating algal cells in hydrogel beads or microcapsules is, once again, the difficulty of extracting and recovering the cells from the materials if required.
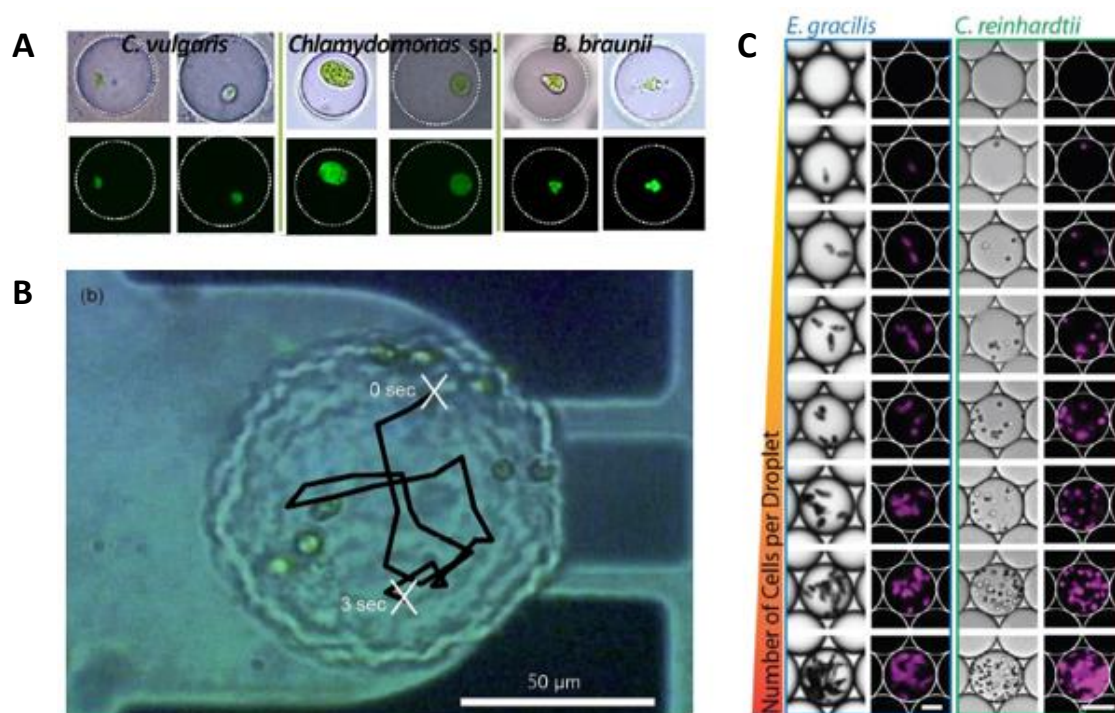
Figure 2.4: A) encapsulation of *Chlorella vulgaris*, *Chlamydomonas sp.*, and *Botryococcus braunii* cells in alginate microcapsules and lipid staining with BODIPY 505/515, adapted from ref.137, B) encapsulation of *C. reinhardtii* cells in alginate-poly-L-lysine (PLL) microcapsules and monitoring of the cell motility, adapted from ref.135, C) encapsulation of *E. gracilis* and *C. reinhardtii* cells in gelatin microdroplets and study of the cell growth over time, adapted from ref.136.

2.1.4. Objectives

In this chapter, the encapsulation and growth of *Phaeodactylum tricornutum* (*Pt*) marine microalgae in microdroplets were investigated. A droplet microfluidic platform was established for the isolation and study of single *Pt* cells and the optimum cell encapsulation parameters for single cell isolation were determined. A density matching solution was used to overcome the issue of cell sedimentation during the encapsulation procedure and to thereby improve the cell encapsulation efficiency. The growth of *Pt* cells in microdroplets over several days was studied and compared to *Pt* growth in bulk.

2.2. Experimental

Algal cell preparation

The *Phaeodactylum tricornutum* (CCAP 1055/1) cells used in all experiments were provided by Professor Alison Smith's group at the Department of Plant Sciences, University of Cambridge. The *Nannochloropsis gaditana* (*Ng*) cells were provided by Professor Saul Purton's group at the Institute of Structural & Molecular Biology, University College London. Both cell species were cultured in Guillard's F/2 medium.[139] The medium was prepared by diluting Guillard's (F/2) marine water enrichment solution 50x (Sigma Aldrich) with artificial sea water. The sea water was prepared by dissolving artificial sea salt (Sigma Aldrich) in Milli-Q water at a concentration of 30 g/L and it was autoclaved before the addition of the enrichment solution.

The cells were cultured in 25 mL plastic cell culture flasks (Nunc™, Thermo Scientific) at room temperature (20 °C), under continuous illumination (115 µmol of photons m^{-2} s^{-1}) and shaking. New cultures were prepared by taking a sample of stationary phase cells and diluting it to the desired cell concentration by adding F/2 medium.

Microfluidic device fabrication and surface treatment

The microfluidic device masters were fabricated, by Dr Ziyi Yu, using photolithography as described by Duffy *et al*.[140] The AutoCAD designs of the devices used throughout this thesis can be found in the Appendix.

To fabricate the PDMS (polydimethylsiloxane) microfluidic devices, a 10:1 mixture of the PDMS precursor and its curing agent (Sylgard 184, Dow and Corning) was thoroughly stirred and poured into a Petri dish containing the master in order to cover it. The mixture was thoroughly degassed under vacuum and the PDMS was cured at 75 °C overnight. The solidified PDMS was peeled off the master and holes for the inlets and outlets were punched in using a 1 mm diameter biopsy punch (Kai medical). The PDMS slab was attached to a glass slide after treatment with oxygen plasma (Femto, Diener Electronic), thereby forming the enclosed microfluidic channels. The device was then cured at 75 °C for a minimum of 10 minutes to strengthen the bonding between the PDMS and the glass substrate and to return the exposed areas back to a hydrophobic state.

The surface of the microfluidic channels was then treated with a 1% v/v solution of trichloro(1H,1H,2H,2H-perfluorooctyl)silane (Sigma Aldrich) in Novec 7500 for 10 seconds to make it more fluorophilic, followed by washing the channels with Novec 7500 for a further 10 seconds and flushing with nitrogen for five seconds to dry the channels.

Cell encapsulation in microdroplets

A *Pt* cell sample was taken from the culture flask under sterile conditions while the cells were in their growth phase. The concentration of the cell sample was determined by cell counting using a bright-line haemocytometer (Sigma-Aldrich) and it was diluted to the desired concentration by the addition of more F/2 medium. The suspension of algal cells in F/2 growth medium, with or without OptiPrep™, was loaded into a 1 mL syringe (HSW NORM-JECT®) fitted with a needle (0.5 x 16 mm, Terumo). The fluorinated oil used as the continuous phase (either Novec™ 7500, 3M™, or FC-40, 3M™, with 1% PicoSurf™ 1 surfactant, Sphere Fluidics) was loaded in another syringe and both syringes were connected to the respective inlets of the flow-focusing device (**Appendix device A**, nozzle dimensions: 40 μm x 40 μm x 25 μm) with fine bore polyethylene tubing (ID = 0.38 mm, OD = 1.09 mm, Smiths Medical International Ltd). Using syringe pumps (Harvard Apparatus PHD 2000 Infusion) the two solutions were injected simultaneously in the device. The oil phase was injected at a rate of 600 μL/hr (16.7 cm/s) and the aqueous phase at a rate of 350 μL/hr (9.72 cm/s). The droplet formation was monitored using a Phantom V72 fast camera mounted on an inverted microscope (IX71, Olympus) set at 20x magnification. The Phantom software was used to monitor the camera feed and record the video of the encapsulation procedure. The generated droplets were collected, through tubing connected to the outlet, into a syringe, for reinjection or a centrifuge tube, for imaging.

Cell growth in microdroplets

After their generation, the droplets containing the *Pt* cells in F/2 medium were stored in a plastic syringe under continuous illumination (115 μmol of photons m^{-2} s^{-1}). Microdroplet samples (4 μL) were taken from the syringe, placed on a glass slide and imaged every day.

<u>Droplet imaging and cell counting in microdroplets</u>

The droplets were imaged using an IX 71 inverted microscope (Olympus) equipped with an EMCCD iXonEM+ DU 897 camera (Andor Technology) at a 32x magnification. The cell counting was performed manually. The droplet diameter and cross-section area were measured using ImageJ, an image processing software. The droplets were manually selected.

<u>OptiPrep optimum concentration determination</u>

The optimum concentration of OptiPrep needed to reduce cell sedimentation was determined by adding 2 mL of F/2 medium with OptiPrep to a 2 mL *Pt* cell sample. The final concentrations of OptiPrep in the samples were 0%, 2%, 4%, 6%, 10% and 20% v/v. The samples were allowed to stand without mixing for 2.5 hours and the precipitation of the cells in each sample was monitored. A photograph of the samples was taken after 2.5 hours.

<u>Growth curve of *Pt* with and without Optiprep in bulk</u>

The growth curves of *Pt* cells in bulk F/2 medium, with and without the addition of 10% v/v OptiPrep, were generated by measuring the optical density at 730 nm of cell samples taken from a fresh culture every day for 12 days. Optical density values were recorded using a spectrophotometer (WPA Biochrome).

2.3.   Results and discussion

2.3.1.   PDMS microfluidic device preparation

As was described in section 2.2, the polydimethylsiloxane (PDMS) microfluidic devices, used throughout this thesis were fabricated through soft lithography. The fabrication process consists of four steps: 1) master fabrication, 2) PDMS polymerisation using the master as a mould, 3) microfluidic device bonding to a glass substrate and 4) surface treatment of the microfluidic channels (**figure 2.5**).[73,140]
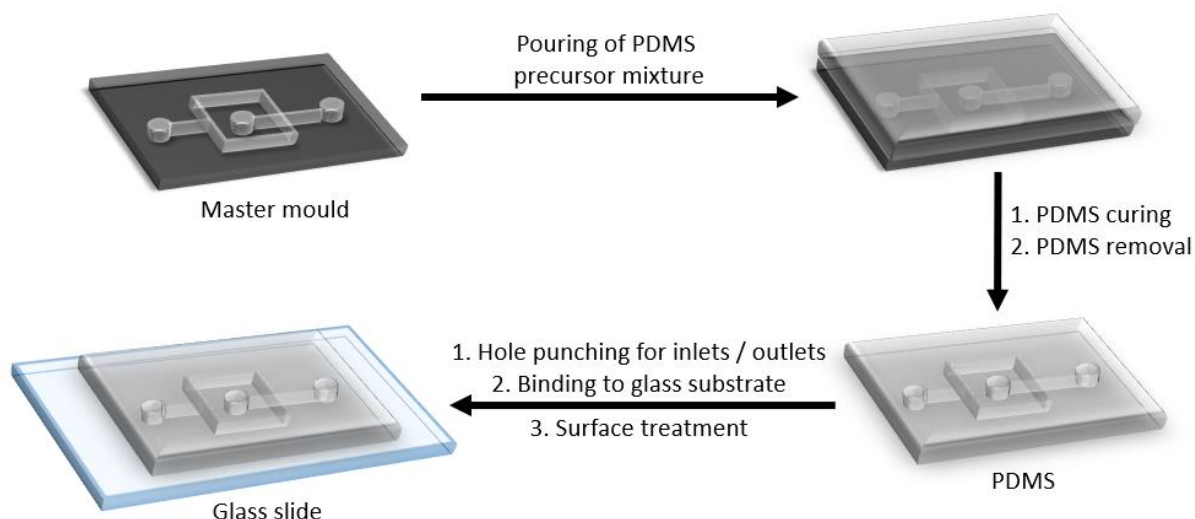
Figure 2.5: Schematic diagram of the microfluidic device fabrication process.

The device master was fabricated by Dr Ziyi Yu using SU-8 photoresist coated on the surface of a silicon wafer and it was subsequently used as the mould for the microfluidic device preparation. A 10:1 mixture of the PDMS base and its curing agent (Sylgard 184, Dow Corning) was poured into a Petri dish containing the master. The curing of PDMS is a platinum-catalysed process during which the vinyl groups on the PDMS base oligomers react with the Si-H groups carried by the crosslinking agent (**figure 2.6**).[141]
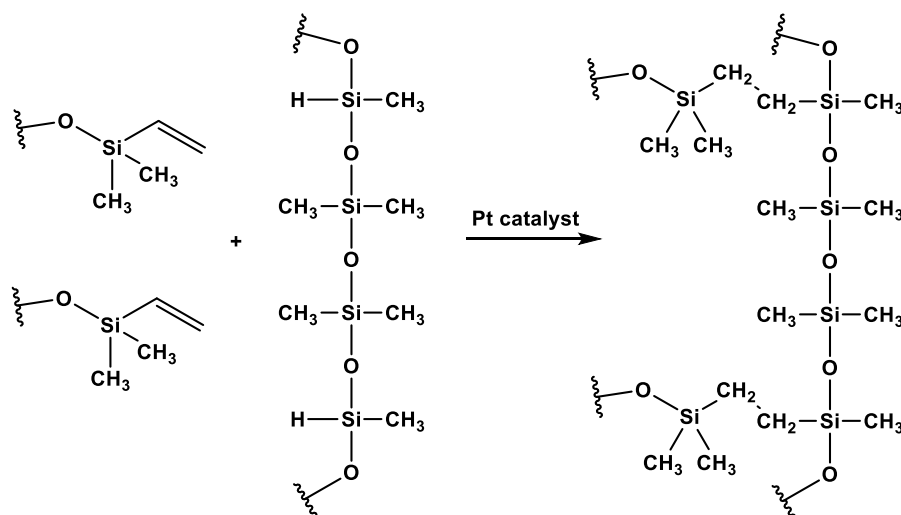
Figure 2.6: PDMS polymerization reaction, adapted from ref.141.

The curing reaction is accelerated through heating, so the PDMS mixture was degassed under vacuum and then cured at 75 °C for a minimum of 4 hours. The solidified PDMS was peeled off the master and holes for the inlets and outlets were punched in using a 1 mm diameter biopsy punch. The PDMS slab was then attached to a glass slide after treatment with oxygen plasma, forming thus the enclosed microfluidic channels. The treatment with oxygen plasma introduces silanol groups (Si-OH) to the surface of the PDMS and the glass slide. When the two surfaces are brought into contact, strong covalent Si-O-Si bonds are formed, sealing the two surfaces together and forming the microfluidic device (**figure 2.7**).
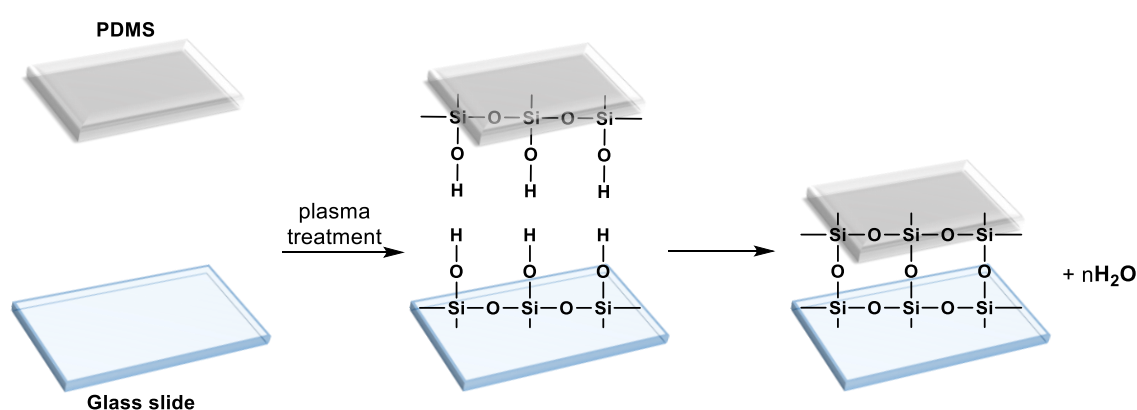
Figure 2.7: Schematic diagram of the plasma treatment process and the bonding between the PDMS and the glass slide.

The device was cured at 120 °C for a minimum of 60 minutes to strengthen the bonding between the PDMS and the glass substrate. Once the microfluidic device was sealed, the surface of the microfluidic channels was treated with a fluorophilic agent. This is done to ensure droplet stability in the devices. The fluorophilic agent used for the surface treatment was 1% v/v trichloro(1H,1H,2H,2H-perfluorooctyl)silane (Sigma Aldrich) solution in Novec 7500. The silane reacts with the exposed silanol groups on the channel walls (**figure 2.8**) changing the hydrophilic surface of the microfluidic device to a fluorophilic surface which is compatible with the oil used for the droplet generation.
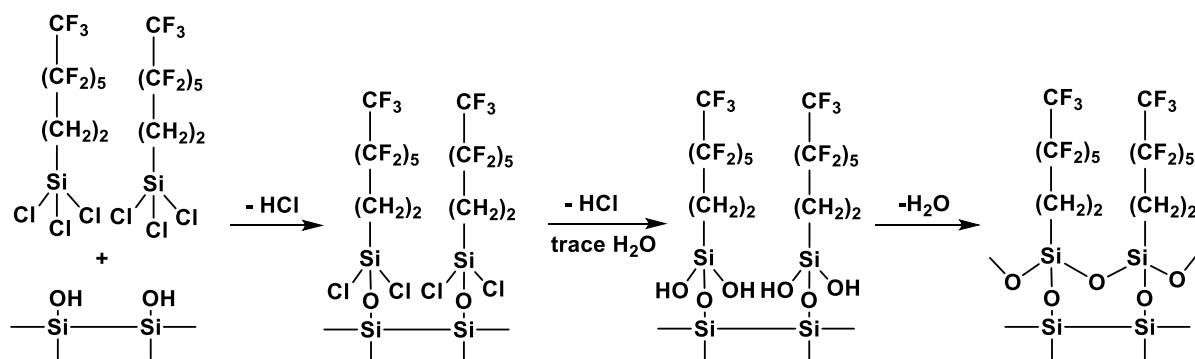
Figure 2.8: Surface treatment of the microfluidic channels with trichloro(1H,1H,2H,2H-perfluorooctyl)silane. Adapted from ref.142.

2.3.2. Encapsulation of algal cells and cell growth assay

The flow-focusing device, shown in **figure 2.9C**, was used to encapsulate Phaeodactylum tricornutum (*Pt*) cells (**Appendix device A**). *Pt* cells are marine microalgae that are ~20 µm in length. The reason why this algal species was selected for this project is explained in section 1.1.6.1. The flow-focusing geometry was selected over other device geometries that have been previously used for droplet generation, because it generates highly monodisperse microdroplets at lower oil-to-water flow rate ratios.[73] The device was placed on a microscope stage during droplet generation (**figure 2.9A-B**), so that the process could be monitored through a high-speed camera.

The fluorous oil that was used as the continuous phase and the suspension of *Pt* cells in F/2 growth medium were injected from different inlets to the device with flow rates of 600 µL/hr (16.7 cm/s) and 350 µL/hr respectively (9.72 cm/s). Novec 7500 or FC-40 (fluorinert oils) were used as the continuous phase with the addition of 1% v/v Pico-Surf™ 1 surfactant.[143] The dimensions of the nozzle in the encapsulation device were 40 µm x 40 µm x 25 µm (length x width x height). The droplets generated had a diameter of approximately 50 µm when Novec 7500 was used (65 ± 4 pL volume) and 40 µm when FC-40 was used (34 ± 2 pL volume). Through microscopic observation and analysis of the microscope images using ImageJ, it was determined that there was less than 2% variation in the diameter of the generated droplets (**figure 2.9D**). The droplet generation frequency achieved was 1.5 kHz when generating droplets that were 50 µm in diameter and 2.8 kHz for droplets that were 40 µm in diameter.
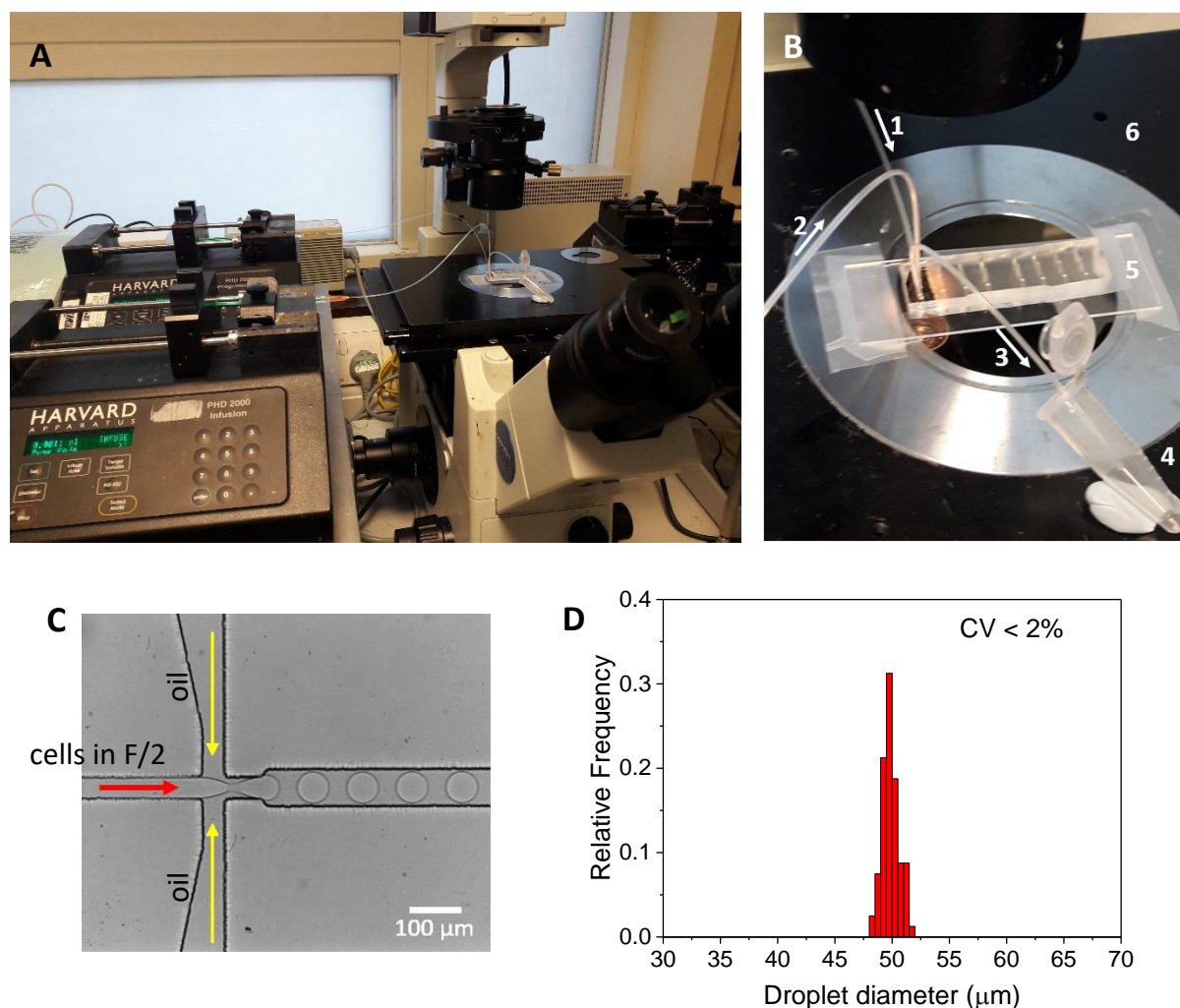
Figure 2.9: A) Photograph of the droplet generation set-up, B) photograph of the microfluidic device during droplet generation; (1) inlet tubing for oil phase, (2) inlet tubing for aqueous phase, (3) outlet tubing, (4) Eppendorf tube for droplet collection, (5) microfluidic droplet generation device, (6) microscope stage, C) droplet generation using the flow-focusing encapsulation device with nozzle dimensions 40 μm x 40 μm x 25 μm (length x width x height), D) distribution of the droplet diameter for the droplets generated.

Both Novec 7500 and FC-40 are fluorinated oils that are widely used for cell encapsulation.[144,145] Both oils are compatible with PDMS and therefore they do not cause swelling and deformation of the microfluidic channels.[146,147] With the selection of an appropriate surfactant, both oils are suitable for the generation of droplets that remain stable in storage for more than two weeks.[147] While they prevent leakage of the droplet contents from taking place, they are permeable to gases, such as O_2 and CO_2,[147] a characteristic which is essential to ensure that the cells in the droplets remain viable over several days. The Pico-

Surf™ 1 surfactant used for droplet stabilisation is a biocompatible surfactant available as a solution in either Novec 7500 or FC-40 fluorocarbon carrier oil. This surfactant is needed to keep the droplets and their contents intact over a wide range of temperatures and over an extended amount of time. Pico-Surf can be used to reliably stabilise droplets that range from 8 pL to 700 pL in volume.[143]

Due to the random nature of the flow of the algal cells in the aqueous inlet channel, the number of cells in the droplets followed a Poisson distribution.[148] Since, the presence of multiple cells in a droplet is undesirable for single cell studies, six different concentrations of the cell suspension were tested to determine the concentration that results in the largest possible percentage of singly occupied droplets while keeping the number of droplets that contain multiple cells to a minimum. The concentrations of the cell suspensions were determined before the encapsulation procedure by cell counting, using a bright field hemocytometer. They were determined to be 4.0×10^5 cells/mL, 1.2×10^6 cells/mL, 1.6×10^6 cells/mL, 2.3×10^6 cells/mL, 2.5×10^6 cells/mL and 7.4×10^6 cells/mL. The droplets generated by each cell suspension were imaged using a brightfield microscope and the number of cells in 190 droplets were counted manually, as such a droplet sample was deemed to be sufficiently large to obtain accurate cell distribution data. The number of cells in the droplets for each of the different cell concentrations tested was found to follow Poisson statistics (**figure 2.10**). As a result, at lower initial cell concentrations (4.0×10^5 cells/mL, 1.2×10^6 cells/mL) as high as 97% of the droplets collected were empty. On the other hand, at higher cell concentrations (7.4×10^6 cells/mL) the percentage of empty droplets decreased but a significant fraction of the occupied droplets contained multiple cells. Based on the distribution data recorded, it was deemed that an initial cell concentration between 1.6×10^6 cells/mL and 2.3×10^6 cells/mL would be optimal for single cell encapsulation, because it results in the greatest percentage of occupied droplets containing just one cell.
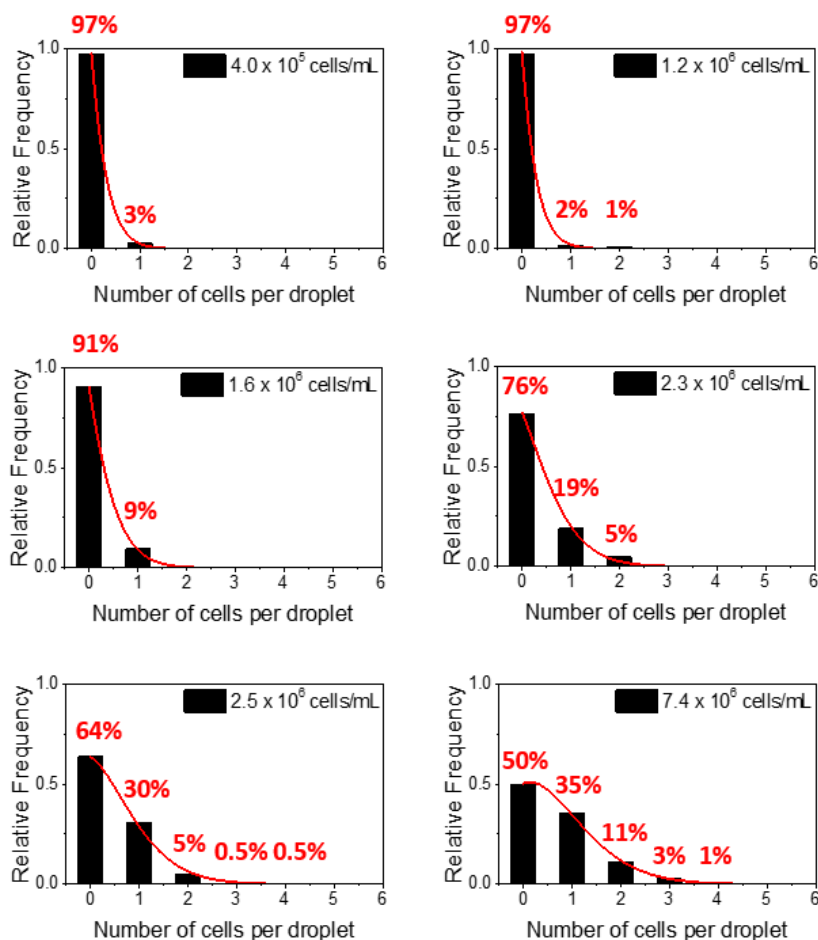
Figure 2.10: Distribution of cells in microdroplets for six different concentrations of *Pt* cells in F/2 medium. The cells were encapsulated into droplets using a 40 µm x 40 µm x 25 µm (length x width x height) flow-focusing device and Novec 7500 with 1% v/v Pico-Surf™ 1 surfactant was used as the continuous phase. The experiment was performed once. The cells in a total of 190 generated droplets were counted for each concentration. Curves have been fitted to show Poisson statistics.

After their generation, the droplets can be stored at room temperature and under continuous illumination for up to two weeks off-chip. The encapsulated cells remain alive in the droplets and continue to grow and multiply. To confirm the viability of the encapsulated cells, the droplets were imaged over 11 days (**Figure 2.11**) to observe the cell growth. The number of cells in each droplet increased at first. On day 0, right after the generation of the droplets, most occupied droplets contained one cell which divided to give two cells on day 1. After this point, the cells continued to multiply, however the growth was non-uniform, resulting in droplets that contained two, three or four cells. After day 4 the cells stopped multiplying due

to the limitation in the volume and the nutrients available within the droplets, which inhibited the cell growth.[74] At that point, the cells entered the stationary phase of their growth cycle with cell death gradually occurring over the following days. A maximum number of four cells per droplet was reached. The final cell concentration in the 34 pL droplets which contained four cells was 1.2×10^8 cells/mL. This concentration is an order of magnitude higher than the *Pt* cell concentration reached in bulk cultures. An explanation which was proposed for this increased cell concentration, is that in bulk cultures some cells which are deeper in the culture receive less light due to shading by the cells near the top, thus inhibiting their growth. In contrast, for the cells that are cultivated in droplets shading is not an issue and cell growth is not inhibited by light limitation.[74]
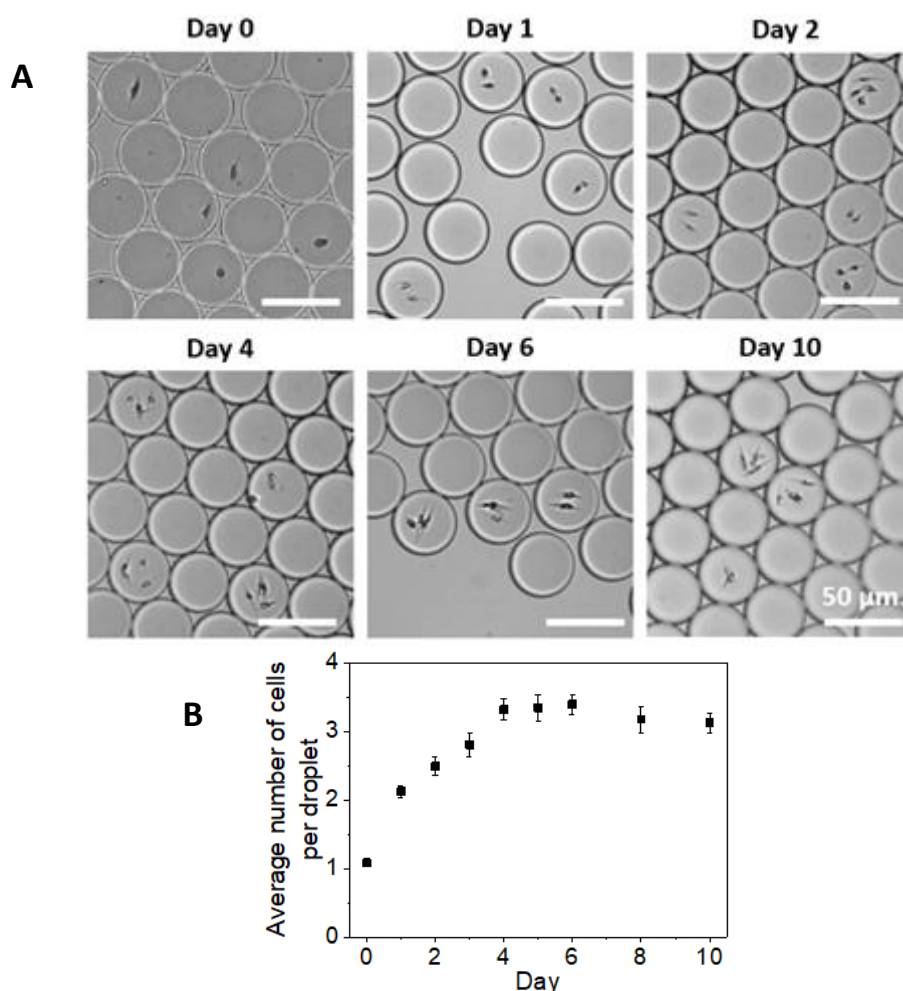
Figure 2.11: A) Microscope images showing the growth of *Pt* cells in 41 μm diameter (36 pL volume) microdroplets over 11 days, B) the average number of cells in the occupied droplets over time. The microdroplets were stored in a plastic syringe and samples were removed every day for imaging. The cells in a total of 50 droplets were counted for each data point. The experiment was performed once.

The growth of the encapsulated *Pt* cells in the microdroplets depends on the size of the droplets. Dr Ziyi Yu performed further experiments on the cultivation of *Pt* cells in microdroplets of different sizes. His results are presented here with permission. While *Pt* cells encapsulated in ~37 µm diameter microdroplets grew until a maximum number of 4 cells was reached, in ~108 µm diameter microdroplets the maximum number of *Pt* cells reached was 16 cells after 7 days of culture (**figure 2.12**). This is further evidence that the viability of the *Pt* cells is not affected by their encapsulation into droplets and that the encapsulated cells will grow as long as they have enough nutrients in the droplets.[74]
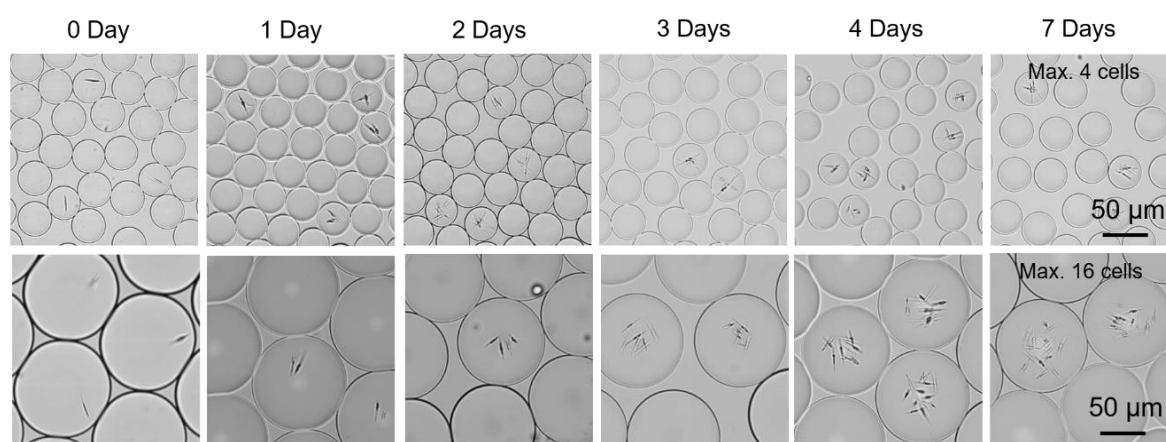
Figure 2.12: Images showing the growth of *Pt* cells over seven days in microdroplets of diameter A) 37 µm (27 pL) and B) 108 µm (660 pL). Data collected by Dr Ziyi Yu and reproduced here with permission.

2.3.3. Overcoming cell sedimentation

A problem that arises when using cells in microfluidics and which particularly affects the encapsulation process, is the sedimentation of the cells. Due to the difference in density between the *Pt* cells and the growth medium, the cells precipitate over time, leading to a change in the distribution of the cells in the droplets and increasing the possibility of blockage of the microfluidic channels.[73,149] This effect therefore restricts the amount of time for which an encapsulation procedure can run, as after only one hour the encapsulation efficiency becomes much lower, and the number of empty droplets collected is much larger. To overcome this problem, density matching solutions, such as OptiPrep™ (iodixanol) can be added to the growth medium to increase its density,[73,149] permitting the cells to stay in solution for longer and reducing the sedimentation taking place.

OptiPrep™ (**figure 2.13A**) is a sterile endotoxin-tested solution of 60% w/v iodixanol in water with a density of 1.32 g/ml. Iodixanol is non-toxic to cells and metabolically inert.[149] OptiPrep has been used in the past for the isolation of different types of mammalian cells,[73,149] but it has not been used along with algal cells. Herein, various concentrations of OptiPrep were added to bulk *Pt* cell cultures in F/2 growth medium to determine the concentration that would provide the best density match and prevent cell precipitation from taking place (**figure 2.13B**). The resulting cell suspensions were allowed to stand for 2.5 hours and they were monitored visually. In cell suspensions containing 0%, 2%, 4% and 6% v/v OptiPrep precipitation was still observed to take place over time. When 10% v/v was used there was no visible precipitation of the cells over time, while when 20% v/v was used the cells floated towards the top because they had a lower density than the surrounding medium. For this reason, the addition of 10% v/v OptiPrep was determined to be sufficient to reduce cell precipitation and it was used in all subsequent experiments.

The growth of *Pt* cells in the bulk density-matched medium was monitored over eleven days to ensure that the growth of the cells was not affected by the addition of OptiPrep (**figure 2.13C**). By measuring the optical density of the bulk sample at 730 nm and comparing it to the optical density of a *Pt* sample that contained no OptiPrep it was determined that the cells in both samples started to grow on day 1 after sub-cultivation and entered a stationary phase on day 11. The sample that contained no OptiPrep reached a higher final cell density than the sample that contained OptiPrep, however that was due to a slightly higher initial cell concentration in that sample. The growth of the cells in the microdroplets was also monitored to ensure that the addition of OptiPrep did not have any negative effects (**figure 2.13D**). Both when OptiPrep was used and when it was not, the cells in the droplets appeared to multiply during the first five days after encapsulation, subsequently entering a stationary phase and no longer multiplying.
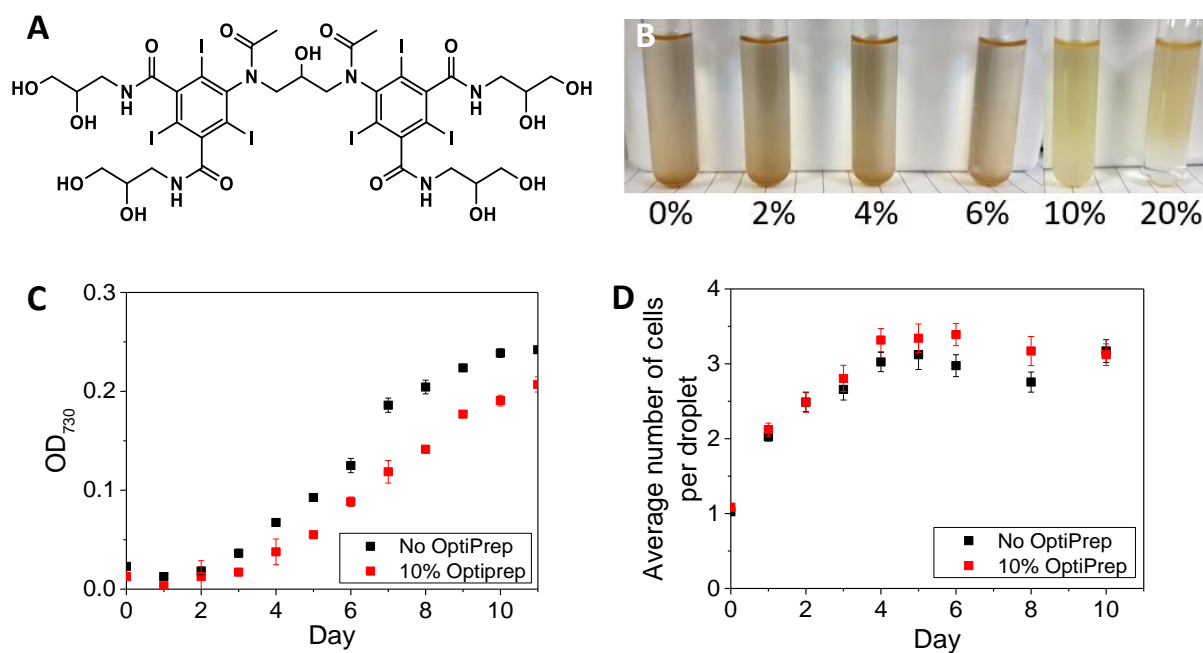
Figure 2.13: A) The chemical structure of OptiPrep (iodixanol), B) *Pt* cell suspensions containing different concentrations of OptiPrep after being left standing for 2.5 hours; from left to right: 0%, 2%, 4%, 6%, 10%, 20% v/v, C) *Pt* cell growth in bulk with and without OptiPrep (initial cell concentration: 5.0×10^5 cells/mL in culture without OptiPrep, 4.4×10^5 cells/mL in culture with 10% v/v OptiPrep), D) growth of *Pt* cells in 52 µm diameter (74 pL) microdroplets with and without OptiPrep. The cells in a total of 50 droplets were counted every time. Each of the experiments was performed once.

Cell encapsulation experiments, for the scope of this thesis, were usually run for 30 to 60 minutes. During this time, cell precipitation took place resulting in a decrease in the cell encapsulation efficiency. To determine where the bulk of this effect comes into play, the residence times of the cells in the syringe, in the tubing and in the microfluidic device were calculated. Under the flow rates used for cell encapsulation (350 µL/hr), the residence time of *Pt* cells in the encapsulation device was 0.02 s (microfluidic channel length: 2 mm, flow rate: 97.2 mm/s) and their residence time in the tubing was approximately 4 minutes (tubing inner diameter: 0.38 mm, length ≈ 20 cm, flow rate: 0.857 mm/s). The bulk of cell precipitation therefore would take place while the cells were in the syringe, as that is where they spend the longest time during the encapsulation procedure. Since the syringe containing the cell sample is placed horizontally on the syringe pump, the cells precipitate at the bottom of the

syringe and they are not injected into the tubing. As a result, over time, the fraction of empty droplets that were collected increased.

The effect that the addition of OptiPrep had over the encapsulation procedure was examined by comparing the droplets obtained by encapsulating a cell sample without any OptiPrep and another sample of the same concentration with 10% v/v OptiPrep. Over time, the distribution of cells in the droplets changed due to cell sedimentation. When no OptiPrep was used, the effect was particularly pronounced (**figure 2.14A**). While at the beginning of the encapsulation procedure approximately 70% of the droplets collected were empty after two hours that percentage increased to 98%. However, the addition of OptiPrep slowed down this effect significantly (**figure 2.14B**). When 10% v/v OptiPrep was added to the cell sample, the percentage of empty droplets increased only slightly, from 58% to 64%, after two hours.
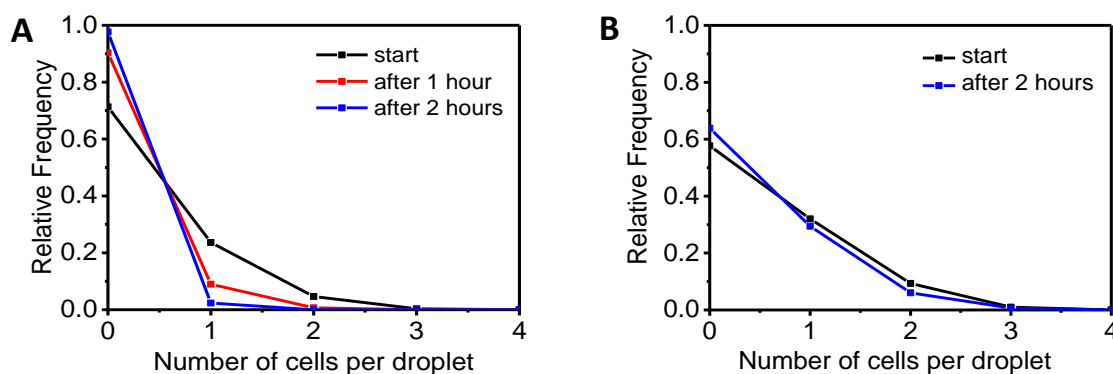
Figure 2.14: Change in the distribution of cells within the droplets over time: A) cell suspension without OptiPrep, B) cell suspension with 10% v/v OptiPrep. Both cell suspensions had a concentration of 8 x 10^6 cells/mL. The cells were encapsulated in 45 μm diameter (48 pL) droplets. Each distribution was generated by counting the cell content of 300 droplets. The experiment was performed once.

2.4.   Conclusions

Droplet microfluidic technology has the potential to provide new insights in the study of single algal cells. In this chapter, a droplet microfluidic platform was successfully established for the encapsulation and study of single *Pt* algal cells. An optimum cell concentration range for single cell encapsulation was determined, which was between 1.6 x 10^6 cells/mL and 2.3 x 10^6 cells/mL. The growth of *Pt* cells in microdroplets over 11 days was also studied and found to

be heterogeneous. This was due to the limitation in the volume of the microdroplets and the amount of nutrients contained within. The growth of the encapsulated cells was compared to *Pt* growth in bulk to ensure that the cells were not negatively affected by their encapsulation in droplets. The final concentrations of cells that were achieved in the droplets were up to a magnitude higher than cell concentrations in bulk culture. Furthermore, a density matching solution was used to overcome the issue of cell sedimentation during the encapsulation procedure. By the addition of 10% v/v Optiprep to the cell suspension, the sedimentation and the clumping of the cells were significantly reduced, minimising their impact on the cell encapsulation efficiency over time. This was evident by the percentage of undesirable empty droplets collected during the encapsulation process, which only increased by 6% over two hours in the presence of OptiPrep, instead of the 28% increase observed when OptiPrep was not used. As droplet encapsulation experiments, for the scope of this thesis, were run for a maximum of 60 minutes, this was determined to be fit for purpose. The addition of OptiPrep improves the cell encapsulation efficiency and enables cell encapsulation over longer periods of time, without any negative effects on the cells and their growth. At the same time, it reduces the unnecessary loss of cells during the encapsulation procedure.

CHAPTER 3

Fluorescence detection and microdroplet sorting

3.1.   Introduction

While the past few years have witnessed the rapid development of the droplet-based microfluidics, a challenge remains in the ability to analyse the content of the microdroplets and to screen rare samples from a large library. In this respect, several analytical detection techniques have been applied to droplet-based microfluidics, including mass spectrometry, SERS, UV-Visible spectrophotometry, Raman and microcoil NMR spectroscopy.[63] Among these methods, fluorescence-based methods have been widely applied due to their high sensitivity.[150] In particular, laser-induced fluorescence (LIF) detection has been frequently used in fluorescence screening studies, when large numbers of particles, cells or droplets need to be assessed.[63,64]

LIF detection relies on illumination by a laser source to excite molecules of interest. Light is spontaneously emitted once these molecules return to their ground state and this light can reveal information about the molecules being probed.[151] LIF detection systems combine high sensitivity with high throughput[63] and have been used in a variety of droplet microfluidic applications, including detecting single molecules in droplets,[152,153] or, when combined with fluorescence resonance energy transfer (FRET), to probe biomolecular interactions.[154]

Fluorescence-Activated Droplet Sorting (FADS) has been developed to screen cells in microdroplets based on their different fluorescence characteristics. This method combines LIF detection with droplet manipulation on-chip, a versatile technique that can separate droplets without damaging the droplets themselves or their contents.

FADS was developed in 2009 by Baret *et al.*[70] based on an earlier droplet sorter design by Ahn *et al.*[109] Baret *et al.* used the FADS platform to sort *E. coli* cells based on whether they expressed the reporter enzyme β-galactosidase or not. The cells were encapsulated into droplets that contained a fluorogenic β-galactosidase substrate. After a 14-hour incubation, the droplets containing cells expressing β-galactosidase had a higher fluorescence from the rest of the droplets and were successfully sorted. FADS has subsequently been used in a

variety of applications due to its versatility, such as in antibody screening,[78] (**figure 3.1A**) in drug screening[78] (**figure 3.1B**) and to detect the secretion of small molecules from cells.[80]
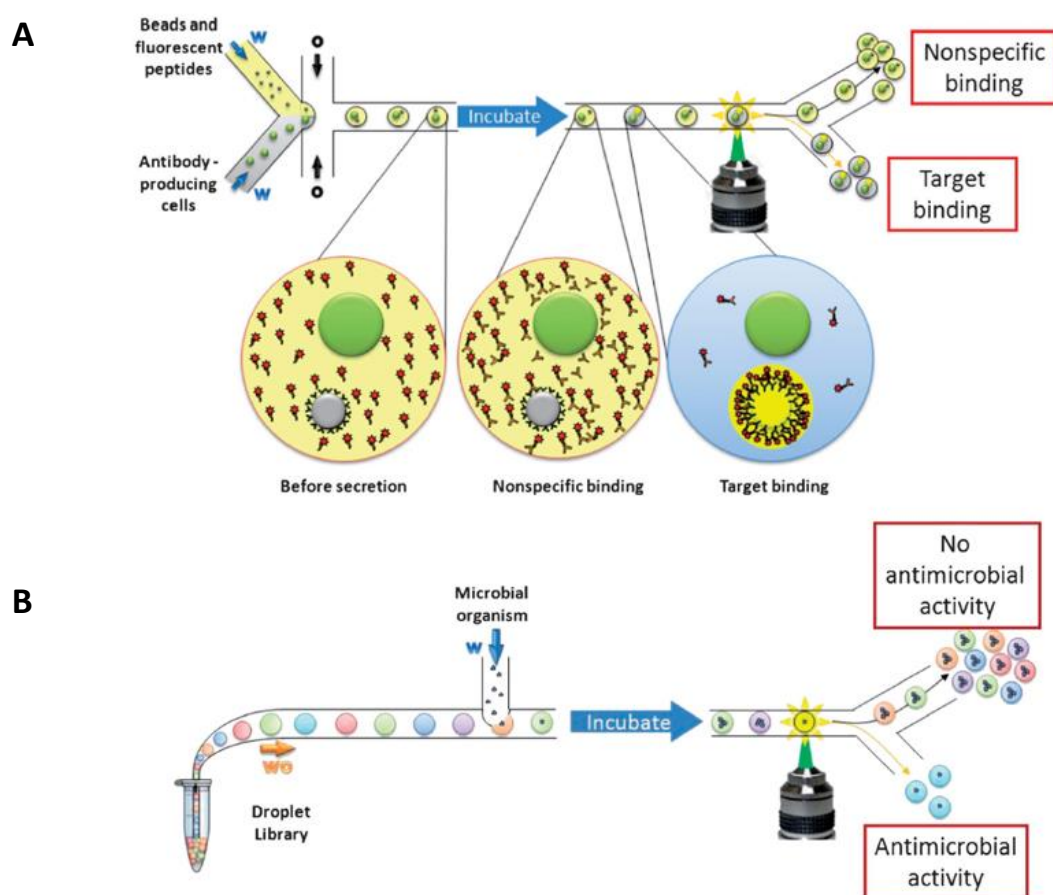
Figure 3.1: A) Droplet based screening of cells to identify cells secreting antibodies of interest, B) screening of a library of small compounds for antimicrobial activity, adapted from ref.78.

By taking advantage of the high throughput fluorescence detection and analysis provided by FADS, the effect of the different environmental conditions on the behaviour and the characteristics of the cells, such as the growth rate and the lipid content, can be examined. It can, therefore, be used to identify and sort algal cells that display specific properties, which might be of interest for applications in biotechnology.

The intrinsic chlorophyll fluorescence of microalgae is of particular interest. Chlorophyll fluorescence is an indicator of the photosynthetic performance of microalgae because it is connected to and can reveal information about the transfer of excitation energy through the photosynthetic apparatus.[82,155] At the beginning of the photosynthetic process, chlorophyll molecules become excited by absorbing light energy. A part of this excitation energy is used

to drive photosynthesis. The rest is either dissipated as heat or emitted as fluorescence. As these processes are connected to each other, studying the fluorescence emitted by the chlorophyll molecules provides information on the efficiency of the photochemistry taking place during photosynthesis.[155]

The chlorophyll content of algae changes over time and is dependent on factors such as the cell growth phase and the environmental conditions.[156] For *P. tricornutum* grown in bulk culture, one of the factors affecting the chlorophyll content of the cells is the light intensity and the light regime (continuous light *vs* a light/dark cycle). According to Laohavisit *et al.*,[157] *Pt* cells that are grown under a light-dark (LD) cycle regime have higher chlorophyll levels than cells grown under constant illumination (LL), even though both populations display similar growth rates (**figure 3.2A-B**). Furthermore, algal cells cultured under light of higher intensity have lower chlorophyll content per cell than cells cultured under low-intensity light.[161]
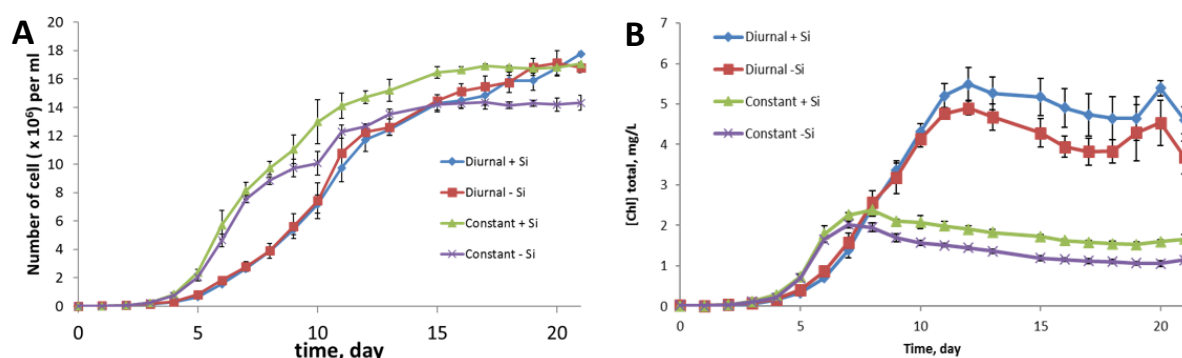
Figure 3.2: A) Growth curves showing the growth of *Pt* cells under different light regimes (16 hours light: 8 hours dark or constant illumination) in the presence (+ Si) or absence (-Si) of sodium metasilicate in the F/2 growth medium, B) chlorophyll content measurement over time for *Pt* cells cultured under the different light regimes, adapted from ref.157.

In the Abell group, Best *et al.*[82] established a FADS platform for the screening and sorting of microalgae and cyanobacteria encapsulated in microdroplets, aiming to screen and identify fast-growing microalgal strains for use in industrial applications. With this system they detected the chlorophyll fluorescence of encapsulated *Synechocystis* PCC 6803, *Synechococcus* PCC 7002 and *C. reinhardtii* cells. The optical components of the set-up they used for chlorophyll fluorescence detection are shown in **figure 3.3A**. Fixed wavelength lasers were used for fluorescence excitation: a 488 nm laser was used for *C. reinhardtii* fluorescence

detection and a 594 nm laser was used for *Synechocystis* PCC 6803 and *Synechococcus* PCC 7002 fluorescence detection. Droplets containing *C. reinhardtii* cells were successfully sorted from empty droplets based on the presence or absence of a chlorophyll fluorescence signal (**figure 3.3B**). A cell sorting frequency of 300 Hz was achieved. A subpopulation of droplets that only contained cells was successfully collected at the positive outlet, however a 4% false negative rate was observed (**figure 3.3C**). Furthermore, Best *et al.* sorted a mixture of cells that displayed high chlorophyll fluorescence from cells that displayed lower chlorophyll fluorescence as a consequence of extended nitrogen limitation. While the cells collected at the negative outlet of the sorting device showed lower chlorophyll levels than the cells in the initial mixture, too few cells were collected at the positive outlet to image. Finally, the growth of two different strains of cyanobacteria was studied in microdroplets and it was suggested that, since the two strains showed different growth rates, the chlorophyll-based sorting platform could be used to sort a mixture of the two strains.
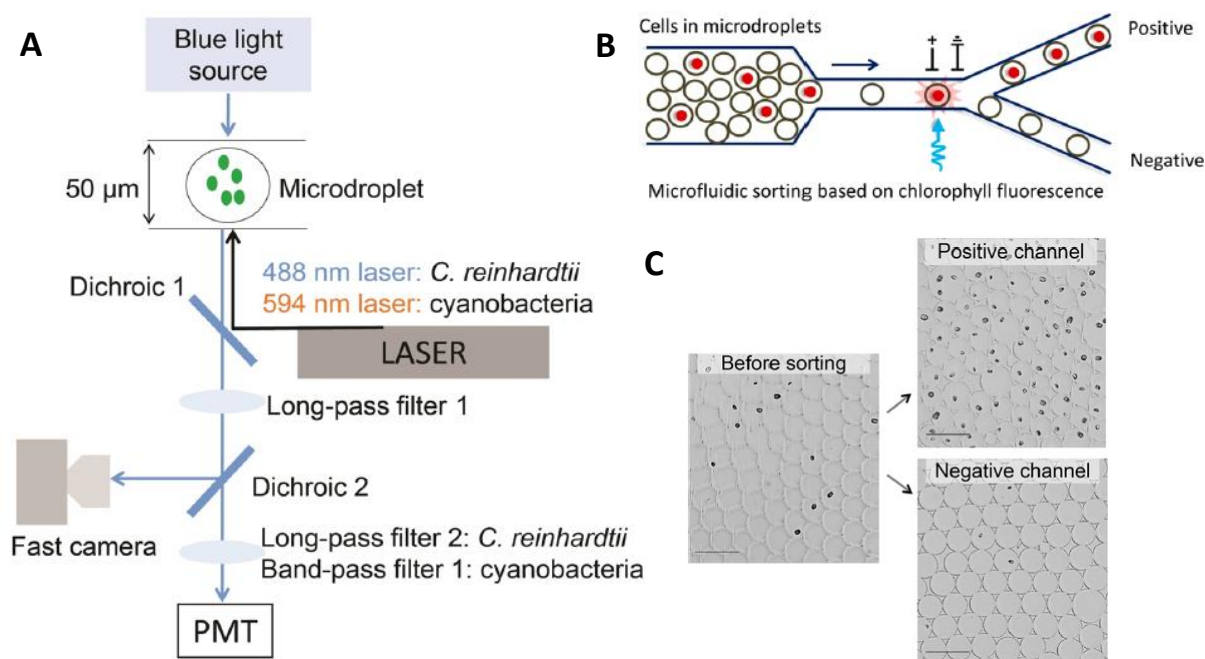
Figure 3.3: A) The setup used for the chlorophyll fluorescence detection and sorting of *C. reinhardtii* and the cyanobacteria *Synechocystis* PCC 6803 and *Synechococcus* PCC 7002 (long-pass filter 1 = 360 nm, dichroic 1 = 488 nm (for *C. reinhardtii*) and 594 nm (for the cyanobacteria), dichroic 2 = 633 nm, long-pass filter 2 = 635 nm, band-pass filter 1 = 629 ± 30 nm), B), C) images of the droplets containing encapsulated *C. reinhardtii* cells before and after sorting (scale bar = 100 μm). Adapted from ref.82.

Besides studying the chlorophyll fluorescence of microalgae, some researchers also use a variety of fluorescent dyes and markers to investigate different characteristics of algal cells, such as viability dyes to assess the viability of the cells and lipophilic dyes, such as Nile Red and BODIPY 505/515, to quantify their lipid content[54]. Fluorescent markers are also widely used as visual selection markers in genetic modification research, thereby facilitating the development of new cell strains.[158]

3.1.1. Objectives

Having successfully encapsulated single microalgal cells into microdroplets, a variety of analytical techniques, including fluorescence detection[82] and Raman spectroscopy,[159] can be applied to identify specific cells which might be of interest. In this chapter, a FADS platform was used for the detection of the intracellular fluorescence of *Pt* cells encapsulated in microdroplets. The optical set-up of the platform was modified to overcome the issue of heterogeneous irradiation of the cells and to therefore improve the accuracy of the fluorescence detection. The fluorescence detection capabilities of the improved platform were then compared to those of a previously used platform, initially by detecting the fluorescence of fluorescent beads encapsulated in droplets and then by detecting the chlorophyll fluorescence of encapsulated *Pt* and *Ng* cells. The detection capabilities of the FADS platform were further tested by detecting the chlorophyll fluorescence of *Pt* cells cultured under different light conditions, since these cells, as a result, contained different levels of chlorophyll. As a final test of the improved platform, it was used to sort droplets containing *Pt* cells from empty droplets, to overcome the issue of the random encapsulation of the cells in droplets. This was done by sorting the droplets based on chlorophyll fluorescence and the sorting results were compared to past results reported for the previous set-up.[82]

Besides chlorophyll fluorescence, the platform was also used to detect GFP fluorescence and to sort GFP-expressing *Pt* cells from a mixture with wild type *Pt* cells. Finally, a Cyto-Mine Single Cell Analysis and Monoclonality Assurance System was used to sort *Pt* cells and to dispense them one-by-one to the wells of a well plate and to obtain monoclonal *Pt* cell cultures.

3.2.   Experimental

<u>Algal cell preparation</u>

The *Phaeodactylum tricornutum* (CCAP 1055/1) cells used in all experiments, wild type and GFP-expressing, were provided by Professor Alison Smith's group at the Department of Plant Sciences, University of Cambridge. The GFP-expressing *Pt* cell samples were kindly provided by Dr Katrin Geisler, Department of Plant Sciences, University of Cambridge. The *Nannochloropsis gaditana* (*Ng*) cells were provided by Professor Saul Purton's group at the Institute of Structural & Molecular Biology, University College London. Both cell species were cultured in Guillard's F/2 medium[139] as detailed in section 2.2.

<u>Sorting device preparation</u>

A PDMS slab with the pattern of the sorting device (**Appendix device B**) was prepared by soft lithography as described in section 2.2. Instead of sealing this slab with a glass substrate, a thin PDMS substrate was used. PDMS is preferred to reduce the amount of scattering which takes place when the laser beam passes through the substrate. After sealing, the device was placed in a 120 °C oven overnight. The sealed device was partially attached to a glass slide as shown in **figure 3.4A** for easier handling. The microelectrodes in the sorting device were created by heating the device on a hotplate (set at 180 °C) and then inserting 51In/32.5Bi/16.5Sn low-temperature solder (Indium Corporation) into the inlets of the electrode channels. The solder melted and filled the channels (**figure 3.4B**). Then, while the solder was still hot, short pieces of electrical wire were inserted into the inlets of the electrode channels to form the electrical connections. Finally, the device was removed from the hotplate and allowed to cool down and the solder to solidify.
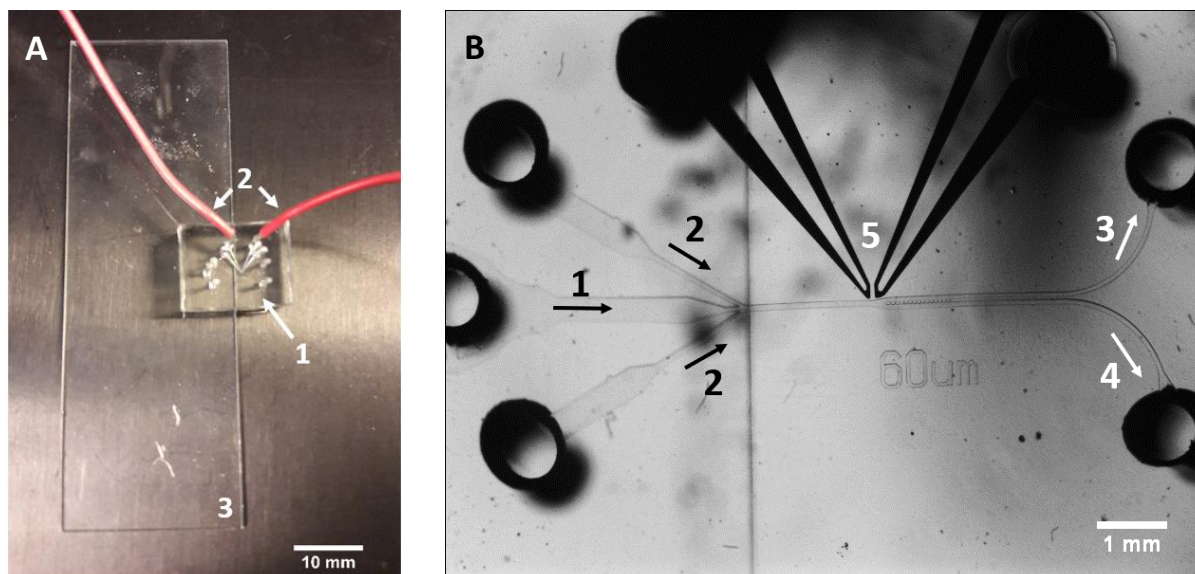
Figure 3.4: A) Photograph of a sorting device; (1) PDMS sorting device, (2) electrodes, (3) glass slide, B) microscope image of the PDMS sorting device, (microfluidic channel dimensions at the fluorescence detection point: 60 µm width x 50 µm height); (1) microdroplet inlet, (2) spacing oil inlets, (3) positive outlet, (4) negative outlet, (5) electrodes formed by melted 51In/32.5Bi/16.5Sn low-temperature solder.

Droplet sorting

    a.   Electrical set-up

A laser of wavelength 491 nm (100 mW, Cobolt) was used as the excitation source. The fluorescence emitted was recorded by a PMT (H8249, Hammamatsu Photonics)(**figure 3.5**) and the data obtained were sent to a computer through a Data Acquisition (DAQ) card (National Instruments). A custom-made program on LabVIEW (National Instruments)[79,82] was used to monitor and analyse the data.

An oscilloscope (TDS2004B, Tektronix) was used to monitor the fluorescence signal and trigger a square signal from the pulse generator (TTi TGP 110, 10 MHz, Thurlby Thandar) if the fluorescence amplitude was above a predetermined value. An amplified pulse was in that case applied to the electrodes of the sorting device by a high-voltage amplifier (PD06087, TREK). A light source was used to illuminate the sorting device during sorting, so that the process could be monitored using a Phantom V72 fast camera. For chlorophyll fluorescence detection the light source used was a blue LED light source (LEDC5, THORLABS). For GFP fluorescence

detection the microscope light was used after being fitted with a 610 nm trans-filter (THORLABS).
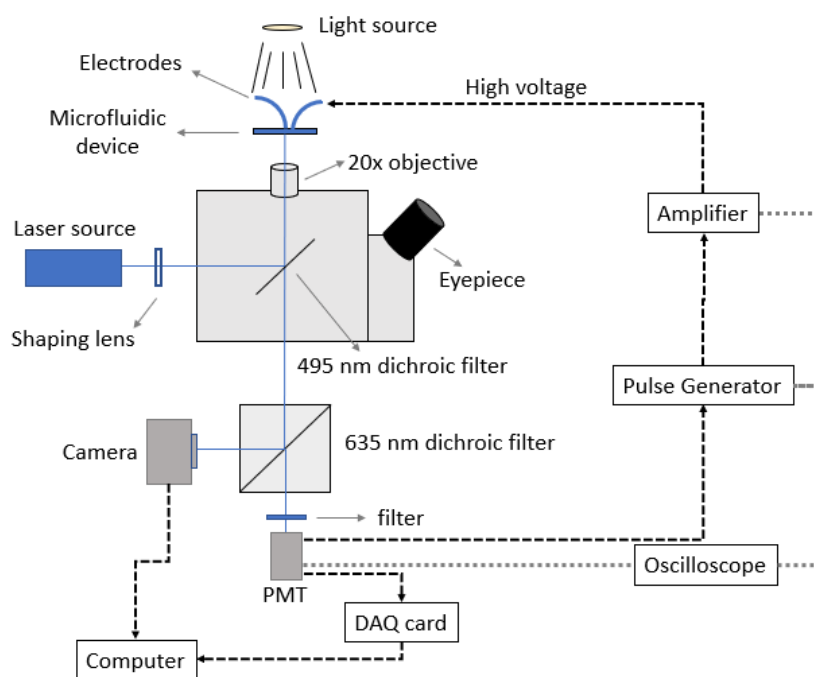
Figure 3.5: Schematic diagram of the laser sheet set-up. The laser beam, shaped into a sheet by a shaping lens (initially a cylindrical lens, later changed to a Powell lens), is directed towards the microfluidic device and the emitted fluorescence is directed towards the PMT and a high-speed camera. A 635 nm dichroic filter splits the signal between the camera and PMT. For chlorophyll fluorescence detection, light of wavelength above 635 nm is directed towards the PMT, which is also fitted with a 635 nm long-pass emission filter. The light of wavelength below 635 nm is directed towards the high-speed camera so that the sorting process can be monitored. For GFP fluorescence detection the positions of the camera and the PMT are reversed, so that the green fluorescence can be detected by the PMT using a 525 nm (bandwidth: 39 nm) emission filter and light at wavelengths above 635 nm can be directed towards the camera.

   b. Sorting procedure

Algal cells were encapsulated into droplets using the same method as in section 2.2. The 1 mL syringe containing the generated microdroplets was loaded on a syringe pump while kept vertical to ensure that the microdroplets remained on top of the oil that was collected along

with the droplets during the encapsulation procedure. The syringe was connected through polyethylene tubing to the corresponding inlet of the sorting device. Two syringes were filled with spacing oil (Novec 7500 with 1% PicoSurf™ 1) and loaded on a syringe pump. They were then connected, through tubing, to the other two inlets of the sorting device. The flow rates applied by the two syringe pumps were adjusted to 10 µL/hr (approximately 0.93 mm/s at the detection region) for the droplets and 160 µL/hr (1.48 cm/s) for the spacing oil, or to 20 µL/hr (approximately 1.85 mm/s) for the droplets and 360 µL/hr (3.33 cm/s) for the spacing oil. Higher flow rates were avoided as they could lead to droplet fusion or errors during sorting. Careful control of the flow rates was required to ensure that the droplets were well separated from each other as they passed through the sorting junction. It was also necessary to ensure that the reinjected droplets all passed through the negative outlet channel when the electrodes were off. The laser beam was aligned so that it would hit the sorting device at a point in the microfluidic channel in-between the two electrodes. Once the PMT started recording fluorescence peaks the gain was adjusted to ensure that only the peaks of the right height would trigger the pulse generator. The voltage applied to the electrodes was increased until droplets could be seen going into the positive channel (approximately 500 – 600 V). The outlet tubing was not moved during the sorting process as any changes in position could result in backpressure changes in the device which affect the sorting procedure, generating false negative or false positive results.

Detection of fluorescence emitted by fluorescent beads after illumination by laser spot and laser sheet

Alignflow™ fluorescent beads (ThermoFisher) were diluted by adding 1 drop of the commercial mixture in 1 mL of distilled water. The resulting solution was encapsulated using Novec 7500 with 1% PicoSurf 1 as the continuous phase. The droplets were then injected into a sorting device and the fluorescence emitted by the microbeads was detected. To detect only the desired fluorescence without interference from background light, a trans-filter (610 nm, THORLABS) was fitted on the light source used to illuminate the sorting device and a 525 nm filter (bandwidth: 39 nm) was fitted before the PMT. The measurement of the emitted fluorescence was repeated using the older laser setup, which was very similar to the new one, but did not have a shaping lens to change the shape of the laser beam.

Detection of *Pt* and *Ng* chlorophyll fluorescence after illumination by laser spot and laser sheet

A 1.5 x 10^6 cells/mL sample of *Pt* cells in F/2 medium was encapsulated into microdroplets. The collected droplets were then divided into two samples. The fluorescence of the first sample was detected after illumination by the laser spot set-up and the fluorescence of the second sample was detected after illumination by the laser sheet. The flow rate of the droplets in both cases was 15 µL/hr (approximately 1.39 mm/s at the fluorescence detection point) and that of the spacing oil was 300 µL/hr (2.78 cm/s). The chlorophyll fluorescence signals emitted were recorded over 6 minutes. The same experiment was performed using a sample of *Ng* cells. In both cases the generated droplets had 7% cell occupancy.

Culture of Pt cells under different light regimes and chlorophyll fluorescence detection

Wild type *Pt* cells and GFP-expressing *Pt* cells at an initial concentration of 1 x 10^5 cells/mL were cultivated in two different 24-well plates. Half of the wells in each plate were used to culture wild type cells and the other half was used to culture GFP-expressing *Pt* cells. The cells in the first plate were cultivated under a low light intensity (30 µmol m^{-2} s^{-1}), light / dark regime (LD, 16 hours light / 8 hours dark), while the cells in the second plate were grown under a continuous illumination regime (LL) of light intensity 75 µmol m^{-2} s^{-1}. The growth of the algae was tracked over 13 days by measuring the OD_{730} using a plate reader (Fluostar Optima, BMG Labtech, USA) and the chlorophyll in the cells was extracted and measured every two days.

To extract the chlorophyll from the cells, 1 mL of each of the cell samples was centrifuged at 15000 g for 10 minutes. The supernatant was discarded and 1 mL of DMF (dimethylformamide; Fisher Scientific, UK) was added to the cell pellet. The samples were agitated at room temperature for 15 minutes using a shaker and then centrifuged for 2 minutes at 10000 g. The absorbance of the supernatant at 630 nm (A630) and 664 nm (A664) was finally recorded using a spectrophotometer (Helios Alpha, Thermo Scientific, UK). The total chlorophyll content of each cell sample was calculated as[160]:
Total chlorophyll content (µg/mL) $= 7.74 \times A664 + 23.39 \times A630$.

On day 8 after the beginning of the experiment, a sample of wild type *Pt* cells grown under a light/dark cycle (LD) and a sample of GFP-expressing *Pt* cells grown under continuous light (LL) were encapsulated into microdroplets and, using the laser sheet set-up, the chlorophyll fluorescence emitted by the cells of each population was recorded and compared.

GFP fluorescence detection and sorting

A 1:1 mixture of GFP-expressing and wild type *Pt* cells was used for the GFP fluorescence sorting experiment. The sample was diluted with F/2 growth medium for single cell encapsulation. The cells were encapsulated in microdroplets and were subsequently re-injected in a sorting device for GFP fluorescence detection and sorting. For GFP fluorescence detection, a trans-filter (610 nm, THORLABS) was fitted on the light source used to illuminate the sorting device and a 525 nm filter (bandwidth: 39 nm) was fitted before the PMT.

Droplet demulsification

The droplets containing GFP-expressing *Pt* cells, that were collected at the positive outlet of the sorting device after the end of the sorting procedure, were demulsified by the addition of 1H,1H,2H,2H-perfluorooctanol (Alfa Aesar) at a 2:1 volume ratio to the volume of the collected droplets. The cells previously contained within the droplets were collected and imaged under a fluorescence microscope.

Fluorescence image analysis

The fluorescence microscope images of the collected cells were analysed using ImageJ image processing software to measure the fluorescence emitted by the cells. The cells were selected manually.

Droplet sorting and dispensing with Cyto-Mine

A sample of GFP-expressing *Pt* cells and a sample of wild type *Pt* cells were mixed at a 1:1 ratio along with 10% v/v Optiprep and 0.1% Pluronic-F68, so that a sample of concentration 3×10^5 cells/mL was obtained. The sample was loaded into Cyto-Mine and the cells were encapsulated by the instrument into 450 pL droplets. The GFP fluorescence and the chlorophyll fluorescence of the encapsulated cells were detected. For GFP fluorescence detection, a 520 nm (bandwidth: 15 nm) emission filter was used, while a 620 nm (bandwidth:

14 nm) filter was used for chlorophyll fluorescence detection. Cells with higher GFP fluorescence were sorted and collected at the positive channel of the droplet sorter. The GFP fluorescence of the collected droplets was then detected once again so that any false positives could be eliminated. The droplets were then dispensed one by one into the cells of two 96- and two 384-well plates. During the dispensing process, the droplets were imaged to determine whether they contained single or multiple cells.

Prior to the dispensing process, each of the wells of the 384-well plates was loaded with 6 µL of F/2 media. Each of the wells of the 96-well plates was loaded with 15 µL of F/2 media. Once the dispensing process was finished, 44 µL of F/2 was added to each of the wells of the first 384-well plate to prevent the cells from dying out. Different volumes of F/2 were added to the wells of the second 384-well plate. This was done as follows: 12 µL were added to the wells of the first four rows, 24 µL to the next four rows, 48 µL to the four rows after that and 72 µL to the final four rows. The wells of the two 96-well plates were all topped up by the addition of 150 µL F/2. The well plates were placed in an incubator and they were cultured at 18 °C under a 16 hr light / 8 hr dark regime for 27 days. The growth of the cells on the well plates was monitored by measuring the OD_{730} with a plate reader (Fluostar Optima, BMG Labtech, USA).

3.3.   Results and discussion

3.3.1. Fluorescence-Activated Droplet Sorting platform

A schematic diagram of the PDMS device that was used for fluorescence-based detection and sorting (**Appendix device B**) is shown in **figure 3.6A**. The sorting device was designed to be separate from the device used for droplet generation, instead of combining droplet generation and droplet sorting modules on the same microfluidic chip. This was done to allow more precise control over the droplet flow during sorting, as well as to limit complications caused by pressure fluctuations in the device which could lead to polydisperse droplet generation and sorting errors.

The sorting device has three inlet channels and two outlet channels. The microdroplets are injected through the inlet channel in the middle and Novec 7500 oil with 1% Picosurf 1 surfactant is provided through the other two inlets to space the microdroplets. The

microdroplets flow through the microfluidic channel until they intercept and are irradiated by a laser beam (**figure 3.6B**) that is positioned between the two sorting electrodes. At that point, the resulting fluorescence emitted by each irradiated droplet is recorded by a PMT. The PMT is connected to an oscilloscope, a Data Acquisition (DAQ) card and a Transistor–transistor logic (TTL) pulse generator. While the oscilloscope is used for the real-time monitoring of the fluorescence detection data, the DAQ card sends the data to a computer for recording and analysis through a custom-made LabVIEW script. The TTL pulse generator receives the PMT voltage and determines whether a triggered signal should be generated based on the voltage magnitude. If the PMT voltage exceeds a defined threshold, the pulse generator will send a signal to the high-voltage supply and the electrodes of the microfluidic device will be activated, applying a dielectrophoretic force on the microdroplet flowing through the microfluidic channel.

In detail, at the sorting junction of the microfluidic device, the microfluidic channel splits into two outlet channels, the positive and the negative. The positive outlet (top channel) is slightly narrower than the negative outlet (bottom channel). As a result, the microdroplets will all flow towards the negative outlet, due to lower fluidic pressure (**figure 3.6C(i)**). However, when the fluorescence intensity of a droplet is above a preselected threshold, the electrodes are activated, and an electric field is applied in the channel. As a result, a dielectrophoretic force is exerted on the microdroplet that drives it towards the positive outlet (**figure 3.6C(ii)**).

The sorting threshold is pre-set by the experimental hardware at 1.25 V and cannot be changed. Instead, the gain of the PMT is adjusted every time and the magnitude of the fluorescence peaks is modified, so that the desired proportion of peaks are above the threshold value (**figure 3.6D**).
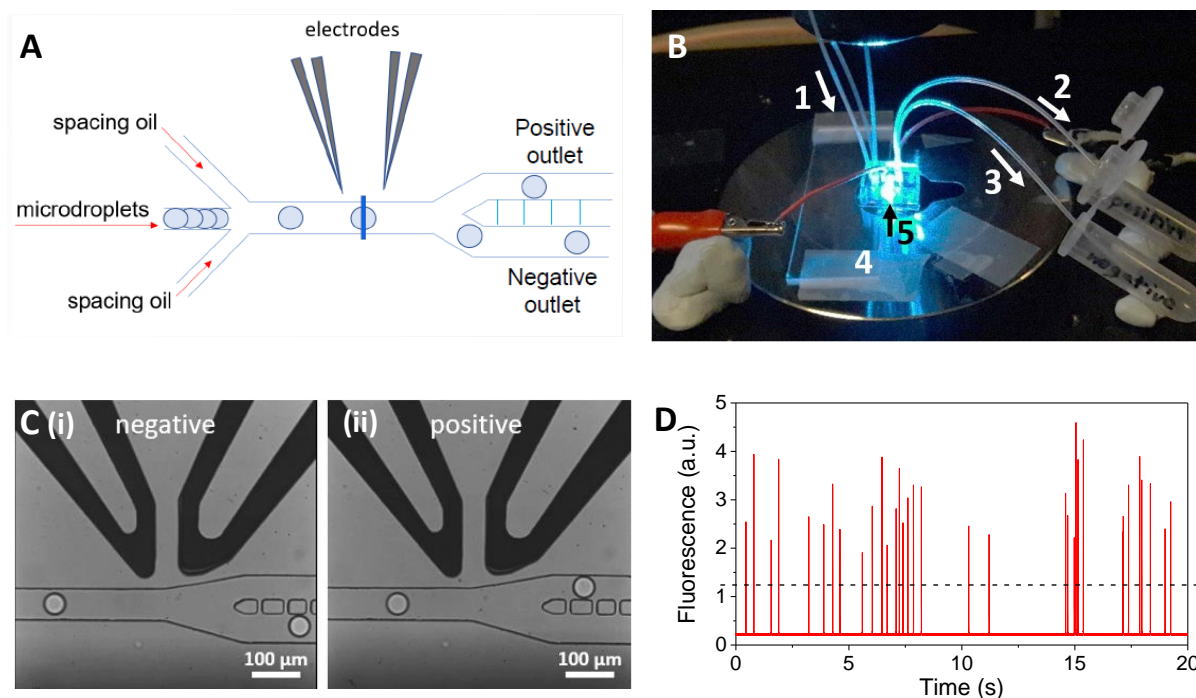
Figure 3.6: A) Schematic diagram showing the structure of the microfluidic device used for fluorescence-activated droplet sorting, B) photograph of the sorting device during a sorting experiment; (1) inlet tubing for microdroplet re-injection and spacing oil supply, (2) positive outlet tubing, (3) negative outlet tubing, (4) sorting microfluidic device on microscope stage, (5) laser beam, C) the droplet sorting process: (i) droplet flowing towards the negative outlet, (ii) droplet redirected towards the positive outlet, D) a typical fluorescence intensity trace recorded during a sorting experiment. The dashed line indicates the sorting threshold.

3.3.2. Laser set-up optimisation for quantitative fluorescence detection

Previous FADS work within the Abell research group was performed using a laser spot with a laser intensity which followed a Gaussian profile and a diameter of approximately 5 µm at half maximum height of the Gaussian profile (**figure 3.7A**). Because the size of the laser spot was smaller than the size of the droplets, only a small part of the microdroplets was irradiated by the laser when they flowed through the channel. For droplets that were 45 µm in diameter (48 pL in volume), approximately one sixth of the droplet volume (8 pL) was actually irradiated by the laser beam. This significantly impacted the fluorescence detection results obtained, because whether the encapsulated cells would be detected depended on the position of the cells relative to the laser beam. Furthermore, the detected fluorescence would frequently be artificially low due to the cells being only partially irradiated by the laser spot.[160]

This system could be improved if the intensity of the laser light used to illuminate the droplets was homogeneous across the microfluidic channel, so that the encapsulated cells are irradiated by the laser regardless of their position in the droplet and so that quantitative fluorescence readings are obtained. To improve the accuracy of the platform, a cylindrical lens was used to turn the circular spot of the laser beam into a sheet that can scan the entire width of the microfluidic channel (**figure 3.7B**). This had a significant impact on the fluorescence intensity values recorded by the PMT, since it eliminates any error that might arise from the relative placement of the laser spot and the cells in the microfluidic channel.

The improved accuracy of the detection set-up was illustrated by using Alignflow™ fluorescent beads which were encapsulated in microdroplets (**figure 3.7C**). These beads are stained internally and are highly uniform with respect to both size (diameter = 2.5 μm) and fluorescence intensity. The generated droplets (diameter = 45 μm) were reinjected in the microfluidic sorting device and their fluorescence was recorded by irradiating them with the laser spot and the laser sheet.
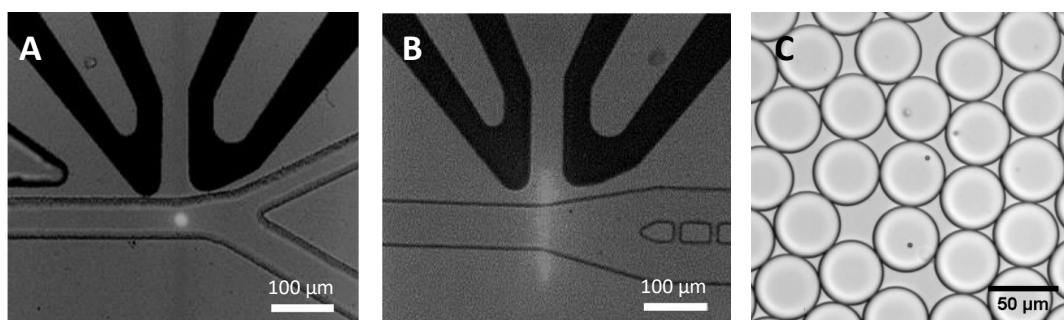
Figure 3.7: Laser beam shape and position in the channel of a microfluidic sorting device: A) laser spot (image provided by Dr Ziyi Yu) and B) laser sheet; C) Alignflow fluorescent beads encapsulated in 45 μm microdroplets.

The detection results obtained from the two different laser set-ups were compared. The fluorescence peaks recorded using the laser spot set-up (**figure 3.8A**) displayed an 87% variation in intensity, while, when the laser sheet was used (**figure 3.8B**), this variation was reduced to 29%. There was, therefore, a three-fold reduction in the CV value of the fluorescence data recorded, with the fluorescence signals recorded through laser sheet irradiation being much more uniform in intensity. This difference in the results is expected

since, when a laser sheet is used, the placement of the beads in the droplet or the placement of the droplet in the channel do not affect the fluorescence read-out.
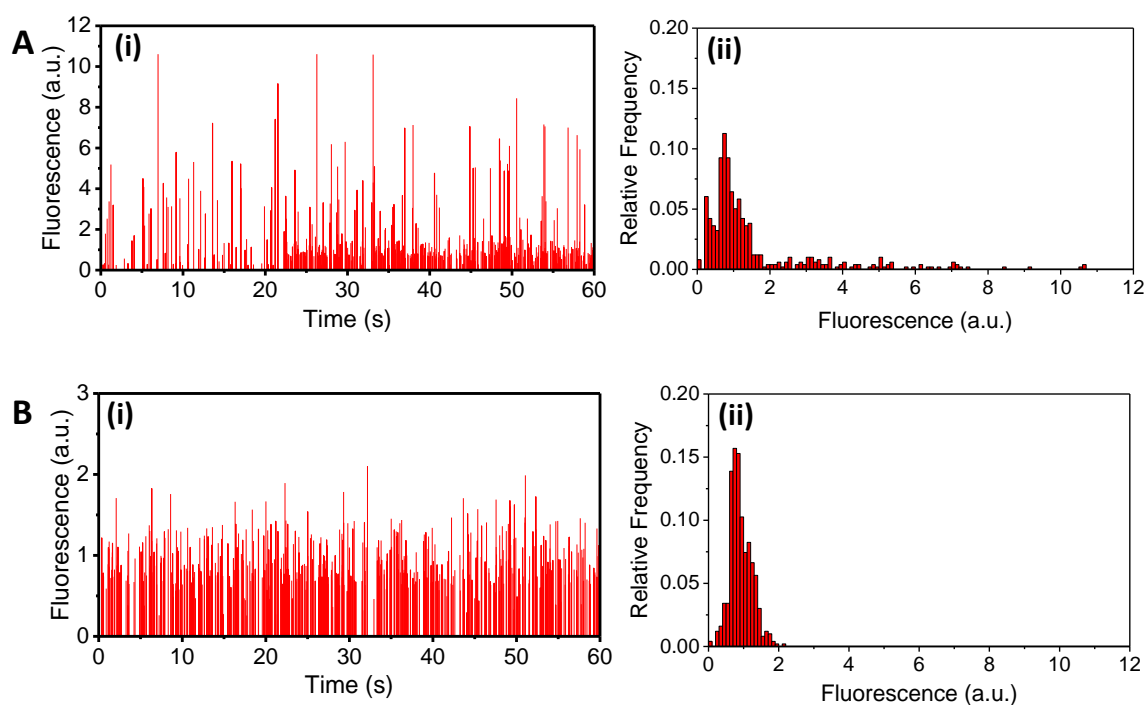
Figure 3.8: A) Microdroplets containing Alignflow™ fluorescent beads used to assess the performance of the laser set-up; fluorescence intensity trace (i) corresponding to fluorescent beads encapsulated in microdroplets and the corresponding fluorescence intensity distribution (ii) when the droplets are irradiated by A) a laser spot and B) a laser sheet. Data collected in collaboration with Dr Ziyi Yu. The experiment was performed twice.

While, using a shaping lens changed the shape of the laser beam into a laser sheet, the intensity of the laser along this sheet was different. The middle section of the laser sheet was more intense than the edges, because of the Gaussian profile of the laser itself.[161] To address this issue, the optics of the laser set up were altered with the help of Dr Aleks Ponjanik from the Klenerman group, Department of Chemistry, University of Cambridge. By substituting the cylindrical lens, previously used to shape the beam, with a Powell lens, the Gaussian distribution of the laser beam was turned into a flattop beam.[161] A Powell lens is capable of converting a gaussian laser beam into a uniform laser sheet that displays less than 30% variation in intensity at the central 80% of its length (**figure 3.9A**).[162] The width of the resulting laser sheet was 5 μm and its length was approximately 150 μm.

This change further improved the performance of the laser sheet system. The optimised laser sheet system could detect and measure the fluorescence emitted by the beads more quantitively than the previous set-up. When tested, there was an 8% variation in the intensity of the fluorescence signals recorded for the single encapsulated beads (**figure 3.9B-C**) as compared to an approximately 29% variation recorded prior to this change (**figure 3.8B**). Subsequent repeat measurements showed that this result was reproducible and an 8 – 10% variation in fluorescence values was recorded in each measurement.

While laser sheet illumination has been used before in FADS to screen droplets, a cylindrical lens was used instead of a Powell lens to shape the beam.[73,163] As seen in **figure 3.9A**, the sheet generated with this lens is less homogeneous in intensity than the sheet that was generated by using a Powell lens and, as a result, it yields less accurate fluorescence data.

While Powell lenses are used in light-sheet microscopy and LIF systems to shape the laser beam and increase fluorescence detection accuracy,[164] there are no references found in literature of them having been used in conjunction with droplet microfluidics to improve fluorescence detection in droplets. With this innovation, which is a methodological improvement over existing literature approaches, more quantitative fluorescence measurements can now be obtained. The improved platform can be used to detect the intracellular fluorescence of algae, in cases where cells with higher fluorescence must be identified, even if the variation in the intensity of the fluorescence emitted is relatively small. For example, as will be seen in Chapter 4, the platform could be used in the identification of cells with higher lipid content, which are stained by a lipophilic fluorescence dye. In this case, the differences in lipid content between cells could be small, so increased detection sensitivity is required to identify cells of interest.
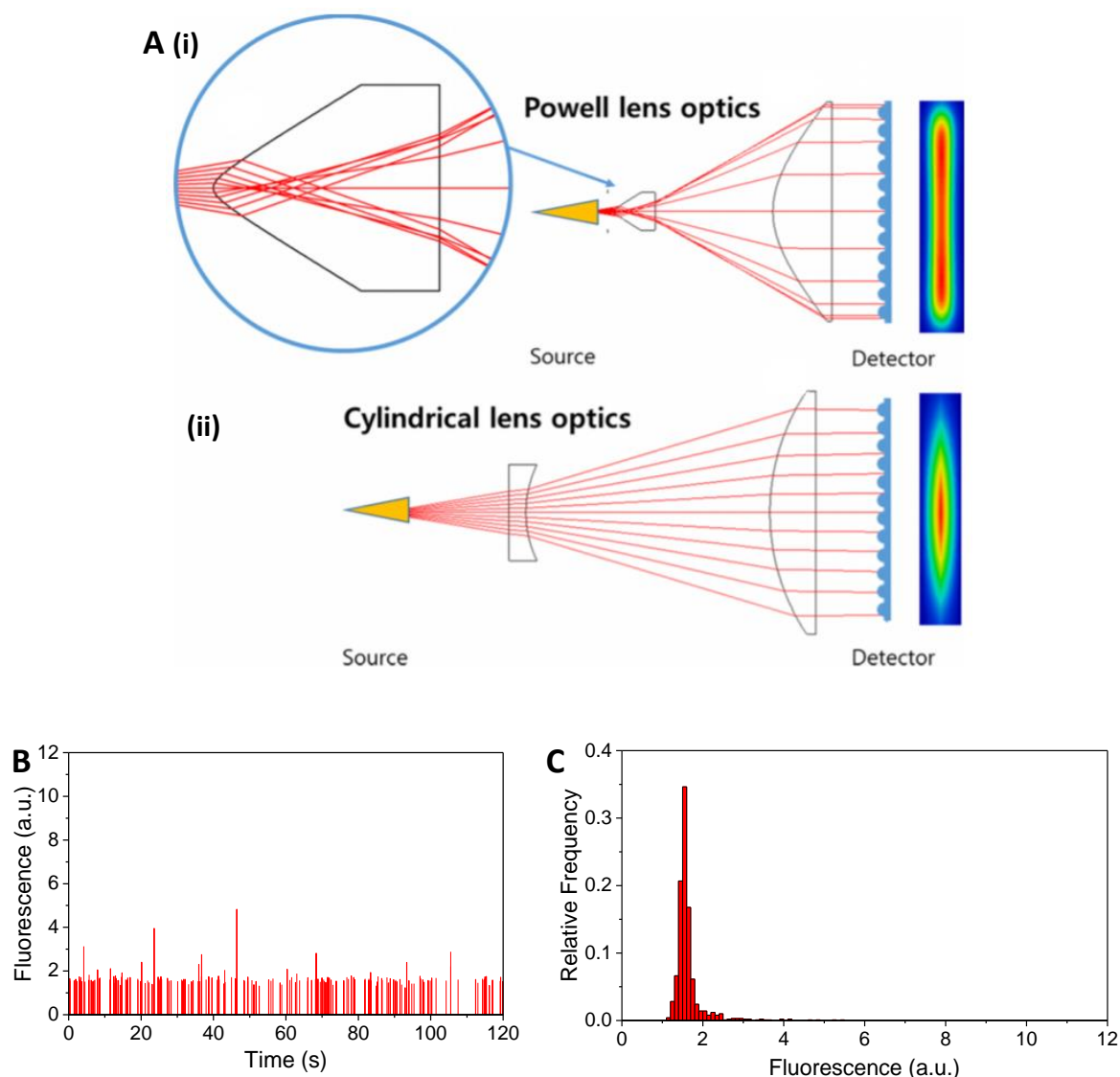
Figure 3.9: A) Ray trajectory diagrams and the corresponding laser intensity distribution patterns on detector plane when using (i) Powell lens optics and (i) cylindrical lens optics, adapted from ref.165, B) fluorescence intensity trace and C) fluorescence intensity distribution of the fluorescence emitted by Alignflow beads encapsulated in 45 µm diameter (48 pL) droplets when they are irradiated by the optimised laser sheet system. This test was performed four times.

3.3.3. Chlorophyll fluorescence detection with the laser sheet set-up

To further compare the capabilities of the two fluorescence detection set-ups, these were used for the detection of the chlorophyll fluorescence emitted by algal cells. Two algal species that are different in size were selected for this purpose, *N. gaditana* (*Ng*) (2 µm in diameter), and *P. tricornutum* (*Pt*) (approximately 20 µm in diameter). *Ng* cells are small in size and, as

they move around in the flowing microdroplets, they can be easily missed by the laser spot illumination, as was observed during previous experimental work conducted within the Abell group.[160] On the other hand, *Pt* cells, while larger in size, can exist in a variety of unusual shapes depending on their culture conditions. These cell species were selected to prove that the improved platform can detect the fluorescence of cells accurately, irrespective of their size or shape.

A sample of *Pt* cells was encapsulated into microdroplets which were 43 μm in diameter (42 pL in volume). Imaging of the generated droplets showed that 8% of the droplets contained cells. The collected droplets were then divided into two samples. The fluorescence of the first sample was detected with the laser spot set-up (**figure 3.10A(i)**) and the fluorescence of the second sample was detected with the laser sheet (**figure 3.10A(ii)**). In both cases, other experimental parameters (microfluidic device used, flow rates of droplets and spacing oil) were kept the same so that direct comparison of the recorded results would be possible.

A trace of the fluorescence emitted by the droplets flowing past the laser beam was recorded over 6 minutes. The number of peaks detected by the laser sheet set-up was then compared to the number of peaks detected by the laser spot set-up (**table 3.1**). This comparison revealed that while 1552 peaks were detected with the laser sheet, in the case of the laser spot this number was only 1075 peaks, showing that 31 % of the cells flowed past the laser spot undetected because the laser beam was too small to cover the entire channel.

The experiment was repeated using *Ng* cells. In this case the difference in the fluorescence detected (**figure 3.10B**) was even more pronounced due to the smaller size of the *Ng* cells. While 1686 peaks were detected with the laser sheet, only 738 peaks were detected with the laser spot, showing that 56 % of the cells were not detected.
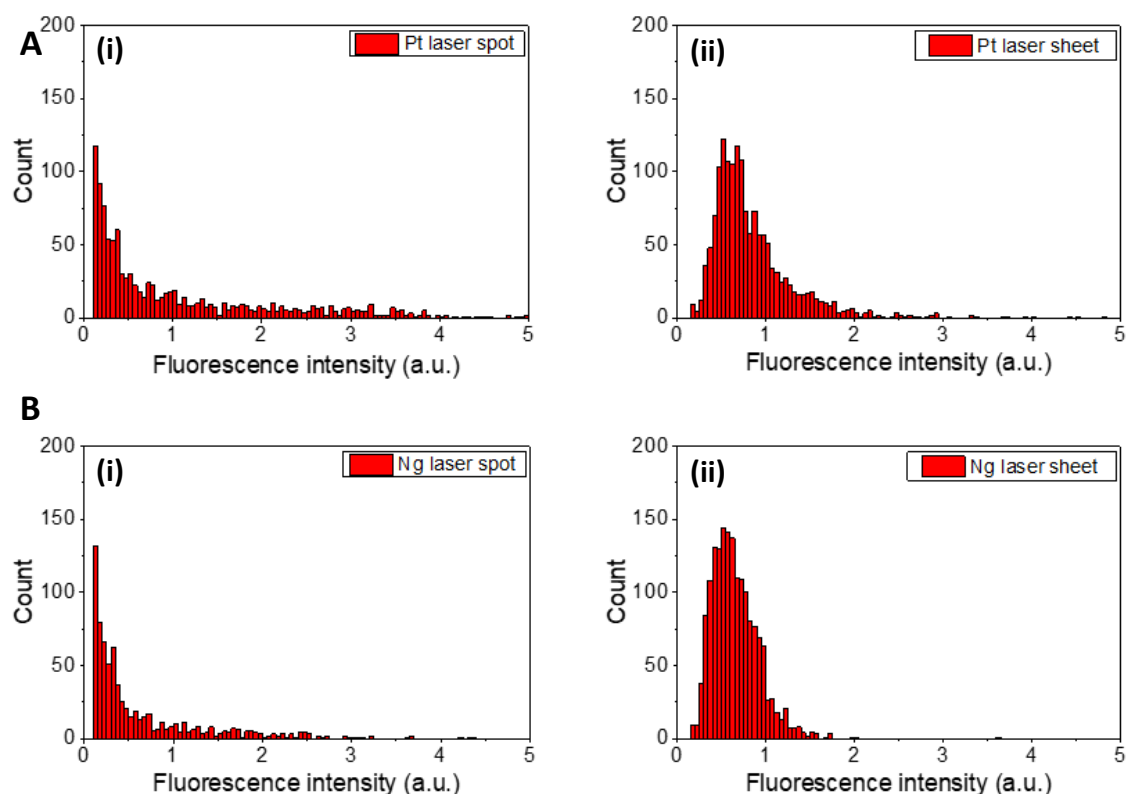
Table 3.1

Number of chlorophyll fluorescence peaks recorded over 6 minutes		
Ng	Laser spot	738
	Laser sheet	1686
Pt	Laser spot	1075
	Laser sheet	1552

Figure 3.10: A) Histograms of the chlorophyll fluorescence emitted by *Ng* cells as detected over 6 minutes with i) the laser spot and ii) the laser sheet; B) histograms of the chlorophyll fluorescence emitted by *Pt* cells as detected over 6 minutes with i) the laser spot and ii) the laser sheet. The experiment was performed once.

The difference in the fluorescence intensity distribution is also readily apparent. When the laser spot is used to irradiate the cells, the irradiation is not uniform. The encapsulated cells are exposed to different amounts of the laser light depending on their position in the channel. This results in large variations in the fluorescence signals recorded and makes quantitative detection impossible. By turning the laser spot into a laser sheet, the distribution of the

fluorescence intensity became narrower, a result of the cell irradiation being more uniform. Since the results obtained using the laser sheet set-up were more quantitative, it was used for all subsequent fluorescence detection experiments.

To test the fluorescence detection capabilities of the laser sheet set-up, it was used to detect the chlorophyll fluorescence of *Pt* cells grown under constant illumination with higher intensity light and *Pt* cells grown under a light-dark cycle and lower intensity light. As mentioned in section 3.1., cells cultured under such light conditions will contain low and high chlorophyll levels respectively. An experiment was designed to determine whether the fluorescence detection set-up is sensitive enough to distinguish between a sample of cells that have high chlorophyll content and another that contains cells that have low chlorophyll levels. The two samples would then be mixed to determine whether they can be successfully sorted based on the current system capabilities. To successfully distinguish which culture the cells came from once they would be mixed together for sorting, it was proposed that one of the cell samples contain GFP-expressing cells so that the GFP fluorescence can serve as an identification feature.

Samples of wild type *Pt* cells and GFP-expressing *Pt* cells with an initial concentration of 1 x 10^5 cells/mL were cultivated in two 24-well plates under different light regimes. Half of the wells in each well plate were used to culture wild type cells and the other half were used to culture GFP-expressing cells. The well plates were both placed in Infors HT shakers which provide uniform LED lighting. The cells in the first plate were cultivated under a low light intensity (30 µmol m^{-2} s^{-1}) light / dark regime (LD, 16 hrs light / 8 hrs dark) and the cells in the second plate were grown under a continuous illumination regime (LL) of higher light intensity (75 µmol m^{-2} s^{-1}). All other growth conditions were the same for both plates (temperature, shaking, nutrients). The growth of the algae was tracked over 13 days by measuring the OD$_{730}$ of the cultures and the chlorophyll in the cells was extracted and measured every two days. The chlorophyll extraction was performed by treating the *Pt* cells with DMF. The absorbance of the extracted chlorophyll at 630 nm (A630) and 664 nm (A664) was recorded using a spectrophotometer (Helios Alpha, Thermo Scientific, UK). The total chlorophyll content of the cells was calculated according to *equation 3.1*:[157]

Total Chlorophyll content (µg/mL) $= 7.74 \times A664 + 23.39 \times A630$ *(Equation 3.1)*

The resulting growth curves (**figure 3.11A**) and the measurements of the bulk chlorophyll content (**figure 3.11B**) were consistent with the results reported by Laohavisit *et al.* (**figure 3.2**).[157] The growth of the cells under continuous light was initially faster than that of the cells grown under a light / dark regime. This could be attributed to the difference in light intensity, as algal cell growth is inhibited by low-intensity light.[156]
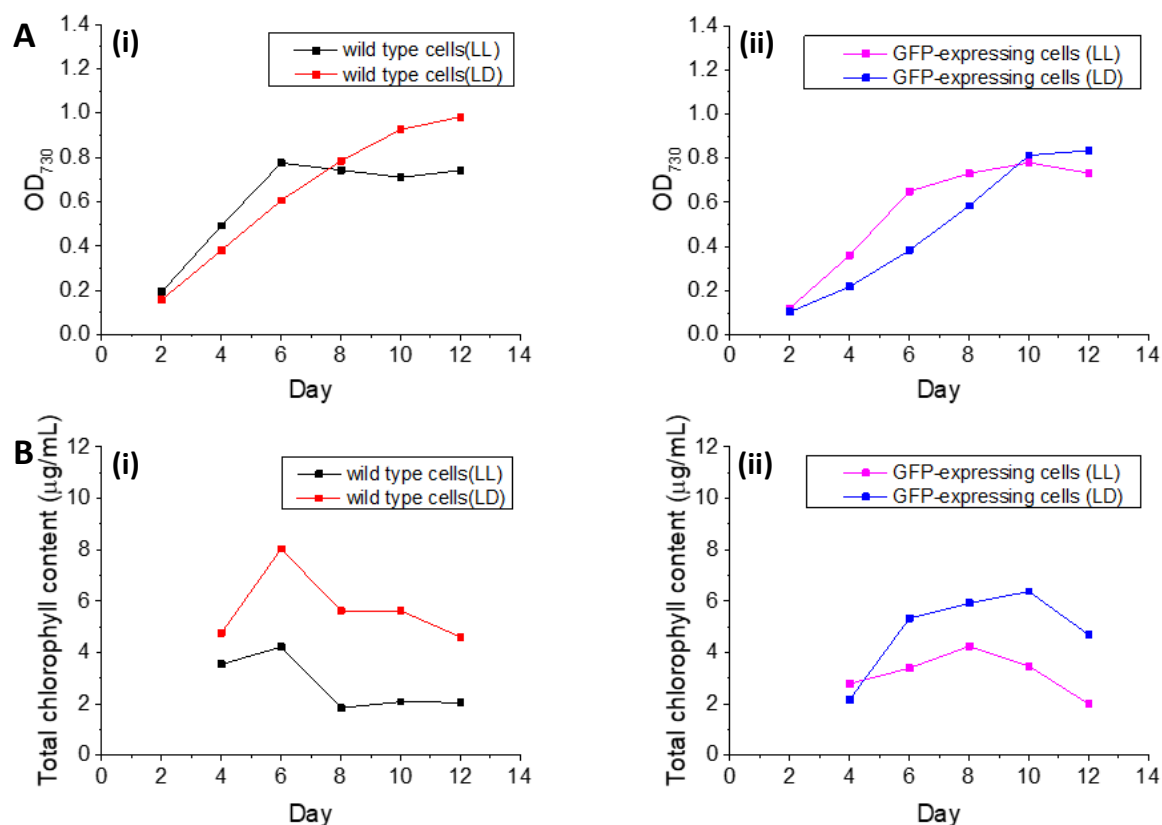
Figure 3.11: A) Growth curves of wild type (i) and GFP-expressing *Pt* cells (ii) grown under continuous illumination (LL) or a 16 hrs light / 8 hrs dark cycle (LD), B) the chlorophyll content of the wild type cells (i) and the GFP-expressing cells (ii) over time, as determined through a bulk measurement. Each data point represents the average of two measurements.

On day 8, a sample of wild type cells grown under a light/dark cycle (LD) and a sample of GFP-expressing cells grown under continuous light (LL) were extracted from the cell cultures and they were encapsulated separately into 40 μm (34 pL) droplets. The chlorophyll fluorescence emitted by the cells of each population was recorded separately using the laser sheet platform (**figure 3.12**). As the chlorophyll fluorescence was filtered using a 635 nm long-pass emission filter, there was no interference by the GFP fluorescence of the GFP-expressing cells

which is emitted at lower wavelengths (emission maximum = 510 nm). Prior to their encapsulation, the concentration of the cell samples was determined with a Coulter counter and the chlorophyll in the cells was extracted and measured through a bulk measurement (**table 3.2**).

Table 3.2: **Results of the bulk measurement of the *Pt* cell concentration and the chlorophyll content on day 8**

	Concentration (cells/mL)	Chlorophyll content on day 8 based on bulk measurement (µg/mL)	Chlorophyll content on day 8 based on bulk measurement (pg/cell)
wt (LD)	4.75×10^{6}	6.3	1.3
GFP (LL)	5.30×10^{6}	4.6	0.9

A comparison of the two fluorescence intensity distributions obtained by the laser sheet set-up, showed that the cells cultured under the light / dark cycle had a higher overall chlorophyll content than the cells cultured under continuous light. Additionally, since the encapsulated cells were screened one by one, the cell-to-cell variation in the chlorophyll content was observed, which was not possible when performing the bulk measurement of the chlorophyll content (**table 3.2**). For the sample cultured under the light / dark cycle a 37% variation in fluorescence intensity was observed (average fluorescence intensity = 1.10 ± 0.41 a.u.), while for the sample cultured under continuous light the variation was approximately 48% (average fluorescence intensity = 0.35 ± 0.17 a.u.).
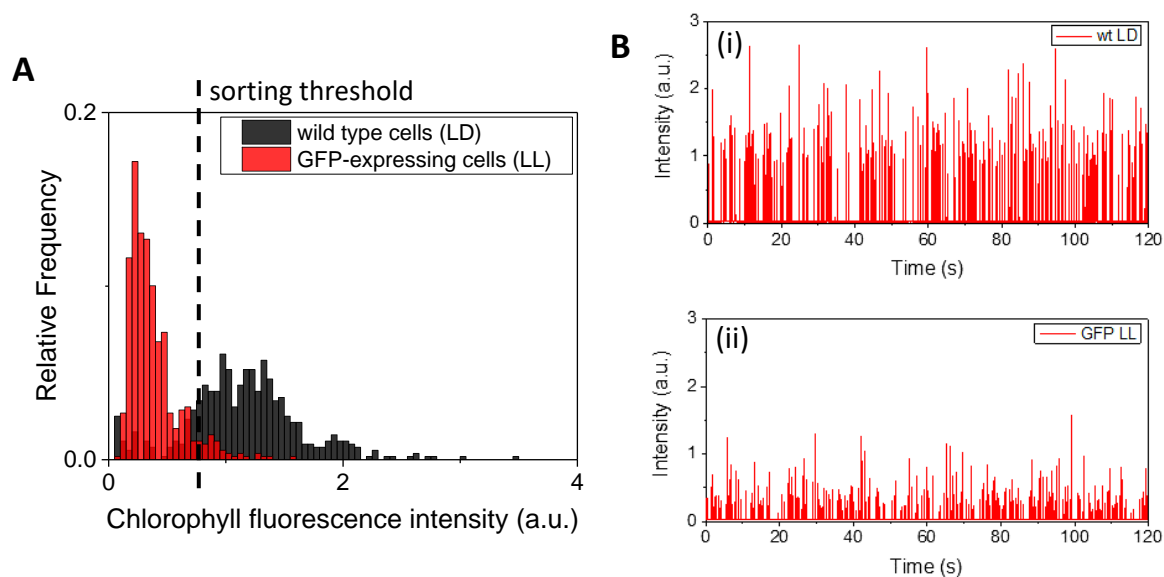
Figure 3.12: A) Chlorophyll fluorescence peak intensity histograms corresponding to wild type cells grown under a 16 hr light / 8 hr dark cycle (black) and GFP-expressing cells grown under continuous light (red) as recorded by the laser sheet on day 8; the dashed line indicates the theoretical sorting threshold, B) chlorophyll fluorescence trace recorded over two minutes for (i) the wild type *Pt* cells cultured under a 16 hr light / 8 hr dark regime and (ii) the GFP-expressing *Pt* cells cultured under a continuous light regime (droplet re-injection rate: 20 µL/hr (1.9 mm/s), spacing oil flow rate: 360 µL/hr (3.3 cm/s)).

Subsequently, droplets containing the two types of cells were mixed at a 1:1 volume ratio and loaded in a syringe. An attempt was made to sort the cells based on their chlorophyll fluorescence and thus to separate the encapsulated wild type cells that had a higher chlorophyll fluorescence from the GFP-expressing cells which had lower chlorophyll fluorescence. At the end of this sorting procedure, the droplets collected at the positive outlet should primarily contain wild type cells. The GFP-expressing cells, as well as wild type cells with lower chlorophyll fluorescence, should be collected at the negative outlet. The GFP fluorescence of the cells could be detected to assess which culture the cells came from.

The PMT output value was adjusted so that only the fluorescence peaks from the encapsulated wild type cells would be above the sorting threshold to ensure that these cells would be collected at the positive outlet, while the GFP-expressing cells would be collected at the negative outlet along with empty droplets. The theoretical sorting threshold is shown in **figure 3.12A**. Due to the adjustment of the gain prior to sorting, the position of the

threshold is just an approximation.The sorting procedure was not successful due to the continuous change in the chlorophyll fluorescence signal of the cells over the multiple hours of the experiment, which resulted in the fluorescence signals of the two cell populations becoming less distinct. Subsequent repeats of the experiment suffered by the same limitation. The sorting process was be carried out in the dark so that background light was at a minimum during the fluorescence detection, however, due to this extended incubation in the dark, the chlorophyll content of the encapsulated cells likely changed over time. This experiment revealed a limitation of the sorting platform. To collect a sample of droplets sizable enough to analyse, a sorting experiment must be run for multiple hours. As a result, the sorting platform cannot be used successfully for samples whose fluorescence can easily change during a short period of time.

3.3.4. Sorting based on chlorophyll fluorescence to eliminate empty droplets

Due to the random flow of the cells in the microfluidic channel during the cell encapsulation procedure, the distribution of the cells in the generated droplets is determined by Poisson statistics.[148] For this reason, and because of the need for having only one cell per droplet, most of the droplets collected after a cell encapsulation procedure are empty, with only a small percentage (up to 20%) of droplets containing cells. The presence of the empty droplets drastically reduces the efficiency of subsequent droplet microfluidic experiments. A possible method to eliminate empty droplets from a sample, is using the droplet sorting platform to enrich the sample with only droplets that contain cells. As has been previously demonstrated by the Abell group, the sorting platform can distinguish between droplets that contain algal cells and droplets that are empty based on the detection of the chlorophyll auto-fluorescence emitted by the encapsulated algal cells.[82]

Pt cells at a concentration of 1.4 x 10^6 cells/mL were encapsulated in microdroplets that were 40 μm in diameter. Imaging of the generated droplets showed that 8% of the droplets contained cells while the rest were empty (**figure 3.13A**). The droplets were collected in a 1 mL plastic syringe, which was then loaded onto a syringe pump so that the droplets could be reinjected into a sorting device.

The droplets were re-injected in the sorting device at a flow rate of 9 μL/hr (approximately 0.83 mm/s at the detection point) and Novec-7500 with 1% Picosurf 1, which was used as the

spacing oil, was injected at a flow rate of 160 μL/hr (1.48 cm/s). The chlorophyll fluorescence of the encapsulated cells was detected using a 635 nm long-pass emission filter. **Figure 3.13B** shows one minute of the chlorophyll fluorescence data recorded by the PMT. The PMT gain was adjusted so that all the chlorophyll fluorescence peaks recorded would be higher in intensity than the sorting threshold. Then the droplets were sorted and all droplets that emitted a chlorophyll signal were collected at the positive outlet.
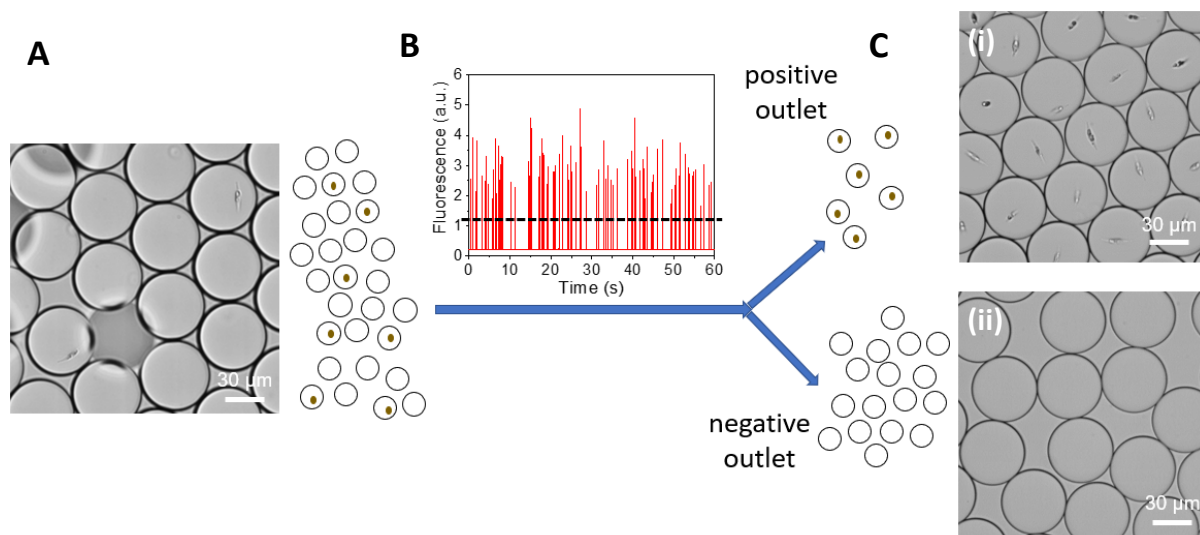
Figure 3.13: Chlorophyll fluorescence detection and sorting of droplets containing *Pt* cells from empty droplets with laser sheet platform (excitation by a 491 nm laser, 80 mW, fluorescence was filtered using a 635 nm long-pass filter). Data collected in collaboration with Dr Ziyi Yu. The experiment was performed once.

At the end of the sorting procedure, the droplets collected at the positive and the negative outlet were imaged with a brightfield microscope. Of the droplets collected at the positive outlet, 99% contained *Pt* cells (**figure 3.13C(i)**). The empty droplets that were collected at the positive outlet could be attributed to false positives that occurred due to pressure fluctuations in the sorting device. Pressure fluctuations occurred likely due to an experimental error and can be eliminated by ensuring that there are no air bubbles in the system and by keeping the sorting device and the tubing fixed in place during the sorting process.

In contrast, the droplets collected at the negative outlet of the sorting device were all empty (**figure 3.13C(ii)**). These results were an improvement over past results by Best *et al.*[82] which were recorded using the laser spot set-up. They observed a small number (~3%) of false

negatives at the negative outlet, after sorting droplets containing *C. reinhardtii* cells from empty droplets, resulting in the loss of a fraction of the cells. Those false negatives were probably the result of their use of a laser spot to irradiate the cells, an issue that has now been resolved, with false negatives no longer being observed.

3.3.5. GFP fluorescence detection and sorting

To improve the productivity of algal cells, in terms of biomass and the production of chemicals of interest, and to reduce the production costs and water consumption which are required for the industrial exploitation of algae, genome editing of algal cells is pursued by researchers. With the recent development of the appropriate tools for the genetic transformation of algal cells,[166-168] the focus is now on developing new strains of cells that display a variety of desirable properties,[169] such as increased biomass and chemical productivity.[170] This effort is aided by fluorescent markers, such as GFP, that are used to show whether a genetic transformation has been successful or not.

Using genetic transformation methods, such as electroporation[171] or biolistic transformation[32], algal cells can be transformed to express fluorescent proteins by the introduction of the corresponding genes in the cells. By detecting the fluorescence emitted by the proteins it is possible to determine which cells have been successfully transformed. However, the cell transformation process has low efficiency, and the identification and recovery of the transformed cells can be a labour-intensive and time-consuming process.

The FADS platform could be used to detect the fluorescence emitted by the fluorescent markers and to screen a mixture of cells at a high throughput to sort the transformed cells from the wild type cells. This can speed up the transformation workflow, therefore facilitating the identification of new high performing microalgal strains.

To test this idea, a 1:1 mixture of GFP-expressing and wild type *Pt* cells was encapsulated in microdroplets. The droplets were reinjected in a sorting device at a flow rate of 10 µL/hr (0.93 mm/s) and Novec 7500 with 1% Picosurf 1, which was used as the spacing oil, was injected at 160 µL/hr (1.48 cm/s). The GFP fluorescence of the encapsulated cells was detected after excitation by the 491 nm laser. **Figure 3.14A** shows one minute of the GFP fluorescence data recorded by the PMT. While the GFP-expressing *Pt* cells displayed strong GFP fluorescence,

the wild type cells displayed weak green autofluorescence resulting in two distinct cell populations, so careful adjustment of the PMT gain was needed to ensure that only GFP-expressing cells would be collected at the positive outlet (**figure 3.14B**).

The droplets collected at the positive channel after the sorting procedure were de-emulsified through the addition of PFO and the cells contained within were imaged under a fluorescence microscope and fluorescence intensity values were obtained from the fluorescence images using ImageJ. The fluorescence emitted by the collected cells was compared to the fluorescence of the cells in the initial mixture. As shown in **figure 3.14C**, the *Pt* cells in the initial mixture had different levels of green fluorescence, while on the other hand, the GFP fluorescence emitted by the cells collected at the positive outlet after the sorting was strong (**figure 3.14D**), which was proof that the FADS platform can be reliably used to isolate transformed cells from a mixture with wild type cells. The empty microdroplets, as well as droplets which contained cells with weak green fluorescence, were collected at the negative outlet. Further work for the optimisation of the GFP fluorescence sorting process was conducted by Dr Ziyi Yu.[172]
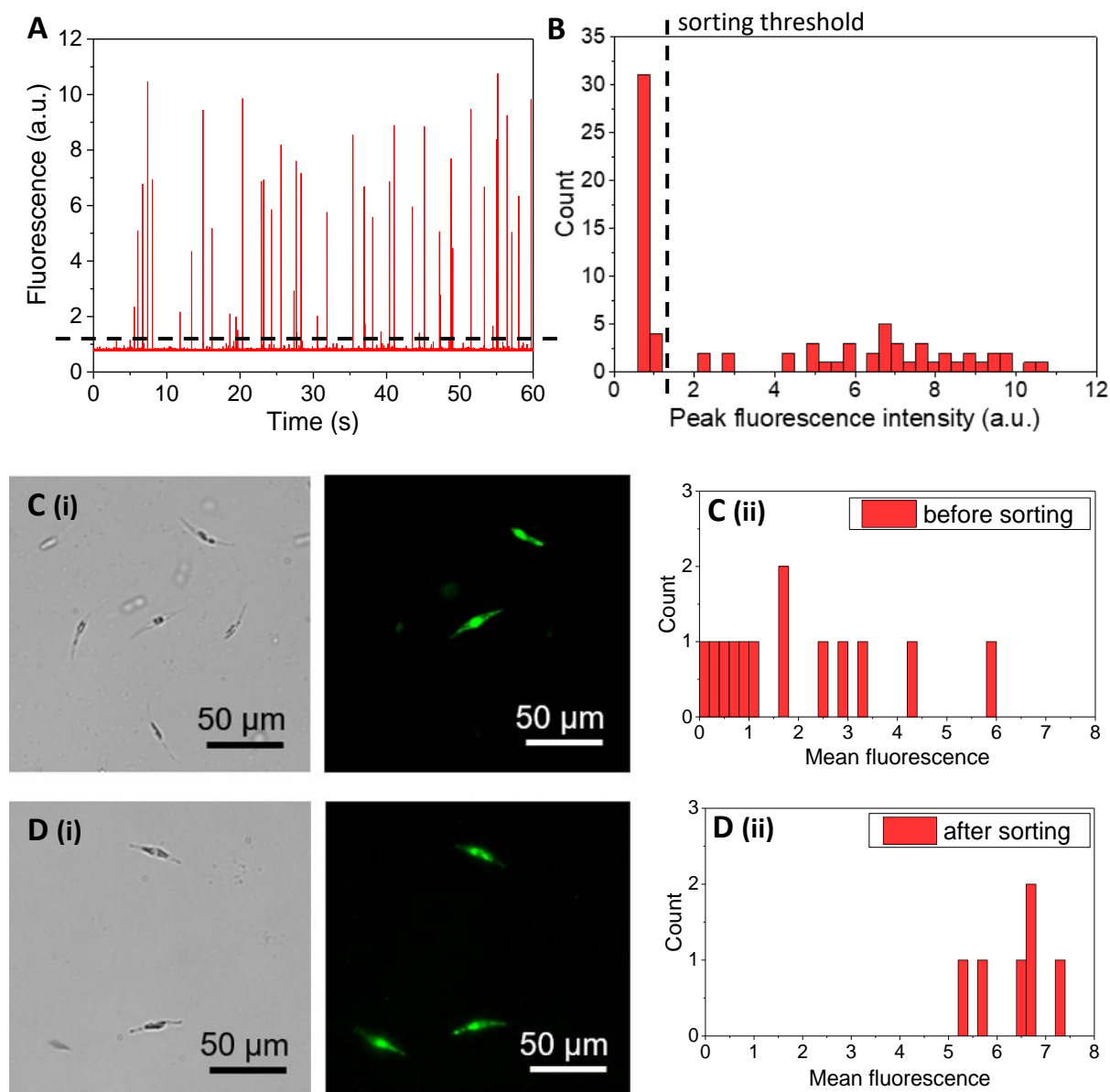
Figure 3.14: A) GFP fluorescence trace obtained as the encapsulated *Pt* cells from a mixture of wild type and GFP-expressing cells pass through the microfluidic channel and are excited by the laser beam, B) histogram of the GFP fluorescence emitted by the *Pt* cells showing the two populations of cells; the dashed line indicates the sorting threshold, C) (i) microscope image of the mixture of GFP-expressing *Pt* cells and wild type cells before encapsulation and sorting and (ii) histogram of the GFP fluorescence emitted by the cells as measured through ImageJ software analysis, D) (i) microscope image of *Pt* cells recovered by de-emulsifying the droplets collected at the positive outlet of the sorting device, imaged by Dr Ziyi Yu and (ii) histogram of the GFP fluorescence emitted by the collected cells. The experiment was carried out once.

3.3.6. Droplet sorting and dispensing with Cyto-mine®

As shown in sections 3.3.3. and 3.3.5., our current droplet sorting platform enables us to collect a subpopulation of high producing cells, however, it is a challenge to dispense and isolate individual cells of interest. An enriched cell population can be obtained, but it is a polyclonal population. A sorting platform which could be used for single cell selection, would enable a wider range of experiments, such as the isolation of rare cell clones from a cell library, and would be invaluable for cell line development. To achieve single droplet selection and to isolate individual cells after sorting, we used the Cyto-Mine Single Cell Analysis and Monoclonality Assurance System developed by Sphere Fluidics.[173]

Cyto-Mine (**figure 3.15A**) is designed to streamline the process of cell line development. It uses an integrated droplet microfluidics platform to automatically screen large populations of cells and then to select and dispense droplets containing cells of interest in the wells of a well-plate.[81] The accurate dispensing of microfluidic droplets after sorting is an invaluable addition to the sorting platform and greatly facilitates the selection of specific cells of interest and the study of those single cells off-chip.[115,174] Cyto-Mine enables users to perform droplet generation, sorting and dispensing on one microfluidic cartridge (**figure 3.15B**).

A cell sample is loaded onto the microfluidic cartridge, as shown in **figure 3.15C**, and it is automatically encapsulated into microdroplets. The generated microdroplets can be incubated on-chip if required. In the next step, the droplets are directed towards a sorting module, where their fluorescence is detected after illumination by a laser sheet. At that point, gating is used to select the droplets of interest and these droplets that have the desired fluorescence are collected at the positive channel of the sorter. Once the sorting process is finished, the fluorescence of each of the collected droplets is detected for a second time to confirm that there have been no false positives. At the same time, the droplets are imaged by a brightfield camera so that the user can check the occupancy of each droplet. Then the droplets are dispensed one by one in the wells of a 96 or a 384 well plate. The data about the droplet fluorescence and occupancy are linked with the well into which the corresponding droplet is dispensed.[81] In this fashion, the culture of specific single cells off-chip can be achieved.
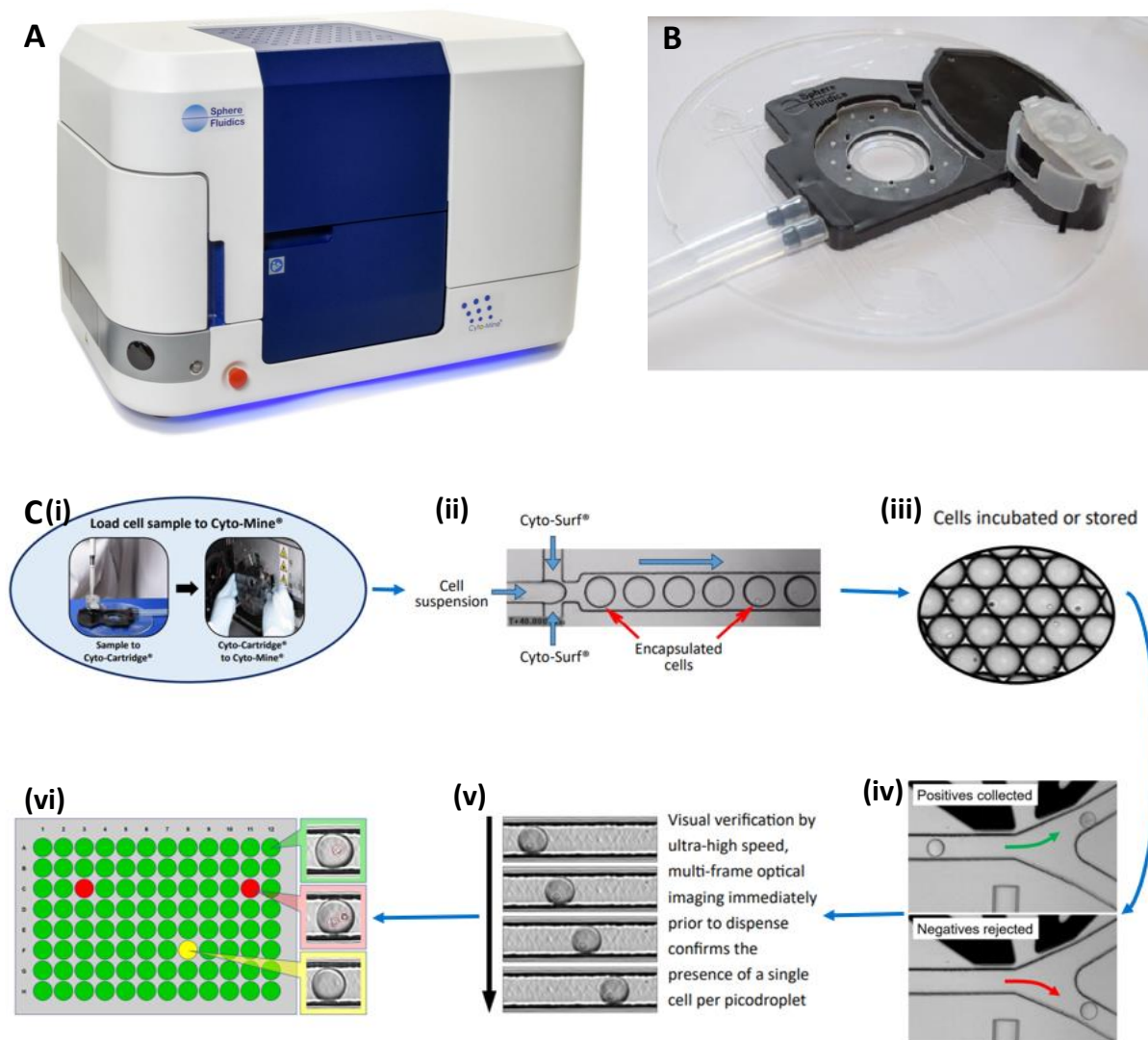
Figure 3.15: A) Cyto-Mine Single Cell Analysis and Monoclonality Assurance System, B) the Cyto-cartridge® used with Cyto-Mine®, adapted from ref.81, C) the Cyto-Mine® operation scheme, adapted from ref.173; (i) sample loading to the Cyto-Mine cartridge using a pipette and insertion of the cartridge into Cyto-Mine, followed by (ii) cell encapsulation into microdroplets, (iii) droplet incubation on-chip, (iv) droplet sorting and (v) imaging of the positive droplets, prior to (vi) dispensing to a 96-well plate.

Cyto-Mine is a very new instrument, which was launched in the market in 2018, and it has never been used to sort algal cells before. An experiment was therefore performed to test whether Cyto-Mine® can be used for the sorting and dispensing of single *Pt* cells. Through this experiment, we examined whether Cyto-Mine® can be used to detect the intracellular fluorescence of *Pt* cells and, based on that fluorescence, to distinguish between transformed

and wild type *Pt* cells. Furthermore, we examined whether Cyto-Mine can successfully dispense single *Pt* cells into the wells of a well-plate after sorting. Finally, we tested whether the dispensed single *Pt* cells can grow on a well plate in a large volume of growth medium or if a volume limitation is required for growth to take place. The work described in this section was performed at Sphere Fluidics in collaboration with Dr Xin Liu who operated Cyto-Mine. The sample preparation, the culture of the collected cells and the data analysis were performed by me.

A cell sample was prepared which contained a 1:1 mixture of wild type and GFP-expressing *Pt* cells in F/2 medium (total concentration 3 x 10^5 cells/mL). The cell sample was loaded onto the Cyto-Mine cartridge and the instrument encapsulated the cells into 450 pL microdroplets. The instrument's capability to detect the fluorescence of the encapsulated cells was tested. The encapsulated cells were excited using a 488 nm laser which was shaped into a sheet. A 520 nm emission filter (bandwidth: 15 nm) was used for the GFP fluorescence detection. For the chlorophyll fluorescence detection, a 620 nm emission filter (bandwidth: 14 nm) had to be used as the present configuration of Cyto-Mine offers fixed filter choices. Unfortunately, the emission band of the filter was too narrow to allow all the chlorophyll fluorescence to come through. As a result, the chlorophyll fluorescence could not be detected and only the GFP fluorescence was successfully recorded (**figure 3.16**).
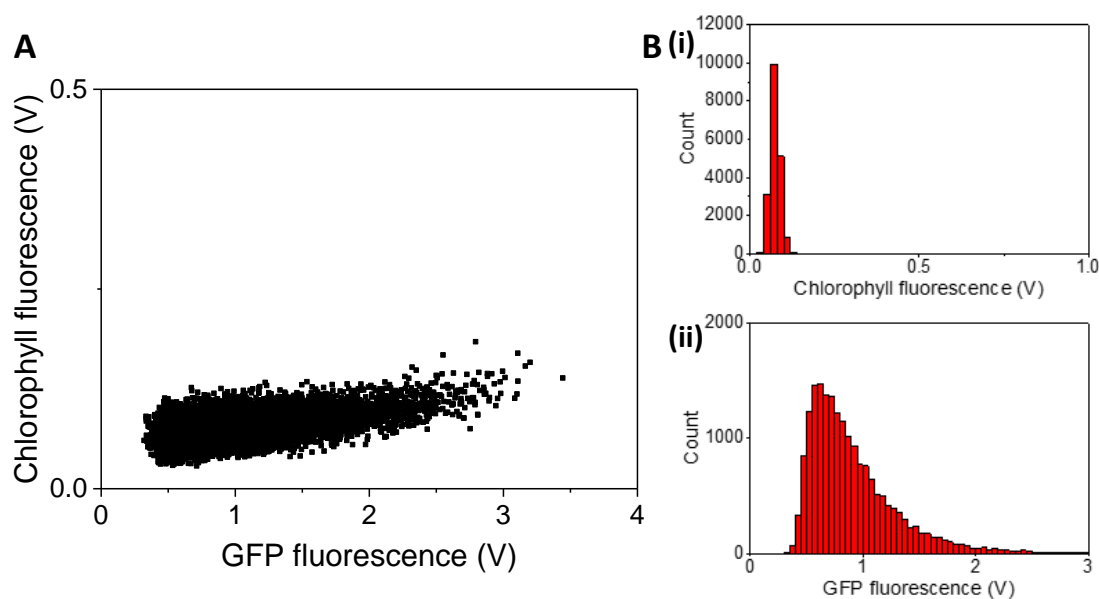
Figure 3.16: A) Scatter plot showing the recorded values of the chlorophyll and the GFP fluorescence of the encapsulated cells, B) histograms of (i) the chlorophyll fluorescence intensity and (ii) the GFP fluorescence intensity.

Despite not being able to detect the chlorophyll fluorescence, the droplets were sorted based on GFP fluorescence. Having thus shown that Cyto-Mine can successfully sort the *Pt* cells, the next question that was explored was whether viable cell cultures could be generated off-chip from single cells. The droplets containing cells with high GFP fluorescence were collected at the positive channel of the sorting device and they were subsequently dispensed into two 96-well plates and one 384-well plate. Imaging of the droplets during the dispensing process revealed that 87% of the dispensed droplets contained single cells, while 12% contained two cells and 1% contained either 3 or 4 cells (**figure 3.17**).
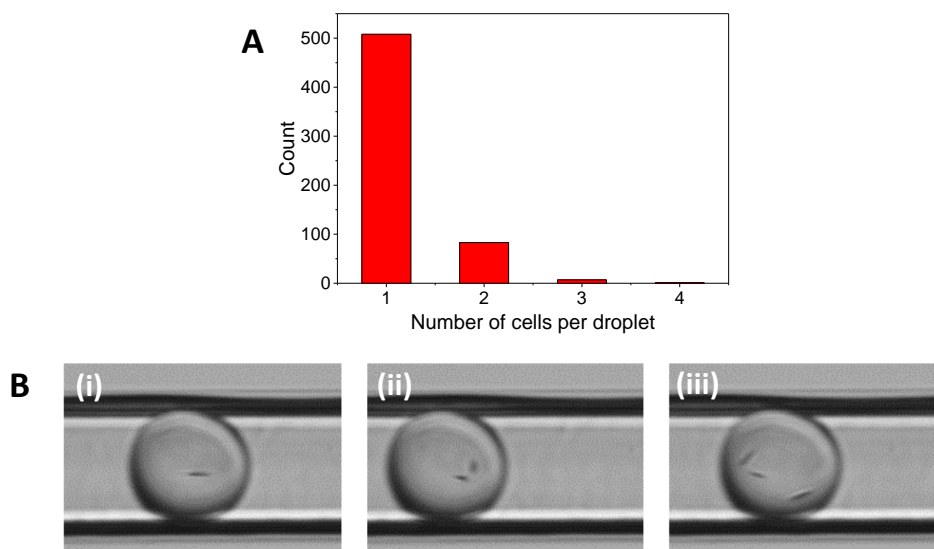
Figure 3.17: A) number of cells per dispensed droplet, B) Images of the droplets collected at the positive channel during the dispensing process; (i) droplet containing one Pt cell, (ii) droplet containing two Pt cells, (iii) droplet containing three Pt cells.

Prior to the dispensing process, each of the wells of the 384-well plate was loaded with 6 μL of F/2 media. Each of the wells of the 96-well plates were loaded with 30 μL of F/2 media. Once the dispensing process was finished, different volumes of F/2 were added to the wells of the 384-well plate, so that the effect of different growth medium volumes on the growth of the cells could be examined. The final F/2 volume in the first four rows of wells was 12 μL, in the next four rows it was 24 μL, in the four rows after that it was 48 μL and in the final four rows it was 72 μL. The wells of the two 96-well plates were all topped with F/2 up a total volume of 150 μL. The well plates were placed in an incubator and they were cultured at 18 °C under a 16 hr light / 8 hr dark regime for 27 days. The growth of the cells on the well plates was monitored by measuring the OD_{730} with a plate reader (**figure 3.18**).

In the 384-well plate cell outgrowth took place, but in the wells that contained smaller volumes of F/2 the cell growth was hindered by the evaporation of the growth medium over time.

Overall, cell growth was more extensive in the 96-well plates. The cells dispensed to these plates grew without any issue in the larger volume of F/2 medium. The measurement of the OD_{730} on day 27 showed that cell growth took place in 133 of the 190 wells (70% viability rate). Of those 133 wells, 114 wells (86%) initially contained single cells, meaning that,

through the dispensing process, 60% of the collected droplets yielded viable monoclonal *Pt* cell cultures.

	1	2	3	4	5	6	7	8	9	10	11	12
A	0.47	0.48	0.43	0.57	0.73	0.32	0.16	0.67	0.56	0.63	0.72	0.16
B	0.09	0.74	0.81	0.90	0.80	0.96	0.08	0.95	1.04	0.08	0.74	0.44
C	0.08	0.69	0.94	0.95	1.01	0.83	0.76	0.08	0.09	0.83	0.09	1.37
D	0.66	0.93	1.16	0.08	0.96	0.09	0.96	0.69	0.81	0.08	0.74	0.08
E	0.62	0.97	0.93	0.87	0.93	1.65	0.51	0.08	0.08	0.92	0.83	0.48
F	0.08	0.83	0.80	0.83	0.81	0.08	0.85	0.88	0.08	0.78	0.65	0.47
G	0.60	0.26	0.13	0.74	0.08	0.36	0.86	0.87	0.70	0.08	0.70	0.14
H		0.09	0.64	0.80	0.58	0.60	0.09	0.08	0.18	0.68	0.08	0.08

	1	2	3	4	5	6	7	8	9	10	11	12
A	0.10	0.24	0.08	0.69	0.70	0.08	0.08	0.88	0.74	0.60	0.65	0.34
B	0.57	0.67	0.92	0.97	0.08	0.08	0.10	0.97	0.08	1.01	0.81	0.08
C	0.08	0.75	0.08	0.08	0.89	1.03	0.86	0.92	0.83	0.97	0.84	0.08
D	0.76	0.91	0.08	0.88	0.08	0.97	1.07	1.04	0.94	0.94	0.67	0.23
E	0.56	0.09	0.08	1.13	1.01	0.95	0.08	1.02	0.08	1.19	0.08	1.38
F	0.08	0.97	0.97	0.84	0.29	1.08	0.96	0.82	0.98	0.69	0.82	0.15
G	0.65	0.08	0.08	0.08	0.10	0.08	0.41	0.08	0.08	0.84	0.84	0.08
H		0.62	0.54	0.89	0.60	0.08	0.09	0.83	0.08	0.08	0.09	0.13

Figure 3.18: The OD_{730} values of the cells cultured on the two 96-well plates which were recorded on day 27. The green cycles denote wells in which cell growth has taken place (OD_{730} > 0.1), while the red and yellow cycles denote wells in which limited or no growth has taken place ($OD_{730} \leq 0.1$). The orange rectangles correspond to wells to which droplets with multiple cells were dispensed.

3.4.   Conclusion

In this chapter, a FADS platform was used for the detection of the intracellular fluorescence of *Pt* cells encapsulated in microdroplets. The optical set-up of the platform was modified to improve the accuracy of the fluorescence detection. The fluorescence detection capabilities of this improved platform were compared to those of a previously used platform, and the fluorescence data recorded using the improved platform were 10 times more accurate. The FADS platform was furthermore able to successfully distinguish between cell cultures containing cells of different fluorescence levels when it was used to detect the chlorophyll fluorescence of *Pt* cells cultured under different light conditions, who, as a result, contained different levels of chlorophyll.

The improved accuracy of the FADS platform was displayed when the platform was used to sort droplets containing *Pt* cells from empty droplets, to overcome the issue of the random

encapsulation of the cells in droplets. This was done by sorting the droplets based on chlorophyll fluorescence. The platform successfully isolated the droplets containing cells from the empty droplets without any false negative results being observed. This was a 3% improvement on previous results recorded by the Abell group, in which false negative droplets were observed, leading to a loss of cells of interest.[82]

Besides chlorophyll fluorescence, the FADS platform was also used to detect GFP fluorescence and to successfully sort GFP-expressing *Pt* cells from a mixture with wild type *Pt* cells. By isolating the transformed GFP-expressing cells from the rest, an enriched population was obtained. The use of FADS to recover transformed cells after the transformation process successfully speeds up the algal transformation workflow which can traditionally take several weeks.[172]

Finally, the possibility was explored of using the Cyto-Mine Single Cell Analysis and Monoclonality Assurance System to sort *Pt* cells and to dispense them one-by-one to the wells of a well plate to obtain monoclonal *Pt* cell cultures. The intracellular GFP fluorescence of transformed *Pt* cells could be detected by the instrument, thereby enabling the sorting of the transformed cells from wild type cells. The sorted GFP-expressing *Pt* cells were dispensed into the wells of 96 and 384-well platesand monoclonal cell cultures were successfully obtained, as the single *Pt* cells could grow in the wells, in a volume as large as 150 μL. This test showed that it is possible to overcome a major limitation of our sorting platformwhich was the difficulty in the collection and handling of small volumes of droplets. Sorting experiments had to be run for longer times to ensure that a large enough number of droplets were collected. As a result, enriched cell subpopulations could be obtained, but it was not feasible to select specific cells of interest. If our sorting platform is combined with automated droplet dispensing for single cell selection and monoclonal culture generation, that would enable a wider range of experiments, such as the isolation of rare cell clones from a cell sample and it would put our platform at the same level as other state of the art systems which combine droplet sorting with droplet dispensing.[115,116]

3.5.   Future work

Due to a lack of available time, it was not possible to complete further experiments using Cyto-Mine. These initial results, however, were very promising and a number of further

experiments could be performed using the platform. While the intracellular GFP fluorescence of the transformed cells could be detected by the Cyto-Mine Single Cell Analysis and Monoclonality Assurance System, the system did not possess the appropriate emission filter to detect the chlorophyll fluorescence of the cells. Further experiments can be performed by updating the emission filter for chlorophyll fluorescence analysis. In the meantime, Cyto-Mine could be further used for GFP fluorescence detection, to identify and isolate mutants with higher GFP fluorescence. Additionally, in future experiments, the GFP fluorescence of the dispensed cells could be tracked as they grow on the well plates, to determine whether GFP expression remains constant over time.

CHAPTER 4

Intracellular lipid staining by BODIPY 505/515 and fluorescence detection

4.1. Introduction

The capability of algal cells to produce lipids through photosynthesis is of interest to both researchers and industry. Microalgae have the ability to accumulate large amounts of lipids. Their lipid content can vary greatly depending on the algal species, as well as the environmental conditions, with some algae containing up to 50-80 % of their dry weight in lipids.[12] Algal lipids can be used in the production of biofuel, such as biodiesel. Furthermore, some microalgae species are a source of high value lipids, such as the omega-3 lipids EPA (eicosapentaenoic acid) and DHA (docosahexaenoic acid), which are not found in large quantities in other natural sources.[175]

Neutral lipids, predominantly triacylglycerols (TAGs), accumulate in the cytoplasm of algal cells in the form of lipid bodies. These lipid bodies act as energy storage for the cells when they are in the stationary phase of growth or when they are under stress conditions.[175] The accumulation of TAGs can be triggered by nutrient limitation or by changes in the salinity and the pH of the growth medium.

Unfortunately, despite extensive efforts to cultivate algae on an industrial scale, the production of algal lipids is often economically unfavourable.[22] As a result, ongoing research is focused on optimizing the production of lipids by algae, either by determining the optimal cell culturing conditions which would result in increased lipid productivity[2,176] or by developing new microalgal strains that display more desirable characteristics.[30]

4.1.1. Intracellular lipid staining

In order to study the production of lipids by the algal cells, a reliable method is needed to determine the intracellular lipid content. The traditional method used to quantify the lipids produced by algal cells requires the use of gravimetric techniques after solvent extraction.[51] This is a laborious method which takes about 3–4 days and requires a cell sample that weighs

at least 10–15 mg.[177,178] Furthermore, as this is a bulk method, it is not possible to determine the lipid content at the single cell level.

As an alternative lipid detection method, fluorescent dyes have been developed that are able to stain the lipid bodies inside the cells without the need of extracting the lipids first. These dyes are lipophilic and fluoresce intensely in lipid rich environments, enabling the visualization of the lipids using fluorescence microscopy or the fluorescence-based screening of cells using flow cytometry.[179]

Due to the intense autofluorescence emitted by algal cells, the fluorescent probes used to stain the lipid bodies inside microalgae must emit at wavelengths distinct from the emission wavelengths of chlorophyll. The fluorescent dyes most commonly used to stain intracellular lipids in algae are therefore Nile Red (**figure 4.1A**) and BODIPY 505/515 (**figure 4.1B**)(as well as its structurally close analogue BODIPY 493/503). Nile Red emits intense yellow light when staining the neutral lipid bodies inside the cells,[180] while BODIPY 505/515 emits green fluorescence at wavelengths similar to fluorescein (FITC). Both dyes are commonly used, however, BODIPY 505/515 appears to have some advantages over Nile Red, when it comes to the study of microalgae. Nile Red cannot easily penetrate thick cellular walls,[181] as shown in lipid staining experiments performed on various green algae, such as *Chlorella vulgaris, Pseudochlorococcum sp*[182] and *Nannochloropsis*.[183] As a result, organic solvents, such as DMSO and acetone, or intense preparation methods, such as microwaving,[184] are needed to increase the solubility of the dye and improve its ability to penetrate the cells. However, these methods can also compromise the viability of the cells.[185] In contrast, BODIPY 505/515 has a high oil / water partition coefficient that allows it to easily cross cell and organelle membranes[181] (**figure 4.1D**).

The fluorescence properties of BODIPY 505/515 also make it preferable for this application. It has a narrow emission spectrum that does not overlap with the emission spectrum of chlorophyll. The green fluorescence of BODIPY 505/515 is spectrally distinct from the red autofluorescence of the chloroplasts, minimizing the background fluorescence during fluorescence detection.[186] This is not the case for Nile Red which has a wider emission spectrum (**figure 4.1C**). Nile Red staining is also affected by changes in the salinity of the growth medium, which can lead to fluorescence quenching. BODIPY 505/515 fluorescence

has been shown to remain unaffected by most changes in its environment.[181] Studies have also shown that BODIPY 505/515 is more photostable than Nile Red.[184]

Additionally, since the goal is to collect and then cultivate the cells that have a higher lipid content, it is important that the cells can stay alive and able to grow after the staining and sorting procedures. Unfortunately, Nile Red has been shown to affect algal cell viability even when used at very small quantities.[187,188] On the other hand, BODIPY 505/515 has been shown to be more biocompatible.[187]
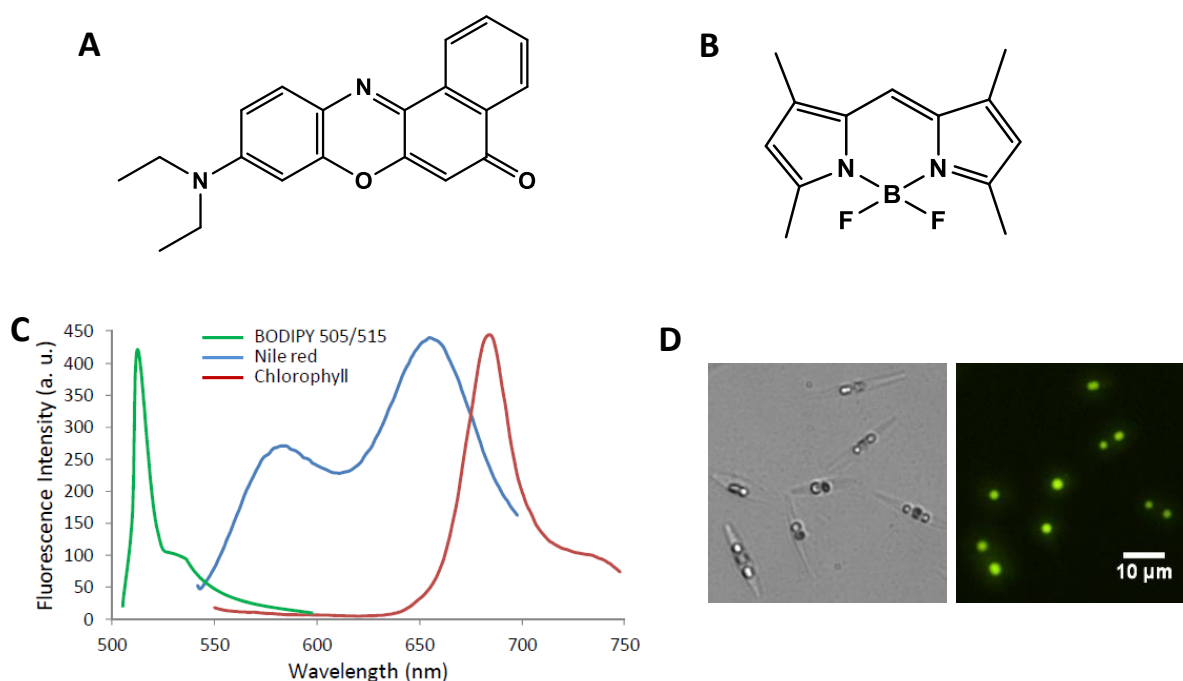
Figure 4.1: Chemical structures of A) Nile Red and B) BODIPY 505/515, C) emission spectra of BODIPY 505/515, Nile Red and chlorophyll excited by light of wavelength 488 nm, adapted from ref.57, D) brightfield and fluorescence images of *Pt* cells in F/2 medium after they were stained with a 1 mM BODIPY 505/515 solution in DMSO and incubated in the dark for 20 minutes.

More recently, alternative dyes have been developed to expand the library of neutral lipid-specific dyes and to compensate for the shortcomings of commercially available dyes (**figure 4.2**). Several of these new dyes show improved behaviour when it comes to parameters such as cell permeability, organelle specificity, photostability and cell toxicity,[189] however they have not yet been used to study algal lipids.
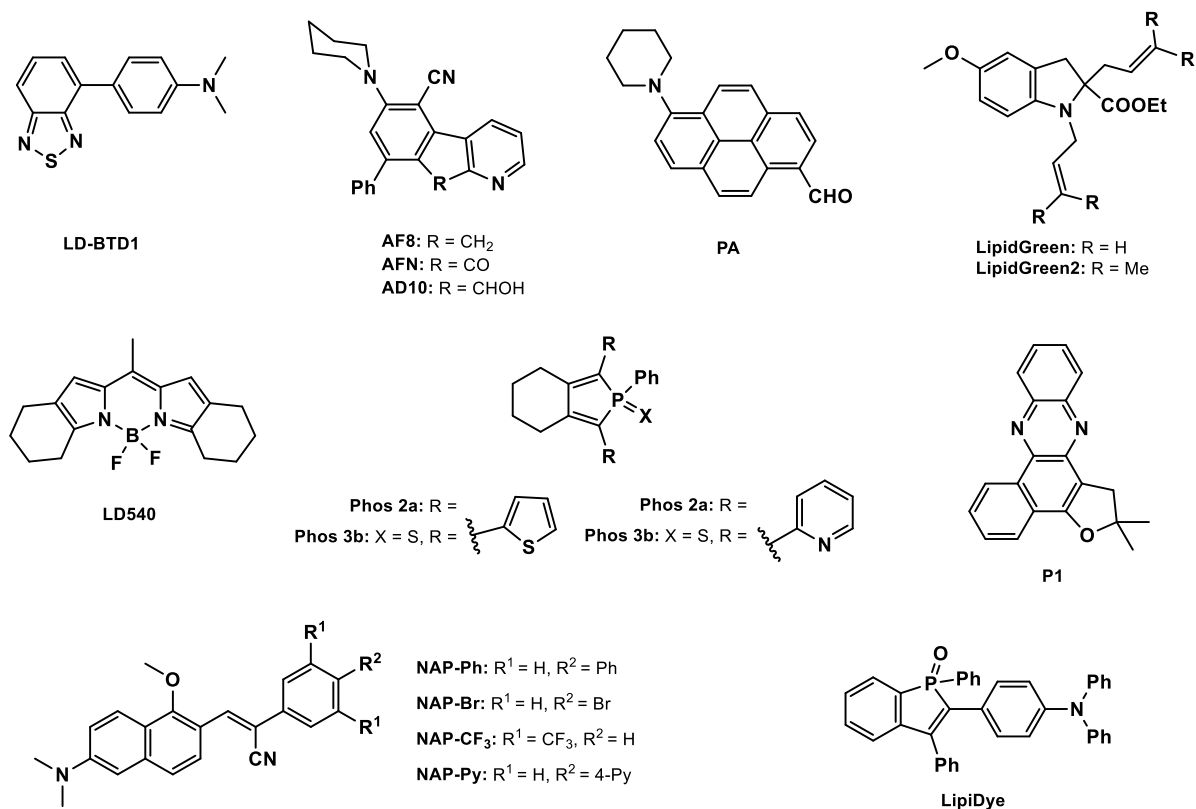
Figure 4.2: Chemical structures of novel green emitting lipophilic dyes, adapted from ref.189.

4.1.2. Intracellular lipid staining in microdroplets

Lipid staining of microalgae in microfluidic droplets is hard to achieve due to the lipophilic nature of the dyes used to stain the cells. The dyes have a high oil / water partition coefficient and consequently they easily diffuse out of the microdroplets and into the continuous oil phase.[83] Additionally, PDMS, which is usually used to fabricate the microfluidic devices in research labs, is porous and hydrophobic.[190] The hydrophobic dyes can be easily absorbed into the PDMS, resulting in a high fluorescence background.

Kim *et al.* developed a droplet microfluidic platform for the analysis of the growth and the oil content of microalgae.[83] This platform combined cell encapsulation and culture with the on-chip staining of the cells with Nile Red and the imaging of the cell lipids. The microalgae were initially encapsulated in microdroplets and then incubated on-chip so that their growth could be monitored. The droplets were afterwards merged with droplets containing Nile Red solution in DMSO and they were incubated so that staining of the encapsulated cells could take place. However, due to the lipophilic nature of Nile Red, the dye diffused out of the droplets during their incubation, resulting in a high fluorescence background. To resolve this

issue, the droplets were transferred to fresh oil that did not contain Nile Red prior to their imaging.

Kim *et al.* further expanded on their work by combining their platform with a droplet sorting module to isolate droplets with higher chlorophyll and BODIPY 505/515 fluorescence (**figure 4.3**).[191] In this case, BODIPY 505/515 in DMSO was used, instead of Nile Red, to stain the encapsulated cells and the droplets were not transferred to fresh oil before the fluorescence detection. The possibility of the leakage of BODIPY 505/515 to the oil or to the PDMS walls of the microfluidic device was not addressed.
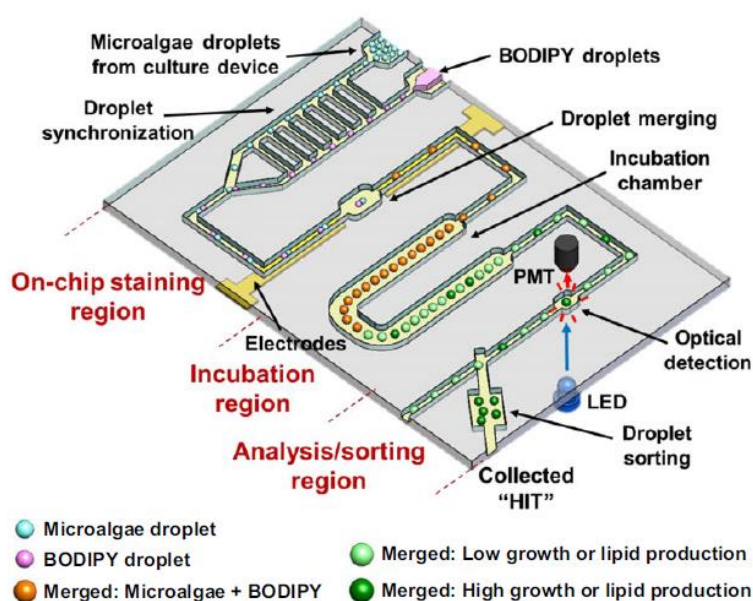
Figure 4.3: Schematic diagram of the platform used for the analysis of microalgal growth and lipid production, adapted from ref.191.

Alternatively, the issue of the dye leakage from the cells can be bypassed by encapsulating the microalgae in hydrogel droplets. Once the droplets have gelled, they can be transferred to an aqueous solution and the oil surrounding the droplets can be removed. The hydrogel beads can then be incubated in a solution of the dye, which crosses into the beads and stains the encapsulated cells. The fluorescence of the beads can then be detected through flow cytometry.[136,137]

4.1.3. Objectives

The work described in this chapter is directed towards the development of a droplet microfluidic platform for the screening of algal cells based on their lipid content. *Pt* cells encapsulated in microdroplets were stained by incubation in a solution of BODIPY 505/515 in FC-40. The diffusion of the dye to and from the droplets was studied. The BODIPY 505/515 fluorescence of the stained droplets was detected with the laser sheet platform established in Chapter 3. The high fluorescence background during these measurements, caused by the BODIPY 505/515 dissolved in the surrounding oil, inhibited the measurement of the cellular fluorescence, so several methods were explored to reduce the background fluorescence.

4.2.   Experimental

<u>Droplet staining with BODIPY 505/515</u>

The staining protocol used was adapted from previous work by Dr Jie Pan.[192] A 300 µM stock solution of BODIPY 505/515 in FC-40 (with 1% PicoSurf 1 as surfactant) was prepared. A 1 x 10^6 sample of *Pt* cells was encapsulated using a 40 µm x 40 µm x 50 µm (length x width x height) flow-focusing device and FC-40 with 1% PicoSurf 1 as the continuous phase. 50 µL of the generated droplet emulsion were added to 50 µL of the BODIPY 505/515 solution and incubated in the dark for up to 2 days. The staining procedure was repeated for the different concentrations of BODIPY 505/515 tested.

<u>Fluorescence imaging</u>

The fluorescence images were obtained using an IX 71 inverted microscope (Olympus) equipped with an EMCCD iXonEM+ DU 897 camera (Andor Technology). An LED illumination system (CoolLED PE300) was used to illuminate the sample and the appropriate filters were used for the fluorophores that needed to be visualized. BODIPY 505/515 fluorescence was imaged using the 'FITC' fluorescence channel (excitation filter 488 (bandwidth: 40 nm), emission filter 535 (bandwidth: 50 nm)). A custom-made LabView program (National Instruments) was used to control the microscope stage, the camera and a shutter. The shutter ensured that the LED light only hit the sample during image acquisition to minimize photobleaching.

Sol-gel coating of microfluidic reservoir device

The sol-gel coating procedure was adapted from Abate *et al.*[193] and modified by Dr Shaohua Ma.[192] The pre-converted sol mixture was prepared by mixing 1 mL tetraethoxysilane (TEOS, Fluka), 0.5 mL (heptadecafluoro-1,1,2,2-tetrahydrodecyl)triethoxysilane (Sigma Aldrich), 1 mL methyltriethoxysilane (MTES, Sigma Aldrich), 2 mL trifluoroethanol (Fluka) and 1 mL DI water of pH 4.5 (adjusted by the addition of HCl). The mixture was heated under reflux for 10 minutes, until it became homogeneous. The mixture was allowed to cool to room temperature and it was then loaded into a 1 mL syringe (HSW NORM-JECT®).

The PDMS reservoir device (**Appendix device C**, height: 75 µm) was bonded onto a glass slide by oxygen plasma treatment. The sealed device was then immediately placed on a hotplate which was heated at 105°C. The prepared sol mixture was injected into the microfluidic device and the device was flushed with 10 ml of air within 20 seconds. A further 10 ml of air was blown into the device slowly over the next 2 minutes. The coated device was heated on the hotplate for a further 2 hours.

Droplet staining on-chip

The inlet of the glass coated reservoir device (**Appendix device C**) was connected by tubing to the outlet of a 40 µm x 40 µm x 50 µm flow-focusing droplet generation device (**Appendix device A**). Droplets were generated in the flow-focusing device by injecting the *Pt* cell sample at a flow rate of 350 µL/hr (4.86 cm/s) and using as the continuous phase a 15 µM solution of BODIPY 505/515 in FC-40 with 1 % Picosurf 1 surfactant which was injected in the device at a flow rate of 600 µL/hr (8.35 cm/s). Once the reservoir device was filled by the droplets, the inlet and the outlet were sealed by pressing together the walls of the tubing with a hot pair of tweezers and the BODIPY 505/515 fluorescence of the collected droplets was monitored over time under a fluorescence microscope.

BODIPY 505/515 fluorescence detection using the laser sheet set-up

Droplets that were incubated in the BODIPY 505/515 solution were reinjected into the cyclic olefin copolymer microfluidic device, provided by Sphere Fluidics (**figure 4.4**). Spacing oil, either the BODIPY 505/515 solution in FC-40 or FC-40 alone, was injected from the second inlet of the device to space the droplets. A 491 nm laser was used to irradiate the droplets

and the resulting BODIPY 505/515 fluorescence was detected through a 525 nm filter (bandwidth: 39 nm) which was fitted before the PMT.
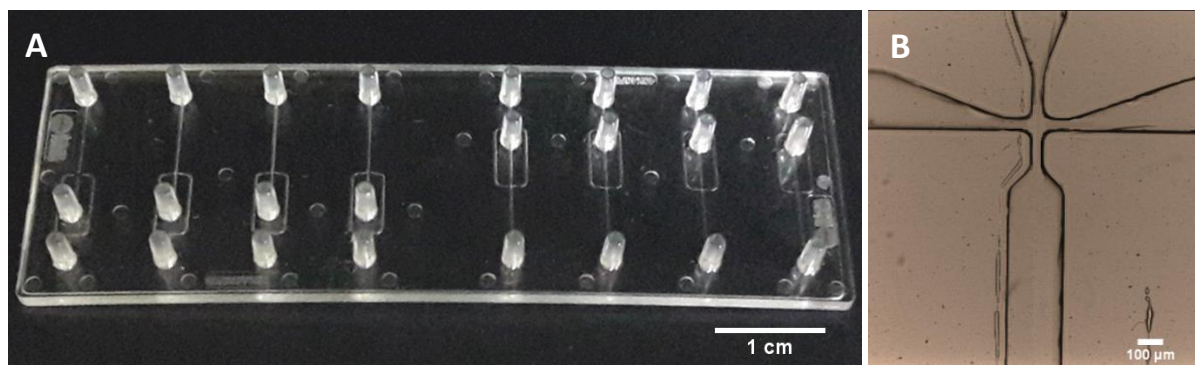
Figure 4.4: A) The cyclic olefin copolymer flow-focusing microfluidic device used for droplet re-injection and BODIPY 505/515 fluorescence detection (flow-focusing junction dimensions: 60 μm x 60 μm x 50 μm(length x width x height)) or 40 μm x40 μm x 30 μm (length x width x height), B) microscope image of the flow-focusing junction of the device (dimensions: 40 μm x40 μm x 30 μm (length x width x height)).

Droplet washing

Pt cells in F/2 medium (1.6 x 10^6 cells/mL) were encapsulated into 45 μm (48 pL) droplets and then 50 μL of the collected droplets were incubated in 50 μL of 150 μM BODIPY 505/515 solution in the dark for two days. The droplets were re-injected in a reservoir device which contained arrays of microfluidic traps. The device was based on the design of Bai *et al*.[194] The droplets were re-injected through one of the inlets at a flow rate of 100 μL/hr, while FC-40 oil with 1% Picosurf surfactant was injected from the second inlet at a flow rate of 300 μL/hr. Once the droplets were immobilised by the microfluidic traps in the device, the flow of droplets into the device was stopped by reducing the injection rate to 0 μL/hr and the flow of oil was reduced to 2 μL/hr. The fluorescence of the encapsulated cells was monitored under the fluorescence microscope.

Dual fluorescence detection

The fluorescence detection set-up was altered, as shown in **figure 4.5**, so that a second PMT could be used to record the fluorescence emitted by the cells at wavelengths above 630 nm.
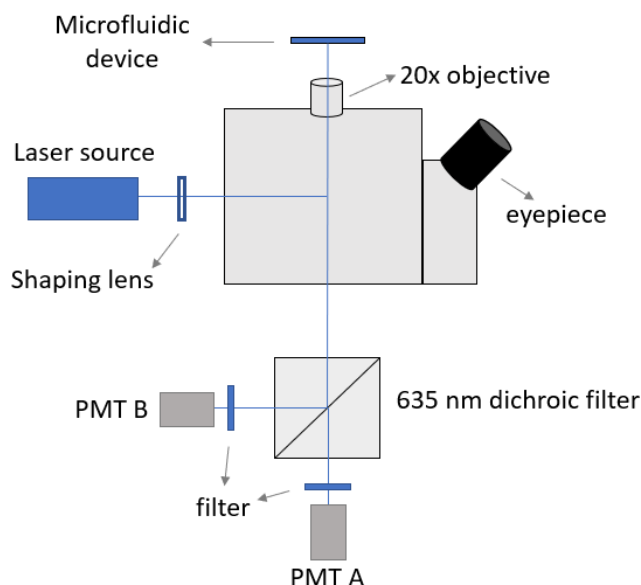
Figure 4.5: Schematic diagram of the set-up used for dual fluorescence detection. The 635 nm dichroic filter splits the signal between the two PMTs. For chlorophyll fluorescence detection, light of wavelength above 635 nm is directed towards PMT A and for BODIPY 505/515 fluorescence detection light of wavelength below 635 nm is directed towards PMT B.

Fluorescence quenching

A stock solution of 50 µM BHQ 1 amine (LGC Biosearch Technologies) in FC 40 was prepared. Different concentrations of the stock solution were mixed with a solution of BODIPY 505/515 in FC-40 so that the final concentration of BODIPY 505/515 in each sample was 60 µM. The fluorescence of the samples was recorded using a plate reader (Fluostar Optima, BMG Labtech, USA) after excitation at 477 nm (bandwidth: 14 nm) using a 525 nm emission filter (bandwidth: 30 nm).

4.3.   Results and discussion

4.3.1.   Staining of encapsulated cells with BODIPY 505/515

A cell staining protocol in microdroplets, first developed by Jie Pan,[192] was used to stain encapsulated *Pt* cells. In accordance with this protocol, instead of staining the cells by adding BODIPY 505/515 in the growth medium and then encapsulating them, the cells were instead encapsulated and then incubated in a solution of BODIPY 505/515 in FC-40, so that they could be stained (**figure 4.6**). Despite the high oil/water partition coefficient of BODIPY 505/515, ta

significant amount of the dye diffused over time from the oil phase to the aqueous phase inside the droplets and eventually accumulated in the lipid bodies inside the cells under a dynamic equilibrium. This staining method was used to avoid the leakage of the fluorescent dye from the aqueous phase to the oil, which would otherwise take place. Jie Pan successfully used this method to stain encapsulated *Chlorella vulgaris* cells. The droplets containing the cells were incubated in a 20 µM solution of BODIPY 505/515 in FC-40 for 1 hour for successful cell staining.[192]
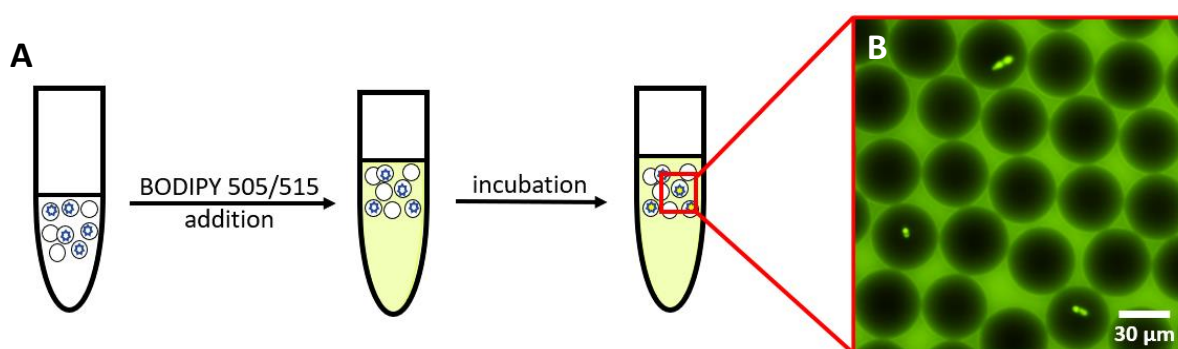
Figure 4.6: A) Schematic diagram of the droplet staining process with BODIPY 505/515 and B) fluorescence image of the encapsulated *Pt* cells after their incubation in a 100 µM solution of BODIPY 505/515 in FC-40 oil.

Pt cells were encapsulated in microdroplets using a 40 µm x 40 µm x 25 µm (length x width x height) flow-focusing device and FC-40 with 1% PicoSurf 1 surfactant as the continuous phase. A 300 µM stock solution of BODIPY 505/515 in FC-40 (with 1% PicoSurf 1 as surfactant) was prepared and dilutions of this stock solution were mixed with the collected droplets at a 1:1 volume ratio to stain the encapsulated cells. Different concentrations of the BODIPY 505/515 solution were tested to determine the ideal concentration for cell staining. The aim was to maximise the fluorescence intensity of the stained lipids, while at the same time keeping the background fluorescence low (**figure 4.7**).
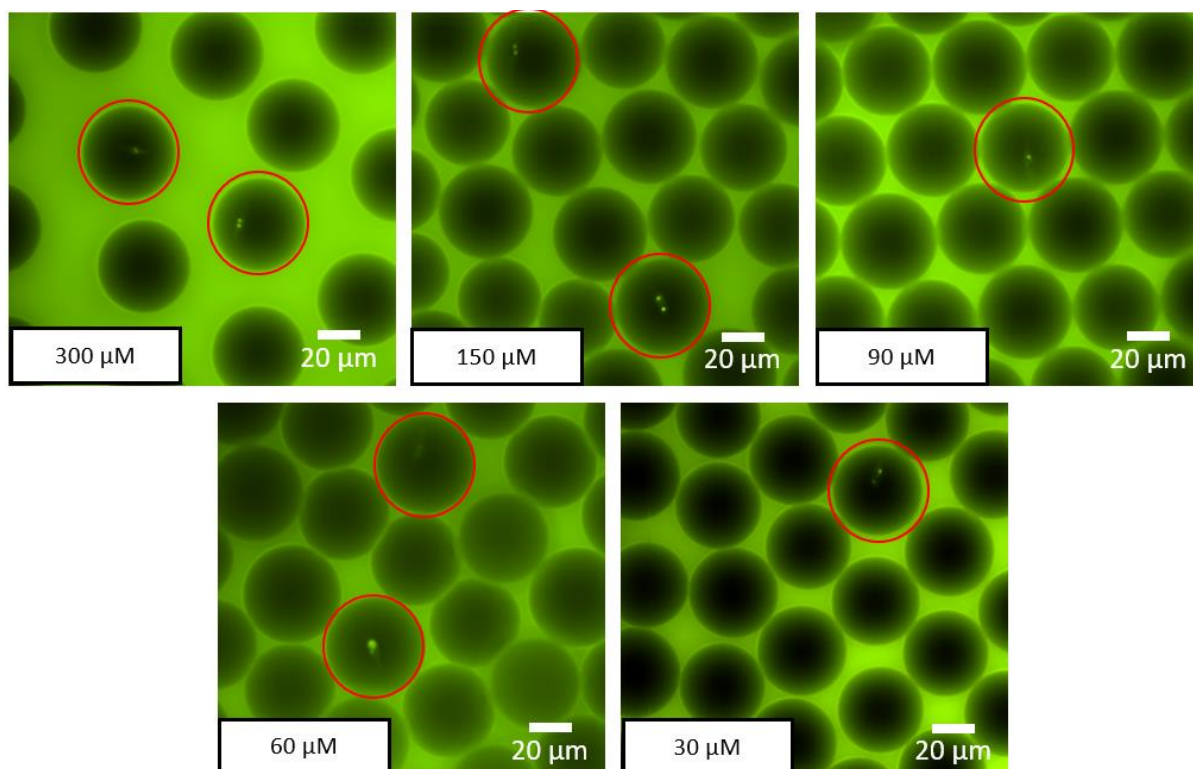
Figure 4.7: Fluorescence imaging of droplets containing single *Pt* cells stained with different concentrations of the BODIPY 505/515 solution: (i) 300 µM, (ii) 150 µM, (iii) 90 µM, (iv) 60 µM and (v) 30 µM. The stained droplets were imaged after 48 hours of incubation in the dark. The droplets that contain cells are indicated by the red circles. The experiment was repeated three times.

The incubation of the droplets in the BODIPY 505/515 solution resulted in successful staining of the intracellular lipids, but also exhibited a strong background fluorescence. The fluorescence images recorded were analysed using ImageJ imaging processing software, however due to the background fluorescence, as well as the fact that this method of fluorescence measurement was not quantitative enough, it was not possible to determine which BODIPY 505/515 solution concentration was most efficient for cell staining.

4.3.2. Droplet staining on-chip

For the staining of the encapsulated cells to take place, BODIPY 505/515 must diffuse from the oil phase surrounding the droplets to the cells inside the droplets. An estimate of the time needed for this diffusion process to take place was generated using *Equation 4.1*:

$$t = \frac{x^2}{6 \cdot D}$$
<div align="right">*(Equation 4.1)*</div>

where t is the time needed for a single molecule to diffuse over a distance x and D is the molecular diffusion coefficient. For this equation to be applied, it was assumed that both the droplets and the cells inside are static, so that diffusion is the only way mixing can take place. The molecular diffusion coefficient of BODIPY 505/515 in aqueous solution has not been calculated before, so an approximate value of 4×10^{-6} cm^2/s was used based on a similar molecular diffusion coefficient value for anthracene (4.2×10^{-6} cm^2/s in water at 25°C).[195] Based on this value of the diffusion coefficient, the time needed for a single BODIPY 505/515 molecule to diffuse from the perimeter to the centre of a 65 μm diameter droplet, was estimated to be 0.4 second. Once the BODIPY 505/515 molecule reaches the cell inside the droplet, however, it will have to cross the cell membrane to stain the intracellular lipids, which is a much slower process. At the same time, only a small amount of the dye will diffuse into the aqueous droplets to begin with, due to the high oil / water partition coefficient of BODIPY 505/515.

To quantitatively determine the rate at which the cells within the droplets were stained, the droplets were incubated on-chip to monitor the change in the cell fluorescence over time. In this case, using a PDMS microfluidic chip for the droplet collection and imaging was not possible, because BODIPY 505/515 is readily absorbed by the PDMS walls of the device, resulting in a high fluorescence background (**figure 4.8**).

To reduce the permeability of PDMS to hydrophobic chemicals, the surface modification of PDMS microfluidic devices has been suggested. A variety of materials have been used to coat PDMS channels, such as transition metal oxides,[196] glass[193] and Teflon.[197,198]
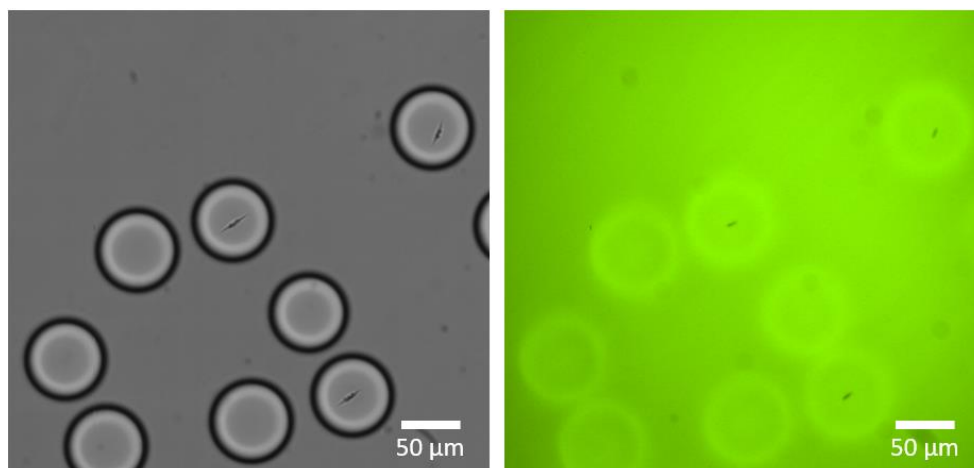
Figure 4.8: Brightfield and fluorescence imaging of 60 µm diameter droplets containing *Pt* cells in F/2 medium. The droplets were incubated in a 30 µM solution of BODIPY 505/515 in FC-40 in a PDMS reservoir device (**Appendix device C**). The images were recorded 5 minutes after the transfer of the droplets to the PDMS device.

To prevent BODIPY 505/515 from leaking into the PDMS, the walls of a PDMS reservoir device were coated with a glass-like layer, using a sol-gel method adapted from Abate *et al*.[193] and subsequently modified by Dr Shaohua Ma.[192] According to this method, a precursor mixture consisting of (heptadecafluoro-1,1,2,2-tetrahydrodecyl)triethoxysilane, tetraethoxysilane (TEOS) and methyltriethoxysilane (MTES) was used to coat the walls of the PDMS reservoir device (height: 75 µm) (**Appendix device C**). Both TEOS and MTES can swell PDMS, so to safely coat the microfluidic device the precursors were oligomerised prior to being injected in the device through an acid-catalysed hydrolysis and condensation reaction (**figure 4.9A**).

The sol mixture was injected to the reservoir device after plasma treatment, so that the silane oligomers could react with the exposed siloxane groups on the PDMS surface. The device was placed on a heated hotplate to initiate the gelation process. At the end of the sol gel coating process the device was filled with a 30 µM BODIPY 505/515 solution in FC-40 and imaged under a fluorescence microscope (**figure 4.9B**). The images showed that the walls of the device were successfully coated, inhibiting the absorption of BODIPY 505/515 by the PDMS.

A   **(i)**   Hydrolysis
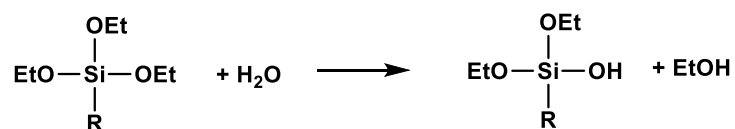
R = OEt or Me

(ii)   Water condensation
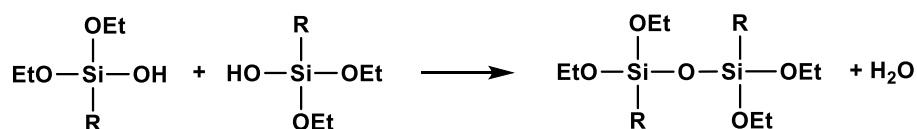
(iii)   Alcohol condensation
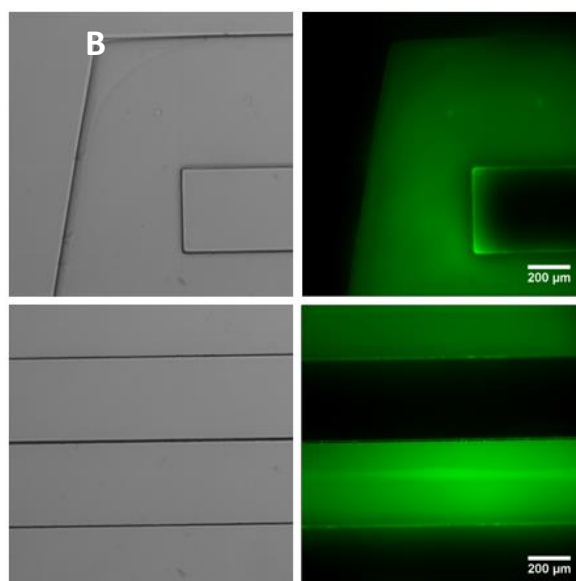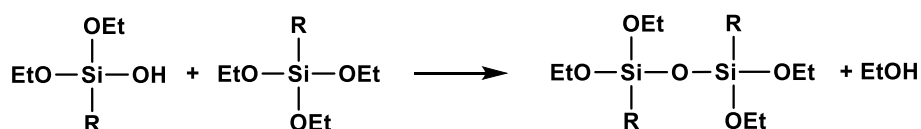
Figure 4.9: A) Oligomerisation of the silane precursors: (i) hydrolysis, (ii) water condensation, (iii) alcohol condensation, adapted from ref.192, B) brightfield and fluorescence images of the coated device after it was filled with a 30 µM BODIPY 505/515 solution in FC-40 (**Appendix device C**).

The inlet of the glass coated reservoir device was connected by tubing to the outlet of a 40 μm x 40 μm x 50 μm flow-focusing droplet generation device. Droplets were generated in the flow-focusing device by injecting a *Pt* cell sample at a flow rate of 350 μL/hr (4.86 cm/s) and using as the continuous phase a 15 μM solution of BODIPY 505/515 in FC-40 with 1 % Picosurf 1 surfactant which was injected in the device at a flow rate of 600 μL/hr (8.35 cm/s). Once the device was full, the inlet and the outlet were sealed by pressing together the walls of the tubing with a hot pair of tweezers and the fluorescence was monitored over time using a fluorescence microscope (**figure 4.10**).

While the glass coating initially slowed down the leakage of the BODIPY 505/515 into the PDMS, a large increase in the background fluorescence was still observed over time. It is thus apparent that dye leakage could still occur through cracks in the coating. An accurate observation of the intracellular fluorescence was therefore not possible. Additionally, due to water evaporation, the droplet size decreased over time. As a result, after just one day in the reservoir, the droplets were much smaller in size and the cells were no longer viable.
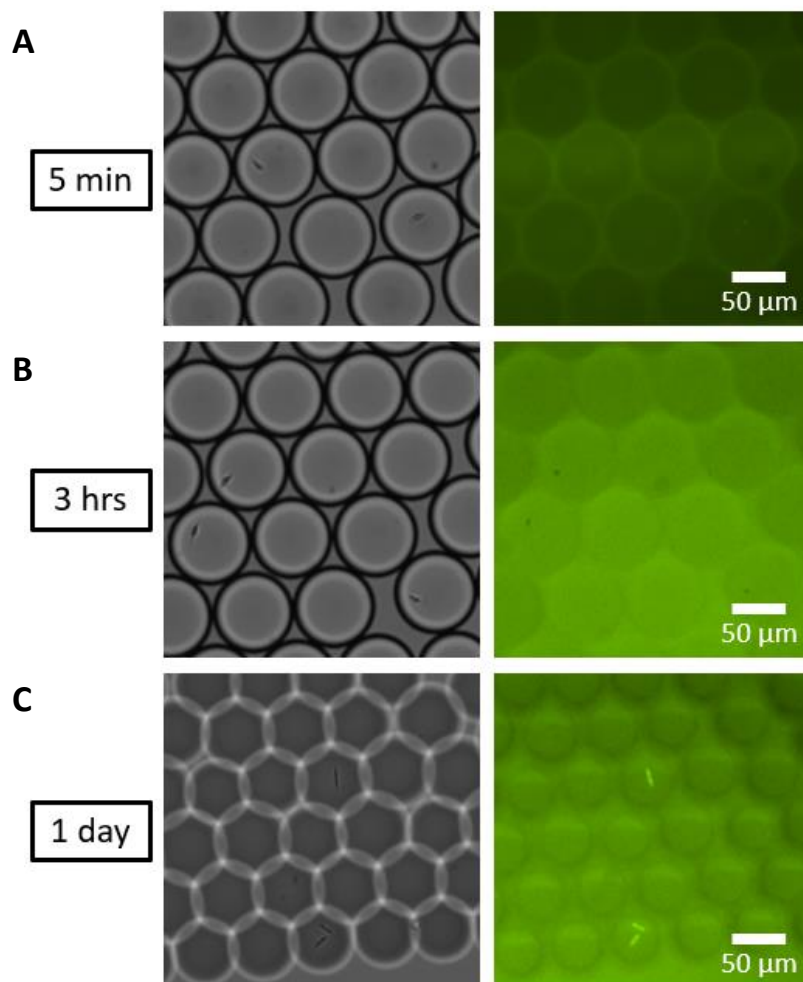
Figure 4.10: Brightfield and fluorescence imaging of 65 µm diameter droplets (144 pL in volume), containing *Pt* cells, that were incubated in a 15 µM solution of BODIPY 505/515 in FC-40 (with 1 % Picosurf 1 surfactant) in the glass-coated reservoir device over A) 5 minutes, B) 3 hours and C) 24 hours. The experiment was conducted twice.

4.3.3. BODIPY 505/515 fluorescence detection with the laser sheet set-up

To quantitatively measure the BODIPY 505/515 fluorescence of the encapsulated cells, after their incubation in the dark, the droplets in the BODIPY 505/515 solution were reinjected in a microfluidic device made from cyclic olefin copolymer (COC), provided by Sphere Fluidics. This device was specifically used, instead of a PDMS device, because the cyclic olefin copolymer was resistant to BODIPY 505/515 adsorption. By using this device, the issue of the BODIPY 505/515 accumulation in the microfluidic channels over time was eliminated, reducing therefore the background fluorescence. The device had two inlets and a flow-focusing geometry. One of the device inlets was used for droplet re-injection and the other

one was used to inject spacing oil, as shown in **figure 4.11A**. The dimensions of the flow-focusing junction were 60 μm x 60 μm x 50 μm (length x width x height). BODIPY 505/515 solution in FC 40, which was used for the incubation step, was also used to space the droplets during the re-injection. The fluorescence was then detected with the laser sheet set-up. Unfortunately, the BODIPY 505/515 dissolved in the incubation oil emitted strong background fluorescence when the laser sheet setup was used to detect the BODIPY 505/515 fluorescence (**figure 4.11B**). The recorded fluorescence intensity trace therefore consisted of a high baseline signal with drops in the fluorescence observed every time droplets flowed past the laser sheet. The background fluorescence from the surrounding oil obscured any fluorescence emitted by the encapsulated cells.
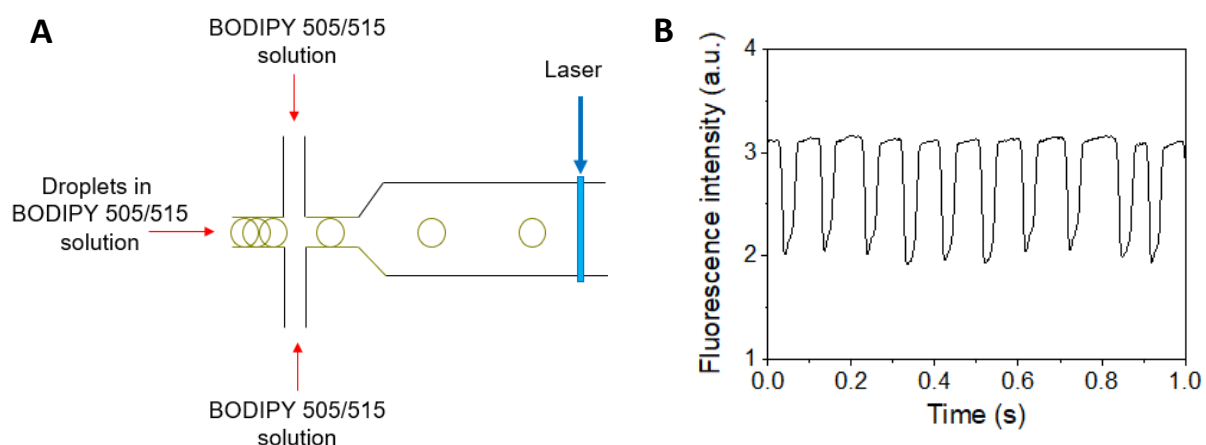
Figure 4.11: A) Diagram showing the reinjection of 65 μm diameter droplets containing *Pt* cells, that were incubated in BODIPY 505/515 solution, into the plastic encapsulation device using a 150 μM solution of BODIPY 505/515 in FC-40 to space out the droplets (microfluidic channel width: 140 μm at the fluorescence detection region), B) the BODIPY 505/515 fluorescence signal detected when the stained microdroplets were reinjected into the plastic microfluidic device.

To determine the BODIPY 505/515 concentration that results in the optimum background fluorescence, Alignflow™ fluorescent beads were encapsulated in microdroplets and incubated in the BODIPY 505/515 solution (**figure 4.12C**). These fluorescent beads emit strong and defined fluorescence, and they were used to bypass the issue of the variability of the fluorescence emitted by each algal cell. It was thereby possible to focus on the background

fluorescence and how it changes when the concentration of BODIPY 505/515 in the oil, as well as the size of the droplets, are varied.
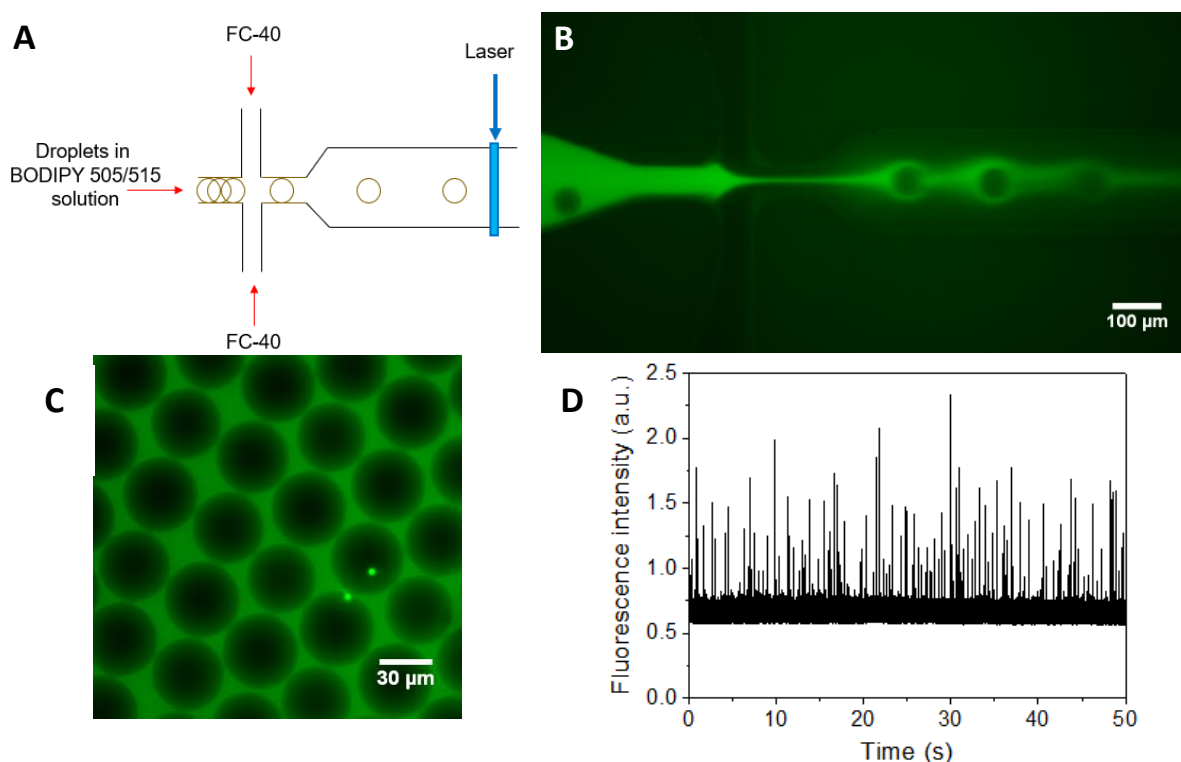
Figure 4.12: A) Diagram showing the reinjection of 65 μm diameter droplets, containing *Pt* cells, that were incubated in BODIPY 505/515 solution, into the plastic encapsulation device using FC-40 to space out the droplets (channel width 140 μm at the fluorescence detection region), B) fluorescence image of the re-injection of aqueous droplets incubated in 150 μM BODIPY 505/515 solution in FC-40 to the plastic device using FC-40 as spacing oil (flow rates: 1 μL/hr droplets, 5 μL/hr FC-40), C) fluorescence image of Alignflow beads encapsulated in aqueous droplets in FC-40 oil containing 30 μM BODIPY 505/515, D) fluorescence trace corresponding to Alignflow beads encapsulated in 65 μm diameter microdroplets, incubated in a 30 μM BODIPY 505/515 solution and then reinjected in a plastic microfluidic device using FC-40 as spacing oil (flow rates: 15 μL/hr droplets (0.59 mm/s at the fluorescence detection point), 150 μL/hr FC-40 (5.94 mm/s)).

The use of FC-40 oil containing BODIPY 505/515 to space the droplets was a major source of background fluorescence, because the laser sheet set-up records the fluorescence emitted along the entire width of the microfluidic channel. To reduce the background fluorescence, FC-40 oil without any BODIPY 505/515 was used to space the droplets during the reinjection

procedure (**figure 4.12A-B**). This resulted in a significant reduction in the background fluorescence. It was determined that, when the beads were encapsulated in 65 μm diameter (144 pL) droplets, incubated in a 30 μM BODIPY 505/515 solution and then reinjected in a plastic microfluidic device using FC-40 as the spacing oil, the background fluorescence was considerably lower than that obtained in the previous attempts and as a result it was possible to distinguish between droplets that contained beads and empty droplets (**figure 4.12D**).

The same set of conditions that resulted in successful bead fluorescence detection, was then used to stain encapsulated *Pt* cells and reinject the microdroplets for fluorescence detection. Peaks corresponding to both empty droplets and droplets with cells inside can be seen in the fluorescence intensity trace recorded over time (**figure 4.13A)**. The peaks that correspond to empty droplets had a peak intensity of approximately 0.9 a.u. (background fluorescence) (**figure 4.13B**). The shape of these peaks was distorted due to the distribution of BODIPY 505/515 dye in the oil surrounding the droplets. As seen in **figure 4.12B**, there was a higher concentration of BODIPY 505/515 at the edges of the droplets resulting in higher fluorescence when those edges passed through the laser sheet. In contrast, the oil surrounding the main body of the droplets contained less BODIPY 505/515, resulting in lower fluorescence. Peaks of higher intensity were also observed, which corresponded to droplets containing cells with high lipid content.

While the fluorescence emitted by *Pt* cells with high lipid content could be successfully detected, the detection of the cells with lower lipid content was difficult, due to the high background fluorescence concealing the weaker fluorescence signals (**figure 4.13A**). The droplets flowed past the laser sheet at a flow rate of 1560 droplets/min. As just 12% of the droplets contained cells, 187 fluorescence signals corresponding to cells should have been observed over 1 minute. However, only 44 distinct peaks per minute were observed, 24% of the expected number of peaks. The staining conditions therefore need further optimisation to achieve a better signal-to-background fluorescence ratio.
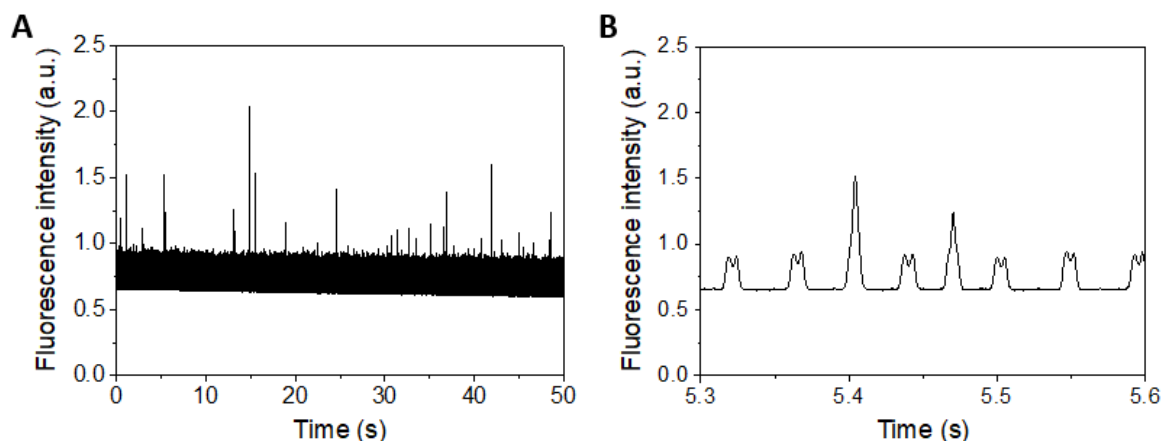
Figure 4.13: Fluorescence signal recorded by the laser sheet setup over A) 50 seconds and B) 0.3 seconds, corresponding to *Pt* cells encapsulated in 65 μm diameter microdroplets, incubated in a 30 μM BODIPY 505/515 solution overnight and then reinjected in a plastic microfluidic device using FC-40 as spacing oil.

4.3.4. Droplet washing

To ensure that the use of spacing oil that does not contain BODIPY 505/515 during re-injection will not affect the fluorescence of the encapsulated cells, an experiment was performed to determine the time needed for the dye to leak out of the encapsulated *Pt* cells when the surrounding oil is replaced by oil without any BODIPY 505/515. To monitor the fluorescence of the encapsulated cells over time, a microfluidic reservoir device containing arrays of traps (**figure 4.14A**) was used to immobilise the droplets. The design of the device was initially used by Bai *et al.*[194]

Pt cells were encapsulated into droplets and then incubated in a 150 μM BODIPY 505/515 solution in the dark for 48 hours. The droplets were re-injected in the device through one of its inlets at a flow rate of 100 μL/hr, while FC-40 oil with 1% Picosurf surfactant was injected from the second inlet at a flow rate of 300 μL/hr. Once the droplets were immobilised by the microfluidic traps in the device (**figure 4.14B**), the flow of droplets into the device was stopped and the flow of oil was reduced to 2 μL/hr to prevent the shearing of the droplets which was observed at higher oil flow rates. The fluorescence of the encapsulated cells was monitored under a fluorescence microscope (**figure 4.14C**) and the fluorescence images recorded were analysed using ImageJ (**figure 4.14D**). The values of fluorescence intensity recorded through this method were impacted by the fact that the cells were not static within

the droplets and they would change positions over time. Despite this source of error, these measurements showed that there was a significant decrease in the cell fluorescence intensity within the span of a few minutes. Furthermore, the time needed for the fluorescent dye to leak out of the cells varied from cell to cell.
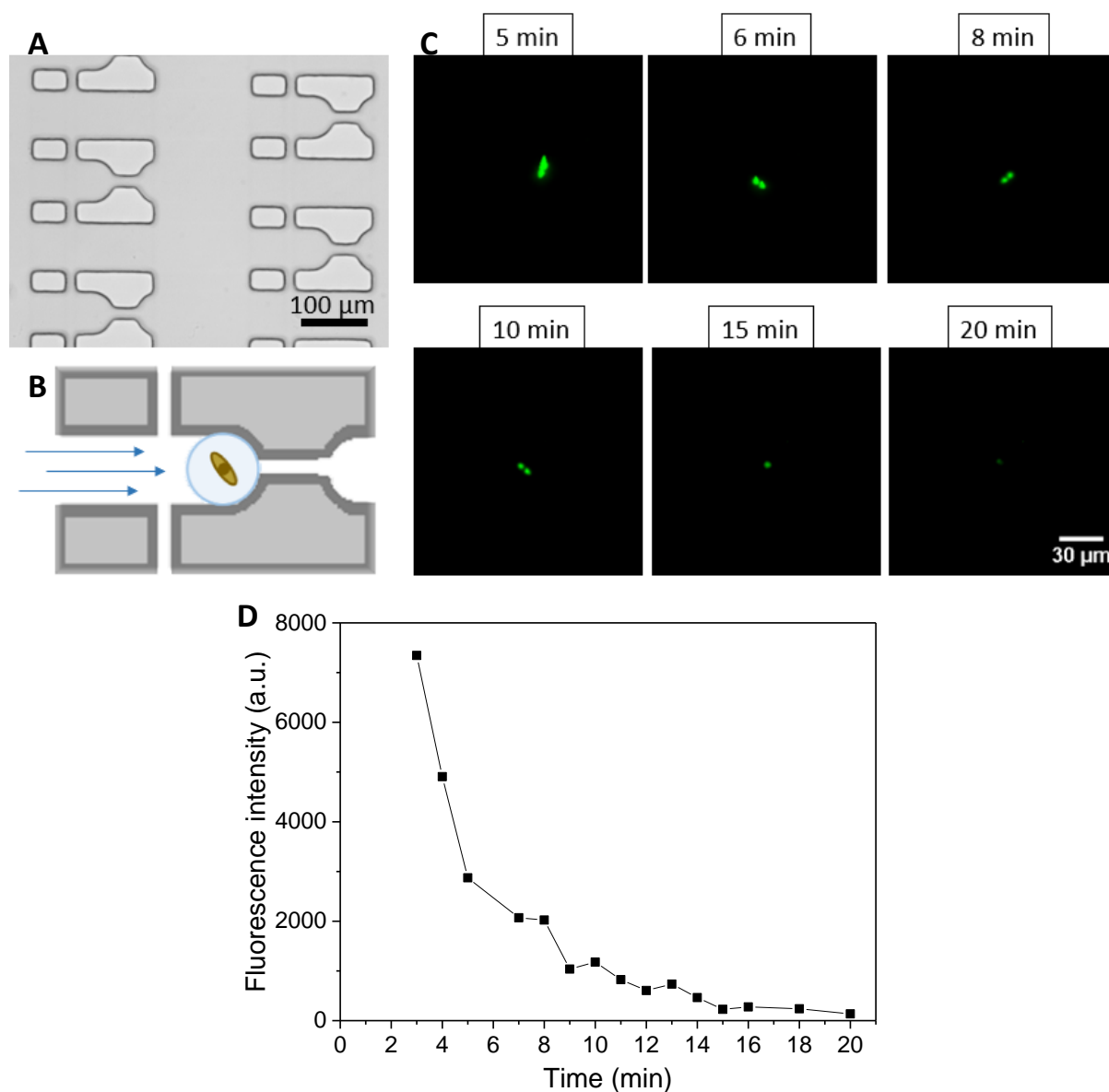
Figure 4.14: A) Microscope image of the microfluidic traps used to immobilise the droplets, B) diagram showing the capture of a droplet containing a Pt cell by the microfluidic trap, C) fluorescence images showing the change in the fluorescence of an encapsulated cell stained with BODIPY 505/515 over time when it is washed with fresh FC-40, D) the fluorescence intensity of the encapsulated cell over time calculated through analysis of the fluorescence images using ImageJ. The experiment was performed twice.

4.3.5. Testing of different droplet staining conditions

The incubation time of the droplets in the dye solution was optimised to maximise the cell fluorescence. *Pt* cells were encapsulated into microdroplets (diameter: 65 μm) and then incubated in a 30 μM BODIPY 505/515 solution for different times, ranging from 1 hour to 48 hours. The fluorescence of each sample of the encapsulated cells was detected using the laser sheet set-up (**figure 4.15**).
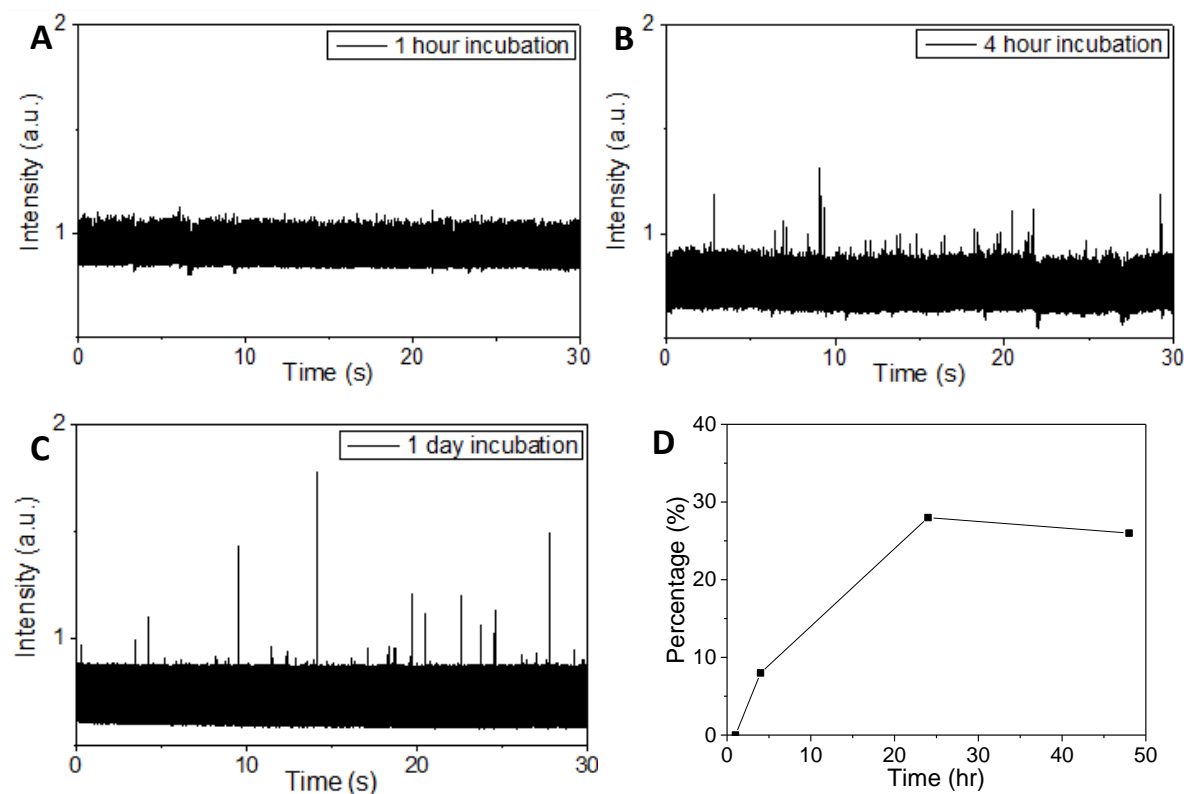
Figure 4.15: BODIPY 505/515 fluorescence signal recorded by laser sheet for cells encapsulated in 65 μm diameter droplets and incubated in a 30 μM BODIPY 505/515 solution for: A) 1 hour, B) 4 hours and C) 24 hours; D) plot of the fractions of the number of detected BODIPY 505/515 fluorescence peaks over the number of expected peaks for each droplet incubation time tested. The experiment was conducted twice.

As 11% of the droplets in the samples contained cells and the droplets were screened at a flow rate of 1920 droplets/min, the number of occupied droplets which result in distinct fluorescence peaks in the fluorescence trace were expected to be approximately 211 per minute. After 1 hour of incubation, the cells were not yet stained by BODIPY 505/515, as no fluorescence peaks could be detected in the fluorescence trace recorded by the laser sheet.

When the incubation time was increased to 4 hours, fluorescence peaks corresponding to cells could be detected. On average, 17 peaks per minute could be seen in the fluorescence trace, a number corresponding to only 8% of the expected number of peaks. After a 24-hour incubation, 44 peaks were recorded on average over one minute, 21% of the expected number of peaks. Longer incubation times did not result in an increase in the fraction of recorded fluorescence peaks. The fluorescence trace of the sample of droplets which were incubated in the BODIPY 505/515 solution for 48 hours displayed on average 43 fluorescence peaks per minute. Based on the fraction of recorded peaks over the number of expected peaks, the optimum incubation time was determined to be 24 hours.

The laser sheet system was also used to assess the effect of the BODIPY 505/515 solution concentration on the staining of the encapsulated cells. *Pt* cells were encapsulated into microdroplets (diameter: 65 μm) and then incubated in BODIPY 505/515 solutions of concentrations ranging from 3 to 50 μM for 24 hours. The fluorescence of each sample was detected using the laser sheet set-up (**figure 4.16**), however the fraction of droplets that resulted in detectable peaks was low for all BODIPY 505/515 concentrations tested. The maximum fraction was observed for the droplets incubated in the 30 μM solution, where approximately 25% of the expected number of BODIPY 505/515 fluorescence peaks was distinct from the background fluorescence. The average amplitude (peak height – baseline) of the detected fluorescence peaks increased with the increase in BODIPY 505/515 concentration for the lower concentrations that were tested (3 and 10 μM), but at higher BODIPY 505/515 concentrations (20 – 50 μM) the average peak amplitude no longer increased (**figure 4.16E**). Occasional changes in the flow of droplets in the microfluidic channel resulted in fluctuations in the baseline fluorescence recorded, as seen in **figure 4.16D**.
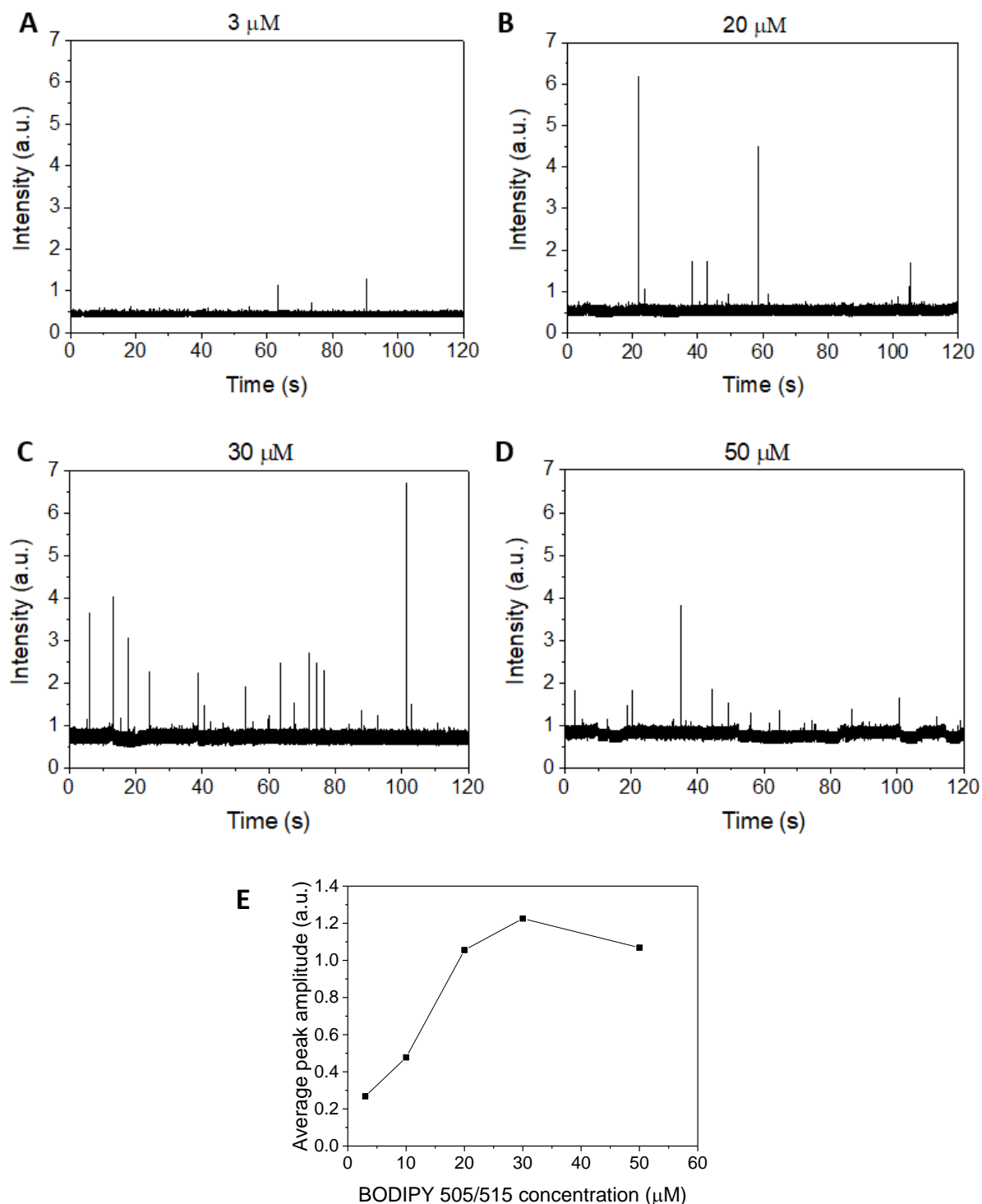
Figure 4.16: BODIPY 505/515 fluorescence signal recorded by laser sheet for cells encapsulated in 65 μm diameter droplets and incubated for 24 hours in BODIPY 505/515 solution of concentration A) 3 μM, B) 20 μM, C) 30 μM and D) 50 μM, E) average amplitude of the peaks in the BODIPY 505/515 fluorescence signals for different concentrations of BODIPY 505/515 in the incubation oil. Each point corresponds to the average of 50 peaks, which correspond to cells. The experiment was repeated three times.

4.3.6. Dual fluorescence detection

In order to eliminate any artifacts and determine the exact fraction of cells that result in a detectable peak in the BODIPY 505/515 fluorescence trace, chlorophyll fluorescence detection was used in conjunction with BODIPY 505/515 fluorescence detection, to determine which droplets contain cells. This was done by altering the fluorescence detection set-up so that a second photomultiplier tube (PMT) could be used to record the fluorescence emitted by the cells at wavelengths above 630 nm. The chlorophyll fluorescence trace obtained by the second PMT was used to identify the droplets which contained *Pt* cells. The chlorophyll fluorescence signal was then compared to the recorded BODIPY 505/515 fluorescence to determine the fraction of cells that emitted detectable BODIPY 505/515 fluorescence (**figure 4.17**). The percentage of BODIPY 505/515 fluorescence peaks relative to chlorophyll fluorescence peaks was found to be approximately 30%. This was because the BODIPY 505/515 fluorescence emitted by most cells was still weaker than the background fluorescence. This could be due to these cells having low lipid content or due to the cells not being fully stained by BODIPY 505/515 even after extended incubation in the BODIPY 505/515 solution.
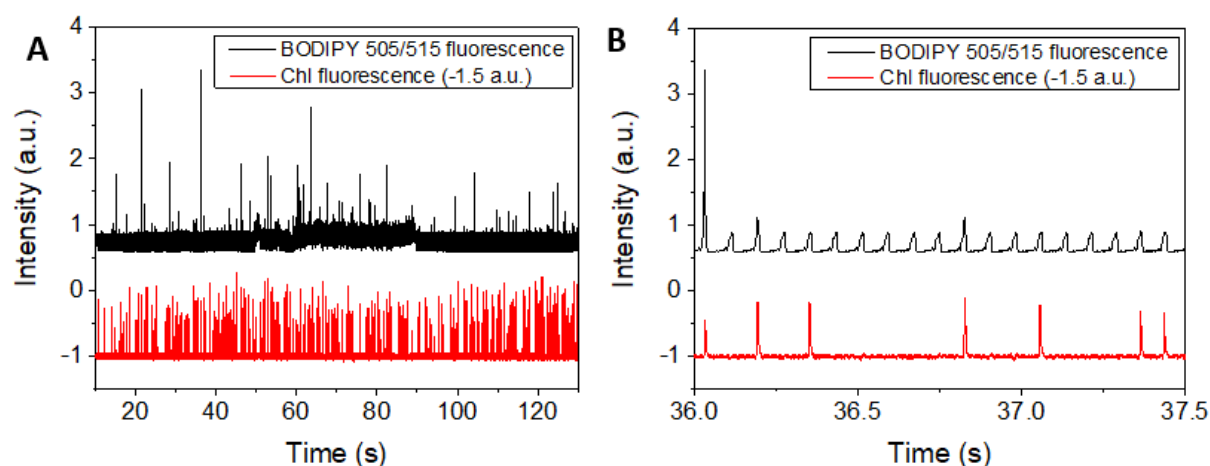
Figure 4.17: Fluorescence trace overlay showing the BODIPY 505/515 (black) fluorescence and the corresponding chlorophyll fluorescence (red) recorded by laser sheet over A) 2 minutes and B) 1.5 seconds, for cells encapsulated in 65 μm diameter droplets that were incubated in a 30μM BODIPY 505/515 solution for 24 hours. The BODIPY 505/515 fluorescence was recorded using a 525 nm (bandwidth: 39 nm) emission filter, while chlorophyll fluorescence was recorded using a 635 nm long pass filter. The experiment was performed twice.

To test whether the fluorescence signals emitted by the cells could be increased, dual fluorescence detection was applied to droplets incubated in a higher concentration of BODIPY 505/515 (60 µM) (**figure 4.18A**) and the fraction of cells that resulted in a detectable BODIPY 505/515 peak was calculated and compared to the fraction obtained at lower concentrations of BODIPY 505/515 (20 µM and 30 µM). However, for the droplets incubated in the 60 µM BODIPY 505/515 solution the fraction of cells that resulted in detectable BODIPY 505/515 fluorescence peaks was only 33%, a result similar to that of the droplets incubated in a 30 µM BODIPY 505/515 solution (**figure 4.18B**).
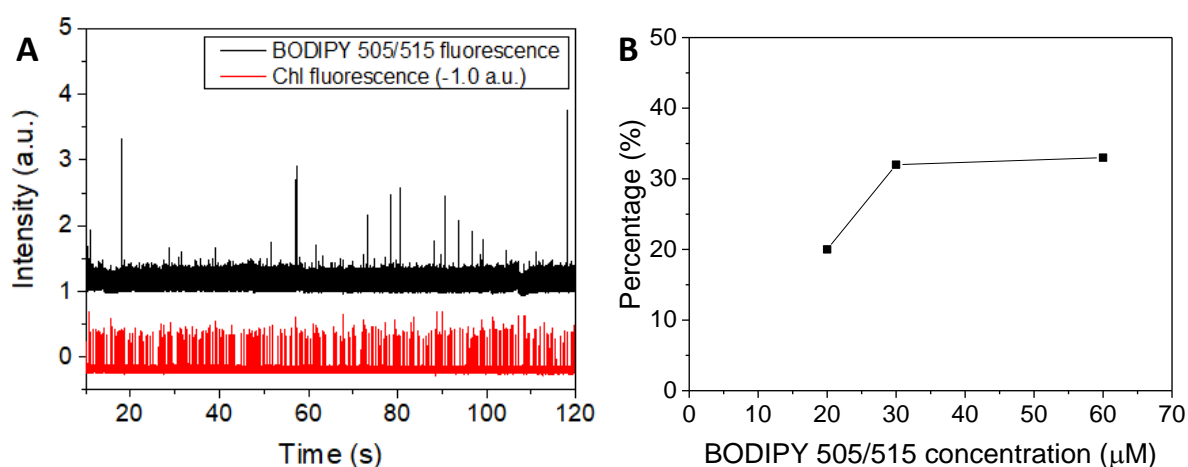
Figure 4.18: A) Fluorescence trace overlay showing the BODIPY 505/515 (black) fluorescence, and the corresponding chlorophyll fluorescence (red), recorded by the laser sheet set-up for cells encapsulated in 65 µm diameter droplets that were incubated in a 60µM BODIPY 505/515 solution for 24 hours, B) plot of the percentages of chlorophyll fluorescence peaks that had a distinct corresponding BODIPY 505/515 fluorescence peak at different concentrations of BODIPY 505/515 in the incubation oil. Each point corresponds to the average of two measurements.

An alternative cell staining method was then tested in an effort to improve the cell staining efficiency. *Pt* cells were stained using a solution of BODIPY 505/515 in DMSO prior to their encapsulation into droplets. The staining conditions used were those suggested as optimal for the staining of *Pt* cells by Wu *et al*. (0.075 µg/mL).[200] The cells were then encapsulated in 65 µm droplets which were transferred to the 30 µM BODIPY 505/515 solution usually used for incubation. The fluorescence of the droplets was finally detected using the laser sheet set-up (**figure 4.19**). While some peaks corresponding to stained cells could be detected, the

peaks were weak and close in magnitude to the background fluorescence. Only 40% of the droplets containing cells resulted in a detectable BODIPY 505/515 fluorescence peak higher than the background fluorescence. It is likely that some of the fluorescence of the stained cells was lost during their encapsulation into droplets due to the BODIPY 505/515 leaking out of the droplets and into the oil phase. This also likely contributed to a higher background fluorescence. These results showed that staining the cells before encapsulating them into the droplets was not a viable method to improve the cell staining efficiency.
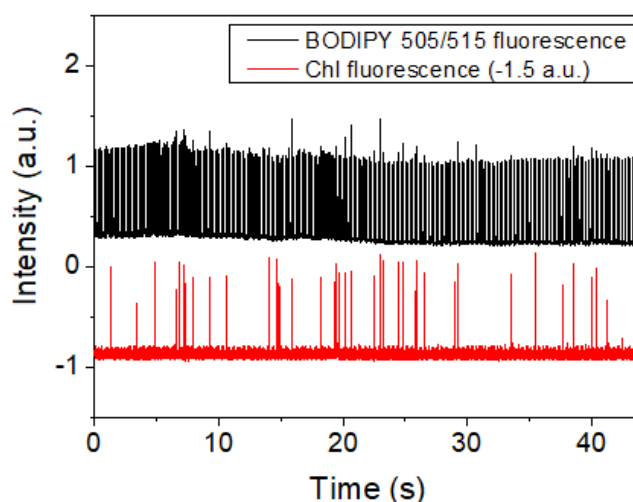
Figure 4.19: Fluorescence trace overlay showing the BODIPY 505/515 (black) fluorescence and the corresponding chlorophyll fluorescence (red) recorded by the laser sheet set-up for cells stained with BODIPY 505/515 in DMSO before being encapsulated in 65 μm diameter droplets and then incubated in 30 μM BODIPY 505/515 solution in FC-40 for one hour. The BODIPY 505/515 fluorescence was recorded using a 525 nm (bandwidth: 39 nm) emission filter, while chlorophyll fluorescence was recorded using a 635 nm long pass filter. The experiment was conducted twice.

4.3.7. BODIPY 505/515 fluorescence detection in narrow channel

To further reduce the BODIPY 505/515 fluorescence background, a microfluidic device with a narrower channel was used for the droplet re-injection. When the droplets flow through a narrow channel which has a smaller cross-section than the droplet diameter, there is less oil between the droplets and the channel wall. This could help to further reduce the background fluorescence. The device used for the droplet re-injection was a cyclic olefin copolymer

microfluidic device, similar to that used in previous experiments (see section 4.4), however the dimensions of the flow-focusing region of the device were 40 μm x 40 μm x 30 μm (length x width x height) (**figure 4.20B**). This device was also provided by Sphere Fluidics.

Pt cells were encapsulated in 65 μm diameter droplets and they were incubated overnight in a 30 μM solution of BODIPY 505/515 in FC-40. The stained droplets were subsequently injected in the device for fluorescence detection using the laser-sheet set-up, as shown in **figure 4.20A**. Lower flow rates were used for the re-injection process to prevent droplet splitting from taking place at the flow-focusing junction. FC-40 oil was used to space out the droplets.
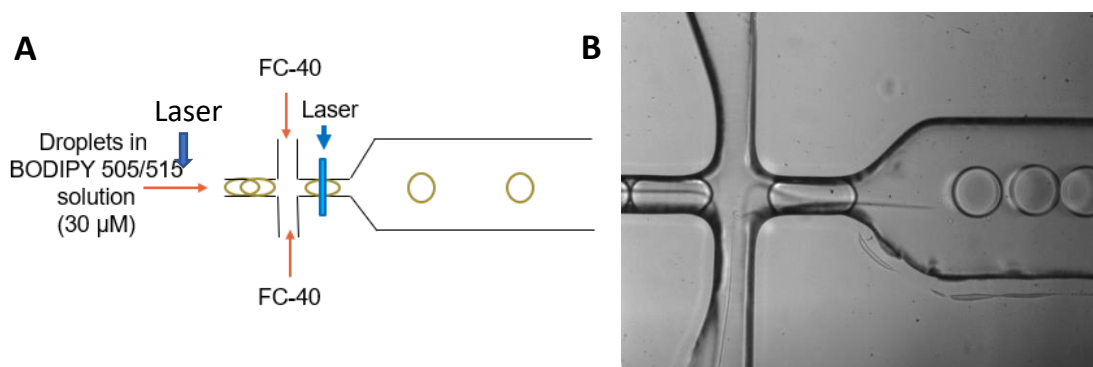
Figure 4.20: A) Schematic diagram showing the reinjection of droplets into the plastic encapsulation device, B) microscope image of the microfluidic device during droplet re-injection and fluorescence detection (droplet diameter: 65 μm, microfluidic channel dimensions at the flow focusing region: 40 μm x40 μm x 30 μm (length x width x height), droplet flow rate: 8 μL/hr (approximately 1.85 mm/s at the detection point), spacing oil flow rate: 25 μL/hr(5.79 mm/s)).

The background BODIPY 505/515 fluorescence was similar in magnitude to the intracellular fluorescence, however due to the lower flow rate used during the re-injection procedure, it was possible to distinguish the peaks corresponding to cells from the background droplet fluorescence since they were higher in magnitude than the background (**figure 4.21**). For droplet screening and sorting to be feasible, the background fluorescence should be reduced further.
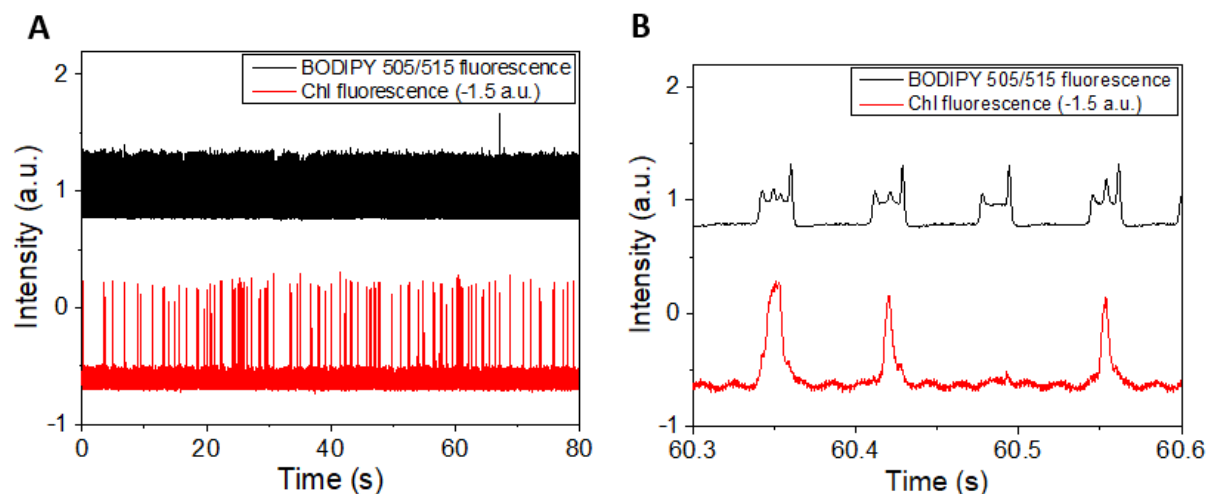
Figure 4.21: Overlay of the BODIPY 505/515 and the chlorophyll fluorescence traces of 65 μm diameter droplets, containing *Pt* cells, as they flowed through the flow focusing region of the plastic device with dimensions 40 μm x 40 μm x 30 μm (length x width x height) (droplet flow rate: 8 μL/hr (1.85 mm/s), FC-40 flow rate: 25 μL/hr (5.79 mm/s)). Prior to the fluorescence detection, the droplets were incubated overnight in a 30 μM solution of BODIPY 505/515. The traces were recorded over A) 80 seconds and B) 0.3 seconds. The BODIPY 505/515 fluorescence was filtered with a 525 nm (bandwidth: 39 nm) emission filter, while chlorophyll fluorescence was recorded using a 635 nm long pass filter. The experiment was conducted three times.

4.3.8. Fluorescence quenching

To test whether the background fluorescence can be reduced any further, the possibility of adding a fluorescence quencher in the oil phase was examined. Fluorescence quenchers are molecules that absorb excitation energy from a fluorophore and re-emit most of this energy as light of a different wavelength, whereas dark quenchers disperse the energy non-radiatively as heat. As a result, the intensity of the fluorescence emitted by the fluorophore is reduced. To achieve efficient fluorescence quenching, there must be significant spectral overlap between the emission spectrum of the donor and the absorption spectrum of the acceptor. Additionally, the donor and the acceptor must be in close contact to each other.

The kinetics of the quenching process follows the Stern-Volmer relationship (*Equation 4.2*):[150]

$$\frac{I_0}{I} = 1 + k_q \tau_0 [Q]$$ *(Equation 4.2)*

where I_0 is the fluorescence intensity without the addition of the quencher, I is the fluorescence intensity after the addition of the quencher, k_q is the quencher rate coefficient, τ_0 is the lifetime of the emissive excited state without any quencher present and $[Q]$ is the concentration of the quencher.

Several dark quenchers can be used to quench fluorescence in the 500 – 550 nm range (**table 4.1**). A dark quencher was preferred over a fluorescent quencher for the quenching of BODIPY 505/515 fluorescence in our system, since any fluorescence emitted by the quencher would interfere with other useful fluorescence readings, such as the detection of the chlorophyll fluorescence.

Table 4.1: **Dark quenchers that absorb in the green fluorescence range (500 – 550 nm)**

Quencher	Absorption maximum / nm	Quenching range / nm
BHQ 1 (Black hole quencher 1)	534	480 – 580
Dabcyl	453	400 – 550
Eclipse	522	390 – 625
TQ2 (Tide quencher 2)	531	440 – 580
Iowa Black FQ	531	420 – 620
QSY 7	560	500 – 600

Black hole quencher 1 (BHQ1, **figure 4.22A**) was selected as the quencher due to its favourable spectral properties. With an absorption maximum at 534 nm, BHQ1 can efficiently quench fluorescence in the 480 – 580 nm range. As shown in **figure 4.22B**, the absorption spectrum of BHQ1 and the emission spectrum of BODIPY 505/515 in FC-40 were recorded and there was a significant overlap between the two spectra.
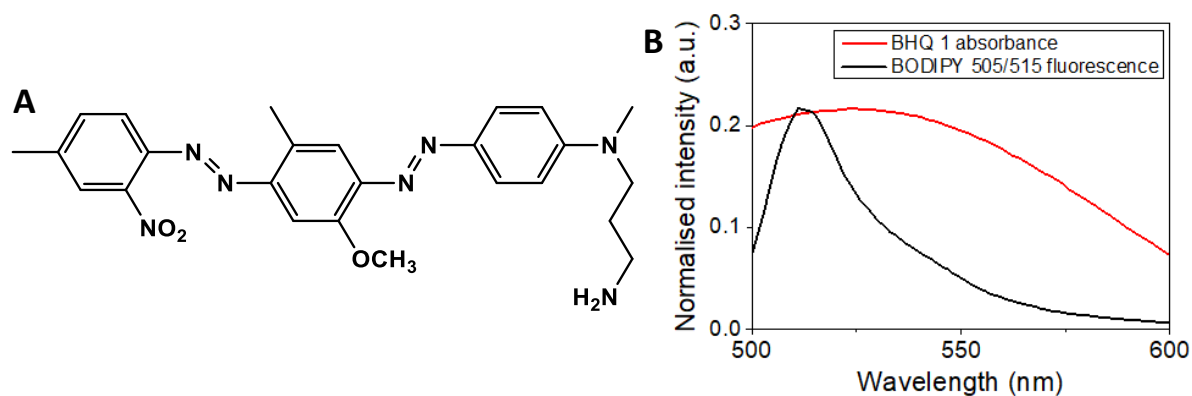
Figure 4.22: A) The structure of BHQ 1 amine, B) normalised plot showing the overlap between the absorption spectrum of BHQ 1 solution in FC 40 and the emission spectrum of BODIPY 505/515 in FC 40 in the 500 nm to 600 nm region.

A stock solution of 50 µM BHQ 1 in FC-40 was prepared. Unfortunately, a more concentrated stock solution could not be obtained due to the low solubility of BHQ 1 in the fluorinated FC-40 oil. Subsequently, a solution of BODIPY 505/515 in FC-40 with 1 % Picosurf 1 surfactant was combined with different concentrations of the BHQ 1 stock solution to observe the effect of the quencher concentration on the fluorescence emitted (**figure 4.23**). The final concentration of BODIPY 505/515 in each sample was 60 µM. At the highest concentration of quencher that could be used (40 µM), the I_0/I ratio was just 1.90. This test showed that, due to the low solubility of the quencher in FC 40, the maximum quenching efficiency (calculated as $\frac{I_0 - I}{I_0} \times 100$) that could be achieved was 47% in the presence of 40 µM BHQ 1.
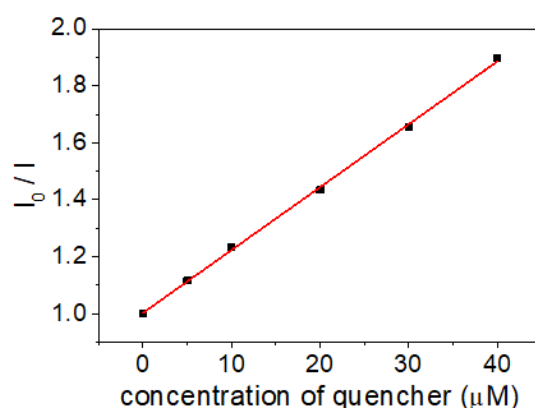
Figure 4.23: Stern-Volmer plot of the change in fluorescence as a function of the concentration of BHQ 1 in a 60 µM solution of BODIPY 505/515. Fluorescence measurements were performed in triplicate.

The stock BHQ1 solution in FC-40 was used to space the droplets during their re-injection, to test whether the quencher solution can reduce the fluorescence background during the droplet fluorescence detection. Unfortunately, the baseline fluorescence signal was not stable during the re-injection and, on average, the background fluorescence remained high despite the addition of the quencher. This indicates that the quenching achieved by the addition of BHQ 1 was too weak. Better quenching could be potentially achieved by identifying a dark quencher which is more soluble in FC-40 than BHQ 1. Such a quencher was not identified during the course of the project, however further investigations could reveal an appropriate quencher given sufficient time.

4.4. Conclusions

The experiments conducted in this chapter aimed towards the development of a droplet microfluidic platform for the screening of algal cells based on their lipid content. Such a platform would be very useful in the effort to screen mutagenized cell populations to identify cell variants that express more lipids. While flow cytometry and FACS have been used in the past to screen algal cell populations based on their lipid content, the use of droplet microfluidics would offer additional advantages. As the cells are encapsulated into droplets, the lipid content of the cells can be monitored in real time while the cellular environment is precisely controlled. In this fashion, cells could be identified that produce a given amount of lipids more quickly or that display enhanced lipid production under a given stimulus.

In this chapter, a novel method was used to stain *Pt* cells encapsulated in microdroplets with BODIPY 505/515. The cells were initially encapsulated in microdroplets which were then transferred in a solution of BODIPY 505/515 in FC-40 so that they could be stained. The diffusion of the dye to and from the droplets was studied by fluorescence imaging. Furthermore, the BODIPY 505/515 fluorescence of the stained droplets was detected with the laser sheet platform established in Chapter 3. The quantitative measurement of the cell fluorescence was not possible due to the high fluorescence background caused by dye dissolved in the oil surrounding the droplets. Several experimental parameters, such as the BODIPY 505/515 concentration, the incubation time, the spacing oil used during the re-injection procedure, and the microfluidic channel width, were modified in an effort to reduce

the background fluorescence. The optimal conditions identified after this effort were the incubation of the droplets in 30 µM BODIPY 505/515 solution in FC-40 for 24 hours, then reinjection of the droplets for fluorescence detection using FC-40 as spacing oil. Re-injecting the droplets through a microfluidic channel that was narrower than the droplet diameter was shown to result in better fluorescence detection.

Besides resulting in a high fluorescence background, the method used to stain the algal cells with BODIPY 505/515 in this chapter was also inefficient when compared to standard methods used to stain cells in bulk solution. Whereas a solution of BODIPY 505/515 in DMSO or a similar organic solvent can be used to successfully stain cells in bulk within less than 10 minutes,[186] the cells in the droplets were stained over multiple hours, as the diffusion of the dye into the droplets was very slow. On the other hand, staining the cells before their encapsulation into droplets is not effective, as the dye leaks out of the cells and into the oil phase surrounding the droplets.

CHAPTER 5

Algal cell staining using micelle / hydrogel composite beads

5.1.   Introduction

The delivery of lipophilic compounds to cells is often hindered by the low solubility of the compounds in aqueous environments. This is a limitation that is readily apparent in cell staining, when lipophilic dyes are used to study cells. It was particularly evident in the experiments conducted in Chapter 4, which were negatively impacted by the inefficient staining of the encapsulated cells with the lipophilic dye, as well as by the leakage of the dye into the oil surrounding the droplets. These issues highlighted the necessity of using a more efficient method to stain the encapsulated cells, as well as ensuring that the cells will remain stained by the dye for longer. The use of beads loaded with dye was thereby proposed. These beads would be co-encapsulated with the cells in the droplets and would serve as localized deposits of the dye. The dye would be slowly and sustainably released from the beads over time, staining the cells and counteracting any loss of dye which takes place due to leakage onto the oil phase.

As seen in Chapter 4, BODIPY 505/515 is a lipophilic dye that is widely used to stain intracellular lipids; however, its hydrophobic nature means that it is only slightly soluble in aqueous solutions. To improve the solubility of lipophilic dyes in bulk solution and their delivery to cells, organic solvents are usually used, such as ethanol,[201,202] acetone[202] and DMSO.[186,201] However, these solvents often compromise the viability of the cells.[201] Several studies have been conducted to determine the optimal conditions for the staining of different cell strains with BODIPY 505/515.[185,186,200,203,204] These conditions should result in maximum cell fluorescence, while at the same time ensuring that the viability of the cells is not affected. However, these staining conditions vary greatly in the literature, depending on the type of cells being stained, the dye and the solvent used.

As the use of organic solvents to improve the solubility of lipophilic dyes has negative effects on the cells, aqueous systems containing appropriate aggregates that work as dye delivery vehicles to the cells have been explored as more biocompatible alternatives.[205] A variety of hydrophobic compound delivery systems have been developed, such as polymer-drug

111

conjugates,[206] liposomes,[207] nanoparticles,[208] microgels[209] and polymeric micelles.[210] Such systems are frequently used in drug delivery applications due to the hydrophobic nature of many drugs.

5.1.1. Hydrogels

Hydrogels are crosslinked polymer networks that swell when in the presence of water due to their hydrophilic nature. Hydrogel materials are highly useful in biotechnological applications due to their biocompatibility, their swelling behaviour in aqueous environments, their high porosity and their highly tuneable nature.[211] Due to these characteristics, they have been used extensively as drug carriers, biosensors, tissue engineering scaffolds etc.[212-214] The properties of hydrogel materials can be modified by changing some parameters of the constituent polymers, such as the molecular weight, the polarity, the charge and the amount of crosslinking.[215,216]

Hydrogels are particularly useful as delivery vehicles, as compounds of interest can be easily incorporated in their matrix. There are three major strategies which are used to load cargo into hydrogels. The first strategy is encapsulation, where the cargo is physically trapped within the cross-linked polymer matrix. The second strategy is tethering, in which a covalent interaction binds the cargo to the hydrogel and the last strategy is affinity binding, where the cargo is incorporated in the matrix due to electrostatic, hydrophobic or peptide interactions.[217] The hydrogel then provides spatial and temporal control over the release of the cargo.[218]

Natural polymers, such as hyaluronic acid,[219] dextran[220] and carboxymethyl cellulose (CMC),[221] are often used to fabricate hydrogels due to their inherent biocompatibility. However, a range of biocompatible synthetic polymers, such as poly(ethylene glycol) (PEG)[222] and poly(vinyl alcohol) (PVA),[223] are also frequently used as they can be easily modified, their mechanical properties can be tuned and they offer limited batch-to-batch variation.[217]

5.1.1.1.   Droplet microfluidics for the generation of biomaterials

Droplet microfluidics is frequently used in materials generation and microfabrication because it provides a high degree of control when working in micro dimensions. Traditional methods used to prepare particulate materials, such as mechanical agitation, precipitation, seeding

polymerisation, emulsion polymerisation etc., often suffer from a lack of control over the particle size and morphology, resulting in a heterogeneity in the particles generated which is undesirable in many applications.[224] In microfluidics the size and the composition of the materials can be tuned by precisely controlling parameters such as the dimensions of the microfluidic device, the flow rates of the continuous and the dispersed phase, the viscosity and the interfacial tension.[224,225] As a result, using microfluidics, a variety of materials can be generated, ranging from microparticles of various shapes, to microfibers and to complex three-dimensional constructs (**figure 5.1**).
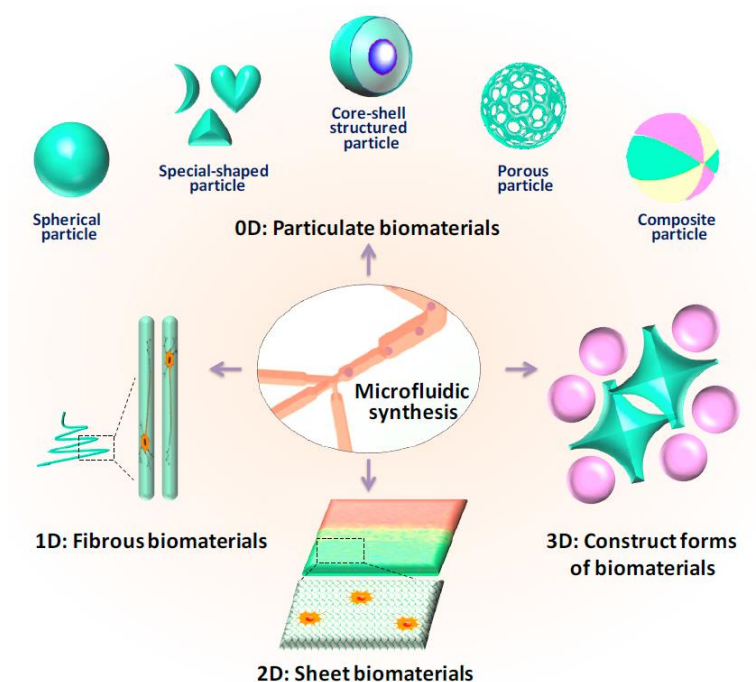
Figure 5.1 : Biomaterials engineered from microfluidics, ranging from particulate biomaterials to three-dimensional constructs, adapted from ref.224.

Hydrogel micromaterials can be easily fabricated using microfluidic technology. The polymer precursors used to form the hydrogel are injected into the appropriate microfluidic device while they are still liquid. Crosslinking of the hydrogel precursors takes place after they have been mixed and they have been given the desired shape by the microfluidic device. Various crosslinking mechanisms have been used to form the hydrogel network, such as Michael-type addition reactions, photo-crosslinking, thermal crosslinking, or enzymatic crosslinking.[226]

5.1.2. Polymeric micelles for hydrophobic compound delivery

Hydrogels are widely used for the delivery of hydrophilic compounds, which can be easily loaded onto the hydrogels due to the hydrophilic nature of the polymer matrix. This hydrophilic nature, however, results in limitations to the quantity of hydrophobic compounds that can be loaded onto the hydrogels. To increase the ability of the hydrogels to uptake and deliver hydrophobic compounds, it is necessary to modify the hydrogels so that they are more hydrophobic in nature. Two main approaches have been used for this purpose. The first approach is the introduction of hydrophobic domains in the hydrogel structure, either by crosslinking the hydrophilic polymer chains with hydrophobic ones or by incorporating molecules that form inclusion complexes within the hydrogel matrix. The second approach involves the introduction of nanoparticles or micelles to the hydrogel matrix.[227]

Polymeric micelles, which are formed through the self-assembly of amphiphilic block co-polymers in aqueous solution, can be efficiently used as delivery systems. The polymers which can be used to form micelles are di- or tri-block co-polymers which consist of hydrophobic and hydrophilic parts.[210] Once the concentration of these polymers in aqueous solution exceeds a certain concentration, known as the critical micelle concentration, these polymers self-assemble so that they form a hydrophobic core with a hydrophilic shell (corona) surrounding it[228] (**figure 5.2**). In this fashion, the hydrophilic polymer chains prevent the hydrophobic chains from interacting with the water. The micelles have the ability to capture hydrophobic compounds in their hydrophobic core and to stabilise them in the aqueous environment.[229]
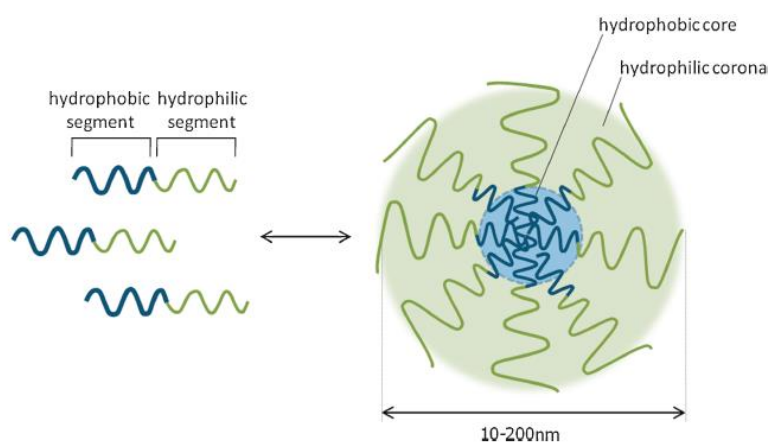
Figure 5.2: Schematic illustration of amphiphilic polymer self-assembly in aqueous solution to form micelles, adapted from ref.210.

Polymeric micelles offer multiple advantages that make them a popular choice as delivery vehicles. They have lower critical micelle concentrations and are generally more stable than micelles formed by small molecule surfactants,[230] leading to increased delivery efficiency and specificity.[231] Furthermore, their small size (10-200 nm) and narrow size distribution make them ideal for drug delivery applications where their ability to penetrate into tissues improves the performance of the drugs in vivo.[231] More recently, research focus has shifted to the development of stimuli-responsive micelles, which release their cargo once exposed to specific environmental stimuli, such as pH or temperature variation.[232,233] This approach increases the specificity of drug release, as only afflicted areas are targeted by the drug and any related side-effects are reduced.[233]

Hydrophobic dyes, such as Nile Red, rhodamine or pyrene, are frequently incorporated into micelles, as a tool to investigate micelle behaviour and to assess their potential as drug delivery vehicles.[234] The dyes can be used to detect changes in the environmental polarity and, as a result, reveal information about the CMC of the micelles[234,235] and about specific interactions within the micelle microenvironment.[236] The micelles have also been used to effectively deliver hydrophobic dyes to cells, however their presence in the aqueous cell medium can result in a high fluorescence background.[205] To eliminate this issue, a method is required to ensure the efficient removal of excess micelles from the solution after the cell staining.

Herein, the formation of micelle/hydrogel composite beads loaded with BODIPY 505/515 is proposed, for the controlled delivery of the dye to cells in aqueous solution without the use of organic solvent (**figure 5.3**). By combining micelles with hydrogel technology, the advantages of both systems can be exploited. The incorporation of the micelles in the hydrogel matrix results in the formation of hydrophobic domains in the hydrophilic hydrogel, thus enhancing the loading capacity of the hydrogel and enabling the uptake of the hydrophobic dye.[227,237] On the other hand, the hydrogel scaffold can prevent the micelles from escaping into the solution during cell staining, thereby reducing the background fluorescence. Instead, the BODIPY 505/515 is released from the micelles into the solution surrounding the beads and then into the cells, where it accumulates in the intracellular lipid bodies. After the completion of the staining process, the beads can be removed easily from the cell sample by filtration.
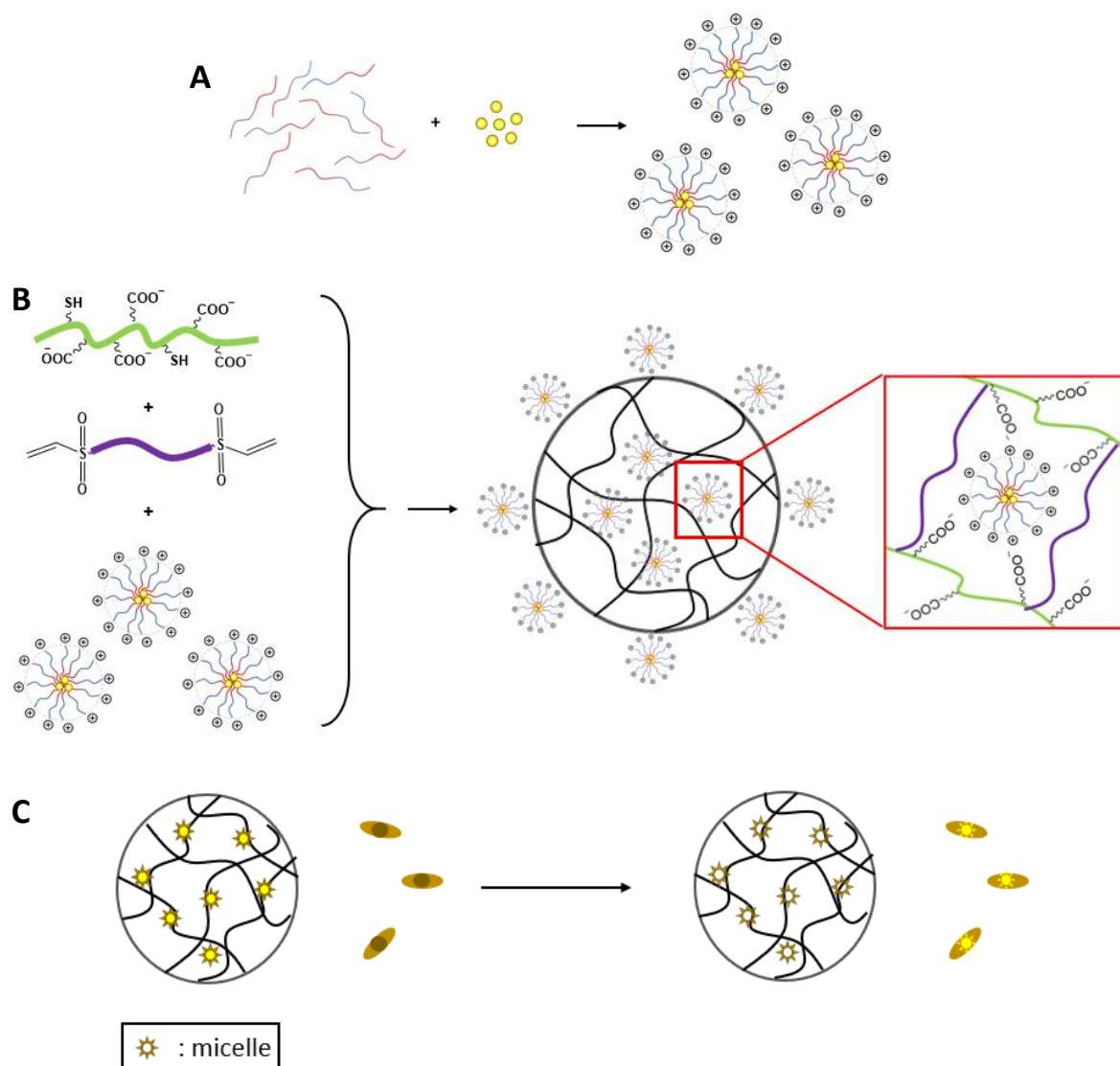
Figure 5.3: Schematic diagram of the proposed generation of micelle / hydrogel composites: A) micelle generation, B) hydrogel / micelle composite bead preparation, C) incubation of micelle / hydrogel composite beads with cells for BODIPY 505/515 staining.

5.1.3. Objectives

In this chapter, an alternative method for the delivery of BODIPY 505/515 to cells was developed. Micelle/hydrogel composite microbeads loaded with BODIPY 505/515 were generated using droplet microfluidics. Positively charged polymeric micelles were formed in aqueous solution and they were subsequently incorporated in a negatively charged hydrogel matrix. Two different methods of loading the micelles to the hydrogel beads were investigated to optimise the incorporation of BODIPY 505/515 to the beads. The first method

that was tested was the mixing of the micelles with one of the polymer precursors prior to the generation of the beads. The second method involved the loading of the micelles onto the beads after the generation of the beads and their transfer to the aqueous phase.

The resulting composite beads were incubated with algal cells to stain the lipids within the cells with BODIPY 505/515. The beads were then removed from the cell sample by filtration once the staining process was complete. The staining of the algal cells was studied through fluorescence microscopy and flow cytometry and the effect of the staining process on the cell viability was assessed. Furthermore, the beads were co-encapsulated with cells in microdroplets to test whether this was a possible way to overcome the issue of the leakage of BODIPY 505/515 from the droplets over time which was observed in Chapter 4.

5.2.   Experimental

<u>PMMA – block - DMAEMA micelle generation</u>

The PMMA – block - DMAEMA polymer (M_n = 19.6 kDa, PDI = 1.16) used for the preparation of the polymeric micelles was kindly provided by Dr Jing Zhang, Nanjing Tech University. Micelles loaded with BODIPY 505/515 were generated using a physical entrapment strategy that is commonly used for insoluble drug loading.[229] The PMMA – block - DMAEMA polymer (4 mg) was dissolved in a 100μM BODIPY 505/515 solution in THF (1 mL). Subsequently, MilliQ water (2 mL) was added dropwise to the solution while it was under continuous stirring. The resulting mixture was stirred for 30 min and then it was dialysed (Spectra/Por®2 dialysis membrane, MWCO: 12,000 – 14,000 g mol^{-1}, Spectrum Laboratories) twice against MilliQ water and twice against PBS buffer (1X, pH 7.4). The concentration of the resulting micellar solution was adjusted to 1.3 mg/mL for subsequent experiments unless otherwise stated.

<u>Critical micelle concentration (CMC) determination</u>

The CMC of PMMA – block - DMAEMA was determined through Nile Red fluorescence detection, according to a method adapted from Chen *et al*.[238] A stock solution of 1 mM Nile Red in THF was prepared. 20 μL of the solution was transferred to each of eight separate glass vials. The vials were placed in a fume-hood for 30 minutes to allow the solvent to evaporate. A 0.1 mg/mL solution of the PMMA – block – DMAEMA polymer in THF was prepared and different amounts of the solution were added to 10 mL of MilliQ water to obtain solutions

with the following concentrations of the polymer: 0.5, 0.4, 0.3, 0.2, 0.1, 0.075, 0.05 and 0.025 mg/mL. Each of the polymer solutions was then transferred to a glass vial containing the Nile Red. The resulting mixtures were mixed overnight in the dark. 200 µL samples from each solution were transferred to a 96-well plate and the Nile Red fluorescence of each mixture was measured using a plate reader (Fluostar Optima, BMG Labtech, USA). The fluorescent emission was measured from 575 to 740 nm at 5 nm intervals after excitation at 550 nm. The maximum fluorescence values in each case were plotted against the logarithm of the corresponding concentration and the CMC was determined by the intersection of the two tangents of the resulting curve.

Functionalisation of carboxymethyl cellulose (CMC) with thiol groups

Thiolated carboxymethyl cellulose (CMC-SH) was synthesized following a procedure adapted by Rakszewska et al.[239] Carboxymethylcellulose sodium salt (125 mg, CMC-Na, MW: 250kDa, DS: 1.2, Sigma Aldrich) was dissolved in 13 mL 2-(N-morpholino) ethanesulfonic acid buffer (MES buffer, pH 4.75, 0.1 M). PDPH (3-(2-pyridyldithio) propionyl hydrazide) (25 mg, Thermo Scientific) was added to the solution. After the PDPH was dissolved, 1-ethyl-3-(3-dimethylaminopropyl)carbodiimide) (150 mg, EDC, Novabiochem, Merck) was added and the reaction was stirred for 3.5 hours at room temperature. The mixture was dialysed using cellulose dialysis tubing (molecular weight cut off: 10,000 g mol^{-1}, Sigma Aldrich) against milliQ water overnight at 4 °C. On the next day, tris(2-carboxyethyl)phosphine (50 mg, 0.2 mmol, TCEP, Sigma Aldrich) was added and the mixture was stirred for 3.5 hours at room temperature. Then it was dialysed three times against 0.1 M NaCl (pH 3.5) and three times against Milli-Q (pH 5), and finally lyophilized over three days using an Alpha 2-4 LDPlus freeze drier.

Ellman's test

The efficiency of the thiol functionalisation of CMC was determined with the Ellman's test.[240] CMC-SH (1 mg) was dissolved in 1 mL of 0.1 M sodium phosphate buffer (pH 8.0), containing 1 mM EDTA (ethylenediaminetetraacetic acid, Sigma Aldrich). The mixture was heated at 37 °C on a shaker plate (Grant Bio PCMT Thermoshaker) to accelerate the dissolution process. Ellman's reagent (4 mg, 5,5'-dithio-bis-(2-nitrobenzoic acid), Thermo Scientific) was dissolved in 1 mL of DMSO (Sigma Aldrich). A set of standards was prepared by dissolving cysteine

hydrochloride in 0.1 M sodium phosphate buffer (pH 8.0), containing 1 mM EDTA (ethylenediaminetetraacetic acid, Sigma Aldrich), at concentrations ranging from 0.25 to 1.5 mM. A set of test tubes was prepared, each containing 2.5 mL of the phosphate buffer and 50 µL of the Ellman's reagent solution. A 250 µL sample of each standard and 250 µL of the CMC-SH solution were added to each of the test tubes. The test tubes were shaken and then incubated in the dark at room temperature for 15 minutes. Three 200 µL samples from each solution were transferred to a 96-well plate and their absorbance at 412 nm was recorded using a plate reader (Fluostar Optima, BMG Labtech, USA). A standard curve was generated from the recorded absorbance values of the cysteine standards. By comparing the absorbance of the CMC-SH solution to the standard curve, the amount of free thiol groups on the polymer was found to range from 0.56 to 0.76 mmol free thiols per g polymer, which corresponded to a 12 to 16% carboxyl transformation efficiency.

Hydrogel bead generation

The aqueous precursor solutions used for the hydrogel generation were prepared as follows:

A solution of CMC-SH was prepared by dissolving CMC-SH in a 10 mM solution of TCEP in PBS buffer at a concentration of 2 % w/v. To accelerate the dissolution process, the solution was heated at 37 °C. The pH of the mixture was then adjusted to 7.4 by the addition of 2M NaOH solution. The pH must be accurately controlled, because at lower pH values the gelation process does not take place while at higher pH values the reaction rate is too fast leading to possible blockages in the microfluidic device. A 10 % w/v solution of vinylsulfone-PEG5K-vinylsulfone (Sigma Aldrich) in the micellar PMMA – block – DMAEMA solution was also prepared.

The two polymer precursor solutions were loaded into SGE 500 µL syringes. The syringes were then connected to the microfluidic device (**Appendix device D**, flow-focusing junction dimensions: 100 µm x 100 µm x 150 µm (length x width x height)) via fine bore polyethylene tubing (ID = 0.38 mm, OD = 1.09 mm, Smiths Medical International Ltd). The precursor solutions were injected into the microfluidic device at a flow rate of 300 µL/hr for CMC-SH (5.55 mm/s) and 200 µL/hr for the PEG crosslinker (3.70 mm/s). Novec 7500 oil with 0.1% Picosurf 1 surfactant was used as the continuous phase and it was injected into the microfluidic device at a flow rate of 1000 µL/hr (1.85 cm/s).

The generated hydrogel droplets were collected into a centrifuge tube and they were subsequently incubated for an hour in the dark so that gelation could take place. 1H,1H,2H,2H-perfluoro-1-octanol was then added to the emulsion, to disrupt the surfactant layer around the microgels, and the microgels were resuspended in F/2 cell growth medium. The oil layer was removed by pipetting and the microgels were washed multiple times with F/2 medium to ensure the complete removal of the oil around the microgels.

Bead fluorescence imaging

The beads were imaged using an IX 71 inverted microscope (Olympus) equipped with an EMCCD iXonEM+ DU 897 camera (Andor Technology) at a 10x magnification. The BODIPY 505/515 fluorescence was imaged using the 'FITC' fluorescence channel (excitation filter 488 nm (bandwidth: 40 nm), emission filter 535 nm (bandwidth: 50 nm)). Micro-Manager Open Source Microscopy Software[241] was used to capture and to analyse the images to determine the fluorescence intensity of the beads. Manual selection of the beads in the images was required.

Cell staining by incubation with micelle/hydrogel composite beads

A *Pt* cell sample of concentration 1×10^6 cells/mL was mixed with beads at a 4:1 volume ratio. The sample was incubated in the dark while shaking on a Grant Bio PCMT Thermoshaker shaker incubator at 500 rpg. Incubation times ranging from 10 minutes to 40 minutes were tested. The beads were then removed from the sample through filtration with a pluriStrainer Mini filter (pore size: 70 µm).

Flow cytometry

Flow cytometry measurements were performed using a CytoFLEX S analyser. Excitation at 488 nm was used to analyse the forward and side scatter, as well as the BODIPY 505/515 fluorescence using a 525 nm filter (bandwidth: 40 nm) and the chlorophyll fluorescence, using a 690 nm filter (bandwidth: 50 nm). For each sample 10,000 events were recorded.

Micelle loading to the beads after generation

Hydrogel beads were prepared following the same procedure as before, but a 10% w/v solution of vinylsulfone-PEG5K-vinylsulfone in PBS buffer was used as the precursor solution,

instead of the micellar PMMA – block – DMAEMA solution. After the transfer of the beads to F/2 medium and the removal of the encapsulation oil, the beads were mixed with the micellar PMMA – block – DMAEMA solution, which had a concentration of 1.3 mg/mL. This mixture was incubated in the dark while shaking on a shaker plate (Grant Bio PCMT Thermoshaker) at 500 rpg. Incubation times ranging from 5 minutes to 120 minutes were tested, as well as different bead : micellar solution volume ratios. At the end of the incubation, the beads were washed multiple times with F/2 medium to remove the excess micelles from the solution.

Confocal imaging of beads

The beads were imaged using a Leica TCS SP5 confocal microscope. Images of the beads at different focal planes which were 4 µm apart were recorded and collated using the Leica Application Suite X software to generate "z-stack" images of the beads, as well as cross-section images.

Bead reloading with micelles

100 µL hydrogel beads were incubated in 200 µL of the 1.3 mg/mL micellar solution for 1 hour. The beads were washed four times with 1 mL F/2 medium and a 5 µL sample was imaged under a fluorescence microscope using the 'FITC' fluorescence channel (excitation filter 488 nm (bandwidth: 40 nm), emission filter 535 nm (bandwidth: 50 nm)). The remaining beads were incubated overnight in a mixture of F/2 medium (500 µL) and Novec 7500 oil (500 µL) to ensure that the BODIPY 505/515 on the beads would be removed. The process of loading micelles to the beads was repeated two more times.

Cell – bead co-encapsulation

A 1.8% w/v solution of CMC-SH in a 10 µM solution of TCEP in PBS buffer and an 8% w/v solution of the PEG crosslinker in PBS buffer were prepared. The precursor solutions were injected into a droplet generation device with a flow-focusing region of dimensions 25 µm x 25 µm x 25 µm (length x width x height) (**Appendix device E**). The precursor solutions were injected at a flow rate of 50 µL/hr for two CMC-SH streams (2.22 cm/s) and 100 µL/hr for the PEG crosslinker (4.44 cm/s). Novec 7500 oil with 0.1% Picosurf 1 surfactant was injected at a flow rate of 1000 µL/hr (44.4 cm/s). The generated droplets were incubated in the dark overnight and they were then transferred to F/2 medium.

The hydrogel beads were incubated in the 1.3 mg/mL PMMA – block – DMAEMA micellar solution for one hour so that they could be loaded with BODIPY 505/515. Once the incubation was over, the beads were washed with F/2 medium and 1% v/v Pluronic™ F-68 non-ionic surfactant was added to the bead suspension to prevent the beads from sticking to the PDMS walls of the microfluidic device during the encapsulation. At the same time, a 200 μL sample of *Pt* cells (1 x 10^6 cells/mL) was stained by the addition of 0.2 μL of a 1 mM solution of BODIPY 505/515 in DMSO.

The cells and the beads were subsequently injected into a droplet generation device with two flow-focusing junctions of dimensions 100 μm x 100 μm x75 μm (length x width x height) (**Appendix device D**). The bead suspension and the cell sample were injected at a flow rate of 100 μL/hr (3.71 mm/s), while FC-40 with 1% Picosurf 1 was injected at a flow rate of 1000 μL/hr (3.71 cm/s). The generated droplets were collected over 10 minutes in a centrifuge tube containing a small volume of 1% Picosurf 1 in FC40 to prevent droplet fusion. Approximately 15 minutes after their generation the droplets were imaged under a fluorescence microscope.

5.3.   Results and discussion

5.3.1. Generation of polymeric micelles

The PMMA – block - DMAEMA polymer (M_n = 19.6 kDa, PDI = 1.16) (**figure 5.4A**) used for the preparation of the polymeric micelles (**figure 5.4B**) was kindly provided by Dr Jing Zhang. The polymer consists of two different polymer blocks: a hydrophobic PMMA (poly(methyl methacrylate)) block and a hydrophilic DMAEMA (2-(Dimethylamino)ethyl methacrylate) block which is positively charged at acidic pH values due to the protonation of the amine functional groups, but becomes neutral at higher pH values.[242] The pKa of poly(DMAEMA) ranges from 7.4 to 7.8 at 0.15M NaCl depending on the chain length.[243] The presence of salts, such as NaCl, results in a relative increase in the protonation of the amine groups due to a reduction in the electrostatic repulsion between adjacent charged monomers.[244]

The critical micelle concentration of the PMMA – block – DMAEMA polymer was determined by Nile Red fluorescence detection, according to a method adapted from Chen *et al*.[238] Nile Red is a dye that is frequently used in the study of heterogeneous systems, such as micelles,[236] liposomes[245] and proteins.[246] It is sensitive to its local environment, exhibiting strong

fluorescence at hydrophobic environments, but weak fluorescence in hydrophilic environments. Due to this characteristic, it has been successfully used to study the local polarity of heterogeneous systems.[234]
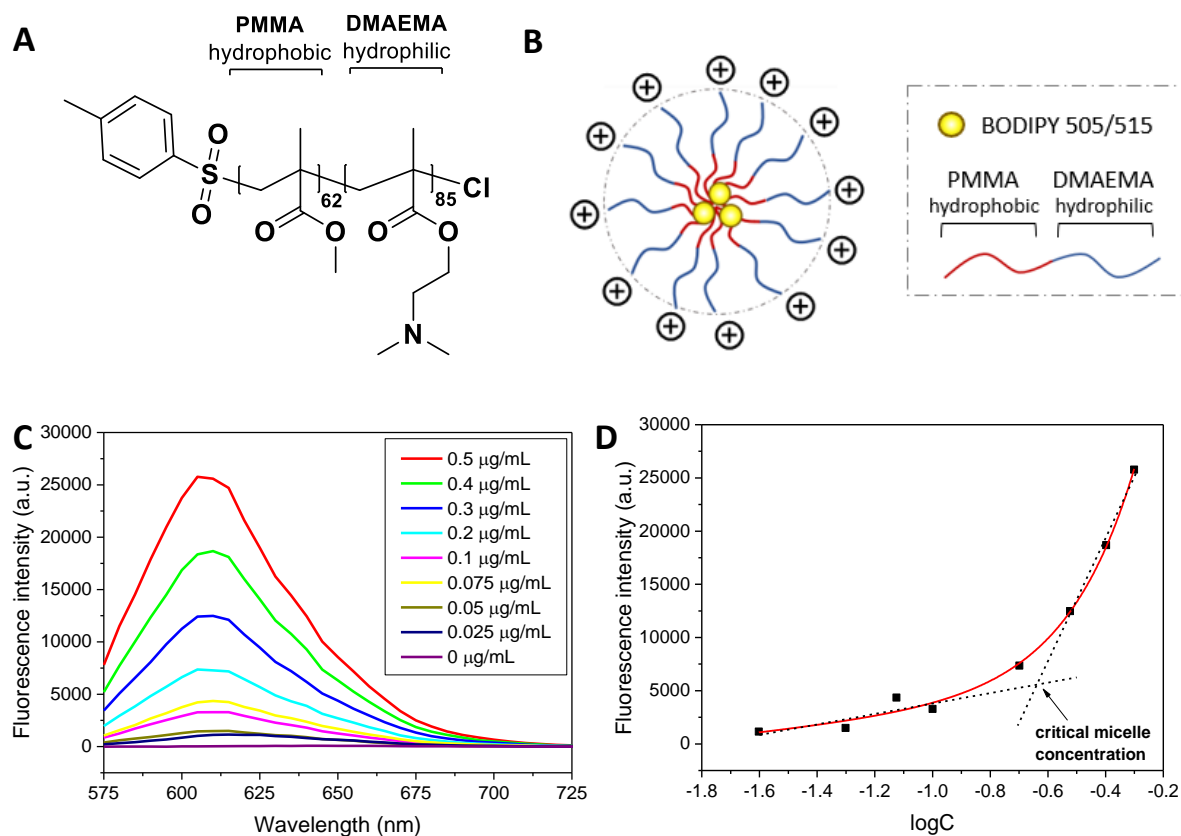
Figure 5.4: A) The structure of PMMA – block – DMAEMA, B) schematic diagram showing the self-assembly of the block copolymer in aqueous solution to form micelles loaded with BODIPY 505/515, C) the emission spectra of PMMA – block – DMAEMA and Nile Red mixtures in MilliQ water for different concentrations of the polymer (excitation: 550 nm, emission recorded at 5 nm intervals), D) plot of the maximum fluorescence against the logarithm of the polymer concentration for each mixture. The fluorescence measurements were performed in triplicate. The intersection point of the two tangents gives the critical micelle concentration value.

Different amounts of a 0.1 mg/mL solution of the PMMA – block – DMAEMA polymer in THF were added to 10 mL of MilliQ water to obtain aqueous solutions with polymer concentrations ranging from 0 to 0.5 µg/mL. Each of the polymer solutions was then transferred to a glass vial containing Nile Red (20 nmol) and the resulting mixtures were

shaken on a shaking plate overnight in the dark. The Nile Red fluorescence emission of each sample was measured after excitation at 550 nm (**figure 5.4C**). The maximum fluorescence values in each case were plotted against the logarithm of the corresponding concentration and the critical micelle concentration was determined by the intersection of the two tangents of the resulting curve (**figure 5.4D**). It was determined to be approximately 0.2 µg/mL. It was not possible to find a literature value of the critical micelle concentration of $MMA_{62} - b - DMAEMA_{85}$ for direct comparison, however, PMMA – block – DMAEMA polymers of larger molar mass (29.4 – 96.7 kDa) and larger DMAEMA/PMMA ratio have reported critical micelle concentration values that range from 0.51 to 1 µg/mL.[247]

The process used to generate BODIPY 505/515-loaded micelles is shown in **figure 5.5** and described in more detail in the Experimental section 5.2. The PMMA – block - DMAEMA polymer was dissolved in a BODIPY 505/515 solution in THF. Subsequently, MilliQ water was added dropwise to the solution under continuous stirring. The resulting mixture was dialysed (dialysis membrane MWCO: 12,000 – 14,000 g mol^{-1}) first against MilliQ water and then against PBS buffer (pH 7.4). The concentration of the micellar solution after the dialysis process was adjusted to 1.3 mg/mL through the addition of PBS buffer when necessary.
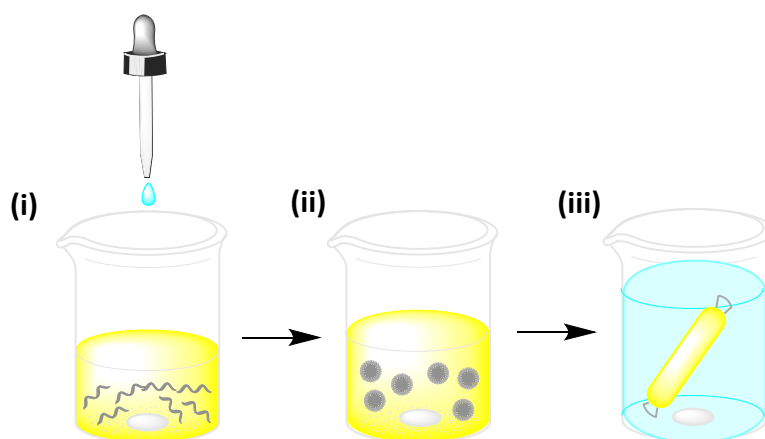
Figure 5.5: Schematic diagram of the process used to generate PMMA – block – DMAEMA micelles loaded with BODIPY 505/515: (i) dropwise addition of MilliQ water to solution of PMMA – block – DMAEMA and BODIPY 505/515 in THF under continuous stirring, (ii) micelle formation, (iii) dialysis of micellar solution against MilliQ water and PBS buffer.

The micelle suspension was mixed with *Pt* cells to test the delivery of the BODIPY 505/515 dye to the cells. A micellar suspension of concentration 1 mg/mL was mixed with a sample of *Pt* cells in F/2 medium (1.5 x 10^6 cells/mL) at a 1:4 volume ratio and the mixture was incubated in the dark for 30 minutes before being imaged under a fluorescence microscope. While the micelles effectively delivered the hydrophobic dye to the cells, they remained in solution causing a high fluorescence background which inhibited the quantitative measurement of the intracellular fluorescence. At the same time, the positively charged micelles would stick to the cell walls due to electrostatic interaction with the negatively charged cell membrane[248] (**figure 5.6**). To eliminate this issue, the incorporation of the micelles into hydrogel beads was proposed.
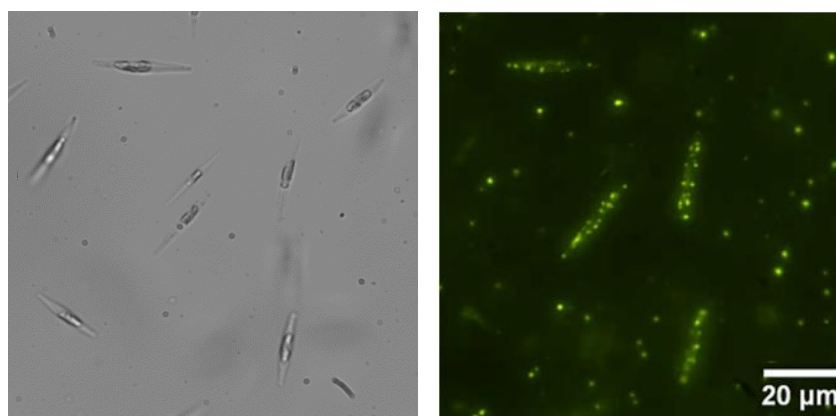
Figure 5.6: Brightfield and fluorescence images of *Pt* cells after a 30-minute incubation with the micelles loaded with BODIPY 505/515 suspension.

5.3.2. Preparation of thiolated carboxymethyl cellulose (CMC-SH)

To generate hydrogel materials, click chemistry reactions are favoured, since they take place at room temperature at fast rates. Click chemistry is a term first used by Sharpless *et al.*[249] to describe reactions that are "modular, wide in scope, give very high yields, generate only inoffensive by-products that can be removed by non-chromatographic methods, and are stereospecific (but not necessarily enantioselective)". The thiol-Michael addition reaction is a type of click reaction that is frequently used to generate hydrogels.[217]

Thiol-Michael type reactions take place at room temperature within the span of a few minutes and usually give high yields. They do not usually result in by-products and can occur without

catalyst.[217,251] Since they can take place under mild, solvent-free conditions, they are particularly attractive for the generation of hydrogel materials for biological applications.[252]

Carboxymethylcellulose (CMC) is a naturally occurring polysaccharide that is widely used in biotechnological applications. It contains numerous carboxyl groups, which are negatively charged at neutral or basic pH values. This would facilitate the capture of the positively charged micelles in the hydrogel matrix. Additionally, the carboxyl groups of CMC can be functionalised through simple chemical reactions .[250] This enables the introduction of thiol groups to the polymer, so that it can be used in a thiol-Michael addition reaction.[217]

Carboxymethylcellulose sodium salt (CMC-Na, MW: 250 kDa, DS: 1.2) was modified using a method adapted from Rakszewska *et al.*,[239] as shown in the reaction scheme in **figure 5.7**.
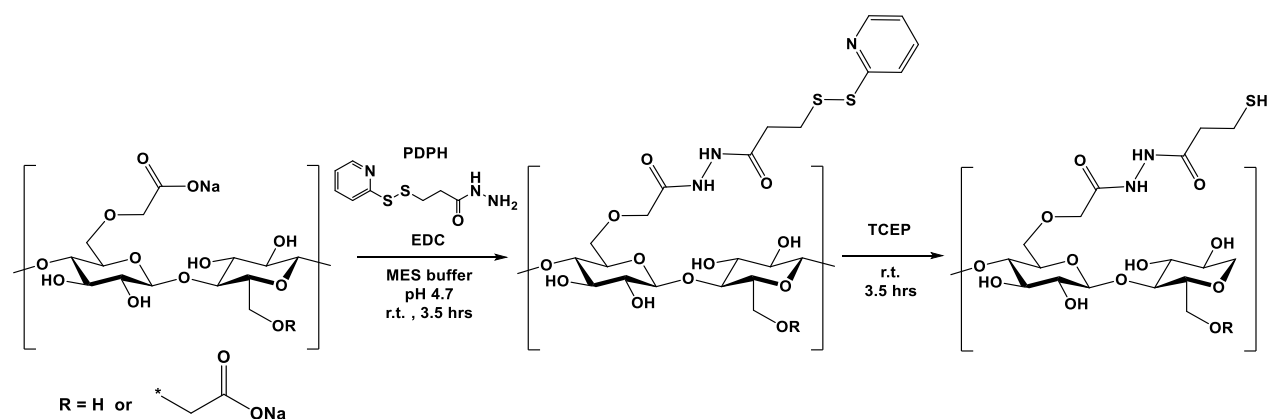
Figure 5.7: The synthesis of CMC-SH.

The Ellman's test was used to determine the amount of free thiol groups added to the polymer.[240] This was found to be 0.66 ± 0.10 mmol free thiols per g polymer, which corresponded to a 14 ± 2% carboxyl transformation efficiency. This transformation efficiency was suitable, as the resulting CMC-SH polymer had sufficient thiol groups to form cross-links, while at the same time still containing a large number of carboxyl groups which would form electrostatic interactions with the positively charged micelles.

5.3.3. Hydrogel bead generation

Besides the thiolated carboxymethyl cellulose (CMC-SH), the other polymer precursor selected for the hydrogel formation was a PEG (polyethylene glycol) cross-linker with two vinylsulfone functional groups purchased from Sigma Aldrich (**figure 5.8**). The vinyl sulfone

groups on the PEG crosslinker react readily with the thiol groups of CMC-SH in neutral to slightly alkaline conditions to form stable thioether sulfone bonds which are resistant to hydrolytic degradation.[217]
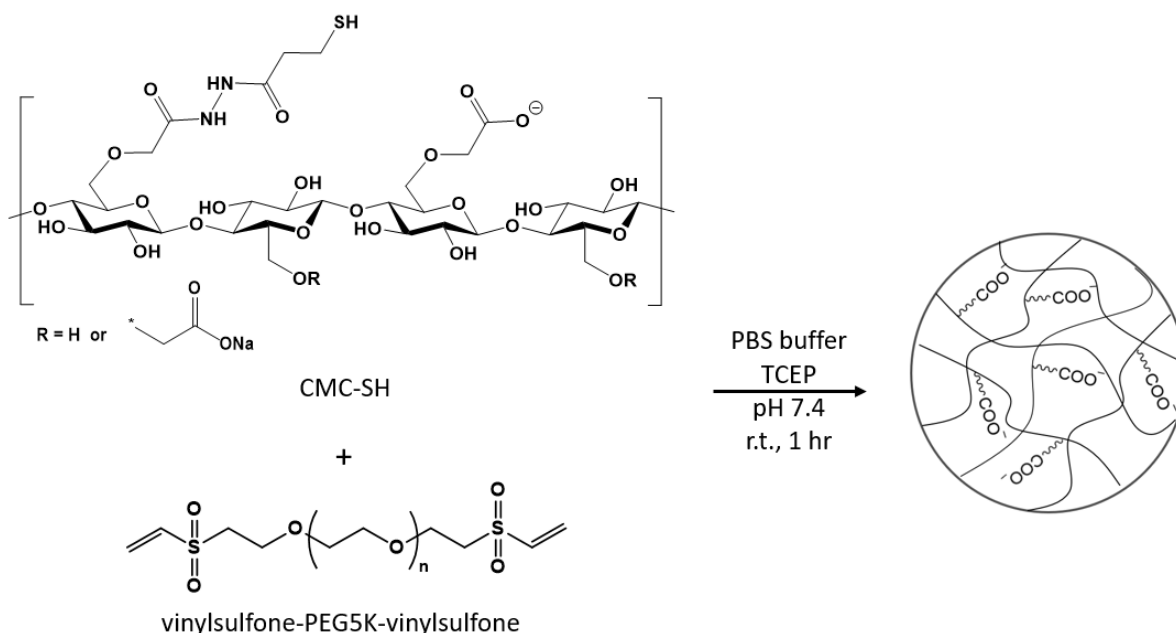
Figure 5.8: The polymer precursors and the reaction conditions used for the hydrogel bead generation.

A PDMS microfluidic device with two flow-focusing junctions was used to generate the hydrogel beads (**figure 5.9A**) (**Appendix device D**). The dimensions of the flow-focusing regions of this device were 100 μm x 100 μm x 150 μm (length x width x height). Two polymer precursor solutions were prepared: a 2% w/v solution of CMC-SH in a 10 μM solution of TCEP in PBS buffer and a 10% w/v solution of the PEG crosslinker in the micellar solution of PMMA – block – DMAEMA in PBS. The precursor solutions were injected into the microfluidic device at a flow rate of 300 μL/hr (5.55 mm/s) for CMC-SH and 200 μL/hr (3.70 mm/s) for the PEG crosslinker. Novec 7500 oil with 0.1% Picosurf 1 surfactant was used as the continuous phase and it was injected into the microfluidic device at a flow rate of 1000 μL/hr (1.85 cm/s). The monodisperse droplets (**figure 5.9B**) (diameter: 200 μm, volume: 4 nL) were collected in an Eppendorf tube and they were subsequently incubated for one hour in the dark, so that the gelation process could take place. Longer incubation times of the droplets in the oil phase were avoided, as, due to the solubility of BODIPY 505/515 in the Novec 7500 oil, the dye

would leak out of the droplets and into the oil over time, leading to a loss of the cargo of the beads. A one-hour incubation was determined to be sufficient for gelation to take place, while, at the same time, minimising the loss of BODIPY 505/515.

After the incubation, the surfactant surrounding the hydrogel beads was removed by the addition of 1H,1H,2H,2H-perfluorooctanol and the beads were transferred to F/2 cell growth medium. The encapsulation oil was removed using a pipette and the beads were centrifuged at 6000 rpm for 90 seconds and washed multiple times with F/2 to ensure complete removal of the oil from the bead suspension (**figure 5.9C**). Once the beads were washed, they were imaged under a fluorescence microscope. The Micro-Manager Open-Source Microscopy Software was used to record the fluorescence images and measure the bead fluorescence intensity. Through the fluorescence images it was determined that the beads were successfully loaded with BODIPY 505/515 (**figure 5.9D**).
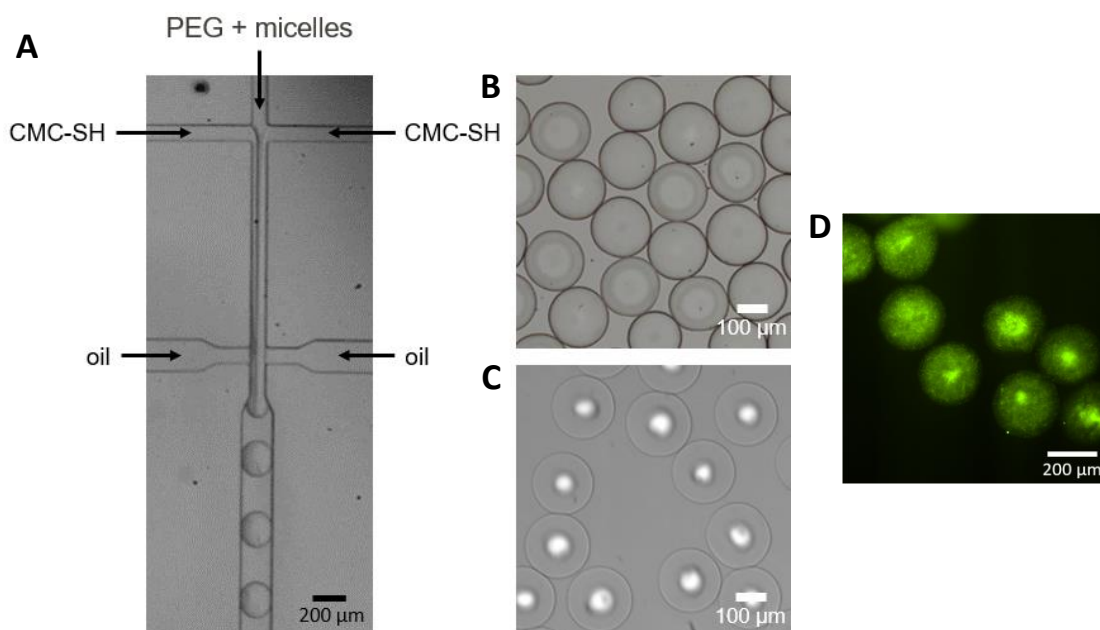
Figure 5.9: Brightfield image of A) the hydrogel droplet generation in the flow-focusing microfluidic device (flow-focusing region dimensions: 100 μm x 100 μm x 150 μm (length x width x height), flow rates: 300 μL/hr for CMC-SH (5.55 mm/s), 200 μL/hr for the PEG crosslinker (3.70 mm/s) and 1000 μL/hr for Novec 7500 oil with 0.1% Picosurf 1 (1.85 cm/s), B) the generated hydrogel droplets in encapsulation oil and C) the hydrogel beads after a 1 hr incubation and transfer to F/2 medium, D) fluorescence imaging of the hydrogel beads after transfer to F/2 medium.

To demonstrate the role that the micelles played in increasing the loading capacity of the beads, two hydrogel bead samples were prepared. The first sample consisted of hydrogel beads that did not contain micelles. They were generated using a solution of the PEG crosslinker in PBS buffer instead of the micellar solution used in **figure 5.9**. The second sample consisted of beads containing 1 mg/mL micelles, although the micelles were not loaded with BODIPY 505/515. The beads of both samples were incubated in a BODIPY 505/515 solution in DMSO for one hour and they were subsequently washed multiple times with F/2 medium. The beads were imaged under a fluorescence microscope and their fluorescence was measured using Micro-Manager Open-Source Microscopy Software[241] (**figure 5.10**). The fluorescence of the micelle/hydrogel composite beads was higher than that of the plain hydrogel beads, showing that the composite beads were more efficient in capturing BODIPY 505/515.
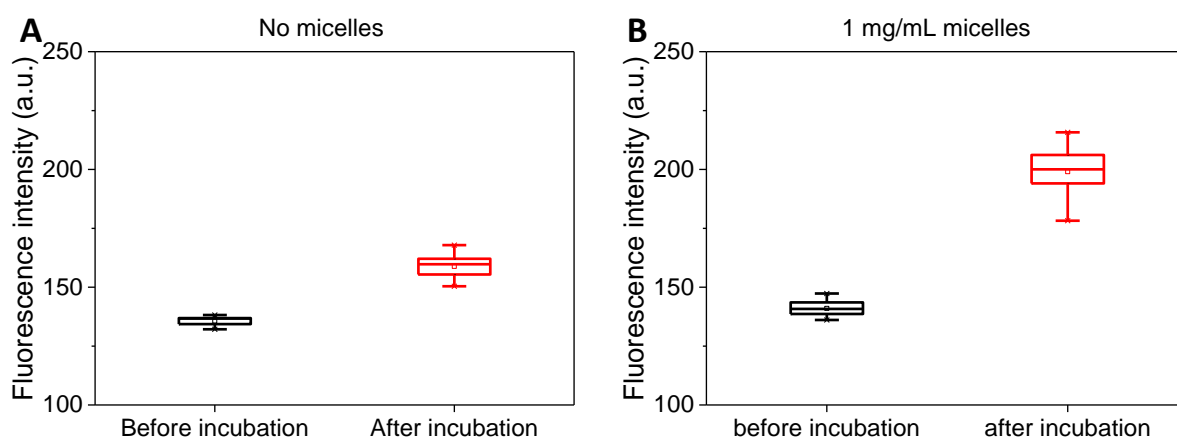
Figure 5.10: A) Box plot showing the fluorescence of hydrogel beads without micelles before and after their incubation in BODIPY 505/515 solution in DMSO, B) box plot showing the fluorescence of micelle/hydrogel composite beads, generated using a 1 mg/mL micellar solution, before and after their incubation in BODIPY 505/515 solution in DMSO. The fluorescence of 20 beads was measured for each sample. The experiment was performed once.

To optimise the loading of micelles to the hydrogel beads, different concentrations of the micellar dispersion used during the bead generation were examined. Solutions with micelle concentrations ranging from 0.5 to 1.5 mg/mL were used to generate hydrogel beads and the

fluorescence of the beads generated with each micellar solution was compared by imaging under a fluorescence microscope. The fluorescence of 45 beads from each sample was measured (**figure 5.11**) and box plots of the fluorescence values were generated for each micelle concentration. The results showed that the optimum loading of BODIPY 505/515 to the beads was achieved when the micellar solution used had a concentration between 1.25 and 1.5 mg/mL. For this reason, in all subsequent experiments, a 1.3 mg/mL micellar solution was used.
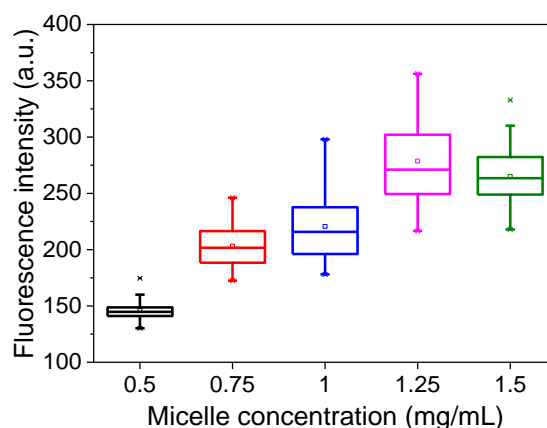
Figure 5.11: Box plot showing the fluorescence intensity of beads generated with different concentrations of the micellar solution (each box corresponds to the fluorescence intensity data of 45 beads). The experiment was repeated three times.

The fluorescence of the generated hydrogel/micelle composite beads loaded with BODIPY 505/515 was monitored over five hours to examine the change in the BODIPY 505/515 content of the beads over time. The fluorescence of 60 beads was measured at every timepoint and a box plot of the bead fluorescence was generated. A decrease in the fluorescence of the beads over time is observed, as the dye slowly leaks out of the beads (**figure 5.12**).
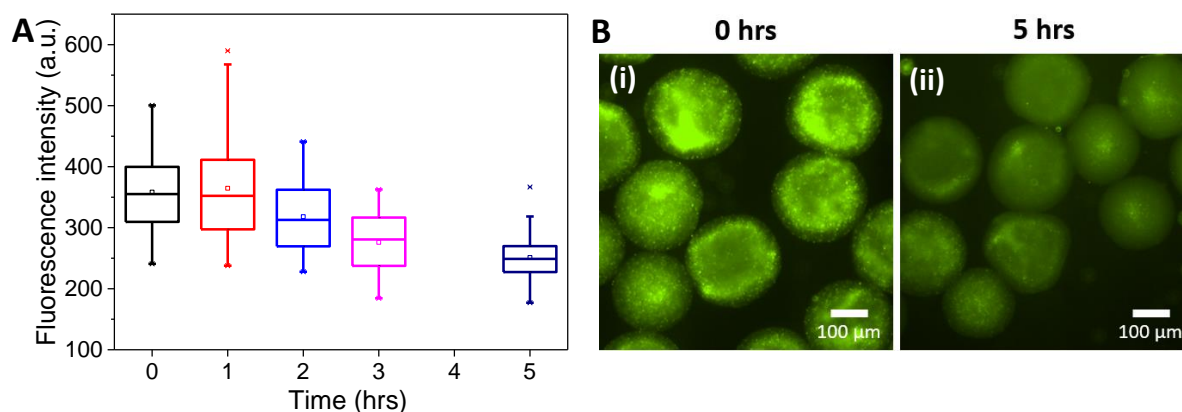
Figure 5.12: A) Box plot showing the change in bead fluorescence intensity over time (each box corresponds to the fluorescence intensity data of 60 beads), B) fluorescence images of the beads (i) at 0 hours (just after the end of the washing procedure) and (ii) after 5 hours. The experiment was performed once.

5.3.4. Cell staining with hydrogel beads

Once the hydrogel beads were successfully generated, they were incubated with *Pt* cells so that staining of the cells with the dye could take place. As the BODIPY 505/515 contained within the beads leaks out over time, the dye crosses the cell membrane of the algal cells and stains the intracellular lipids due to its high oil / water partition coefficient.[181]

A cell sample of density 1 x 10^6 cells/mL was mixed with beads at a 4:1 volume ratio. The sample was incubated in the dark while shaking on a shaker incubator for 40 minutes. The beads were then removed from the sample through filtration with a pluriStrainer Mini filter (pore size: 70 µm) (**figure 5.13A**) and the cells were imaged under a fluorescence microscope, so that their intracellular fluorescence could be assessed (**figure 5.13B(ii)**). Comparison of the cell fluorescence to the fluorescence of the cells before their incubation with the beads (**figure 5.13B(i)**), revealed that the *Pt* cells were successfully stained with BODIPY 505/515.

The stained cells were transferred to fresh F/2 medium and they were cultured over five days. On each day, the density of the cell culture was measured using a hemocytometer. The cells grew normally in the fresh medium, showing that their viability was not affected by the staining process (**figure 5.13C**).

131
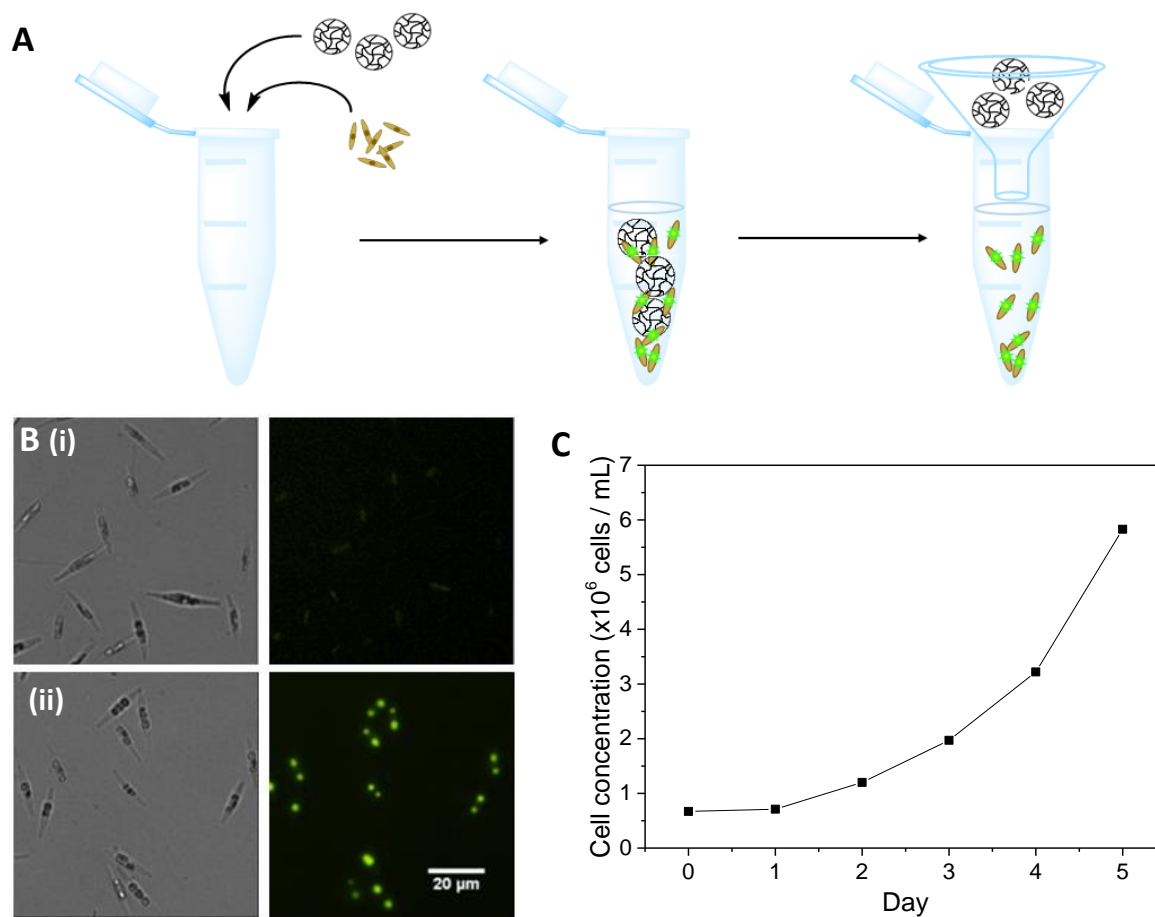
Figure 5.13: A) Schematic diagram showing the staining of *Pt* cells by co-incubation with the micelle/hydrogel conjugate beads and the removal of the beads by filtration after the staining, B) *Pt* cells (i) before the cell staining and (ii) after the cell staining, C) *Pt* cell re-culture in fresh F/2 medium after their staining by co-incubation with the conjugate beads. Cell density measured with a haemocytometer over five days of culture. The experiment was conducted once.

To obtain a more quantitative measure of the cell fluorescence, the fluorescence of the recovered cells was analysed through flow cytometry. Flow cytometry is a powerful technique which is frequently used to detect the fluorescence of single cells at a high throughput.

A *Pt* cell sample of concentration 1×10^6 cells/mL was mixed with beads at a 4:1 volume ratio. The sample was incubated in the dark while shaking on a shaker incubator for 30 minutes. The beads were then removed from the sample through filtration and the fluorescence of the cells was analysed with a CytoFLEX S analyser, using a 488 nm laser as the illumination source. For comparison, the fluorescence of *Pt* cells that had not been stained was also recorded.

Data of the BODIPY 505/515 fluorescence emitted by the cells were collected using a 525 nm band pass filter (bandwidth: 40 nm). 10,000 events were recorded for each sample. An increase in the fluorescence recorded was observed in the sample of cells that had been incubated with the beads (**figure 5.13A**). The mean fluorescence emitted by the unstained *Pt* cells was 1.8×10^4 a.u., while the mean fluorescence emitted by the cells that had been incubated with the beads was 1.74×10^6 a.u., two degrees of magnitude higher.

The beads and a 1×10^6 cells/mL *Pt* cell sample were mixed at different volume ratios to determine the minimum number of beads that resulted in successful staining of the *Pt* cells. 200 µL of the cell sample was mixed with 50 µL, 100 µL and 150 µL beads. After 40 minutes of incubation the beads were removed by filtration and the fluorescence of the cells was recorded through flow cytometry (**figure 5.14B**). The mean fluorescence intensity values of the *Pt* cells in each sample were compared and were found to be close in value for the three cell : bead ratios tested (**figure 5.14C**). Based on the results of this test, a 4:1 cell : bead volume ratio (50 µL beads : 200 µL cell sample) was determined to be enough for cell staining and was used for all subsequent experiments, as it would require the preparation of the smallest amount of beads.
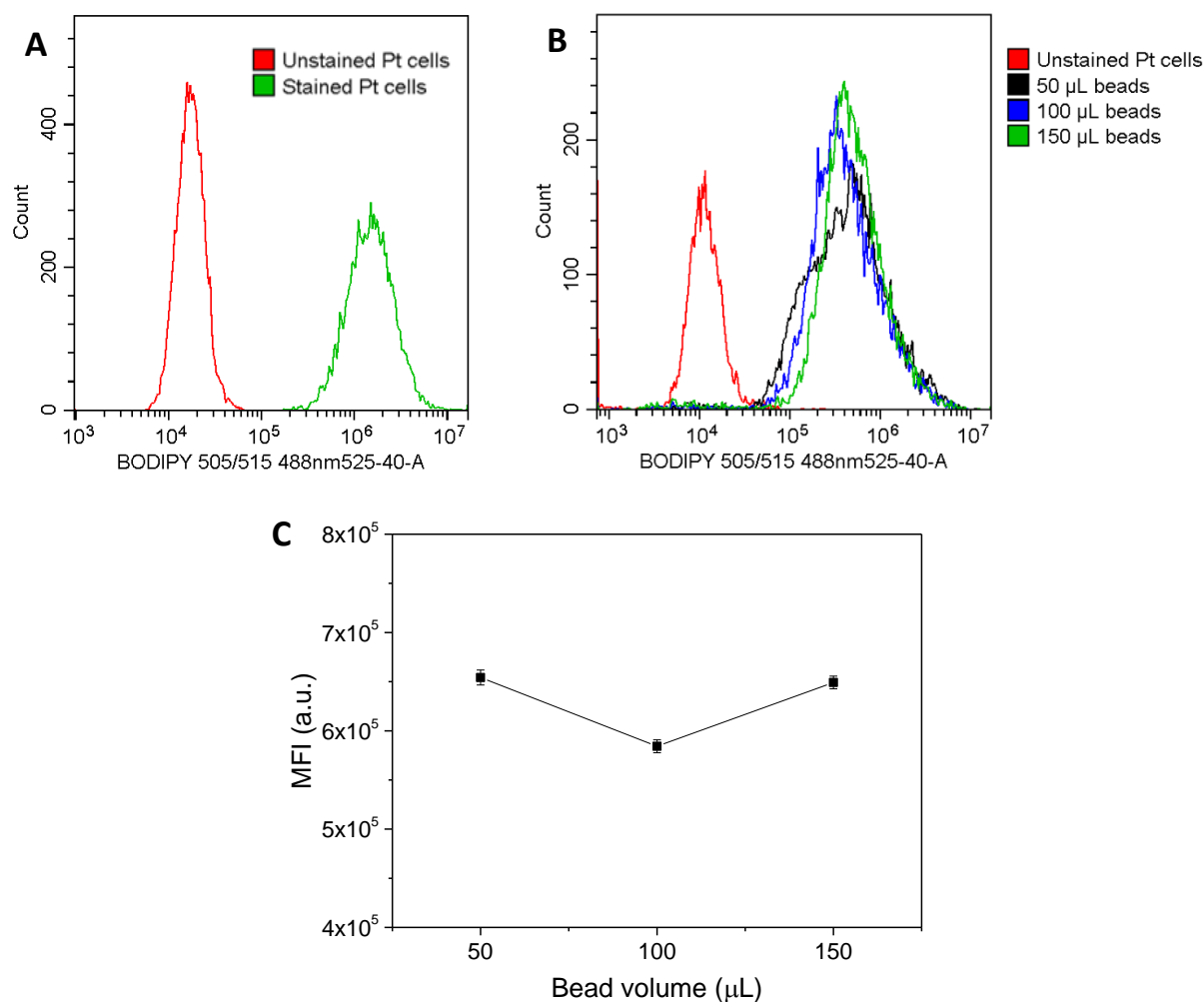
Figure 5.14: A) Fluorescence intensity distributions corresponding to the green fluorescence emitted by the *Pt* cells before and after their incubation with hydrogel beads for 40 minutes, B) fluorescence intensity distributions of *Pt* cells stained with different amounts of hydrogel beads and C) the mean fluorescence intensity values of each of the *Pt* cell samples stained with different amounts of beads. Excitation at 488 nm was used to analyse the BODIPY 505/515 fluorescence using a 525 nm filter (bandwidth: 40 nm). For each sample 10,000 events were recorded. The experiment was performed once.

The effect of the incubation time on the staining of the cells by the beads was examined by flow cytometry to determine the optimum incubation time. *Pt* cell samples of concentration 1×10^6 cells/mL were mixed with beads at a 4:1 volume ratio. Each of the samples was incubated for a different amount of time, ranging from 10 to 40 minutes. The BODIPY 505/515 fluorescence of each cell sample was measured through flow cytometry (**figure 5.15A**) and

the median fluorescence intensity values were calculated (**figure 5.15B**). The results showed that 30 minutes of incubation time were optimum for the staining of the *Pt* cells.
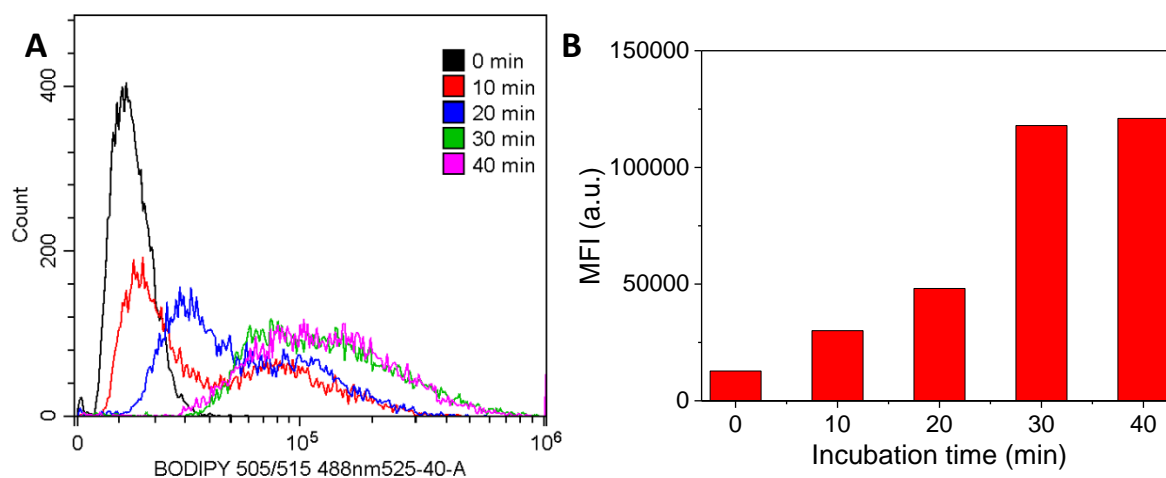
Figure 5.15: Flow cytometry measurements of the fluorescence emitted *Pt* cells after different incubation times with the hydrogel beads: A) fluorescence intensity distributions, B) the median fluorescence intensity (MFI) values (excitation at 488 nm, emission filter: 525 nm (bandwidth: 40 nm). For each sample 10,000 events were recorded. The experiment was repeated twice.

To better understand the factors that affect the cell staining time, a rough estimate of the time needed for BODIPY 505/515 molecules to diffuse from the beads to the cells was generated. Based on the bead concentration used for cell staining (a 4:1 cell : bead volume ratio, which is equal to 3×10^4 beads/mL), and under the assumption that the beads and the cells in the sample are well mixed, an approximate value of the mean distance between the beads in the solution was calculated using *Equation 5.1*.

$$d = \frac{1}{\sqrt[3]{c}} \qquad \text{(Equation 5.1)}$$

where c is the bead concentration and d is the mean distance. The distance was thus estimated to be 320 µm. As the bead radius was 100 µm, the distance from the surface of one bead to the surface of the other was therefore 120 µm. As the cells could be at any point in the solution between the beads, the distance of a cell from the nearest bead was assumed to be in the range of 60 µm.

Using this estimate of the diffusion distance and Equation 4.1., which was previously used in section 4.3.2., the time needed for a molecule of BODIPY 505/515 to diffuse from a bead to a cell was calculated.

$$t = \frac{x^2}{6 \cdot D}$$ *(Equation 4.1)*

In this case, x is the diffusion distance, t is the diffusion time and D is the molecular diffusion coefficient. An approximate value of 4 x 10^{-6} cm^2/s was used for the molecular diffusion coefficient, as in section 4.3.2. The diffusion time was estimated to be approximately 2 s. The diffusion of the dye in the solution is therefore a relatively quick process which is further accelerated by the continuous mixing of the cells and the beads. This indicates that most of the time needed for the cell staining to take place is consumed by the two other processes taking place: the release of the dye from the composite beads and the crossing of the cell membrane, once the dye reaches the cell, to stain the intracellular lipids.

The micelle/hydrogel composite beads can be used to stain other algal cell species besides *Pt*. A *Nannochloropsis gaditana* (*Ng)* cell sample of concentration 1 x 10^6 cells/mL was mixed with beads at a 4:1 volume ratio and they were incubated together for 30 minutes. The beads were then filtered off the cell sample and the BODIPY 505/515 fluorescence of the cells was measured through flow cytometry (**figure 5.16**). Fluorescence compensation was applied to the recorded fluorescence values to compensate for the high chlorophyll autofluorescence of the *Ng* cells. The median fluorescence emitted by the cells after the incubation process was two degrees of magnitude higher than that emitted by the *Ng* cells that had not been stained by beads. The flow cytometry results therefore showed that the staining of the cells with the beads was successful.
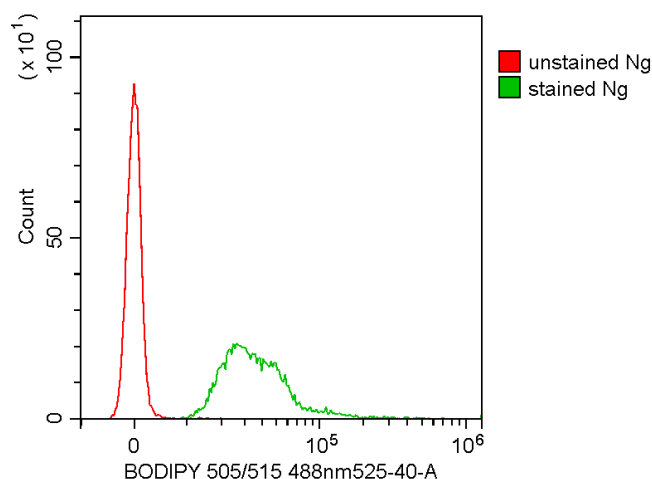
Figure 5.16: Fluorescence intensity distributions corresponding to the green fluorescence emitted by *Ng* cells before and after their incubation with hydrogel beads for 30 minutes. Each distribution corresponds to 10,000 cells. The experiment was carried out once.

5.3.5. Optimisation of the loading of BODIPY 505/515 to the beads

While it has been demonstrated that the BODIPY 505/515 loaded micelle / hydrogel composite beads are able to stain the cells, further optimisation was required to enhance the dye loading and thus to increase the staining efficiency. As was mentioned in section 5.3.3., during the preparation process of the micelle / hydrogel composite beads, the hydrogel microdroplets containing BODIPY 505/515 were incubated in the Novec 7500 oil. Because the BODIPY 505/515 is partially soluble in the Novec 7500 oil, there was a significant loss of dye during the incubation (**figure 5.17**).
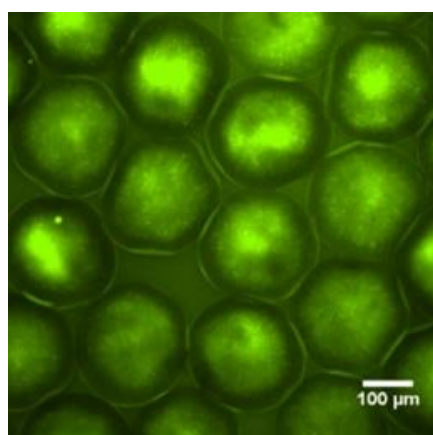
Figure 5.17: Fluorescence image of the micelle/hydrogel composite beads during a four-hour incubation in the Novec 7500 encapsulation oil. BODIPY 505/515 fluorescence is emitted by the oil phase due to leakage of the dye from the beads.

An alternative method of loading the micelles into the hydrogel beads was tested to reduce the loss of the dye during the preparation of the beads. According to this method, the polymeric micelles which contained the dye were incorporated onto the beads after the transfer of the beads to aqueous medium.

Hydrogel beads were prepared following the same procedure as before (**figure 5.9A**), however, the PEG crosslinker was dissolved in PBS buffer instead of the micellar solution. The generated droplets were incubated for one hour for the crosslinking to take place and they were then resuspended in F/2 medium. Once the hydrogel beads were transferred to the aqueous phase, a 1.3 mg/mL solution of the PMMA – block – DMAEMA micelles loaded with BODIPY 505/515 was added to the beads for incubation. Finally, the beads were collected, and the excess micelles were washed away with F/2 medium (**figure 5.18A**).

During the incubation of the hydrogel beads in the micellar solution, the positively charged micelles were captured by the hydrogel beads due to electrostatic interaction between the micelles and the negatively charged carboxyl groups of the CMC-SH. Once the micelles were successfully incorporated into the hydrogel matrix, the excess micelles were removed from the surrounding solution by washing the beads multiple times with F/2 medium.

As shown in **figure 5.18B**, the loading of the hydrogels with BODIPY 505/515 was successful. The collected beads after the incubation in the micellar solution, displayed high fluorescence in the FITC channel (excitation at 488 nm (bandwidth: 40 nm) and emission at 535 nm (bandwidth: 50 nm)) when imaged under a fluorescence microscope (**figure 5.18C**).
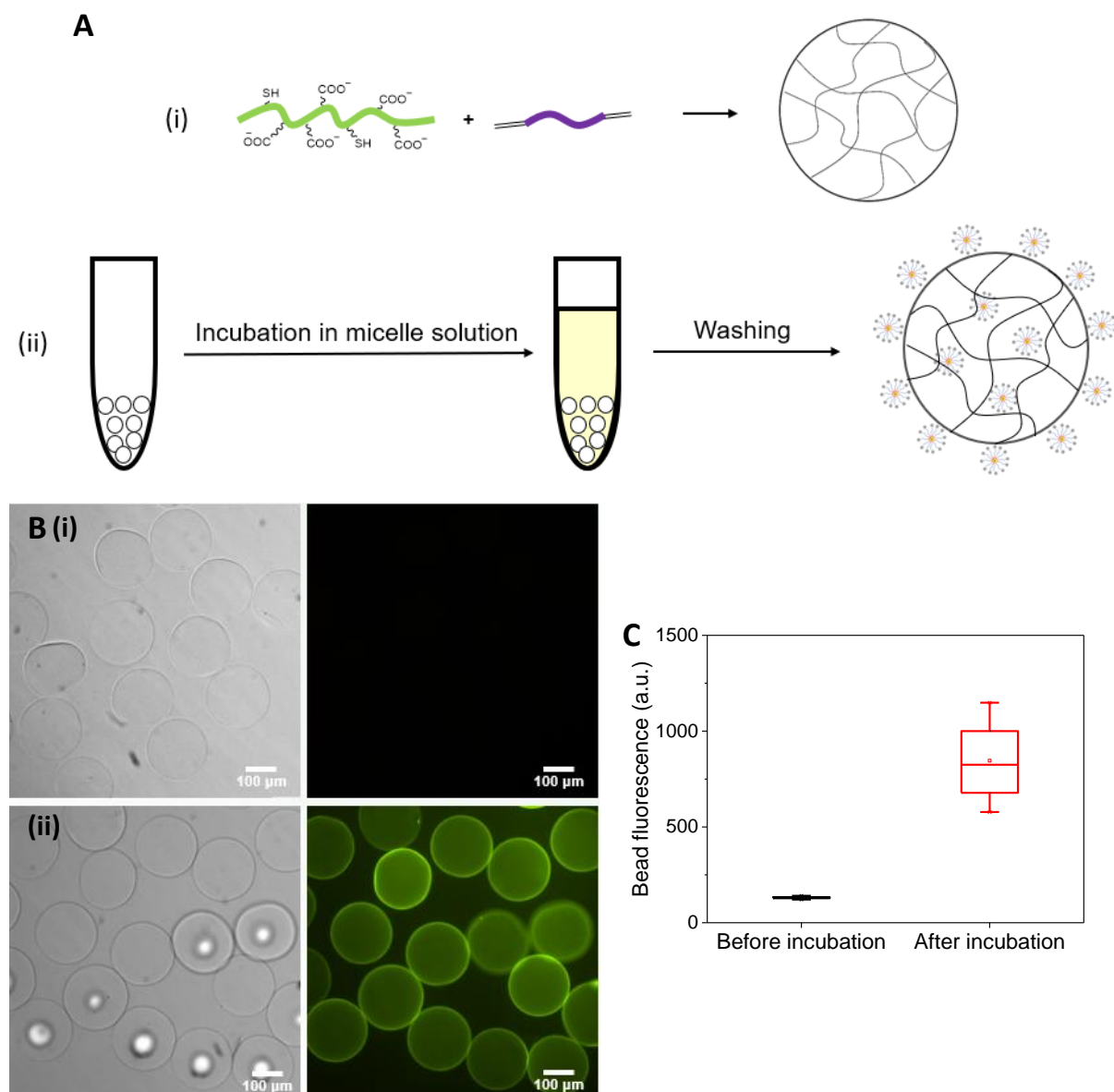
Figure 5.18: A) Schematic diagram showing (i) the generation of hydrogel beads and (ii) the incubation of the hydrogel beads in micellar solution to load the micelles onto the beads, followed by the washing of the beads to remove excess micelles, B) bright-field and fluorescence images of hydrogel beads (i) before and (ii) after their incubation in 1.3 mg/mL micellar solution C) box plot showing the measured bead fluorescence before and after the incubation of the hydrogel beads in the micellar solution. The fluorescence of 60 beads was measured.

Various incubation times of the beads in the micellar solution were tested to determine the optimal incubation time for the capture of the micelles by the hydrogel beads (**figure 5.19A**). 20 µL of the beads were incubated in the dark with 40 µL of the micellar solution under continuous shaking on a shaker plate. Each sample was washed five times with F/2 medium after the incubation, to ensure the removal of excess micelles and the beads were imaged under a fluorescence microscope. The average fluorescence of each bead sample was determined using the image analysis software of Micro-Manager. An incubation time of one hour was determined to be sufficient for the optimal loading of micelles to the beads.

Furthermore, 20 µL samples of the beads were mixed with different volumes of the micellar solution (10 µL, 20 µL, 30 µL and 40 µL) and incubated for 90 minutes to identify the ideal bead : micellar solution volume ratio to be used during the incubation process. In this case, it was determined that a 1:2 volume ratio was sufficient for the optimal loading of the beads with the micelles (**figure 5.19B**).

After the loading of the beads with micelles, a confocal microscope was used to access the distribution of the micelles within the beads. Images of the beads at different focal planes which were 4 µm apart were recorded and collated to generate "z-stack" images of the beads (**figure 5.19C(i)**), as well as cross-section images (**figure 5.19C(ii)**, xz section) (**figure 5.19C(iii)**, yz section) showing the placement of the micelles at different heights. These images showed that the micelles were concentrated mainly on the outer surface of the beads, with the centre of the beads remaining relatively free of micelles. This implies that the pore size of the hydrogel is smaller than the size of the micelles, so the micelles cannot pass into the inside of the hydrogel beads. Further optimisation to the bead composition and adjustment of the cross-linking density is required to achieve uniform distribution of the micelles in the beads.
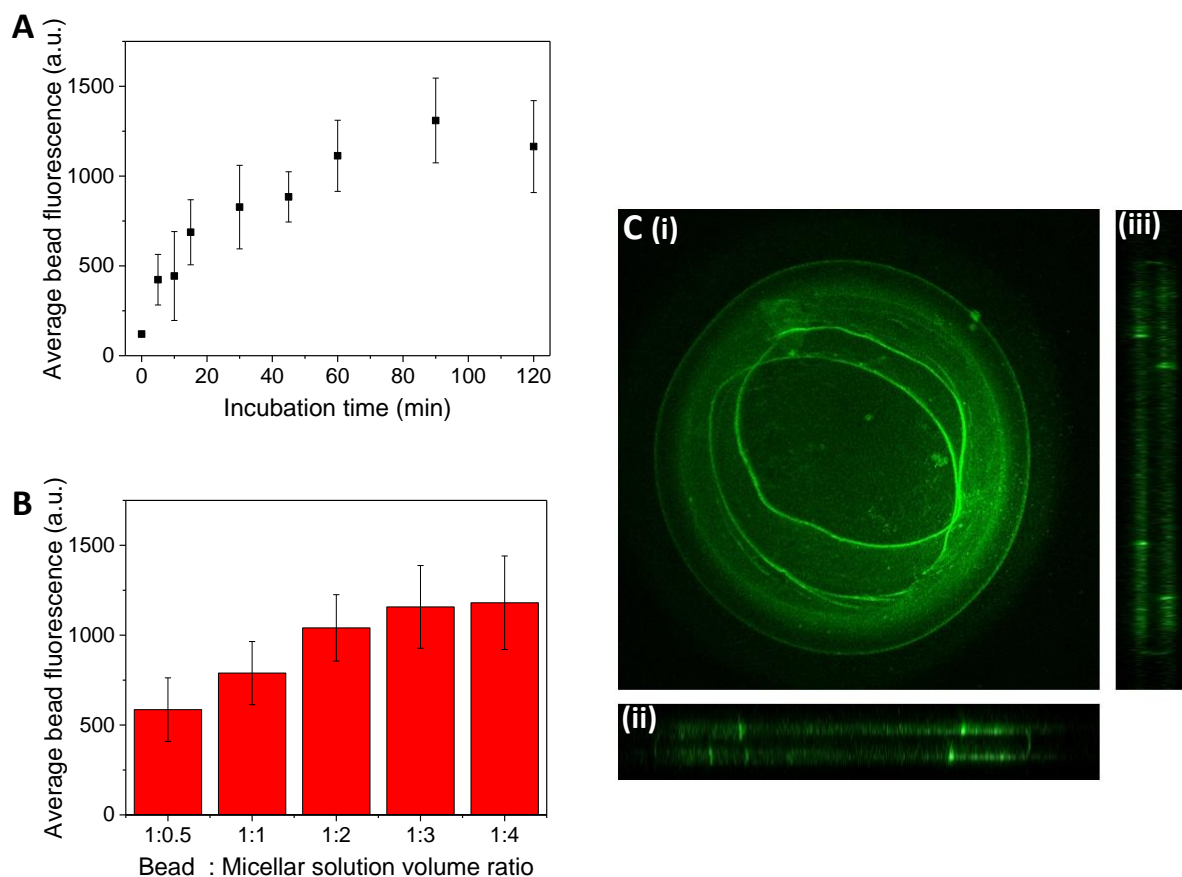
Figure 5.19: A) Testing of different incubation times of the hydrogel beads in the micellar solution to optimise the loading of micelles to the hydrogel beads; the fluorescence of 70 beads was measured for each datapoint and the test was carried out three times, B) testing of different bead : micellar solution volume ratios used during the incubation process to optimise the loading of micelles to the hydrogel beads; the fluorescence of 70 beads was measured for condition tested and the test was carried out twice, C) confocal imaging of a hydrogel bead after its incubation in the micellar solution: (i) z-stack image generated by compiling images of the bead at focal planes which were 4 μm apart, (ii) xz bead cross-section, (iii) yz bead cross-section.

By using this method of loading micelles to the beads, it should be possible to reuse beads that have already been used and drained of BODIPY 505/515. To test this theory, 100 μL beads were incubated in 200 μL of the micellar solution for 1 hour. The beads were washed four times with F/2 medium and a 5 μL sample was imaged under a fluorescence microscope. The remaining beads were incubated overnight in a mixture of F/2 medium and Novec 7500 oil to ensure that the BODIPY 505/515 on the beads would be removed. On the next day, the beads,

which no longer contained BODIPY 505/515, were incubated once more in the micellar solution. Fluorescence imaging of the beads after the incubation showed that, through this process, they were successfully reloaded with BODIPY 505/515. Overall, the beads were successfully loaded with micelles three times over the span of three days (**figure 5.20**).
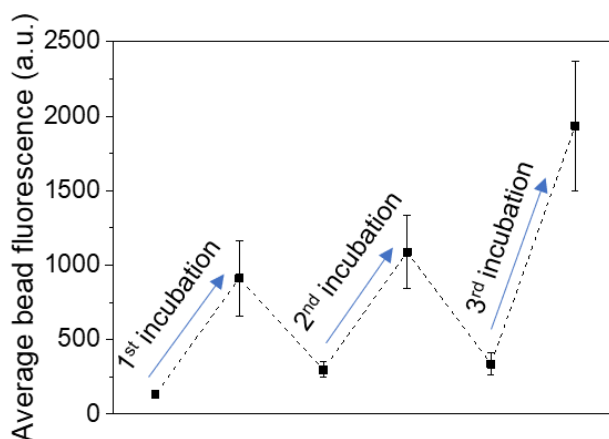
Figure 5.20: Reloading of the hydrogel beads with BODIPY 505/515 by incubation in a 1.3 mg/mL solution of micelles loaded with BODIPY 505/515. Between each incubation step, the beads were stored overnight in a mixture of F/2 medium and Novec 7500 oil to remove all the BODIPY 505/515 from the beads. The fluorescence of 40 beads was measured for each datapoint. The experiment was performed twice.

The staining of *Pt* cells with beads that had been loaded with micelles after their generation was tested. Hydrogel beads were incubated in the 1.3 mg/mL micellar solution for one hour at a 1:2 bead: micellar solution volume ratio. The beads were then washed with F/2 medium to remove the free micelles from the medium surrounding the beads and they were mixed with a *Pt* cell sample of concentration 1×10^6 cells/mL. The beads and the cells were incubated together for 40 minutes. Then, the beads were removed from the sample and the cells were imaged under a fluorescence microscope. The staining of the cells with BODIPY 505/515 appeared to be heterogeneous. There were some free micelles in the solution which became attached to the cell wall of some cells (**figure 5.21**).
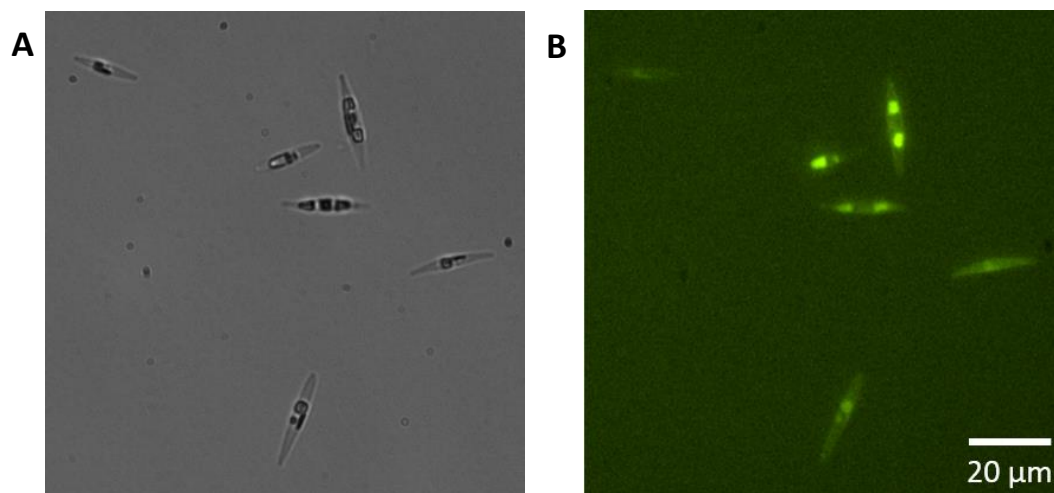
Figure 5.21: A) Bright-field and B) fluorescence images of *Pt* cells stained with BODIPY 505/515 by incubation with the micelle/hydrogel beads for 40 minutes.

5.3.6. Bead / cell co-encapsulation for sustained cell staining in droplets

A proposed solution to the issue of the leakage of BODIPY 505/515 from microdroplets over time, is to encapsulate hydrogel beads loaded with BODIPY 505/515 in the droplets. As the beads release BODIPY 505/515 slowly over time, they could act as localised deposits of BODIPY 505/515 to counteract the effect of the BODIPY 505/515 diffusing out of the droplets. To test whether this approach is viable, hydrogel beads of diameter 40 μm (34 pL in volume) were generated and encapsulated with *Pt* cells in microdroplets.

Two polymer precursor solutions were prepared: a 1.8% w/v solution of CMC-SH in a 10 μM solution of TCEP in PBS buffer and an 8% w/v solution of the PEG crosslinker in PBS buffer. The precursor solutions were injected into the microfluidic device shown in **figure 5.22A (Appendix device E)**. The device had four inlets and the dimensions of the flow-focusing region were 25 μm x 25 μm x 25 μm (length x width x height). The precursor solutions were injected at a flow rate of 50 μL/hr for each CMC-SH stream (2.22 cm/s) and 100 μL/hr for the PEG crosslinker (4.44 cm/s). Novec 7500 oil with 0.1% Picosurf 1 surfactant was injected at a flow rate of 1000 μL/hr (44.4 cm/s).

The generated droplets were incubated in the dark overnight and they were then transferred to F/2 medium. The hydrogel beads, which were approximately 40 μm in diameter, were incubated in the PMMA – block – DMAEMA micellar solution for one hour so that they could

be loaded with BODIPY 505/515. Once the incubation was over, the beads were washed with F/2 medium and 1% v/v Pluronic™ F-68 non-ionic surfactant was added to the bead suspension to prevent the beads from sticking to the PDMS walls of the microfluidic device during the encapsulation. At the same time, a 200 μL sample of *Pt* cells (1 x 10^6 cells/mL) was stained by the addition of 0.2 μL of a 1 mM solution of BODIPY 505/515 in DMSO.

The cells and the beads were subsequently injected into a droplet generation device to be co-encapsulated into droplets. The device used was similar in geometry to the device in **figure 5.9A (Appendix device D),** however, the dimensions of the flow-focusing junctions were 100 μm x 100 μm x75 μm (length x width x height). The bead suspension and the cell sample were injected at a flow rate of 100 μL/hr (3.71 mm/s), while FC-40 with 1% Picosurf 1 was injected at a flow rate of 1000 μL/hr (3.71 cm/s) (**figure 5.22B**).

The generated droplets (droplet diameter: 120 μm, volume: 0.9 nL) were collected in a centrifuge tube containing a small volume of 1% Picosurf 1 in FC40 to prevent droplet fusion. Approximately 15 minutes after their generation the droplets were imaged under a fluorescence microscope (**figure 5.22C**). While the hydrogel beads displayed strong BODIPY 505/515 fluorescence, the fluorescence of the cells was weaker than it was before their encapsulation, implying that the rate at which BODIPY 505/515 leaks out from the cells to the FC-40 oil surrounding the droplets is faster than the rate at which the dye is transferred from the hydrogel bead to the cells.
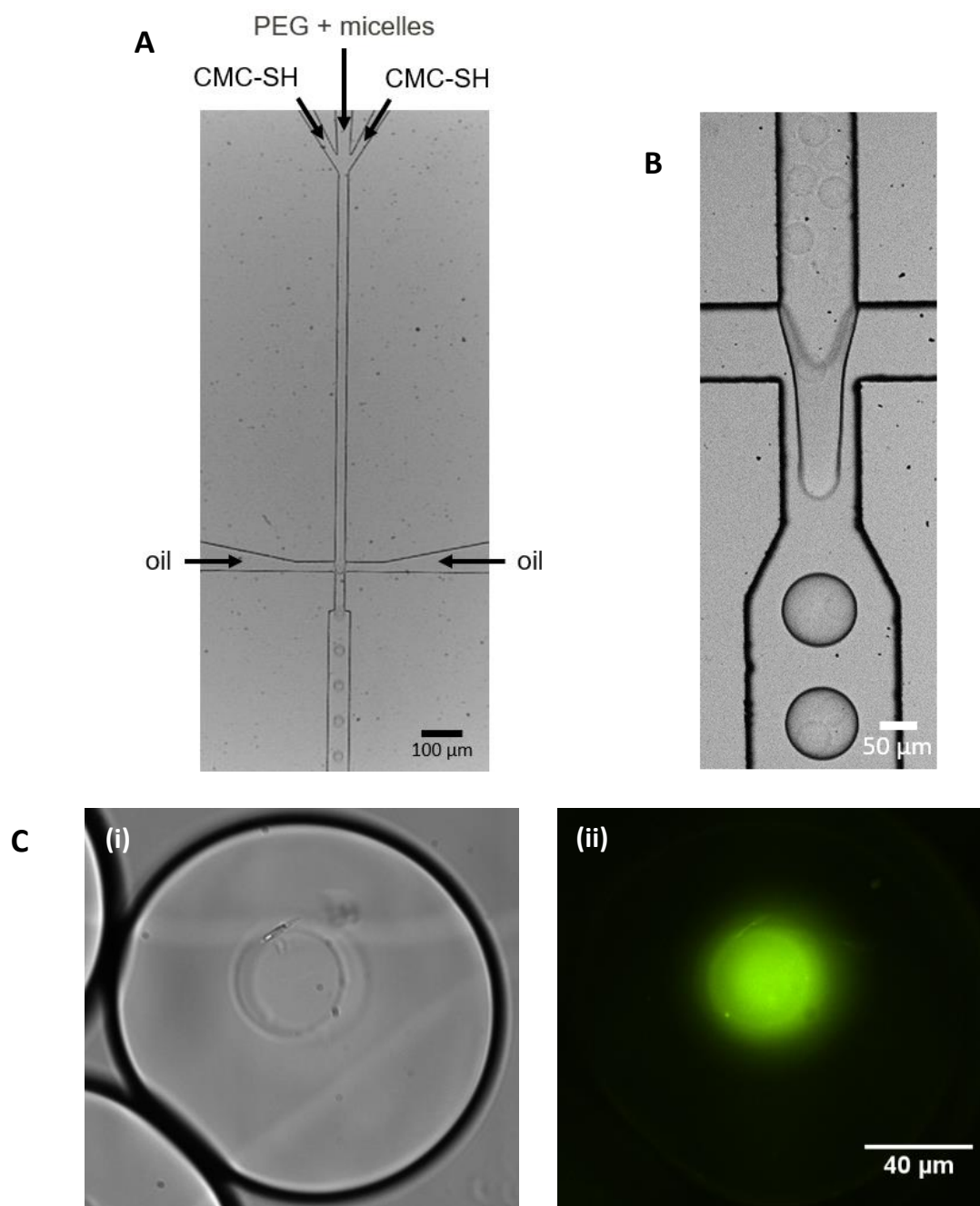
Figure 5.0.22: A) Image of the device (**Appendix device E**) used to generate 40 µm diameter hydrogel beads (flow-focusing region dimensions: 25 µm x 25 µm x 25 µm (length x width x height), flow rates: 2 x 50 µL/hr for CMC-SH, 100 µL/hr for the PEG crosslinker and 1000 µL/hr for the oil), B) the device used to co-encapsulate the 40 µm beads with *Pt* cells (**Appendix device D**, flow-focusing region dimensions: 100 µm x 100 µm x75 µm (length x width x height), flow rates: 100 µL/hr for the beads and the *Pt* cells and 1000 µL/hr for the oil), C) brightfield (i) and fluorescence (ii) images of a *Pt* cell co-encapsulated with a 40 µm bead in a 120 µm droplet 15 minutes after the droplet generation. The experiment was performed twice.

5.4.   Conclusions

In this chapter, a new algal cell staining method was developed using micelles-hydrogel composite beads loaded with BODIPY 505/515. Positively charged PMMA – block – DMAEMA micelles loaded with BODIPY 505/515 were successfully generated. The micelles were then incorporated in a hydrogel formed by the reaction between CMC-SH and a PEG crosslinker to form micelle/hydrogel composite microbeads. The beads were mixed and incubated with algal cells to stain them and the success of this new staining method was assessed with fluorescence microscopy and flow cytometry measurements. An alternative approach to loading the micelles to the hydrogel beads was examined to reduce the loss of BODIPY 505/515 during the preparation process. This new approach could be applied to load the beads with BODIPY 505/515 several times, ensuring that the beads can be reused for staining. Finally, the micelle/hydrogel composite beads were co-encapsulated with *Pt* cells in microdroplets to test whether this was a possible way to keep the encapsulated cells stained with BODIPY 505/515 for a longer time. Unfortunately, the rate at which BODIPY 505/515 leaked out of the droplets was faster than the rate at which the dye was transferred from the hydrogel bead to the cells.

5.5.   Future work

Loading the micelles to the hydrogel beads after the transfer of the beads to aqueous medium helped reduce the loss of BODIPY 505/515 during the bead preparation process. However, the distribution of the micelles in the beads was very uneven and, as a result, most of the micelles were concentrated on the outer surface of the beads. Further work is required to optimise the loading of BODIPY 505/515 to the beads and achieve uniform distribution of the micelles in the beads. A possible way to ensure that the micelles can penetrate deeper into the hydrogel beads is to increase the pore size of the hydrogel by adjusting the cross-linking density.

Co-encapsulating cells and beads loaded with BODIPY 505/515 in microdroplets could potentially keep the cells stained for longer, however for that to be achieved the rate at which the dye is transferred from the beads to the cells must be equal to the rate at which the dye leaks out of the droplets. In the case of the beads used in section 5.3.6, the rate at which the dye was transferred from the beads to the cells was too slow. Further work is required to

adjust the release rate of BODIPY 505/515 from the beads, perhaps by modifying the composition of the micelles or by switching to a different encapsulation oil.

CHAPTER 6

Conclusions

Algae are promising microorganisms for the production of biofuel and high value chemicals. Increased interest in their industrial exploitation has revealed gaps in our knowledge of the physiology and behaviour of microalgae at the single cell level. As a result, single cell methods are increasingly applied to study algal cells.[57,253] The aim of this thesis was to use droplet microfluidic technology to establish a platform for the study and high throughput screening of single algal cells, mainly focusing on the determination of the lipid content of the cells.

A droplet microfluidic platform could offer multiple advantages over other screening methodologies currently used in algal research. Plate-based screening, which is commonly used in algal studies, is limited by the relatively small number of cells that can be examined in a single screen and the relatively slow screening rate.[73] FACS, which has also been used to screen single algal cells,[255,256] enables high-throughput screening of larger cell samples, however it suffers from its own limitations. Some cells can be damaged due to the hydrodynamic stress that they experience during sorting. *Terashima et al*.[255] were only able to obtain viable colonies from about 5% of the *C. reinhardtii* mutants that they recovered after Nile red staining and FACS. In contrast, the droplets in the droplet-based sorting process shield the cells from damage, resulting in recovered cells that are almost 100% viable.[82,191] Furthermore, the ability to control the cellular environment which is provided by droplet microfluidics, enables the screening of both the cells and their microenvironment, something that is not possible through FACS.[160]

In this thesis, single *Phaeodactylum tricornutum* cells were successfully encapsulated in microdroplets of diameter ∼ 40 μm using a PDMS flow-focusing microfluidic device. The growth of the encapsulated cells was monitored over 11 days and was found to be heterogeneous. To overcome the issue of cell sedimentation during the encapsulation procedure and to increase the time over which the procedure could be run, 10% v/v OptiPrep density matching medium was added to the cell suspension prior to the encapsulation. The addition of OptiPrep significantly reduced cell sedimentation, minimising its impact on the cell encapsulation efficiency over time. As a result, the percentage of undesirable empty droplets collected during the encapsulation process, only increased by 6% over two hours, as

compared to the much larger increase (28%) observed when OptiPrep was not used. Furthermore, it was confirmed that the presence of OptiPrep had no impact on the algal cell growth.

A fluorescence-activated droplet sorting (FADS) platform was used for the detection of the intracellular fluorescence of *Pt* cells encapsulated in microdroplets. Following the modification of the optical components of a previously existing fluorescence detection platform,[160] the accuracy of the fluorescence detection increased by nearly tenfold, reducing the fluorescence measurement variation from 87%, which was achieved by a previously used platform,[82,160] to 8%. This increase in accuracy was confirmed initially by detecting the fluorescence of fluorescent beads encapsulated in droplets and then by detecting the chlorophyll fluorescence of encapsulated *Pt* and *Ng* (*N. gaditana*) cells. The detection capabilities of the FADS platform were also tested by detecting the chlorophyll fluorescence of *Pt* cells which contained different chlorophyll levels. These tests confirmed that the detection platform can be used for the screening of cells of different sizes and shapes. This was not possible with the previous platform, as when it was used to screen small cells, such as *Nannochloropsis gaditana*, a large fraction of them (as high as 43 %) would pass by the sides of the laser beam undetected.

Through chlorophyll fluorescence detection and screening, droplets containing *Pt* cells were successfully sorted from empty droplets, showing that the FADS platform can be used to overcome the issue of the random encapsulation of the cells in droplets, improving the efficiency of any further screening experiments. Due to the improved accuracy of the fluorescence detection, false negatives were eliminated, minimising the loss of cells during the sorting procedure.

Besides chlorophyll fluorescence, the FADS platform was also used to detect GFP fluorescence and to successfully sort GFP-expressing *Pt* cells from a mixture with wild type *Pt* cells. GFP is frequently used as a transformation marker in transgenics, to determine whether the cells have been successfully transformed. Due to the low efficiency of the current cell transformation processes, reliable methods are required for the identification and recovery of the transformed cells. The FADS platform could be used for the high throughput sorting of transformed cells from wild type cells. When used in this context, some time-consuming steps

in the traditional transformation workflow can be bypassed and the time needed to identify and confirm stably expressing transformants can be reduced from 6 - 7 weeks to 4 weeks.[172]

A major limitation of the FADS platform, noted during this work, was that the collection and handling of small volumes of droplets was hard to achieve, resulting in the loss of several droplets during the post-sorting collection process. Consequently, sorting experiments had to be run for longer times to ensure that a sufficient number of droplets were collected and, while enriched cell subpopulations were obtained, there was no method to manually select specific cells of interest. This limitation was addressed in this thesis through the application of droplet dispensing technology. In a proof-of-concept experiment, the Cyto-Mine Single Cell Analysis and Monoclonality Assurance System was used to sort GFP-expressing *Pt* cells from a mixture with wild type *Pt* cells. After the end of the sorting procedure, images of the collected droplets were obtained to determine their cell occupancy and the droplets containing GFP-expressing cells were dispensed off-chip one-by-one to the wells of 96- and 384-well plates. The cells were cultured in the well plates for 4 weeks and monoclonal cell cultures were obtained with a 60% success rate. By applying an off-the-shelf that has been successfully launched to the market, it was demonstrated that the combination of droplet sorting and dispensing can be efficiently used for single cell handling and the selection of specific cells of interest. This is a real advantage, as it enables the screening of mutagenized libraries of cells and the selection of potentially rare cell clones from a cell sample. Combining automated droplet dispensing with our optimised droplet sorting platform would therefore be a useful next step in the development of our own algal biotechnology platform. It would put our platform at the same level as other state of the art systems which combine droplet sorting with droplet dispensing for cell selection.[115,116]

While the GFP fluorescence of the transformed *Pt* cells could be detected by Cyto-Mine, the system did not possess the appropriate emission filter to detect the chlorophyll fluorescence of the cells. To expand the range of experiments on algal cells which can be performed by the instrument, an emission filter should be added for chlorophyll fluorescence detection. In the meantime, through GFP fluorescence detection, mutants with higher GFP fluorescence could be identified and isolated using Cyto-Mine. Additionally, in future experiments, the GFP fluorescence of the dispensed cells could be tracked as they grow on the well plates, to determine whether GFP expression remains constant over time.

In a separate investigation, *Pt* cells encapsulated in microdroplets were stained with BODIPY 505/515 to identify and screen cells with higher lipid content. Algal lipids are a valuable resource, because they can be used in the production of biodiesel, one of the most promising biofuels available in the market. Furthermore, certain algae contain large amounts of high value lipids and fatty acids, such as the omega-3 fatty acids EPA and DHA, which are a highly beneficial part of human diet and are used in nutritional supplements.[21,254]

A major challenge in using a lipophilic dye, such as BODIPY 505/515, in droplet microfluidics is the tendency of the dye to leak out of the aqueous droplets and into the oil surrounding them, as well as into PDMS, resulting in a decrease in the stained cell fluorescence over time and in a significant increase in the background fluorescence. To prevent this decrease in the fluorescence of the stained cells, the cells were initially encapsulated in microdroplets using FC-40 with 1% Picosurf 1 surfactant as the continuous phase and they were then transferred to a solution of BODIPY 505/515 in the same oil so that they could be stained. The BODIPY 505/515 fluorescence of the stained droplets was detected with the laser sheet platform. The possibility of BODIPY 505/515 leakage into PDMS was addressed by the substitution of the PDMS microfluidic device, usually used for fluorescence detection, with a cyclic olefin copolymer microfluidic device. Unfortunately, quantitative measurement of the cell fluorescence was not possible due to the high fluorescence background caused by BODIPY 505/515 dissolved in the oil surrounding the droplets. Several experimental parameters were modified in an effort to reduce the background fluorescence. The optimal conditions identified through this effort were the incubation of the droplets in 30 µM BODIPY 505/515 solution in FC-40 for one day, then reinjection of the droplets for fluorescence detection using FC-40 as spacing oil. However, this method of cell staining was not reliable, and the fluorescence emitted by the cells was still weak in comparison to the background fluorescence. Furthermore, this staining method was very slow in comparison to the standard protocols used to stain algal cells with BODIPY 505/515 in bulk, which require less than 10 minutes.[186,200,204]

To alleviate the problem, a new cell staining method was successfully developed using micelle/hydrogel composite beads loaded with BODIPY 505/515. Positively charged PMMA – block – DMAEMA micelles loaded with BODIPY 505/515 were generated. The micelles were then incorporated in a hydrogel formed by the reaction between CMC-SH and a PEG

crosslinker to form micelle/hydrogel composite microbeads. The micelles were bound to the hydrogel through electrostatic interactions with the carboxyl groups of CMC-SH. The composite beads were then mixed and incubated with *Pt* cells to stain them and the success of this new staining method was assessed with fluorescence microscopy and flow cytometry measurements. Specifically, the flow cytometry measurements showed that *Pt* cells could be stained by the beads within 30 minutes and that the beads could also be used to stain other cells types, such as *Ng* cells. The cells could still grow after the staining by the beads and fresh cells cultures could be obtained.

An alternative approach to loading the micelles to the hydrogel beads was examined to reduce the loss of BODIPY 505/515 during the bead preparation process. According to this approach, the micelles could be loaded onto the beads after their transfer to the aqueous phase. Unfortunately, the distribution of the micelles in the beads after this loading process was uneven, with most of the micelles being concentrated on the outer surface of the beads. Further work is required to achieve uniform distribution of the micelles in the beads. A possible way to ensure that the micelles can penetrate deeper into the hydrogel beads is to increase the pore size of the hydrogel by adjusting the cross-linking density. Once this loading method is optimised, it should, as an additional advantage, enable the recharging of the beads with BODIPY 505/515 after each use, ensuring that the beads can be reused multiple times for staining. This should eliminate the need to generate fresh beads for each staining experiment, resulting in a significant reduction in labour and in research cost.

The micelle/hydrogel composite beads were also co-encapsulated with *Pt* cells in microdroplets to test whether this was a possible way to keep the encapsulated cells stained with BODIPY 505/515 for a longer time. For this to be achieved, the rate at which the dye is transferred from the beads to the cells must be equal to the rate at which the dye leaks out of the droplets. Unfortunately, in the experiments performed to test this theory, the rate at which the dye was transferred from the beads to the cells was too slow. Further work is required to increase the release rate of BODIPY 505/515 from the beads and to decrease the rate at which the dye leaks out of the droplets. Some possible ways to achieve these changes is by modifying the composition of the micelles or by switching to a different encapsulation oil.

Overall, despite the difficulties faced in the detection of the lipid content of algal cells, the FADS platform has been further optimised during this project and it can now be efficiently used to study other types of fluorescence, such as GFP or chlorophyll fluorescence, which are very significant in algal research. Furthermore, multiple types of fluorescence can be detected at the same time. While this was demonstrated for dual BODIPY 505/515 and chlorophyll fluorescence detection, it can also be applied to detect GFP and chlorophyll fluorescence and, with the selection of the right optical filters, it can be extended to the detection of other types of fluorescence. As such, some of the requirements about the microfluidic platform, that were set in section 1.3, have been met. The platform can now generate more quantitative and reproducible experimental results and the range of experiments that can be performed with the platform has also been expanded. At its current state, the platform is not straight-forward to use for people that don't have the proper training, as careful control of some experimental parameters is required for its operation. Making the platform more accessible to non-specialists was not within the scope of this thesis, however, it could be achieved by directing future efforts towards the automation of some experimental processes, such as the sample injection to the microfluidic device or the gain adjustment during sorting, so that less input is required by the user.

While other efforts have been made by researchers to develop droplet-based platforms for use in algal research,[83,129-134,191] these platforms are not yet at a stage where they can be widely used by non-specialists. Most of these platforms are limited to the monitoring of cell growth in droplets and the measurement of cell fluorescence with fluorescence microscopy.[129-134] *Kim et al.*[191] developed a droplet-based screening platform, similar to the one described in this thesis, which was capable of identifying faster growing and lipid-rich *C. reinhardtii* lines from an ethyl methanesulfonate (EMS)-mutagenized population. Eight strains showing faster growth and higher lipid content were identified by combining chlorophyll fluorescence detection with BODIPY 505/515 staining and screening. However, the platform had a very low optical analysis throughput (5 Hz) and it was unclear whether the platform was sensitive enough to pick up fluorescence intensity differences at the single cell level. Furthermore, the platform was complex, with multiple droplet operations taking place on one chip and a large number of parameters that had to be carefully controlled. This made the operation of the platform complicated.

With our platform now established, it is possible to achieve the transition from mainly proof-of-concept experiments on algal cell fluorescence detection to targeted experiments aimed towards answering specific biological questions. Future experiments could take advantage of the unique feature of droplets microfluidics which makes it distinct from other analytical methods: the ability to control and study both the encapsulated cells and their microenvironment. A range of experiments can be performed only in droplets, such as the detection of chemicals secreted from the algal cells or the co-culture of microalgae with symbiotic bacteria. The FADS platform can be used in such experiments to identify cell strains or experimental conditions that might be promising for larger scale investigation.

BIBLIOGRAPHY

1. W. Fu, A. Chaiboonchoe, B. Khraiwesh, D. R. Nelson, D. Al-Khairy, A. Mystikou, A. Alzahmi and K. Salehi-Ashtiani, *Mar. Drugs*, 2016, **14**, 225(1-20).

2. G. Sibi, V. Shetty and K. Mokashi, *J. Energy Inst.*, 2016, **89**, 330–334.

3. M. Hlavova, Z. Turoczy and K. Bisova, *Biotechnol. Adv.*, 2015, **33**, 1194–1203.

4. V. Ebenezer, L. K. Medlin and J. Ki, *Mar. Biotechnol.*, 2012, **14**, 129–142.

5. A. Kumar, S. Ergas, X. Yuan, A. Sahu, Q. Zhang, J. Dewulf, F. X. Malcata and H. van Langenhove, *Trends Biotechnol.*, 2010, **28**, 371–380.

6. M. K. Lam and K. T. Lee, *Biotechnol. Adv.*, 2012, **30**, 673–690.

7. H. C. Greenwell, L. M. L. Laurens, R. J. Shields, R. W. Lovitt and K. J. Flynn, *J. R. Soc. Interface*, 2010, **7**, 703–726.

8. D. P. Ho, H. Hao and W. Guo, *Bioresour. Technol.*, 2014, **169**, 742–749.

9. R. Harder and H. von Witsch, *Ber. Deutsch. Bot. Ges.*, 1942, **60,** 146–152.

10. K. Kumar, S. Ghosh, I. Angelidaki, S. L. Holdt, D. B. Karakashev, M. A. Morales and D. Das, *Renew. Sustain. Energy Rev.*, 2016, **65**, 235–249.

11. F. Alam, A. Date, R. Rasjidin, S. Mobin and H. Moria, *Procedia Eng.*, 2012, **49**, 221–227.

12. Y. Chisti, *Biotechnol. Adv.*, 2007, **25**, 294–306.

13. REN21, *Renewables 2020 Global Status Report*, REN21 Secretariat, Paris, 2020.

14. A. K. Koyande, K. W. Chew, K. Rambabu, Y. Tao, D. Chu and P. Show, *Food Sci. Hum. Wellness*, 2019, **8**, 16–24.

15. K. W. Chew, J. Y. Yap, P. L. Show, N. H. Suan, J. C. Juan, T. C. Ling, D. Lee and J. Chang, *Bioresour. Technol.*, 2017, **229**, 53–62.

16. J. L. Harwood and I. A. Guschina, *Biochimie*, 2009, **91**, 679–684.

17. Q. Hu, M. Sommerfeld, E. Jarvis, M. Ghirardi, M. Posewitz, M. Seibert and A. Darzins, *Plant J.*, 2008, **54**, 621–639.

18. Y. Gong and M. Jiang, *Biotechnol. Lett.*, 2011, **33**, 1269–1284.

19.   B. Sajjadi, W. Chen, A. Aziz, A. Raman and S. Ibrahim, *Renew. Sustain. Energy Rev.*, 2018, **97**, 200–232.

20.   O. P. Ward and A. Singh, *Process Biochem.*, 2005, **40**, 3627–3652.

21.   K. Lane, E. Derbyshire, W. Li and C. Brennan, *Crit. Rev. Food Sci. Nutr.*, 2014, **54**, 572–579.

22.   P. Singh, S. Kumari, A. Guldhe, R. Misra, I. Rawat and F. Bux, *Renew. Sustain. Energy Rev.*, 2016, **55**, 1–16.

23.   Y. T. T. Doan and J. P. Obbard, *J. Appl. Phycol.*, 2015, **27**, 2203–2208.

24.   W. Park, G. Yoo, M. Moon, C. W. Kim, Y.-E. Choi and J. Yang, *Appl. Biochem. Biotechnol.*, 2013, **171**, 1128–1142.

25.   T. R. Zalogin and U. Pick, *Algal Res.*, 2014, **3**, 8–16.

26.   Y. Taoka, N. Nagano, Y. Okita, H. Izumida, S. Sugimoto and M. Hayashi, *J. Biosci. Bioeng.*, 2011, **111**, 420–424.

27.   Y. Choi, R. S. Kumaran, H. J. Jeon, H. Song, Y. Yang, S. H. Lee, K. Song, K. J. Kim, V. Singh and H. J. Kim, *Spectrochim. Acta Part A Mol. Biomol. Spectrosc.*, 2015, **145**, 245–253.

28.   Y. H. Seo, Y. Lee, D. Y. Jeon and J. Han, *Bioresour. Technol.*, 2015, **181**, 355–359.

29.   D. Cho, R. Ramanan, J. Heo, J. Lee, B. Kim, H. Oh and H. Kim, *Bioresour. Technol.*, 2015, **175**, 578–585.

30.   W. Yu, W. Ansari, N. G. Schoepp, M. J. Hannon, S. P. Mayfield and M. D. Burkart, *Microb. Cell Fact.*, 2011, **10**, 91–102.

31.   S. Seo, H. Jeon, S. Hwang, E. Jin and K. Suk, *Algal Res.*, 2015, **11**, 50–54.

32.   K. E. Apt, P. G. Kroth-Pancic and A. R. Grossman, *Mol. Gen. Genet.*, 1996, **252**, 572–579.

33.   M. A. Borowitzka and B. E. Volcani, *J. Phycol.*, 1978, **14**, 10–21.

34.   N. N. Zulu, K. Zienkiewicz, K. Vollheyde and I. Feussner, *Prog. Lipid Res.*, 2018, **70**, 1–16.

35.   M. J. Griffiths and S. T. L. Harrison, *J. Appl. Phycol.*, 2009, **21**, 493–507.

36.   Z. Lari, N. Moradi-kheibari, H. Ahmadzadeh, P. Abrishamchi, N. R. Moheimani and M. A. Murry, *J. Appl. Phycol.*, 2016, **28**, 3235–3250.

37.   K. W. M. Tan and Y. K. Lee, *Biotechnol. Biofuels*, 2016, **9**, 255–268.

38.   L. Alipanah, J. Rohloff, P. Winge, A. M. Bones and T. Brembu, *J. Exp. Bot.*, 2015, **66**, 6281–6296.

39.   J. Longworth, D. Wu, M. Huete-Ortega, P. C. Wright and S. Vaidyanathan, *Algal Res.*, 2016, **18**, 213–224.

40.   N. Yodsuwan and S. Sawayama, *Agric. Nat. Resour.*, 2017, **51**, 190–197.

41.   X. Bai, H. Song, M. Lavoie, K. Zhu, Y. Su, H. Ye and S. Chen, *Sci. Rep.*, 2016, **6**, 25494.

42.   M. S. Chauton, Y. Olsen and O. Vadstein, *Biomass Bioenergy*, 2013, **58**, 87–94.

43.   J. L. Salgueiro, A. Cancela, A. Sánchez, R. Maceiras and L. Pérez, *Eur. J. Sustain. Dev.*, 2015, **4**, 89–96.

44.   N. Zou, C. Zhang, Z. Cohen and A. Richmond, *Eur. J. Phycol.*, 2010, **35**, 127–133.

45.   D. Simionato, M. A. Block, N. La Rocca, J. Jouhet, G. Finazzi and T. Morosinotto, *Eukaryot. Cell*, 2013, **12**, 665–676.

46.   M. Cecchin, S. Berteotti, S. Paltrinieri, I. Vigliante, B. Iadarola, B. Giovannone, M. E. Maffei, M. Delledonne and M. Ballottari, *Biotechnol. Biofuels*, 2020, **13**, 78.

47.   R. Radakovits, R. E. Jinkerson, S. I. Fuerstenberg, H. Tae, R. E. Settlage, J. L. Boore and M. C. Posewitz, *Nat. Commun.*, 2012, **3**, 686.

48.   I. Ajjawi, J. Verruto, M. Aqui, L. B. Soriaga, J. Coppersmith, K. Kwok, L. Peach, E. Orchard, R. Kalb, W. Xu, T. J. Carlson, K. Francis, K. Konigsfeld, J. Bartalis, A. Schultz, W. Lambert, A. S. Schwartz, R. Brown and E. R. Moellering, *Nat. Biotechnol.*, 2017, **35**, 647–652.

49.   E. C. Carpinelli, A. Telatin, N. Vitulo, C. Forcato, M. D. Angelo, R. Schiavon, A. Vezzi, G. Mario and T. Morosinotto, *Mol. Plant*, 2014, **7**, 323–335.

50.   D. Simionato, E. Sforza, E. Corteggiani, A. Bertucco, G. Mario and T. Morosinotto, *Bioresour. Technol.*, 2011, **102**, 6026–6032.

51.   E. G. Bligh and W. J. Dyer, *Can. J. Biochem. Physiol.*, 1959, **37**, 911–917.

52.   V. Challagulla, S. Nayar, K. Walsh and L. Fabbro, *Crit. Rev. Biotechnol.*, 2017, **37**, 566–578.

53.   Z. Gitai, *Curr. Opin. Microbiol.*, 2009, **12**, 341–346.

54.   P. Hyka, S. Lickova, P. P, K. Melzoch and K. Kovar, *Biotechnol. Adv.*, 2013, **31**, 2–16.

55.   H. Pereira, P. S. C. Schulze, L. Maylin, T. Santos and L. Barreira, *Algal Res.*, 2018, **30**, 113–120.

56.   M. Díaz, M. Herrero, L. A. García and C. Quirós, *Biochem. Eng. J.*, 2010, **48**, 385–407.

57.   Y. Juang and J. Chang, *Biotechnol. J.*, 2016, **11**, 327–335.

58.   P. Bodénès, H.-Y. Wang, T.-H. Lee, H.-Y. Chen and C.-Y. Wang, *Biotechnol. Biofuels*, 2019, **12**, 33.

59.   A. Huebner, S. Sharma, M. Srisa-art, F. Hollfelder, B. Edel and A. J. De Mello, *Lab Chip*, 2008, **8**, 1244–1254.

60.   S. Mashaghi, A. Abbaspourrad, D. A. Weitz and A. M. Van Oijen, *Trends Anal. Chem.*, 2016, **82**, 118–125.

61.   O. J. Dressler, X. Casadevall i Solvas and A. J. de Mello, *Annu. Rev. Anal. Chem.*, 2017, **10**, 1–24.

62.   X. Casadevall i Solvas and A. deMello, *Chem. Commun.*, 2011, **47**, 1936–1942.

63.   Y. Zhu and Q. Fang, *Anal. Chim. Acta*, 2013, **787**, 24–35.

64.   T. W. Murphy, Q. Zhang, L. B. Naler, S. Ma, C. Lu and T. Murphy, *Analyst*, 2018, **143**, 60–80.

65.   M. G. Simon and A. P. Lee, in *Microdroplet Technology: Principles and Emerging Applications in Biology and Chemistry*, ed. P. Day, A. Manz and Y. Zhang, New York, 2012, ch. 2, pp. 23–50.

66.   F. Ismagilov, *Philos. Trans. R. Soc. Lond. A.*, 2004, **362**, 1087–1104.

67.   N. Bremond, A. R. Thiam and J. Bibette, *Phys. Rev. Lett.*, 2008, **100**, 024501.

68.   A. Huebner, D. Bratton, G. Whyte, M. Yang, A. J. De Mello and F. Hollfelder, *Lab Chip*, 2008, **9**, 692–698.

69.   D. R. Link, S. L. Anna, D. A. Weitz and H. A. Stone, *Phys. Rev. Lett.*, 2004, **92**, 054503–054506.

70.   J. Baret, O. J. Miller, V. Taly, M. Ryckelynck, A. El-harrak, L. Frenz, C. Rick, M. L. Samuels, J. B. Hutchison, J. J. Agresti, D. R. Link, D. A. Weitz and A. D. Griffiths, *Lab Chip*, 2009, **9**, 1850–1858.

71.   A. R. Abate, T. Hung, P. Mary, J. J. Agresti and D. A. Weitz, *Proc. Natl. Acad. Sci. U. S. A.*, 2010, **107**, 19163–19166.

72.   K. C. Lowe, *J. Fluor. Chem.*, 2002, **118**, 19–26.

73.   L. Mazutis, J. Gilbert, W. L. Ung, D. A. Weitz, A. D. Griffiths and J. A. Heyman, *Nat. Protoc.*, 2013, **8**, 870–891.

74.   J. Pan, A. L. Stephenson, E. Kazamia, W. T. S. Huck, J. S. Dennis, A. G. Smith and C. Abell, *Integr. Biol.*, 2011, **3**, 1043–1051.

75.   J. Park, A. Kerner, M. A. Burns and X. N. Lin, *PLoS One*, 2011, **6**, e17019.

76.   M. He, J. S. Edgar, G. D. M. Jeffries, R. M. Lorenz, J. P. Shelby and D. T. Chiu, *Anal. Chamistry*, 2005, **77**, 1539–1544.

77.   T. D. Rane, H. C. Zec, C. Puleo, P. Lee and T. Wang, *Lab Chip*, 2012, **12**, 3341–3347.

78.   M. T. Guo, A. Rotem, J. A. Heyman and D. A. Weitz, *Lab Chip*, 2012, **12**, 2146–2155.

79.   S. Abalde-Cela, A. Gould, X. Liu, E. Kazamia, A. G. Smith and C. Abell, *J. R. Soc. Interface*, 2015, **12**, 20150216.

80.   J. Abatemarco, M. F. Sarhan, J. M. Wagner, J. Lin, L. Liu, W. Hassouneh, S. Yuan, H. S. Alper and A. R. Abate, *Nat. Commun.*, 2017, **8**, 332–341.

81.   D. Josephides, S. Davoli, W. Whitley, R. Ruis, R. Salter, S. Gokkaya, M. Vallet, D. Matthews, G. Benazzi, E. Shvets, F. Gesellchen, D. Geere, X. Liu, X. Li, B. Mackworth, W. Young, Z. Owen, C. Smith, D. Starkie, J. White, B. Sweeney, M. Hinchliffe, S. Tickle, D. J. Lightwood, M. Rehak, F. F. Craig and D. Holmes, *SLAS Technol.*, 2020, **25**, 177–189.

82.   R. J. Best, J. J. Lyczakowski, S. Abalde-Cela, Z. Yu, C. Abell and A. G. Smith, *Anal. Chem.*, 2016, **88**, 10445–10451.

83.   H. S. Kim, A. R. Guzman, H. R. Thapa, T. P. Devarenne and A. Han, *Biotechnol. Bioeng.*, 2016, **113**, 1691–1701.

84.   J. Q. Boedicker, L. Li, T. R. Kline and R. F. Ismagilov, *Lab Chip*, 2008, **8**, 1265–1272.

85.   F. Chen, Y. Zhan, T. Geng, H. Lian, P. Xu and C. Lu, *Anal. Chem.*, 2011, **83**, 8816–8820.

86.   B. Qu, Y.-J. Eu, W.-J. Jeong and D.-P. Kim, *Lab Chip*, 2012, **12**, 4483–4488.

87.   D. Pekin, Y. Skhiri, J.-C. Baret, D. Le Corre, L. Mazutis, C. Ben Salem, F. Millot, A. El Harrak, J. B. Hutchison, J. W. Larson, D. R. Link, P. Laurent-Puig, A. D. Griffiths and V. Taly, *Lab Chip*, 2011, **11**, 2156–2166.

88.   S. C. Kim, I. C. Clark, P. Shahi and A. R. Abate, *Anal. Chem.*, 2018, **90**, 1273–1279.

89.   E. Z. Macosko, A. Basu, R. Satija, J. Nemesh, K. Shekhar, M. Goldman, I. Tirosh, A. R. Bialas, N. Kamitaki, E. M. Martersteck, J. J. Trombetta, D. A. Weitz, J. R. Sanes, A. K. Shalek, A. Regev and S. A. Mccarroll, *Cell*, 2015, **161**, 1202–1214.

90.   P. B. Umbanhowar, V. Prasad and D. A. Weitz, *Langmuir*, 2000, **16**, 347–351.

91.   S. Jin, X. Wei, Z. Liu, J. Ren, Z. Jiang, C. Abell and Z. Yu, *Sensors Actuators B. Chem.*, 2019, **291**, 1–8.

92.   A. J. T. Teo, M. Yan, J. Dong, H.-D. Xi, Y. Fu, S. H. Tan and N.-T. Nguyen, *Microfluid. Nanofluidics*, 2020, **24**, 21.

93.   T. Trantidou, M. S. Friddin, A. Salehi-reyhani, O. Ces and Y. Elani, *Lab Chip*, 2018, **18**, 2488–2509.

94.   A. B. Theberge, F. Courtois, Y. Schaerli, M. Fischlechner, C. Abell, F. Hollfelder and W. T. S. Huck, *Angew. Chem. Int. Ed.*, 2010, **49**, 5846–5868.

95.   P. Zhu and L. Wang, *Lab Chip*, 2017, **17**, 34–75.

96.   T. P. Lagus and J. F. Edd, *J. Phys. D: Appl. Phys.*, 2013, **46**, 114005–114025.

97.   S. Köster, F. E. Angilè, H. Duan, J. J. Agresti, A. Wintner, C. Schmitz, A. C. Rowat, C. A. Merten, D. Pisignano, D. Griffiths and D. A. Weitz, *Lab Chip*, 2008, **8**, 1110–1115.

98.   J. F. Edd, D. Di Carlo, K. J. Humphry, S. Köster, D. Irimia, D. A. Weitz and M. Toner, *Lab Chip*, 2008, **8**, 1262–1264.

99.   E. W. M. Kemna, R. M. Schoeman, F. Wolbers, I. Vermes, D. A. Weitz and A. van den Berg, *Lab Chip*, 2012, **12**, 2881–2887.

100.   M. A. Schwarz and P. C. Hauser, *Lab Chip*, 2001, **1**, 1–6.

101.   L. M. Fidalgo, G. Whyte, B. T. Ruotolo, J. L. P. Benesch, F. Stengel, C. Abell, C. V. Robinson and W. T. S. Huck, *Angew. Chem. Int. Ed.*, 2009, **48**, 3665–3668.

102.   E. E. Kempa, C. A. Smith, X. Li, B. Bellina, K. Richardson, S. Pringle, J. L. Galman, N. J. Turner and P. E. Barran, *Anal. Chem.*, 2020, **92**, 12605–12612.

103. A. R. Salmon, R. Esteban, R. W. Taylor, J. T. Hugall, C. A. Smith, G. Whyte, O. A. Scherman, J. Aizpurua, C. Abell and J. J. Baumberg, *Small*, 2016, **12**, 1788–1796.

104. J. Choo, C. Lim, L. Chen, H. Chon, G. Wang, J. Hong and A. J. DeMello, *Anal. Bioanal. Chem.*, 2009, **394**, 1827–1832.

105. Q. Y. Wong, N. Liu, C. Koh, H. Li and W. S. Lew, *Microfluid. Nanofluid.*, 2016, **20**, 139–147.

106. A. Barani, H. Paktinat, M. Janmaleki, A. Mohammadi, P. Mosaddegh, A. Fadaei-Tehrani and A. Sanati-Nezhad, *Biosens. Bioelectron.*, 2016, **85**, 714–725.

107. A. R. Abate, J. J. Agresti and D. A. Weitz, *Appl. Phys. Lett.*, 2010, **96**, 203509–203511.

108. Z. Cao, F. Chen, N. Bao, H. He, P. Xu, S. Jana, S. Jung, H. Lian and C.Lu, *Lab Chip*, 2013, **13**, 171–178.

109. K. Ahn, C. Kerbage, T. P. Hunt, R. M. Westervelt, D. R. Link and D. A. Weitz, *Appl. Phys. Lett.*, 2006, **88**, 024104–024106.

110. S. S. Schütz, T. Beneyton, J. Baret and T. M. Schneider, *Lab Chip*, 2019, **19**, 2220–2232.

111. A. Sciambi and A. R. Abate, *Lab Chip*, 2015, **15**, 47–51.

112. M. Chabert and J. Viovy, *Proc. Natl. Acad. Sci. U. S. A.*, 2008, **105**, 3191–3196.

113. S. Buryk-iggers, J. Kieda and S. S. H. Tsai, *AIP Adv.*, 2019, **9**, 075106.

114. M. Sesen and G. Whyte, *Sci. Rep.*, 2020, **10**, 8736.

115. Y. Qin, L. Wu, J. Wang, R. Han, J. Shen, J. Wang, A. L. Paguirigan, J. L. Smith, J. P. Radich and D. T. Chiu, *Anal. Chem.*, 2019, **91**, 6815–6819.

116. R. H. Cole, S. Tang, C. A. Siltanen, P. Shahi, J. Q. Zhang, S. Poust, Z. J. Gartner and A. R. Abate, *Proc. Natl. Acad. Sci. U. S. A.*, 2017, **114**, 8728–8733.

117. N. Wen, Z. Zhao, B. Fan, D. Chen, D. Men, J. Wang and J. Chen, *Molecules*, 2016, **21**, 881–894.

118. H. S. Kim, T. P. Devarenne and A. Han, *Algal Res.*, 2018, **30**, 149–161.

119. K. Matsumura, T. Yagi and K. Yasuda, *Biochem. Biophys. Res. Commun.*, 2003, **306**, 1042–1049.

120. K. Matsumura, T. Yagi and K. Yasuda, *Jpn. J. Appl. Phys.*, 2003, **42**, 784–787.

121. K. Matsumura, T. Yagi, A. Hattori, M. Soloviev and K. Yasuda, *J. Nanobiotechnology*, 2010, **8**, 23–35.

122. X. Ai, Q. Liang, M. Luo, K. Zhang, J. Pan and G. Luo, *Lab Chip*, 2012, **12**, 4516–4522.

123. S. Bae, C. W. Kim, J. S. Choi, J.-W. Yang and T. S. Seo, *Anal. Bioanal. Chem.*, 2013, **405**, 9365–9374.

124. Y. Eu, H. Park, D. Kim and J. W. Hong, *Biomicrofluidics*, 2014, **8**, 024113–024125.

125. B. J. Kim, L. V Richter, N. Hatter, C. Tung, B. A. Ahner and M. Wu, *Lab Chip*, 2015, **15**, 3687–3694.

126. P. J. Graham, J. Riordon and D. Sinton, *Lab Chip*, 2015, **15**, 3116–3124.

127. H. S. Kim, T. L. Weiss, H. R. Thapa, T. P. Devarenne and A. Han, *Lab Chip*, 2014, **14**, 1415–1425.

128. H. S. Kim, T. P. Devarenne and A. Han, *Lab Chip*, 2015, **15**, 2467–2475.

129. A. Dewan, J. Kim, R. H. Mclean, S. A. Vanapalli and M. N. Karim, *Biotechnol. Bioeng.*, 2012, **109**, 2987–2996.

130. Y. J. Sung, J. Y. H. Kim, K. W. Bong and S. J. Sim, *Analyst*, 2016, **141**, 989–998.

131. M. G. Saad, N. S. Dosoky, M. S. Khan, M. S. Zoromba, L. Mekki, M. El-Bana, D. Nobles and H. M. Shafik, *Biomolecules*, 2019, **9**, 276–287.

132. M. G. Saad, A. Selahi, M. S. Zoromba, L. Mekki, M. El-Bana, N. S. Dosoky, D. Nobles and H. M. Shafik, *Algal Res.*, 2019, **44**, 101657–101666.

133. T. P. Lagus and J. F. Edd, *RSC Adv.*, 2013, **3**, 20512–20522.

134. S. P. Damodaran, S. Eberhard, L. Boitard, J. G. Rodriguez, Y. Wang, N. Bremond, J. Baudry, J. Bibette and F. Wollman, *PLoS One*, 2015, **10**, e0118987.

135. Y. Morimoto, W. Tan, Y. Tsuda and S. Takeuchi, *Lab Chip*, 2009, **9**, 2217–2223.

136. M. Li, M. Van Zee, C. T. Riche, B. Tofig, S. D. Gallaher, S. S. Merchant, R. Damoiseaux, K. Goda and D. Di Carlo, *Small*, 2018, **14**, 1803315.

137. D. Lee, C. Y. Bae, J. Han and J. Park, *Anal. Chem.*, 2013, **85**, 8749–8756.

138. J. Ohan, B. Pelle, P. Nath, J. H. Huang, B. Hovde, M. Vuyisich, A. E. K. Dichosa and S. R. Starkenburg, *Biotechniques*, 2019, **66**, 218–224.

139. R. R. Guillard and J. H. Ryther, *Can. J. Microbiol.*, 1962, **8**, 229–239.

140. D. C. Duffy, J. C. McDonald, O. J. A. Schueller and G. M. Whitesides, *Anal. Chem.*, 1998, **70**, 4974–4984.

141. U. J. Ana, G. W. Critchlow, K. M. Ford, N. R. Godfrey, D. B. Grandy and M. A. Spence, *Int. J. Adhes. Adhes.*, 2010, **30**, 781–788.

142. K. Kim, J. Kim, H. Lee and S. Lee, *J. Mech. Sci. Technol.*, 2010, **24**, 5–12.

143. Pico-Surf™ User Guide, https://www.spherefluidics.com/wp-content/uploads/2016/11/Pico-Surf-User-Guide-2016-12-02-V1.pdf, (accessed November 2020)

144. T. S. Kaminski, O. Scheler and P. Garstecki, *Lab Chip*, 2016, **16**, 2168–2187.

145. L. Weng and J. E. Spoonamore, *Micromachines*, 2019, **10**, 734–755.

146. R. Dangla, F. Gallaire and C. N. Baroud, *Lab Chip*, 2010, **10**, 2972–2978.

147. P. Gruner, B. Riechers, L. A. C. Orellana, Q. Brosseau, F. Maes, T. Beneyton, D. Pekin and J. Baret, *Curr. Opin. Colloid Interface Sci.*, 2015, **20**, 183–191.

148. D. J. Collins, A. Neild, A. Liu and Y. Ai, *Lab Chip*, 2015, **15**, 3439–3459.

149. H. Liu, M. Li, Y. Wang, J. Piper and L. Jiang, *Micromachines*, 2020, **11**, 94–106.

150. J. R. Lakowicz, *Principles of Fluorescence Spectroscopy,* Springer, Boston, MA, 3rd edn., 2006.

151. J. L. Kinsey, *Annu. Rev. Phys. Chem.*, 1977, **28**, 349–372.

152. M. Srisa-art, A. J. DeMello and J. B. Edel, *Chem. Commun.*, 2009, 6548–6550.

153. M. H. Horrocks, H. Li, J.-U. Shim, R. T. Ranasinghe, R. W. Clarke, W. T. S. Huck, C. Abell and D. Klenerman, *Anal. Chem.*, 2012, **84**, 179–185.

154. M. Srisa-art, E. C. Dyson, A. J. DeMello and J. B. Edel, *Anal. Chem.*, 2008, **80**, 7063–7067.

155. N. R. Baker, *Annu. Rev. Plant Biol.*, 2008, **59**, 89–113.

156. V. da Silva Ferreira and C. Sant'Anna, *World J. Microbiol. Biotechnol.*, 2016, **33**, 20(1-8).

157.   A. Laohavisit, A. Anderson, P. Bombelli, M. Jacobs, C. J. Howe, J. M. Davies and A. G. Smith, *Algal Res.*, 2015, **12**, 91–98.

158.   L. Doron, N. Segal and M. Shapira, *Front. Plant Sci.*, 2016, **7**, 505–529.

159.   H. S. Kim, S. C. Waqued, D. T. Nodurft, T. P. Devarenne, V. V Yakovlev and A. Han, *Analyst*, 2017, **142**, 1054–1060.

160.   R. Best, PhD thesis, University of Cambridge, 2015.

161.   A. Laskin and V. Laskin, in *Proc. SPIE 8843, Laser Beam Shaping XIV*, ed. A. Forbes and T. E. Lizotte, 2013, 88430C.

162.   Thorlabs Powell lenses, https://www.thorlabs.com/newgrouppage9.cfm?objectgroup_id=13875 (assessed April 2021)

163.   H. Jiang, T. Zhu, H. Zhang, J. Nie, Z. Guan, C. Ho, S. Liu and P. Fei, *Lab Chip*, 2017, **17**, 2193–2197.

164.   I. Khaw, B. Croop, J. Tang, A. Möhl, U. Fuchs and K. Y. Han, *Opt. Express*, 2018, **26**, 943–945.

165.   Y. B. Nam, D. J. Lee, J. Lee, C. Kim, G. S. Yun, W. Lee and H. K. Park, *Rev. Sci. Instrum.*, 2016, **87**, 11E130 (1–3).

166.   M. A. Scranton, J. T. Ostrand, D. R. Georgianna, S. M. Lofgren, D. Li, R. C. Ellis, D. N. Carruthers, A. Dräger, D. L. Masica and S. P. May, *Algal Res.*, 2016, **15**, 135–142.

167.   T. Moses, P. Mehrshahi, A. G. Smith and A. Goossens, *J. Exp. Bot.*, 2017, **68**, 4057–4074.

168.   P. Crozet, F. J. Navarro, F. Willmund, P. Mehrshahi, K. Bakowski, K. J. Lauersen, M. Pérez-Pérez, P. Auroy, A. Gorchs Rovira, S. Sauret-gueto, J. Niemeyer, B. Spaniol, J. Theis, R. Trösch, L. Westrich, K. Vavitsas, T. Baier, W. Hübner, F. de Carpentier, M. Cassarini, A. Danon, J. Henri, C. H. Marchand, M. de Mia, K. Sarkissian, D. C. Baulcombe, G. Peltier, J.-L. Crespo, O. Kruse, P.-E. Jensen, M. Schroda, A. G. Smith and S. D. Lemaire, *ACS Synth. Biol.*, 2018, **7**, 2074–2086.

169.   R. Radakovits, R. E. Jinkerson, A. Darzins and M. C. Posewitz, *Eukaryot. Cell*, 2010, **9**, 486–501.

170.   Y. Maeda, T. Yoshino, T. Matsunaga, M. Matsumoto and T. Tanaka, *Curr. Opin. Biotechnol.*, 2018, **50**, 111–120.

171. Y. Niu, Z. Yang, M. Zhang, C. Zhu, W. Yang, J. Liu and Y. Li, *Biotechniques*, 2012, **52**, 1–3.

172. Z. Yu, K. Geisler, T. Leontidou, R. E. B. Young, S. E. Vonlanthen, S. Purton, A. G. Smith and C. Abell, *Algal Res.*, in press.

173. Cyto-Mine brochure, https://spherefluidics.com/wp-content/uploads/2019/03/Cyto-Mine-Brochure-12-page-March-2019.pdf, (accessed on November 2020)

174. L. Nan, M. Y. A. Lai, M. Y. H. Tang, Y. K. Chan, L. L. M. Poon and H. C. Shum, *Small*, 2020, **16**, 1902889.

175. S. K. Hess, B. Lepetit, P. G. Kroth and S. Mecking, *Eur. J. Lipid Sci. Technol.*, 2018, **120**, 1700152.

176. J. K. Pittman, A. P.Dean and O. Osundeko, *Bioresour. Technol.*, 2011, **102**, 17–25.

177. D. Elsey, D. Jameson, B. Raleigh and M. J. Cooney, *J. Microbiol. Methods*, 2007, **68**, 639–642.

178. T. Mutanda, D. Ramesh, S. Karthikeyan, S. Kumari, A. Anandraj and F. Bux, *Bioresour. Technol.*, 2011, **102**, 57–70.

179. V. Benito, F. Goñi-de-Cerio and P. Brettes, *J. Appl. Phycol.*, 2015, **27**, 233–241.

180. G. Diaz, M. Melis, B. Batetta, F. Angius and A. M. Falchi, *Micron*, 2008, **39**, 819–824.

181. J. Rumin, H. Bonnefond, B. Saint-Jean, C. Rouxel, A. Sciandra, O. Bernard, J. Cadoret and G. Bougaran, *Biotechnol. Biofuels*, 2015, **8**, 42–57.

182. W. Chen, C. Zhang, L. Song, M. Sommerfeld and Q. Hu, *J. Microbiol. Methods*, 2009, **77**, 41–47.

183. T. Y. Doan and J. P. Obbard, *J. Appl. Phycol.*, 2011, **23**, 895–901.

184. W. Chen, M. Sommerfeld and Q. Hu, *Bioresour. Technol.*, 2011, **102**, 135–141.

185. J. T. Cirulis, B. C. Strasser, J. A. Scott and G. M. Ross, *Cytometry Part A*, 2012, **81A**, 618–626.

186. T. Govender, L. Ramanna, I. Rawat and F. Bux, *Bioresour. Technol.*, 2012, **114**, 507–511.

187. N. Velmurugan, M. Sung, S. S. Yim, M. S. Park, J. W. Yang and K. J. Jeong, *Bioresour. Technol.*, 2013, **138**, 30–37.

188. A. de la Jara, H. Mendoza, A. Martel, C. Molina, L. Nordströn, V. de la Rosa and R. Díaz, *J. Appl. Phycol.*, 2003, **15**, 433–438.

189. T. K. Fam, A. S. Klymchenko and M. Collot, *Materials (Basel).*, 2018, **11**, 1768.

190. N. Li, M. Schwartz and C. Ionescu-Zanetti, *J. Biomol. Screen.*, 2009, **14**, 194–202.

191. H. S. Kim, S.-C. Hsu, S.-I. Han, H. R. Thapa, A. R. Guzman, D. R. Browne, M. Tatli, T. P. Devarenne, D. B. Stern and A. Han, *Plant Direct*, 2017, **1**, e00011.

192. J. Pan, PhD thesis, University of Cambridge, 2013.

193. A. R. Abate, D. Lee, T. Do, C. Holtze and D. A. Weitz, *Lab Chip*, 2008, **8**, 516–518.

194. Y. Bai, X. He, D. Liu, S. N. Patil, D. Bratton, A. Huebner, F. Hollfelder, C. Abell and W. T. S. Huck, *Lab Chip*, 2010, **10**, 1281–1285.

195. K. E. Gustafson and R. M. Dickhut, *J. Chem. Eng. Data*, 1994, **39**, 281–285.

196. G. T. Roman and C. T. Culbertson, *Langmuir*, 2006, **22**, 4445–4451.

197. J. W. Park, S. Na, M. Kang, S. J. Sim and N. L. Jeon, *BioChip J.*, 2017, **11**, 180–187.

198. V. Arima, M. Bianco, A. Zacheo, A. Zizzari, E. Perrone, L. Marra and R. Rinaldi, *Thin Solid Films*, 2012, **520**, 2293–2300.

199. S. Yu, T. K. S. Wong, X. Hu and K. Pita, *J. Electrochem. Soc.*, 2003, **150**, F116–F121.

200. S. Wu, B. Zhang, A. Huang, L. Huan, L. He, A. Lin, J. Niu and G. Wang, *J. Appl. Phycol.*, 2014, **26**, 1659–1668.

201. H. De la Hoz Siegler, W. Ayidzoe, A. Ben-Zvi, R. E. Burrell and W. C. McCaffrey, *Algal Res.*, 2012, **1**, 176–184.

202. D. M. Wong and A. K. Franz, *J. Microbiol. Methods*, 2013, **95**, 122–128.

203. L. Brennan, A. Blanco Fernandez, A. S. Mostaert and P. Owende, *J. Microbiol. Methods*, 2012, **90**, 137–143.

204. D. Xu, Z. Gao, F. Li, X. Fan, X. Zhang, N. Ye, S. Mou, C. Liang and D. Li, *Bioresour. Technol.*, 2013, **127**, 386–390.

205. K. M. Hackman, B. S. Doddapaneni, C. W. Barth, I. H. Wierzbicki, A. W. G. Alani and S. L. Gibbs, *Mol. Pharm.*, 2015, **12**, 4386–4394.

206. I. Ekladious, Y. L. Colson and M. W. Grinstaff, *Nat. Rev. Drug Discov.*, 2019, **18**, 273–294.

207. L. Sercombe, T. Veerati, F. Moheimani, S. Y. Wu, A. K. Sood and S. Hua, *Front. Pharmacol.*, 2015, **6**, 286.

208. S. A. A. Rizvi and A. M. Saleh, *Saudi Pharm. J.*, 2018, **26**, 64–70.

209. M. E. Wechsler, R. E. Stephenson, A. C. Murphy, H. F. Oidenkamp, A. Singh and N. A. Peppas, *Biomed. Microdevices*, 2019, **21**, 31.

210. S. C. Owen, D. P. Y. Chan and M. S. Shoichet, *Nano Today*, 2012, **7**, 53–65.

211. Q. Chai, Y. Jiao and X. Yu, *Gels*, 2017, **3**, 6.

212. N. A. Peppas, J. Z. Hilt, A. Khademhosseini and R. Langer, *Adv. Mater.*, 2006, **18**, 1345–1360.

213. M. G. A. Mohamed, P. Ambhorkar, R. Samanipour, A. Yang, A. Ghafoor and K. Kim, *Biomicrofluidics*, 2020, **14**, 021501.

214. Y. Ding, P. D. Howes and A. J. DeMello, *Anal. Chem.*, 2020, **92**, 132–149.

215. P. Gupta, K. Vermani and S. Garg, *Drug Discov. Today*, 2002, **7**, 569–579.

216. A. S. Hoffman, *Adv. Drug Deliv. Rev.*, 2012, **64**, 18–23.

217. P. M. Kharkar, M. S. Rehmann, K. M. Skeens, E. Maverakis and A. M. Kloxin, *ACS Biomater.*, 2016, **2**, 165–179.

218. J. Li and D. J. Mooney, *Nat. Rev. Mater.*, 2016, **1**, 16071.

219. H. Labie, A. Perro, V. Lapeyre, B. Goudeau, B. Catargi, R. Auzély and V. Ravaine, *J. Colloid Interface Sci.*, 2019, **535**, 16–27.

220. Y. Liu, N. O. Nambu and M. Taya, *Biomed. Microdevices*, 2017, **19**, 55.

221. Y. Ke, C. Liu, Y. Wang, M. Xiao, J. Fan, P. Fu, S. Wang and G. Wu, *Artif. Cells, Nanomedicine, Biotechnol.*, 2018, **46**, 140–151.

222. Y. Dong, Y. Qin, M. Dubaa, J. Killion, Y. Gao, T. Zhao, D. Zhou, D. Duscher, L. Geever, G. C. Gurtner and W. Wang, *Polym. Chem.*, 2015, **6**, 6182–6192.

223. S. Ma, S. Wang, Q. Li, Y. Leng, L. Wang and G. Hu, *Ind. Eng. Chem. Res.*, 2017, **56**, 7971–7976.

224. J. Ma, Y. Wang and J. Liu, *Micromachines*, 2017, **8**, 255–283.

225. L. Wang and J. Wang, *Nanoscale*, 2019, **11**, 16708–16722.

226. T. Kamperman, M. Karperien, S. Le Gac and J. Leijten, *Trends Biotechnol.*, **36**, 850–865.

227. E. Larrañeta, S. Stewart, M. Ervine, R. Al-Kasasbeh and R. F. Donnelly, *J. Funct. Biomater.*, 2018, **9**, 13.

228. J. Nicolas, S. Mura, D. Brambilla, N. Mackiewicz and P. Couvreur, *Chem. Soc. Rev.*, 2013, **42**, 1147–1235.

229. M.-C. Jones and J.-C. Leroux, *Eur. J. Pharm. Biopharm.*, 1999, **48**, 101–111.

230. K. Cholkar, A. Patel, A. D. Vadlapudi and A. K. Mitra, *Recent Patents Nanomed.*, 2012, **2**, 82–95.

231. Y. Lu, E. Zhang, J. Yang and Z. Cao, *Nano Res.*, 2018, **11**, 4985–4998.

232. Q. Zhou, L. Zhang, T. Yang and H. Wu, *Int. J. Nanomedicine*, 2018, **13**, 2921–2942.

233. D. Liu, F. Yang, F. Xiong and N. Gu, *Theranostics*, 2016, **6**, 1306–1323.

234. I. N. Kurniasih, H. Liang, P. C. Mohr, G. Khot, J. P. Rabe and A. Mohr, *Langmuir*, 2015, **31**, 2639–2648.

235. A. Fluksman and O. Benny, *Anal. Methods*, 2019, **11**, 3810–3818.

236. M. C. A. Stuart, J. C. van de Pas and J. B. F. N. Engberts, *J. Phys. Org. Chem.*, 2005, **18**, 929–934.

237. M. Pekař, *Front. Mater.*, 2015, **1**, 35.

238. C. Chen, G. Liu, X. Liu, S. Pang, C. Zhu, L. Lv and J. Ji, *Polym. Chem.*, 2011, **2**, 1389–1397.

239. A. Rakszewska, R. J. Stolper, A. B. Kolasa, A. Piruska and W. T. S. Huck, *Angew. Chemie - Int. Ed.*, 2016, **55**, 6698–6701.

240. G. L. Ellman, *Arch. Biochem. Biophys.*, 1959, **82**, 70–77.

241. A. Edelstein, N. Amodaj, K. Hoover, R. Vale and N. Stuurman, *Curr. Protoc. Mol. Biol.*, 2010, **92**, 14.20.1-14.20.17.

242. G. Kocak, C. Tuncer and V. Bütün, *Polym. Chem.*, 2017, **8**, 144–176.

243. P. van de Wetering, N. J. Zuidam, M. J. van Steenbergen, O. A. G. J. van der Houwen, W. J. M. Underberg and W. E. Hennink, *Macromolecules*, 1998, **31**, 8063–8068.

244. H. Lee, S. H. Son, R. Sharma and Y. Won, *J. Phys. Chem. B*, 2011, **115**, 844–860.

245. S. Mukherjee, H. Raghuraman and A. Chattopadhyay, *Biochim. Biophys. Acta*, 2007, **1768**, 59–66.

246. D. L. Sackett and J. Wolff, *Anal. Biochem.*, 1987, **167**, 228–234.

247. V. V. De Souza, M. L. de C. Noronha, F. L. A. Almeida, C. A. R. Prado, A. C. Doriguetto and F. H. Florenzano, *Polym. Bull.*, 2011, **67**, 875–884.

248. J. Li, Z. Li, T. Zhou, J. Zhang, H. Xia, H. Li, J. He, S. He and L. Wang, *Int. J. Nanomedicine*, 2015, **10**, 6027–6037.

249. H. C. Kolb, M. G. Finn and K. B. Sharpless, *Angew. Chemie - Int. Ed.*, 2001, **40**, 2004–2021.

250. A. Pettignano, A. Charlot and E. Fleury, *Polym. Rev.*, 2019, **59**, 510–560.

251. C. E. Hoyle and C. N. Bowman, *Angew. Chemie Int. Ed.*, 2010, **49**, 1540–1573.

252. D. P. Nair, M. Podgórski, S. Chatani, T. Gong, W. Xi, C. R. Fenoli and C. N. Bowman, *Chem. Mater.*, 2014, **26**, 724–744.

253. S. C. Pierobon, X. Cheng, P. J. Graham, B. Nguyen, E. G. Karakolis and D. Sinton, *Sustain. Energy Fuels*, 2018, **2**, 13–38.

254. X. Ma, T. Chen, B. Yang, J. Liu and F. Chen, *Mar. Drugs*, 2016, **14**, 61 (1–18).

255. M. Terashima, E. S. Freeman, R. E. Jinkerson and M. C. Jonikas, *Plant J.*, 2015, **81**, 147–159.

256. D. C. Iago Teles, M. Van Der Zwart, D. M. M. Kleinegris, R. H. Wijffels and M. J. Barbosa, *Biotechnol Biofuels*, 2016, **9**, 183 (1–12).
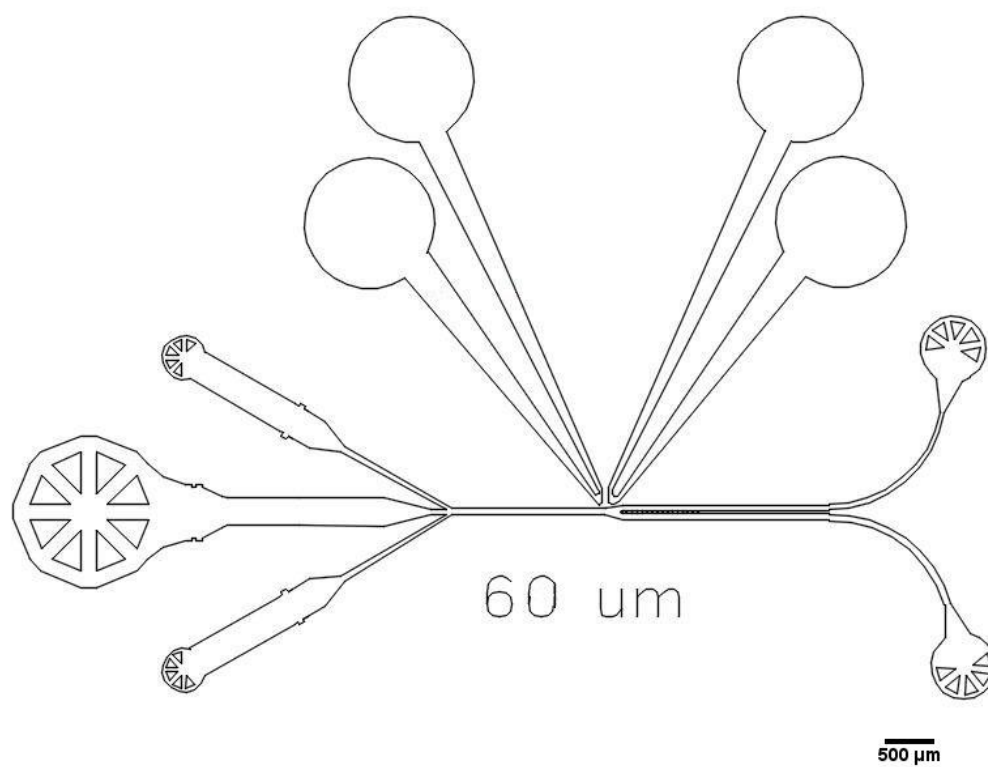
APPENDIX

Device A
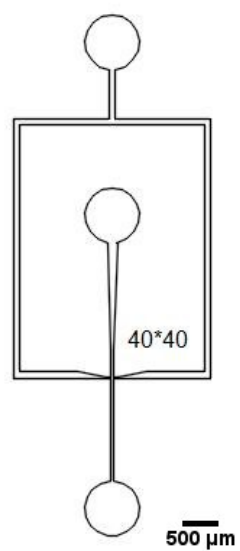
AutoCAD design of the flow-focusing droplet generation device used for cell encapsulation. Dimensions at the flow-focusing region: 40 µm x 40 µm x 25 µm (length x width x height), for experiments in Chapters 2 and 3, 40 µm x 40 µm x 50 µm (length x width x height) for experiments in Chapter 4.
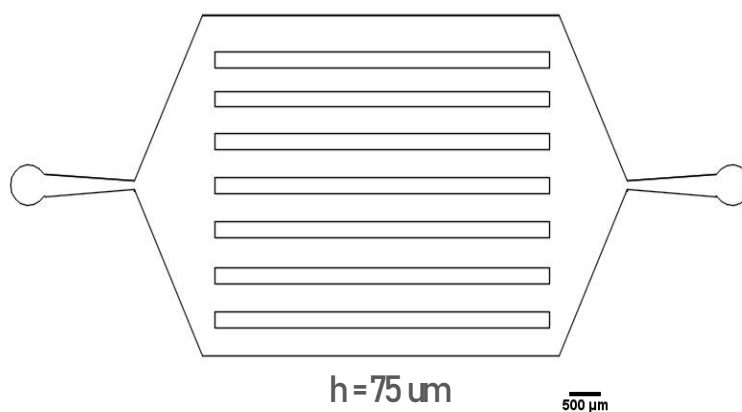
Device B

AutoCAD design of the microfluidic device used for droplet sorting. Microfluidic channel dimensions at the fluorescence detection point: 60 μm width x 50 μm height.
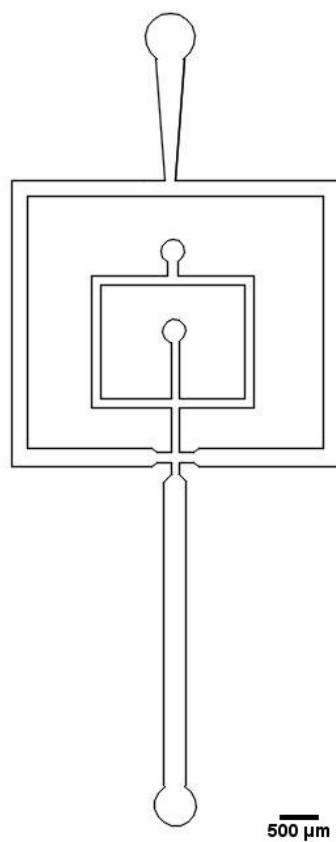
Device C

h=75 um

500 μm

AutoCAD design of the microfluidic reservoir device that was coated using the sol-gel method and used for droplet BODIPY 505/515 fluorescence monitoring over time. Reservoir height 75 μm.
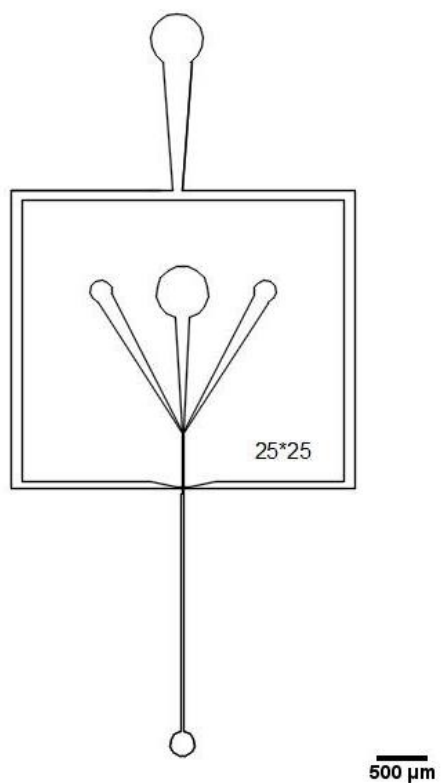
Device D

500 µm

AutoCAD design of the microfluidic device with two flow-focusing modules that was used for hydrogel and micelle/hydrogel composite bead generation. Dimensions at the flow focusing regions: 100 µm x 100 µm x 150 µm (length x width x height). A device of the same design was used for the co-encapsulation of beads and cells in microdroplets (device dimensions 100 µm x 100 µm x 75 µm (length x width x height) at the flow-focusing region).

Device E

AutoCAD design of the microfluidic device that was used for the generation of 40 μm diameter hydrogel beads. Dimensions at the flow focusing region: 25 μm x 25 μm x 25 μm (length x width x height).